INVESTIGATION OF BLOCKAGE EFFECTS ON CIRCULAR CYLINDERS IN A TWO-DIMENSIONAL WIND TUNNEL

Thesis by

Edwin Pounder

In Partial Fulfillment of the Requirements

for the Degree of

Aeronautical Engineer

California Institute of Technology

Pasadena, California

1951

ACKNOWLEDGEMENT

The author wishes to express his appreciation to Mr. Richard W. Bell, Mr. Josiah E. Smith and Mr. Louis Schmidt for their comments and assistance during the course of this investigation. He is greatly indebted to the members of the GALCIT ten-foot wind tunnel staff for their work in the preparation of the figures and the manuscript.

ABSTRACT

These investigations include some experimental and theoretical studies upon blockage effects in a two-dimensional wind tunnel. The shape chosen to represent a body in the tunnel is that of a circular cylinder since such a body will eliminate circulation as a variable and will produce large blockage effects.

In experimental studies, three cylinders of different size are tested in a two-dimensional tunnel. It is found that interference effects are of such a magnitude that it is impossible to obtain two-dimensional flow with the basic models. Two-dimensional flow is obtained through the use of separation devices, but a quantitative blockage study is not attained.

The theoretical work attempts to show the blockage effects of a two-dimensional tunnel upon a circular cylinder of arbitrary size with and without a wake. The potential flow theory is used throughout, and some correlations with the experimental data are indicated.

TABLE OF CONTENTS

INDEX OF RUNS

Date	Run	Configuration	Test	q_o, $\frac{lb}{ft^2}$	α_g	Remarks
3-30-48	1	Clear Tunnel	P_2+P_2'	10		
"	2	" "	" + "	20		
"	3	" "	" + "	40		
"	4	" "	" + "	80		
4-1-48	5	C_1	P_1+P_2	Vary	-4.37°	
"	6	$C_1 + R_1$	$P_1+P_2+P_3$	80	"	
"	7	" $+ R_2$	P_3	"	"	
"	8	" $+ R_3$	"	"	"	
"	9	" $+ R_4$	"	"	"	
"	10	" $+ R_5$	"	"	"	
"	11	" $+ R_6$	"	"	"	
"	12	" $+ R_7$	"	"	"	
4-2-48	13	C_1	P_2'	"	"	
"	5A	"	P_1	"	0°	Repeat of Run 5 at $\alpha_g = 0^\circ$
"	14	$C_1 + T_1 + R_1$	$P_1+P_2+P_3$	"	"	
"	15	" + " $+ R_2$	P_3	"	"	
"	16	" + " $+ R_3$	"	"	"	
4-5-48	17	" $+ T_2$	P_1	"	"	
"	18	" $+ T_3 + R_3$	$P_1+P_2+P_3$	"	"	

INDEX OF RUNS (Continued)

Date	Run	Configuration	Test	q_o, $\frac{lb}{ft^2}$	α_g	Remarks
4-5-48	19	$C_1 + T_3$	P_2+P_1(Vis.)	80	0°	
"	20	" + " + R_2	P_3	"	"	
"	21	" + " + R_1	"	"	"	
4-6-48	22	" + T_4 + "	"	"	"	
"	23	" + " + R_2	P_3+P_1(Vis.)	"	"	
"	24	" + " + R_3	$P_1+P_2+P_3$	"	"	
"	25	" + "	P_2'	"	"	
"	26	" + T_2	P_2+P_1(Vis.)	"	"	
"	27	Clear Tunnel	P_2'	Vary		
4-7-48	28	C_3	P_1	"	0°	
"	29	$C_3 + R_1$	$P_1+P_2+P_3$	10	"	
4-8-48	30	$C_3 + R_2$	P_3	"	"	
"	31	"	P_2'	"	"	
"	32	" + T_5 + R_1	$P_1+P_2+P_3$	"	"	
"	33	" + " + R_2	P_3	"	"	
"	34	" + "	P_2'	"	"	
"	35	" + T_6 + R_2	P_1+P_2	"	"	
"	36	" + T_7 + "	$P_1+P_2+P_3$	"	"	
4-9-48	37	" + " + R_1	P_3	"	"	
"	38	" + "	P_2'	"	"	

INDEX OF RUNS (Continued)

Date	Run	Configuration	Test	$q_o, \frac{lb}{ft^2}$	α_g	Remarks
4-28-48	39	Clear Tunnel	Press.			Calibration of Rake Statics
4-29-48	40	$C_1 + R_5$	P_3	80	0°	Model Orifices Taped
"	41	" $+ R_4$	"	"	"	Model Orifices Taped
"	42	" $+ R_1$	"	"	"	Model Orifices Taped
"	43	" $+ R_4$	P_3(Vis.)	"	"	Model Orifices Taped, Tape on Model in Front of Rake
"	44	" $+ R_1$	"	"	"	Model Orifices Taped, Tape on Model in Front of Rake
"	45	" + "	P_3	"	"	Cylinder Orifices Waxed
4-30-48	46	" $+ R_5$	"	"	"	Cylinder Orifices Waxed
"	46A	" + "	"	"	"	Cylinder Orifices Waxed, Wiped Model of Surface Oxidation
"	47	" $+ R_4$	"	"	"	Cylinder Orifices Waxed
"	48	" $+ R_8$	"	"	"	Cylinder Orifices Waxed

INDEX OF RUNS (Continued)

Date	Run	Configuration	Test	q_o, $\frac{lb}{ft^2}$	α_g	Remarks
4-30-48	48A	$C_1 + R_8$	P_3	80	0°	Cylinder Orifices Waxed
"	49	" $+ R_8'$	P_3(Vis.)	"	"	
5-1-48	50	" $+ T_8 + R_8'$	"	"	"	Sandpaper Separation Strips Blew Loose
"	50A	" + " + "	"	"	"	Repeat of Run 50
"	51	" $+ T_9$ + "	"	"	"	
5-3-48	52	" $+ T_{10}$ + "	P_3(Vis.)+P_4	"	"	End Plate Unsealed
"	49A	" $+ R_8$	" +"	"	"	Cylinder Orifices Waxed, End Plate Unsealed
"	49B	" + "	" +"	"	"	Cylinder Orifices Waxed, End Plate Sealed
"	53	" $+ X_1 + R_8'$	" +"	"	"	
"	54	" + " $+ R_8''$	P_3(Vis.)	"	"	
5-4-48	55	" $+ S_1 + R_8'$	"	"	"	
"	56	" $+ R_8$	P_2+P_3	"	"	
"	57	" $+ R_9$	" + "	"	"	
"	58	" $+ R_9'$	P_3(Vis.)	"	"	
"	49C	" $+ R_8'$	"	"	"	Cylinder Orifices Waxed, End Plate Sealed, Repeat of Run 49B

INDEX OF RUNS (Continued)

Date	Run	Configuration	Test	q_o, $\frac{lb}{ft^2}$	α_g	Remarks
5-5-48	59	$C_1 + T_2 + R_8$	P_2+P_3	80	0°	
"	60	" + " + R_9	P_3	"	"	
"	61	" + T_4 + "	P_2+P_3	"	"	
"	62	" + " + R_8	P_3	"	"	
"	63	" + T_3 + "	P_2+P_3	"	"	
"	64	" + " + R_9	P_3	"	"	
5-6-48	65	$C_2 + R_9$	P_4	24	"	
"	66	" + "	$P_1+P_2+P_3$	"	"	
"	67	C_2	P_1	Vary	"	
"	68	" + R_8	$P_2'+P_3$	24	"	
5-7-48	69	" + T_{11} + R_8	$P_1+P_2+P_3$	"	"	
"	70	" + " + R_9	$P_2'+P_3$	"	"	
"	71	" + T_{12} + "	$P_1+P_2'+P_3$	"	"	
"	72	" + " + R_8	P_2+P_3	"	"	
5-8-48	73	$C_3 + R_8$	" + "	10	"	
"	74	C_1 + "	$P_2+P_2'+P_3$	80	"	
"	75	" + R_8'	P_3(Vis.)	"	"	

INDEX OF FIGURES

Miscellaneous

Experimental Data

INDEX OF FIGURES (Continued)

INDEX OF FIGURES (Continued)

INDEX OF FIGURES (Continued)

Page

Results of Analysis

TABLE 1

A. NOMENCLATURE

Definition of Tests

P_1 = Static pressure measurements made on cylinder using cylinder orifices. Measurements were recorded photographically.

P_1(Vis.) = Visual observation and recording of P_1 pressure measurements.

P_2 = Static pressure measurements made at floor and ceiling of test section using flush mounted orifices which were coincident with vertical plane through tunnel centerline. Measurements were indicated on a multimanometer and recorded photographically.

P_2' = P_2 static pressure measurements made visually using a Zahm type precision micromanometer.

P_3 = Static and total head measurements of the wake made using the survey rake. Measurements were indicated on a multimanometer and recorded photographically.

P_3(Vis.) = Visual observation and recording of P_3 pressure measurements.

P_4 = Visual observation and recording of static pressures on cylinder endplate support as indicated on a multimanometer.

Definition of Angular and Linear Measurements

α_g = Angle of attack of reference cylinder diameter with zero defined by rotating the cylinder in the windstream until orifice number 1 indicated that it was measuring the forward stagnation pressure. Positive angular displacement occurs when the nose is raised or trailing edge is lowered (as a tunnel observer would see it).

θ = Angular measurement of point on cylinder relative to reference diameter (when model is at $\alpha = 0^o$). See sketch to right.

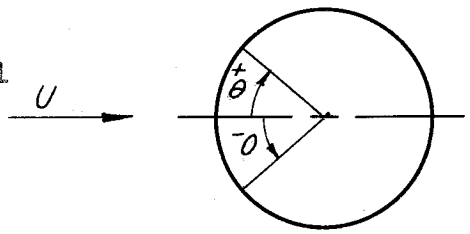

TABLE 1 (Continued)

x = Distance from trunnion axis measured in direction parallel to tunnel centerline. Positive value corresponds to downstream direction.

y = Distance from trunnion axis measured in vertical direction. Positive value corresponds to measurement above trunnion axis.

z = Distance from tunnel centerline measured parallel to trunnion axis (i.e. horizontal). Positive value corresponds to measurement to left (North) of tunnel centerline (observer looking upstream).

d = Diameter of cylinder.

Definition of Coefficients

C_p = Total or static pressure coefficient. Figures on which the scales are labeled C_p have the curves marked so as to identify the pressure coefficient presented.

$$C_p = \frac{P_x - P_{ref.}}{q_o} \quad \text{or} \quad \frac{H_x - P_{ref.}}{q_o}$$

$$R = \text{Reynolds number} = \frac{\rho d U_o}{\mu}$$

Where the foregoing coefficients are associated with the following quantities:

q_o = Dynamic pressure in clear tunnel test section as indicated when using calibrated tunnel piezometer rings. ($1/2\ \rho U_o^2$ in lb/ft.^{2})

$q = H_x - p_x$ = True dynamic pressure measured in tunnel when model is present ($1/2\ \rho u^2$ in lb/ft.^{2})

H_x = Total head as indicated by measurements made using the rake.

P_x = Static pressure measurements made at "x" where subscripts used are:

TABLE 1 (Continued)

x = denotes location of static pressure orifice as indicated on figures. (i.e. Rake, model, or endplate static orifices)

w = denotes static pressure measurement made on the wall (floor and ceiling) when model is present in tunnel.

$P_{ref.}$ = Reference static pressure measurement where subscript "ref." may be:

20 ~ denotes static pressure measurements made at the 20 ft. piezometer ring

3-1/2 ~ denotes static pressure measurements made at the 3-1/2 ft. piezometer ring

o ~ denotes static pressure measurements made at the intersection of the tunnel centerline with the trunnion axis when no model is present

$\mathbb{C}$ ~ denotes static pressure measurements made when no model is present at points on the tunnel centerline other than at intersection with the trunnion axis

w_o ~ denotes static pressure measurements made on the wall (floor and ceiling) when no model is present

U_o = Freestream velocity when no model is present.

u = Local velocity when model is present.

ρ = Mass density of air (note: A correction is applied in the tunnel airspeed calibration so that in the above formulae ρ is to be taken as the free air density unaffected by compressibility).

μ = Absolute viscosity of air (for T = 15° C., h = 760 mm.) =

$$3.726 \times 10^{-7} \frac{\text{lb - wgt x sec}}{\text{ft}^2}$$

In addition to the preceding definitions, new definitions are given in the text when they occur in conjunction with derivations, etc.

TABLE 1 (Continued)

B. NOTATIONS USED TO DESCRIBE CONFIGURATIONS TESTED

C_1 = Steel cylinder machined and ground to a high polish. Length is 36.0 inches and diameter is 6.598 inches. It is equipped with 20 static pressure orifices made by installing 3/32" O.D. copper tubing flush to the surfaces. Orifices are spaced evenly apart with number 1 orifice being on the leading edge. The orifices were mounted on tunnel centerline in an unstaggered (axially) position.

C_1' = C_1 with static pressure orifices filled in with brass rod. Slight surface irregularities still existed.

C_2 = Steel cylinder similar to C_1 but of 12.613 inch diameter. It is equipped with 36 static pressure orifices mounted in a vertical plane coincident with the tunnel centerline.

C_3 = Steel cylinder similar to C_2 but of 17.838 inch diameter.

R_1 = Standard 80 tube GALCIT traversing total head rake installed so as to make a vertical total head survey 20-1/2 inches aft of the trunnion axis and 6 inches South of tunnel centerline. Rake also equipped with static pressure tubes.

R_2 = Rake mounted 32-1/2 inches aft of the trunnion axis and 6 inches South of tunnel centerline.

R_3 = Rake mounted 44-1/2 inches aft of the trunnion axis and 6 inches South of tunnel centerline.

R_4 = Rake in same axial position as R_1 but mounted 12 inches South of tunnel centerline.

R_5 = Rake in same axial position as R_1 but mounted on tunnel centerline.

R_6 = Rake in same axial position as R_1 but mounted 6 inches North of tunnel centerline.

R_7 = Rake in same axial position as R_1 but mounted 12 inches North of tunnel centerline.

TABLE 1 (Continued)

R_8 = Rake mounted 20-1/2 inches aft of trunnion axis. Differs from previous rake notation in that this location allows a complete horizontal traverse in addition to the vertical traverse. Actual position of rake in traverse plane is noted on pressure data.

R_8' = Rake R_8 with total head tube mounted on outside of static pressure tube mount so as to permit total head measurements to be taken close to the South tunnel wall. (Total head tube was mounted on South side of rake).

R_8'' = Rake R_8 with total head tube mounted to flanges on North side of rake so as to permit total head survey close to the North wall.

R_9 = Rake mounted 38-1/2 inches aft of trunnion axis. Similar to R_8 in that notation is used to denote rake being used for complete traverse with actual rake position noted on pressure data.

R_9' = Rake R_9 with total head tube mounted as in R_8' so as to permit total head survey near South wall.

T_1 = 0.041-inch diameter (piano wire) separation strips taped spanwise on model at $\theta = \pm 65^\circ$. Used in conjunction with cylinder C_1.

T_2 = 0.018-inch diameter (piano wire) separation strips taped spanwise on cylinder C_1 at $\theta = \pm 65^\circ$.

T_3 = Separation strips similar to T_2 except taped at $\theta = \pm 85^\circ$.

$T_4 = T_2 + T_3$.

T_5 = 0.039-inch diameter (piano wire) separation strips taped spanwise on cylinder C_3 at $\theta = \pm 65^\circ$.

T_6 = 0.0675-inch diameter (welding rod) separation strips taped spanwise on cylinder C_3 at $\theta = \pm 55^\circ$.

T_7 = Separation strips similar to T_6 except taped at $\theta = \pm 85^\circ$.

TABLE 1 (Continued)

T_8 = One-inch wide chordwise separation strips (sandpaper) mounted on each end of cylinder. Extended around leading edge from $\theta = +100^\circ$ to $\theta = -100^\circ$.

T_9 = 0.0675-inch diameter (welding rod) separation strips taped spanwise on cylinder C_1 at $\theta = \pm 65^\circ$.

T_{10} = Separation strips similar to T_9 but modified such that they only extended to within 2 inches of each wall.

T_{11} = 0.0675-inch diameter (welding rod) separation strips taped spanwise on cylinder C_2 at $\theta = \pm 65^\circ$.

T_{12} = 0.0675-inch diameter (welding rod) separation strips taped spanwise on cylinder C_2 at $\theta = \pm 65^\circ$ and $\pm 85^\circ$.

S_1 = 1/2-inch wide cellulose tape strips mounted parallel to chord plane of cylinder C_1 and spaced 3 inches apart across the span.

X_1 = Wax fillet installed at intersection of front side of cylinder C_1 and North tunnel wall.

Clear Tunnel = Test section of wind tunnel devoid of models so as to permit preliminary calibrations of air flow.

TABLE 1 (Continued)

C. NOTATION USED FOR THE THEORETICAL ANALYSIS

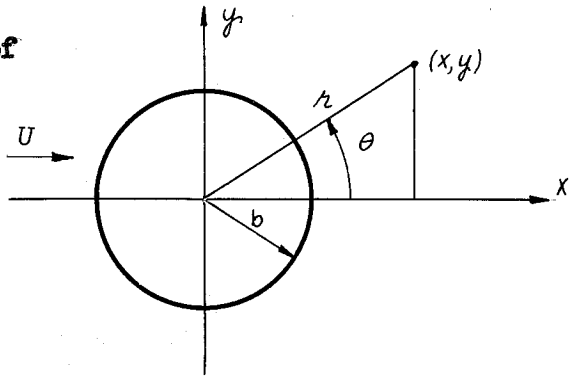

x = $r \cos \theta$ = coordinate in direction of undisturbed flow

y = $r \sin \theta$ = coordinate perpendicular to undisturbed flow

r = $\sqrt{x^2 + y^2}$ = polar coordinate

θ = $\tan^{-1} \frac{y}{x}$ = polar argument

z = $x + iy = re^{i\theta}$ = complex coordinate

d = diameter of circular cylinder

b = radius of circular cylinder

a = height of channel

c = polar distance of wake source from origin

ϕ = angular location of wake source from origin

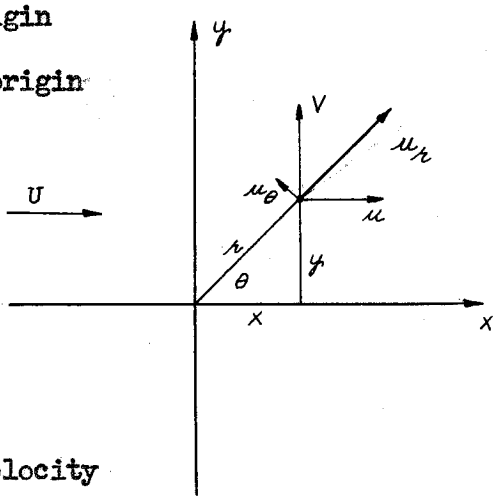

U = undisturbed velocity

u = velocity in x direction

v = " " y "

u_r = radial velocity

u_θ = tangential velocity

$w(z) = u - iv = (u_r - i\, u_\theta) e^{-i\theta}$ = complex velocity

$F(z) = \bar{\phi} + i\psi$ = complex potential

$\bar{\phi}$ = velocity potential, ψ = stream function

$u = \frac{\partial \bar{\phi}}{\partial x} = \frac{\partial \psi}{\partial y}$ $\quad v = \frac{\partial \bar{\phi}}{\partial y} = -\frac{\partial \psi}{\partial x}$

$\mu_{1,2}$ = strengths of doublets for the cylinder without wake in the channel

TABLE 1 (Continued)

μ' = strength of doublet which corrects wake disturbance at $x = -\infty$

$\mu_1 + \mu'$ = strength of doublet for the cylinder with wake in the channel

Q = strength of sources which simulate wake

TABLE 2

IMPORTANT PHYSICAL DATA

Cylinder	d (inches)	$\frac{d}{a}$	$\frac{b}{a}$	$\frac{\text{Span}}{d}$
C_1	6.598	.06468	.03234	5.46
C_2	12.613	.12366	.06183	2.85
C_3	17.838	.17488	.08744	2.02

APPROXIMATE REYNOLDS NUMBERS, R x 10^{-5}

q lb/ft^2	C_1	C_2	C_3
2		2.1	
5		3.8	5.4
10	3.1	5.7	8.4
12.5	3.5		
15	3.7	7.0	10.3
17.5	4.1		
20	4.4	8.1	11.4
24		8.9	
30	5.4	9.9	14.5
40	6.2		
60	7.6		
80	8.8		

APPROXIMATE MACH NUMBERS

q(lb/ft^2)	M
10	.082
24	.128
80	.235

I INTRODUCTION

The following is a summary of some experimental and theoretical studies of flow about right circular cylinders in a two-dimensional wind tunnel. The attempt is made to draw some conclusions concerning the effects of tunnel walls upon the flow. In the absence of any circulation about the body in the tunnel, all such effects are generally grouped together under the term "blockage effects", and the effects will be so designated hereafter in this report.

The reason for interest in blockage effects is simply that in all wind-tunnel tests the data obtained in the tunnel must be applied to cases in free air. Consequently, such data must be corrected for the effects of the tunnel if they are to be used with assurance. Corrections, associated with circulation, are based on a well developed theory which has been checked by experiment with some success; while corrections for blockage effects are not so well developed or so thoroughly substantiated by experiment.

It has always been customary to keep all corrections as small as possible by keeping the sizes of the models small in comparison to the tunnel dimensions, but if the corrections were well understood large models would be desirable for many reasons. As Mach numbers increase, this consideration becomes even more critical, since all corrections increase markedly with M.

The present investigation was undertaken with these things in mind. It was decided to use a large two-dimensional wind tunnel and to use as models three right circular cylinders of different diameters, each spanning the tunnel working section. All models were to be tested at the

same Reynolds number and at low Mach numbers. The cylinder shape was chosen to eliminate circulation as a variable, and the two-dimensional flow was used because of the comparative simplicity and because most of the detailed theory is for this case. Comparatively large cylinder diameters were chosen to assure large wakes and large blockage effects. Comprehensive pressure surveys were taken in the flow about each model, and it was believed that the differences in data between models would be solely due to blockage effects. Therefore, these data could be used to check the theoretical treatments. Wake sizes were to be varied by the use of devices to induce separation.

As it turned out, the experimental work was complicated by some unforeseen circumstances. It was found that the flow about the models was far from two-dimensional, with the interference between the boundary layers on the tunnel walls and the cylinder surface having a profound effect on the wake pattern. Since the ratio between cylinder diameter and span was different for each model, this interference varied greatly between models and made direct two-dimensional flow correlation impossible. In addition, some static pressure tubes set flush in the model surfaces induced early separation, and any surface irregularities such as small spots of corrosion, which were almost imperceptable, had similar effects. As a consequence of these troubles, a good deal of the testing time was spent in studying and eliminating their effects.

It was found that reasonably good two-dimensional flows could be obtained by moving the general location of the separation forward. This was done by laying wires spanwise along the model surface upstream of the maximum thickness point, and several of these configurations were

tested. Sets of data for all models with wires located in similar positions are available and can be compared for blockage effects. However, the data from the clean models cannot be compared at all in this sense.

Some attempts were made to eliminate the wall interference by fillets and similar devices, but it is quite clear that the only effective method would be to remove the wall boundary layer just ahead of the cylinder through a porous surface or a slot.

In addition to these experimental surveys a theoretical study was made of the potential flow about a circular cylinder in a tunnel with and without singularities downstream to simulate wake effects.

The experimental data which were obtained and a summary of the theoretical treatment are presented here, along with a general discussion of results.

A complete outline of the tests is presented in the Index of Runs, and the definitions of model configurations and test nomenclature are found in Table I. The experimental setup and instrumentation are described in Section II, and the methods of data reduction and presentation are outlined in Section III.

II PHYSICAL AND CALIBRATION DATA

A. Physical Data

The facility used for the experimental studies is the GALCIT 10-Foot Wind Tunnel with the two-dimensional working section installed. A complete description of this installation is given in References (1) and (2). The working section is three feet wide, eight feet high and ten feet long, and models are mounted horizontally between two end plates which are set flush to the walls. The contraction ratio is about 12-1/2 to 1, and five turbulence screens are provided in the settling section between the last turn and the contraction section. A very smooth flow is achieved with a turbulence level (ratio of the root mean square of velocity fluctuations to mean velocity) of 0.08% parallel to and 0.12% perpendicular to the flow direction.

The models consisted of three 36.0 inch lengths of steel tubing ground to an accurate circular shape on a centerless grinder, and finished to a high polish. Their diameters were 6.598, 12.613, and 17.838 inches, and they were mounted between the standard end plates. Each model was equipped with a chordwise row of static pressure orifices located at the center of the span and extending around the entire circumference.

Wake surveys were made with the standard survey rake for the two-dimensional tunnel. This rake consists of 80 total head tubes mounted 0.1 inches apart and of 5 static pressure tubes mounted on the side of the rake frame. The rake mount incorporates horizontal and vertical leadscrews to facilitate surveys, while fore and aft movement of the rake must be accomplished by unclamping the rake support strut from the mount and moving it manually.

Static pressure surveys on the working section floor and ceiling were made using 38 orifices set flush in the walls on lines defined by the intersection of the fore and aft vertical plane of symmetry with the floor and ceiling.

The north end plate was equipped with 27 static pressure orifices, from which data were taken during several runs of the test.

All pressure tubes were connected by rubber tubing to back-lighted multi-manometer banks, and most of the data were recorded photographically from these banks. In several instances, where interest centered on only a few readings, data were taken visually. The floor and ceiling pressures were recorded both from the multi-manometers and from a precision micro-manometer, since it was found that pressure differences were often too small to record accurately from the former.

The wake rake was in general too short to cover the large wakes encountered, and so surveys were taken in two or three steps with the rake moved about two thirds of its length across the wake for each step. Several pictures were taken during each reading so that the continually fluctuating wake pattern could be satisfactorily averaged. The wake patterns all fluctuated about 5 or 10% about their mean values, and were in no cases unstable or subject to violent variations with time, so that this survey procedure was considered adequate.

A drawing of the working section is presented in Figure 1 which shows the model support system, the wake rake mount, and the locations of the floor and ceiling orifices. Figure 2 shows the cylinders and Figure 3 the location of the end plate orifices.

B. Tunnel Calibrations

The results of the clear tunnel flow calibrations are shown in Figures 4 through 9.

The tunnel flow parameter to which all data are referred is the free stream dynamic pressure q_o, which is completely defined in Table I. This dynamic pressure was set during the testing by measuring the static pressure difference between two sets of pressure orifices in the settling and contraction sections of the tunnel. The calibration between this pressure difference and q_o was obtained by taking simultaneous measurements of the two, using a standard pitot-static tube located at the reference point to measure q_o. A compressibility correction was applied, so that the true q_o was known at all times. The calibration is shown in plotted form in Figure 4.

Figures 5 through 8 illustrate the clear tunnel variations in static pressure along the reference axis in the working section and along the floor and ceiling. It should be noted that at the farthest aft rake position (44-1/2 inches aft of trunnion axis) q had varied only 1% from q_o. Since this was so, q_o was used as the reference value in the denominators of all pressure coefficients. In general, static pressure references were taken from the calibration plots at the place in the working section where the measurements were taken.

Figure 9 illustrates the calibration of the static pressure tubes on the wake rake. No calibration was made for the total head tubes.

III DATA PRESENTATION

All experimental data presented in this report were obtained from pressure measurements. They are all reduced to the form of pressure coefficients by subtracting the value of a suitable reference pressure and dividing the difference by the dynamic pressure, q_o, which was used when the data were taken. Definitions of the coefficients used are found in Table I. All space coordinates are made dimensionless by dividing them by the diameter, d, of the cylinder to which they refer. The coordinate system used is shown at right and is defined completely in Table I.

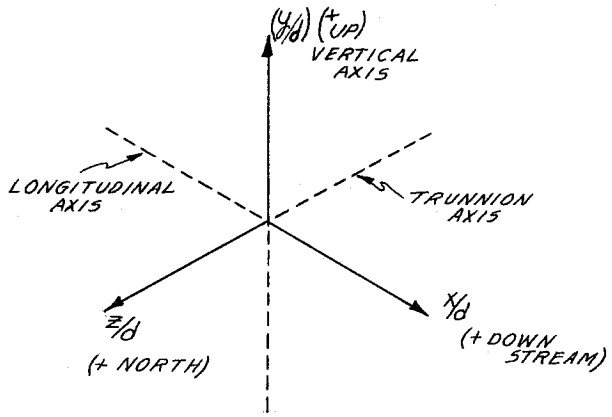

All data are shown in plotted form, with the type of plot depending on the kind of data in question. Essentially four kinds of data were recorded as follows:

a) Wake surveys behind the models.

b) Static pressure surveys around the models at their midspans.

c) Static pressure surveys on the tunnel wall near the tunnel-model intersection.

d) Static pressure surveys along the floor and ceiling covering the length of the working section.

The data in each of these categories are presented together, and the presentation of each group will be described separately in the following discussion.

a) Wake Surveys: Wake data are presented in Figures 10 to 32. In general, surveys were taken vertically through the wake. A series

of such surveys taken at a given distance downstream (x/d) and at several spanwise stations (z/d) are considered a complete picture of the wake at that value of (x/d). These groups are presented together, each under one Figure number. In some cases, only one spanwise station was studied and in these instances the plots usually appear individually. Each vertical survey is plotted on a separate sheet. Plotted are

$$\frac{H - p_{20}}{q_o} \text{ , } \frac{p - p_{20}}{q_o} \text{ and } \frac{p_{\mathbb{C}} - p_{20}}{q_o} \text{ vs. } (y/d)$$

Also, indicated is the value of $\frac{p_w - p_{20}}{q_o}$ existing at the floor and ceiling at that value of (x/d). The points without symbols represent experimental values of $\frac{H - p_{20}}{q_o}$ and the circled points values of $\frac{p - p_{20}}{q_o}$. In some cases where the amount of data is insufficient, no fairing has been shown for the static pressure curves.

It is to be noted that, for this tunnel contraction ratio, $\frac{H_o - p_{20}}{q_o} =$ .0064 or about 1/2 mm. on these plots, so that the coefficients are nominally referenced to H_o. The difference between the static pressure and total head curves is essentially q/q_o.

In several cases, groups of surveys are cross-plotted to show contours of constant total head values at a given value of (x/d) (a few cross plots of static pressure also appear). These cross-plots illustrate the three dimensional character of the wake when transition wires are not used, and the two dimensional qualities when they are. In the case of cylinder C_1 two detailed total head surveys were made near the model-wall intersection and these are included on the appropriate cross-

plots (Figures 10 and 14).

b) Static Pressure Surveys on Models: These data are presented in Figures 33 to 47, and were obtained from static pressure orifices located around the cylinders at their midspan. Plotted is $\frac{p - p_o}{q_o}$ vs. θ. In cases where no differences existed between corresponding orifices on the top and bottom of the model only one point is plotted. When differences did exist, the data for the lower surface are given tagged symbols. The dotted line on each plot represents the static pressure distribution on a cylinder in potential flow (no walls).

It may be noted here for reference later that the pressure drag coefficient can be computed from these data using the relation

$$C_{D_1} = \frac{1}{2} \int_0^{2\pi} \left[\frac{p - p_o}{q_o} \right] \cos \theta \, d\theta \qquad \text{-----(1)}$$

c) Surveys on the End Plates: Here several complete surveys were taken, and results are plotted as lines of constant static pressure in Figures 49 and 50. It was found that differences between cylinders C_1 and C_2 were slight in this case and so data taken in these cases are plotted together in Figure 49. No data appear for C_3 since this model covered most of the orifices. Figure 48 presents the potential flow solution corresponding to these plots.

The points shown on these Figures are not experimental values but are obtained from cross-plotting the data and picking even values of $\frac{p - p_o}{q_o}$.

d) Floor and Ceiling Surveys: Data from these studies are plotted

on Figures 51, 52 and 53. They are presented as $\frac{p_w - p_{w_o}}{q_o}$ vs. x/d for a series of model configurations. Each curve is an average of floor and ceiling pressures, with values of the reference pressure, p_{w_o}, being taken from Figure 7.

The curves are a combination of data taken on both the multi-manometer and a micro-manometer. The latter was used to accurately establish the level of the readings, since in some cases the differences were quite small and hard to read from the manometer film.

The velocities at the wall can be computed from the relation

$$\frac{u_w}{u_{w_o}} = \sqrt{\frac{1 - \frac{p_w - p_{w_o}}{q_o}}{1 - \frac{p_{w_o} - p_o}{q_o}}} \qquad -----(2)$$

IV DISCUSSION OF EXPERIMENTAL RESULTS

The experimental data will be discussed qualitatively here, and some of the difficulties encountered will be pointed out in detail. Wake surveys, model pressures, and floor and ceiling data will be discussed separately, and then some general results concerning drag and blockage will be indicated.

a) Wake Surveys: The data on configurations without separation strips may be considered first. These are presented in Figures 10-14, 22, 23 and 28. The first thing to notice is the interference due to the wall-model intersection (see the cross plots of constant total head decrements). For all three cylinders, an area of large total head loss exists adjacent to the wall, and outside this area a region of almost negligible total head loss exists. The center of the latter area is at about one diameter from the wall in every case, and the amount of loss depends only on the distance x/d downstream of the model. The ratio of cylinder diameter to span is never small enough for effects of this interference to be very well defined farther than one diameter from the wall, but presumably, if the cylinders were longer the effects would die out and a predominately two-dimensional wake would be established at two or three diameters distance. Some probing at the intersection indicated that a double vortex is formed off the top and bottom of the model, and evidently this forces high energy air down into the wake at about one diameter out causing the low loss observed at that point.

The data also show that the static pressure orifices caused some wake distortion by moving the point of separation at the center of the span somewhat forward. This effect is not nearly as well defined as the wall intersection interference, since it is a weaker disturbance and occurs close to or within the area in which the wall effect predominates. Figures 11-13 illustrate attempts to eliminate orifice interference by waxing, taping, and plugging the orifices as smoothly as possible. It is seen that the waxing (Figure 11c) and plugging (Figure 13f) were effective, but that the taping (Figure 12c) was not. In the first two cases, there is still an area of larger total head loss at the center, but this must be mainly caused by the attempt of the wake to form in a two-dimensional manner since the wall effect is comparatively small at center of the span for this case.

The remaining Figures in the group illustrate the effects of the separation wires, and it is apparent that all these configurations have wakes which are predominately two dimensional. Separation wires at 85° have the least effect; those at 65° are intermediate; and those at both 65° and 85° develop the largest wakes. It was found that the size of wire was relatively unimportant.

Note that in all cases the spanwise variations in static pressure are comparatively minor, but that through the wake vertically, large gradients are exhibited which are of the same order of magnitude as those in total head pressure.

b) Static Pressure Surveys on Models: The data under this category are shown in Figures 33-47. Reynolds number comparisons are presented in Figures 33, 39 and 43 for the cylinders without

separation strips, and a table of R is included in Table 2. It is apparent that a marked change in pressure distribution occurs at a value of R of about 3.7×10^5, and this is to be expected as a manifestation of the transition from laminar to turbulent separation which occurs in the flow over any smooth body. Most of the data in this thesis were taken at a Reynolds number of about 8.6×10^5 so as to be well above this critical range.

Since none of these data were taken with separation strips, the pressures shown are only good at the center of the model spans. It is seen that the region of separation below $R = 3.7 \times 10^5$ is at about $\theta = 90^\circ$, while after transition separation occurs at about $\theta = 115^\circ$. This leads to the possibility that the wakes below $R = 3.7 \times 10^5$ might be much more two dimensional than those which were observed for the cases without separation strips, but since no wake surveys were actually made at the low Reynolds numbers this cannot be proved. Such tests would be interesting if any further experimental surveys are undertaken on the cylinders, as wakes of a somewhat different nature would certainly be produced.

The remaining Figures illustrate pressure distributions with the separation strips in use, and it may be reasonably assumed that these surveys apply across the model spans. Note that as the cylinder size increases for a given separation strip location (cf. Figures 36, 41 and 45) the point of separation remains reasonably constant while the peak negative pressure (point of highest velocity) increases somewhat. Such behavior can be considered as a bonafide effect of blockage.

One other fact is worthy of note here. Figure 43 shows data on cylinder C_3, and it will be remembered (cf. Figure 28) that these data are taken in the region of minimum total head loss mentioned previously as being associated with the wall interference. Figure 43 shows that the separation point is moved back to about $\theta = 140^{\circ}$ for this case and that the peak negative pressure is very large. This can only occur if high energy air is being forced over the back side of the cylinder to delay the separation, since the blockage itself does not move the separation point appreciably. Presumably then, the delayed separation is due to the formation of the double vortex which was observed in the visual studies. However, the whole interference pattern is surprising and still somewhat obscure.

c) Surveys on The End Plates: These data are shown on Figures 49 and 50 and may be compared with the potential distribution (in free air) shown on Figure 48. As they are made on the wall surface, they represent the static pressure distribution as observed through the boundary layer and wall interference effect. Therefore, they are of qualitative interest only. The effect of the separation strip is seen to be very large (Figure 50) in that the static pressure behind the model is considerably reduced.

d) Floor and Ceiling Surveys: Floor and ceiling pressure distributions are shown in Figures 51, 52 and 53 for the three models with and without separation strips. The separation strips increase the disturbance at the wall as expected due to the increased wake sizes. At about four diameters upstream of the cylinders the disturbance is about -.02 in all cases. The peak change occurs slightly aft of the cylinders,

moving forward and increasing markedly as the ratio d/a increases. Downstream, the curves all tend to some final negative value which indicates a higher velocity than that in the free stream, and this may be considered as an indication of the wake blockage. However in no case was the final value of static pressure established, so that it is clear that the working section was somewhat short for these investigations.

e) Other Observations: Figures 54-61 summarize the data on the wakes which were considered to be two-dimensional. Averages of the wake surveys are shown, and plots of maximum wake losses as functions of x/d are presented. Figures 54, 58 and 61 show the latter.

It is seen here that at about six diameters downstream when the wake is perhaps three diameters wide, the velocity recovery in the center of the wake is almost complete, so that the losses apparently appear almost immediately as decreases in static pressure and not as velocity gradients as is usually the case. This is an unexpected result, and must mean that the wake is diffusing into the tunnel free stream flow in a manner quite different from that of the usual wakes observed in two-dimensional work.

In Figure 61 no fairing was attempted since it is clear that the rake was too close to the model to allow the total head tubes to function properly. This highlights another difficulty encountered which may be mentioned here. Ideally the wake surveys should have been taken at the same values of x/d for all cylinders, but this was impossible because of the relatively short working section length. From the experience here it would seem that values of about 4, 6 and 8 for x/d would be about right.

Because such a procedure could not be adopted with the model sizes used, exact wake correlations are impossible.

Figures 62 and 63 show results of some drag coefficient computations made from the experimental data. The first figure is a plot of C_{D_1} vs. R for cylinder C_1, computed from equation (1). The data are taken from Figures 33-38. This again illustrates the critical Reynolds number effect at about $R = 3.8 \times 10^5$, which is typical for such cases. For C_1 without the separation strips the values of C_{D_1} are of qualitative interest only, because of the interference effects. The effect of the separation strips on C_{D_1} is clearly indicated here.

Figure 63 is a tabulation of pressure and wake drag coefficients computed for the cases with two-dimensional wakes. Here C_{D_1} was again computed from equation (1) using Figures 35-47. These values indicate that C_{D_1} generally increases as cylinder size increases for a given separation strip, but there is too much scatter for any exact correlations considering the number of values available.

The values of C_{D_w} are computed from the averaged wake plots, Figures 55-60, using a relation derived in reference 3), page 128, from the momentum equation. This relation was chosen because it restricts the computations to the region of the wake, and is presumably quite general. In the nomenclature used here, the equation can be written as

$$C_{D_w} = 2 \int_W \left[\frac{H_o - H_w}{q_o} \right] d \left(\frac{Y}{d} \right) - \left[2W + \frac{d}{a} W^2 \right] \qquad -----(1a)$$

where

$$W = \int_W \left[\sqrt{\frac{q_w}{q_o}} - \sqrt{\frac{q_w}{q_o}} \right] d \left(\frac{y}{d} \right)$$

$( )_w$ refers to data in the wake

$$q_w = H_w - p_w$$

$$q_w' = H_o - p_w$$

The values, thus computed, do not correlate very well with corresponding values of C_{D_1}, nor do values for the same cylinder at different values of x/d correspond. In general, the values of C_{D_w} are slightly less than those of C_{D_1} and decrease somewhat as x/d increases. This probably means that equation (1a) cannot be accurately applied so close to the body and/or that the data are not accurate because of instrument errors close to the body. No values of C_{D_w} were computed for C_3 since the wake surveys were made at very small values of x/d for this model.

In summary then, it is plain that the drag data are not adequate for any quantitative blockage study, although the general trends are in the correct direction. This is due in part to the lack of complete similarity between the cylinders, and also due to the manner in which wake data were taken.

f) Comment on the Tests: As a result of the experience gained from these investigations, several rules concerning experimental techniques may be laid down which should aid in any future studies of this nature.

First, geometric similarity must be maintained to a higher degree than was possible here. Ideally, of course, the only geometric parameter to be varied should be d/a, with the ratio of span to diameter and the values of x/d at the wake rake stations held constant. If this could be done, good quantitative results could almost certainly be obtained, but several working sections of different dimensions would be required, and this would introduce many new difficulties. The alternatives are either to eliminate the wall interference effect so that the span to diameter ratio would lose its significance or to make the ratio

quite large (at least 10) to reduce the importance of the wall interference. Either approach should give essentially two-dimensional wakes. The wall effects could be presumably eliminated by boundary layer removal on the wall just upstream of the model either through a slot or a porous surface.

Second, the practice of using a complete ring of orifices to measure pressures on the model is not too sound, and a much better approach might be to use one orifice and rotate the model. However, the latter approach would require much more testing time for equivalent results, so a probable compromise might be to locate a row of orifices on a helical line around the model. The orifice size should also be reduced to as small a diameter as possible (the model orifices used here had diameters of about 3/64") and the orifice holes should be drilled directly into the surface of the model and connected to pressure tubing on the inside.

Third, the use of separation wires to vary the wake size is well established by these tests, and the locations for maximum effectiveness are pretty well fixed as between $\theta = 65^{\circ}$ and 85°. If similar strips are to be used on several cylinders as was done for this report, some care should be taken to see that all strips are fastened in the same manner with as much geometric similarity between models as possible. The variations in wire size which were investigated (cf. Table 1B) did not seem to be very important as far as wake size was concerned, but it would probably be wise to use geometrically similar diameters.

Fourth, the surface condition of the cylinders is of extreme importance, and any practice leading to the possibility of corrosion should be avoided. It might be well to use some kind of a lacquer to insure complete uniformity of the surface over a reasonable period of time.

Fifth, it might be very interesting to study the wall-cylinder interference effect in some detail, so that it can be defined and understood completely. The two primary variables if compressibility is neglected should be R, the Reynolds number of the cylinder and R_W the Reynolds number along the wall (R_W would define the character of the wall boundary layer in the vicinity of the wall-cylinder intersection if the cylinder were not present). If the effect is completely defined as a function of R and R_W , it should be easy to eliminate it or at least exercise some measure of control.

If the above points are considered, it is reasonably certain that good quantitative data on the basic two-dimensional blockage effects can be obtained with circular cylinders. These points must therefore be considered as the main results of the experimental part of the thesis, as they indicate the way to the final solution of the problem as originally outlined. It is now pertinent to present the theoretical considerations which may also act as a guide in any future experimental work.

V. Theoretical Considerations on Two Dimensional Blocking in a Channel Due to the Presence of a Circular Cylinder

The two dimensional flow around cylinders has been treated extensively both for the cases with and without channel walls. Some elaboration will be given here with special emphasis on circular cylinders of comparatively large dimensions. The two dimensional potential theory is employed throughout, and correlation with the experimental data is discussed wherever necessary. The analysis is presented in four parts for reasons of clarity. These are:

1). Flow about a circular cylinder without a wake in free air (rectilinear flow).

2). Flow about a circular cylinder without a wake in a channel.

3). Flow about a circular cylinder with a wake in free air (rectilinear flow).

4). Flow about a circular cylinder with a wake in a channel.

The presence of the wake is simulated by a suitable arrangement of sources.

The two primary purposes of the analysis are first to simulate the wake by a potential flow, and second to preserve the shape of the body in the channel as completely as possible.

1). Cylinder without wake in a simple rectilinear flow.—This case is derived by combining a doublet with rectilinear flow and is well known. The results will simply be listed here without derivation for a circular cylinder at the origin of the coordinate system (the cylinder will be maintained at this location throughout).

The complex potential is

$$F(z) = Uz + \frac{c}{z}$$

and if we let the doublet have the strength

$$c = \frac{a\mu}{\pi} = Ub^2$$

then

$$F(z) = U\left[z + \frac{b^2}{z}\right] \qquad \text{------ (3)}$$

The potential is

$$\phi(x,y) = Ux\left[1 + \frac{b^2}{x^2 + y^2}\right] \qquad \text{------ (3a)}$$

and the stream function is

$$\psi(x,y) = Uy\left[1 - \frac{b^2}{x^2 + y^2}\right] \qquad \text{------ (3b)}$$

The streamline $\psi = 0$ lies along the x axis and on a circle of radius b.

The velocities are

$$\left.\begin{aligned} &\frac{u}{U} = 1 - \frac{b^2(x^2 - y^2)}{(x^2 + y^2)^2} \quad ; \quad \frac{v}{U} = \frac{-2b^2xy}{(x^2 + y^2)^2} \\ &\frac{u_r}{U} = \left[1 - \left(\frac{b}{r}\right)^2\right]\cos\theta \quad ; \quad \frac{u_\theta}{U} = -\left[1 + \left(\frac{b}{r}\right)^2\right]\sin\theta \end{aligned}\right\} \qquad \text{--- (4)}$$

On the cylinder r = b and

$$\frac{u_r}{U} = 0 \quad ; \quad \frac{u_\theta}{U} = -2\sin\theta$$

The pressure coefficient is obtained from the incompressible Bernoulli equation as

$$C_p = 1 - \frac{u^2 + v^2}{U^2} = \frac{2b^2(x^2 - y^2) - b^4}{(x^2 + y^2)^2} = -\left(\frac{b}{r}\right)^4 + 2\left(\frac{b}{r}\right)^2(\cos^2\theta - \sin^2\theta)$$

and on the cylinder

$$C_p = 1 - 4\sin^2\theta$$

2). Cylinder without wake in a channel of height a.--This case is obtained approximately by placing an infinite row of doublets on the y axis and combining the resultant flow with rectilinear flow (5). If the doublets are spaced a distance, a, apart, the wall boundary condition at $y = \pm \frac{a}{2}$ is satisfied, but a slightly distorted circular cylinder is created.

Here the complex potential is

$$F(z) = Uz + \frac{a\mu}{\pi} \sum_{n=-\infty}^{\infty} \frac{1}{z - ina}$$

$$= Uz + \mu \coth \frac{\pi z}{a} \qquad \text{------ (5)}$$

The potential is

$$\phi = Ux + \frac{\mu \sinh \frac{2\pi x}{a}}{\cosh \frac{2\pi x}{a} - \cos \frac{2\pi y}{a}} \qquad \text{------ (5a)}$$

and the stream function is

$$\psi = Uy - \frac{\mu \sin \frac{2\pi y}{a}}{\cosh \frac{2\pi x}{a} - \cos \frac{2\pi y}{a}} \qquad \text{------ (5b)}$$

When $y = 0$; $\psi = 0$ and when $y = \pm \frac{a}{2}$, $\psi = \pm \frac{Ua}{2}$ satisfying the wall boundary condition.

The velocities may be written as

$$\frac{u}{U} = 1 + \frac{2\pi\mu}{Ua} \frac{\left[1 - \cosh \frac{2\pi x}{a} \cos \frac{2\pi y}{a}\right]}{\left[\cosh \frac{2\pi x}{a} - \cos \frac{2\pi y}{a}\right]^2}; \quad \frac{v}{U} = \frac{-2\pi\mu}{Ua} \frac{\sinh \frac{2\pi x}{a} \sin \frac{2\pi y}{a}}{\left[\cosh \frac{2\pi x}{a} - \cos \frac{2\pi y}{a}\right]^2} \qquad (6)$$

We now wish to evaluate μ which determines the size of the cylinder in relation to the channel. Probably the most critical dimension when comparing this case with case 1 is the thickness or maximum y coordinate, so we would like to maintain this at a constant

value, b. To do this, use equation (5b) letting $\Psi = 0$, $x = 0$ and $y = b$ and solve for μ. Then rigorously

$$\left(\frac{2\pi\mu}{Ua}\right)_1 = 2\pi \frac{b}{a} \tan\left(\frac{\pi b}{a}\right) \qquad \text{- - - - - (7)}$$

gives the result desired (the form for the doublet strength parameter used here is written because of its convenience later). If this expression is expanded and only the first term written, the strength is

$$\left(\frac{2\pi\mu}{Ua}\right)_2 = 2\pi^2 \left(\frac{b}{a}\right)^2 \qquad \text{- - - - - (7a)}$$

which is the value used in reference (5). If (7a) is used the y semi-diameter varies with $\left(\frac{b}{a}\right)$ and this variation can be expressed by the relation

$$\frac{\pi y}{a} \tan \frac{\pi y}{a} = \left(\frac{\pi b}{a}\right)^2$$

In any case the x semi-diameter is given by the relation

$$\left[\frac{x}{b}\right]_{\substack{\mu=0 \\ y=0}} = \frac{1}{2\pi}\left(\frac{a}{b}\right) \cosh^{-1}\left[\frac{2\pi\mu}{Ua} + 1\right] \qquad \text{- - - - - (8)}$$

Equations (7), (7a), and (8) are plotted in Figures 64,65 and here the doublet strength required and the distortion of the cylinder as a function of $\left(\frac{b}{a}\right)$ are clearly shown.

To further study the shape of the cylinder expand (5b) for $\Psi = 0$.

Here $$\cosh \frac{2\pi x}{a} = \cos \frac{2\pi y}{a} + \left[\frac{2\pi\mu}{Ua}\right] \frac{a}{2\pi y} \sin \frac{2\pi y}{a}$$

and if this expression is expanded and rewritten, we get

$$\left(\frac{x}{a}\right)^2 + \left(\frac{y}{a}\right)^2 \left[1 + \frac{1}{3}\left(\frac{2\pi\mu}{Ua}\right)\right] - \frac{1}{a^2}\left[\frac{\mu a}{\pi U}\right] =$$

$$- \left[3.3\left(\frac{x}{a}\right)^4 + 4.35\left(\frac{x}{a}\right)^6 + \cdots\right]$$

$$+ \left[3.3\left(\frac{y}{a}\right)^4 - 4.35\left(\frac{y}{a}\right)^6 + \cdots\right]$$

$$+ \frac{1}{2\pi^2}\left[\frac{2\pi\mu}{Ua}\right]\left[13.1\left(\frac{y}{a}\right)^4 - 12.2\left(\frac{y}{a}\right)^6 + \cdots\right]$$

If the size of the cylinder is such that anywhere on it $\frac{x^2 + y^2}{a^2} \ll 1$ (a maximum value for this report is 0.01) then $\frac{2\pi\mu}{Ua}$ is of the same order, from equation (7), and the following can be said. On the right-hand side of the above expression the 4^{th} order terms are the only ones of any importance, and they have a maximum value of about 3% of the terms on the left. On the left, therefore, since $\left[\frac{2\pi\mu}{Ua}\right] \ll 1$, is the equation of a figure very near to a circle of radius $b = \sqrt{\frac{\mu a}{\pi U}}$. This gives a physical interpretation to the value for μ given in (7a) i.e.,

$$\mu = \frac{\pi b^2 U}{a}$$

The velocities $\frac{u}{U}$ and $\frac{v}{U}$ are not so easy to interpret in relation to those of case (1), but if they are expanded in power series, the second order terms give expressions identical to those of case (1) with 4^{th} order terms providing the first corrections.

2a). A comparison between velocities in cases (1) and (2).--Velocities on the lines x = 0 and y = 0 can be profitably compared here as an indication of the blockage. The doublet strength $\left[\frac{2\pi\mu}{Ua}\right]_1$ will be used here for complete generality, and in fact will be used exclusively hereafter.

Let $\Delta\left(\frac{u}{U}\right) = \left(\frac{u}{U}\right)_{\text{channel}} - \left(\frac{u}{U}\right)_{\text{free air}}$ ~effect of channel walls

Then

$$\left.\begin{aligned}\Delta\left(\frac{u}{U}\right)_{x=0} &= \frac{2\pi b}{a}\,\frac{\tan\frac{\pi b}{a}}{\left[1-\cos\frac{2\pi y}{a}\right]} - \frac{(b/a)^2}{(y/a)^2}\\ \text{and } \Delta\left(\frac{u}{U}\right)_{y=0} &= \frac{(b/a)^2}{(x/a)^2} - \frac{2\pi b}{a}\,\frac{\tan\frac{\pi b}{a}}{\left[\cosh\frac{2\pi x}{a}-1\right]}\end{aligned}\right\} \quad \text{- - - - - (9)}$$

where we are interested in the regions $0 \le y/a \le 1/2$, $0 \le x/a < \infty$, $0 \le b/a < 1/2$. Since these quantities obviously approach 0 as $(b/a)^2 \to 0$, a more significant form can be written as

$$\left.\begin{aligned}\left(\frac{a}{b}\right)^2\Delta\left(\frac{u}{U}\right)_{x=0} &= \left[\frac{2\pi\tan\frac{\pi b}{a}}{b/a}\right]\,\frac{1}{1-\cos\frac{2\pi y}{a}} - \frac{1}{(y/a)^2}\\ \text{and } \left(\frac{a}{b}\right)^2\Delta\left(\frac{u}{U}\right)_{y=0} &= \left[\frac{2\pi\tan\frac{\pi b}{a}}{b/a}\right]\,\frac{1}{1-\cosh\frac{2\pi x}{a}} + \frac{1}{(x/a)^2}\end{aligned}\right\} \quad \text{- - - - (9b)}$$

In addition when considering small values of x/a and y/a it is convenient to expand (9b) in power series with the result that

$$\left.\begin{aligned}\left(\frac{a}{b}\right)^2\Delta\left(\frac{u}{U}\right)_{x=0} &= \left[\frac{\tan\frac{\pi b}{a}}{\frac{\pi b}{a}}-1\right]\,\frac{1}{(y/a)2} + \frac{\pi^2}{3}\left[\frac{\tan\frac{\pi b}{a}}{\frac{\pi b}{a}}\right] + \sum_{n=1}^{\infty} C_{2n}\,(y/a)^{2n}\\ \text{and}\\ \left(\frac{a}{b}\right)^2\Delta\left(\frac{u}{U}\right)_{y=0} &= -\left[\frac{\tan\frac{\pi b}{a}}{\frac{\pi b}{a}}-1\right]\,\frac{1}{(x/a)2} + \frac{\pi 2}{3}\left[\frac{\tan\frac{\pi b}{a}}{\frac{\pi b}{a}}\right] + \sum_{n=1}^{\infty} K_{2n}\,(x/a)^{2n}\end{aligned}\right\} \text{- (9c)}$$

where C_{2n} and K_{2n} are constants of the expansions.

Using (9b) and (9c) the two functions have been computed over the range of interest and are presented in plotted form in Figures 66 and 67. The limits shown there at x/a = y/a = 0 can be clearly seen in (9c), since, if we let b/a approach zero faster than y/a or x/a both limits are

$$\left(\frac{a}{b}\right)^2 \Delta\left(\frac{u}{U}\right)_{\substack{x=0 \\ y/a=0,\ b/a=0}} = \left(\frac{a}{b}\right)^2 \Delta\left(\frac{u}{U}\right)_{\substack{y=0 \\ x/a=0,\ b/a=0}} = \frac{\pi^2}{3}$$

but if b/a, y/a, x/a all approach zero at the same rate then the limits become

$$\left(\frac{a}{b}\right)^2 \Delta\left(\frac{u}{U}\right)_{\substack{x=0 \\ y/a=b/a=0}} = \frac{2\pi^2}{3}\ ;\quad \left(\frac{a}{b}\right)^2 \Delta\left(\frac{u}{U}\right)_{\substack{y=0 \\ x/a=b/a=0}} = 0$$

The range of practical interest on the Figures lies in the areas where y/a and x/a are larger than b/a, since elsewhere the coordinates are inside the body. The effects which are indicated are generally referred to as "solid blockage", when b/a = 0.

Although these expressions specifically represent results for a circular cylinder, they may be used to illustrate the general effect of finite body size, and can be compared directly with results given in Reference (4) which has considered "solid blockage" for a general body shape in the limiting case of very small size. For instance Figures 66 and 67 may be compared directly with Figures 6 and 7 of Reference (4). It is seen that the curves for b/a = 0 correspond directly to the blockage increments (F_2) indicated there, but that as soon as finite size is considered marked differences occur. The most notable is in the velocity increment at the maximum thickness of the body, which differs from the value at b/a = 0 (the reference would show this) where b/a is finite. Such differences are of considerable importance when high subsonic Mach numbers are considered.

3). Cylinder with wake in a simple rectilinear flow.--The real flow behind a cylinder cannot be represented by the potential theory since the irrotationality condition is not maintained throughout. However, the effects of the wake upon the irrotational part of the real flow can be

approximated by the introduction of singularities near the body on its downstream side. These create a "displacement thickness" behind the body, which influences the rest of the flow in a manner similar to the way the wake influences the rest of the real flow. However, the pressures and velocities in the potential flow downstream of the cylinder become meaningless in any region where the wake has been dissipated into the real flow to an appreciable extent.

Considering circular cylinders, the addition of singularities in the free stream (rectilinear flow) is easy, because a system of sources and simks, say, can be set up which have a circle as a streamline, and then this solution can be superimposed on that in part (1) using a circle of the same radius. Because of the linearity the circle streamline will be retained in the combined solution.

In the channel case however, the source sink solution will give a body streamline slightly distorted from a circle and different from that of part (2). Therefore, superposition of these solutions will not necessarily yield results which can be compared directly with the free air case. If the two shapes are not grossly different, the superposition is plausible.

In this regard, the effect of one source behind the cylinder is first investigated, and then a pair of sources on the cylinder surface are studied. It will be shown that the latter can be matched to the experimental results much more closely. In this section the problem will be studied in free air and in the following section, part (4), the channel case will be attacked.

The flow about a circular cylinder due to a source of strength Q at z = c has the complex potential

$$F(z) = Q \ln (z - c) + Q \ln \left(z - \frac{b^2}{c}\right) - Q \ln z \qquad \text{------ (10)}$$

The potential is

$$\frac{\phi}{Q} = \ln \left[\frac{(\alpha^2 + \beta^2)^{\frac{1}{2}}}{x^2 + y^2}\right] = \ln \left[\frac{(\alpha^2 + \beta^2)^{\frac{1}{2}}}{r^2}\right] \qquad \text{------ (10a)}$$

and the stream function is

$$\frac{\psi}{Q} = \tan^{-1} \frac{\beta}{\alpha} \qquad \text{------ (10b)}$$

where

$$\alpha = x (x^2 + y^2 + b^2) - (x^2 + y^2)\left(\frac{c^2 + b^2}{c}\right)$$

$$= r \cos \theta (r^2 + b^2) - r^2\left(\frac{c^2 + b^2}{c}\right)$$

$$\beta = y (x^2 + y^2 - b^2) = r \sin \theta (r^2 - b^2)$$

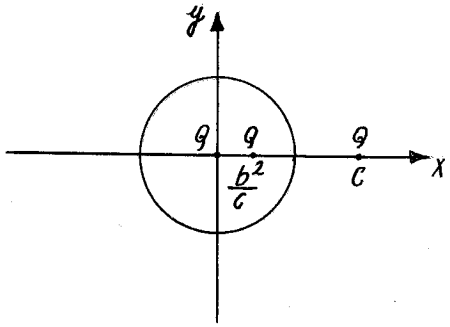

When $r = b$ or $y = 0$, $x < c$; $\frac{\psi}{Q} = \pi$

The velocities are

$$\left.\begin{aligned}
&\frac{u}{Q} = \frac{1}{\alpha^2 + \beta^2}\left[\alpha \frac{\partial \beta}{\partial y} - \beta \frac{\partial \alpha}{\partial y}\right], \quad \frac{v}{Q} = \frac{-1}{\alpha^2 + \beta^2}\left[\alpha \frac{\partial \beta}{\partial x} - \beta \frac{\partial \alpha}{\partial x}\right] \\
&\frac{u_r}{Q} = \frac{1}{r}\frac{\partial \psi}{\partial \theta} = \frac{1}{\alpha^2 + \beta^2}\left[r (r^4 - b^4) - r^2 (r^2 - b^2)\left(\frac{c^2 + b^2}{c}\right) \cos \theta\right] \\
&\frac{u_\theta}{Q} = -\frac{\partial \psi}{\partial r} = \frac{-1}{\alpha^2 + \beta^2}\left[\alpha \frac{\partial \beta}{\partial r} - \beta \frac{\partial \alpha}{\partial r}\right]
\end{aligned}\right\} \qquad \text{--- (11)}$$

These solutions can be immediately added to those of part (1) to give the result desired, as follows:

$$
\left.
\begin{aligned}
F(z) &= U\left[z + \frac{b^2}{z}\right] + Q \ln \left[\frac{(z - c)\left(z - \frac{b^2}{c}\right)}{z}\right] \\
\phi &= Ux\left[1 + \frac{b^2}{x^2 + y^2}\right] + Q \ln \frac{\sqrt{\alpha^2 + \beta^2}}{x^2 + y^2} \\
\psi &= Uy\left[1 - \frac{b^2}{x^2 + y^2}\right] + Q \tan^{-1} \frac{\beta}{\alpha} \\
\frac{u}{U} &= 1 - \frac{b^2(x^2 - y^2)}{(x^2 + y^2)^2} + \frac{Q}{U} \frac{1}{\alpha^2 + \beta^2}\left[\alpha \frac{\partial \beta}{\partial y} - \beta \frac{\partial \alpha}{\partial y}\right] \\
\frac{v}{U} &= \frac{-2b^2 xy}{(x^2+y^2)^2} - \frac{Q}{U} \frac{1}{\alpha^2 + \beta^2}\left[\alpha \frac{\partial \beta}{\partial x} - \beta \frac{\partial \alpha}{\partial x}\right]
\end{aligned}
\right\} \quad ----- (12)
$$

On the cylinder ($r = b$)

$$
\left.
\frac{u_r}{U} = 0; \quad \frac{u_\theta}{U} = -2 \sin \theta \left[1 - \frac{Q}{U} \frac{c}{c^2 + b^2 - 2bc \cos \theta}\right]
\right\}
$$

The body downstream of the cylinder formed by the source is defined by the streamline $\psi = \pi Q$, and as $x \to \infty$, the value of y for this streamline approaches $\frac{\pi Q}{U}$, so that the width of the so-called displacement thickness becomes $\frac{2\pi Q}{U}$ far downstream from the body. This fact gives a method of picking a value of Q/U to match experimental data, obtained by wake surveys, from which a pseudo displacement thickness can be computed.

When Q/U has been picked in an attempt to simulate a real flow by the above equations, the only remaining unknown is c. Therefore, one more condition in the real flow can be matched in the potential flow, and since c is the location of the source, the logical thing to do is to match some pressure on the cylinder surface. This pressure must be upstream of the separation point but should be close enough to it to be influenced profoundly by the wake presence. A convenient point to use is the maximum thickness point where $\theta = \pi/2$.

For this case from equation (12) we can write

$$\left(\frac{u_\theta}{U}\right)_{\theta=\pi/2} = -2\left[1 - \frac{Q}{bU}\,\frac{c/b}{1+\left(\frac{c}{b}\right)^2}\right] = -\sqrt{1 - C_p\,(\pi/2)}$$

which can be solved for c/b since $\frac{Q}{bU}$ and $C_p(\pi/2)$ are picked from experimental data.

This method and several variations of it were used in attempting to match the experimental data of this report (Figures 33-47) and a sample result is shown in Figure 68. It was soon apparent that to match the pressure distributions on the cylinder using one source is generally not feasible; the closest approach is to let c = b as was done in the example, but even here the matching cannot be complete.

This last statement can best be illustrated by a variation of the above method. Here, match the following experimental quantities

$C_p(\theta)$ at $\theta = \pi/2$ and $C_p(\theta)$ at $\theta = \theta_s$

where θ_s = angle at which separation occurs.

Then from equation (12), it can be shown that

$$(c/b) = A + \sqrt{A^2 - 1}$$

where

$$A = \frac{2\left[1 - \frac{1}{2\sin\theta_s}\sqrt{1 - C_p(\theta_s)}\right]\cos\theta_s}{\left[\sqrt{1 - C_p\left(\frac{\pi}{2}\right)} - \frac{1}{\sin\theta_s}\sqrt{1 - C_p(\theta_s)}\right]}$$

Now obviously A must be greater or equal to one, and a few computations will quickly show that for the data of this report at least, θ_s in the above expression for A must always be smaller than the observed θ_s if $A \geq 1$. When A = 1 the closest matching is obtained, but it is still not very good. Therefore, the best possible position for the single source is at c/b = 1.

Since one source fails to match the wake influence properly, the next step is to try two sources on the downstream surface of the cylinder, symmetrically spaced about the x axis. They will be located by the coordinates $(b, \pm \phi)$, and the velocity on the surface can be obtained immediately by the simple $\theta = \theta' - \phi$ (see diagram)

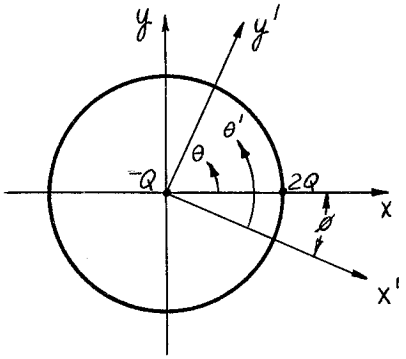

From equation (11)

$$\left(\frac{u_\theta}{Q}\right)_{\substack{c=b \\ r=b}} = \frac{\sin \theta}{b - b \cos \theta}$$

so that

$$\left(\frac{u_\theta'}{Q}\right)_{\substack{c=b \\ r=b}} = \frac{\sin (\theta' - \phi)}{b - b \cos (\theta' - \phi)}$$

Dropping the prime on the new coordinate system and using two sources and the rectilinear flow we get

$$\left(\frac{u_\theta}{U}\right)_{r=b} = -2 \sin \theta + \frac{Q}{bU} \left[\frac{\sin (\theta - \phi)}{1 - \cos (\theta - \phi)} + \frac{\sin (\theta + \phi)}{1 - \cos (\theta + \phi)} \right]$$

$$= -2 \sin \theta \left[1 - \frac{Q}{bU} \left(\frac{1}{\cos \phi - \cos \theta} \right) \right] \qquad \text{- - - - (13)}$$

In matching this new flow to a real case, two parameters are again available; $\frac{Q}{bU}$ and ϕ. Therefore, for example, the displacement thickness and C_p ($\pi/2$) can be matched as was done previously (these seem to be the most logical quantities to use for this purpose, and so will be employed exclusively hereafter). Since the displacement thickness is to be used to find the source strength, it might be well to write down in detail here the relations concerning the displacement thickness which will be employed.

For the potential flows, the displacement thicknesses are clearly defined by the following equations

$$\left(\frac{\delta}{2b}\right)_{\text{free air}} = \frac{1}{2b}\left[\frac{2\pi nQ}{U}\right]$$

$$\left[\frac{\delta}{2b}\right]_{\text{channel}} = \frac{1}{2b}\left[\frac{2\pi nQ}{U}\right]\left[\frac{1}{1+\frac{2\pi nQ}{Ua}}\right] = \frac{1}{2b}\left[\frac{2\pi nQ}{U}\right]\sqrt{\frac{q_o}{q_1}}$$

where n = number of sources used to simulate the wake
q_o = dynamic pressure far ahead of the body
q_1 = dynamic pressure far behind the body

The second equation can be derived easily from relations appearing later. n is of course 2 for the case under consideration. For the real flow in the wind tunnel it will now be assumed that

$$\left(\frac{\delta}{2b}\right)_{WT} = \frac{1}{2(b/a)}\left[1-\sqrt{\frac{q_o}{q_1}}\right]$$

where here
q_o = free stream dynamic pressure without cylinder
q_1 = dynamic pressure downstream of cylinder outside of wake

Further, it will be assumed that the ratios q_o/q_1 in the potential and real flows are equivalent for the matching to be done. Therefore, we can immediately write from the above relations

$$\frac{Q}{bU} = \frac{1}{2\pi n(b/a)}\left[\sqrt{\frac{q_1}{q_o}}-1\right]$$

$$\text{or} \quad \frac{2\pi Q}{Ua} = \frac{1}{n}\left[\sqrt{\frac{q_1}{q_o}}-1\right] \qquad \text{- - - - - (14)}$$

which will be used to pick the wake source strength in the potential flow from the measurements in the real flow. The value of q_1/q_o to be used in an actual case must of course be picked with care, but no basic difficulty should exist if the working section is reasonably long. If the wake has entirely dissipated, the ratio must be 1 with the velocity increment being replaced by a static pressure loss, and here the simile breaks

down. Probably the only thing to be done here is to replace q_1/q_o by $1 + \frac{p_o - p_1}{q_o}$ where p is the downstream value of static pressure.

To return to the main discussion, Q/bU may be picked from (14) and then ϕ may be chosen if $C_p(\pi/2)$ in free air is known. This can be computed from the expression

$$\cos \phi = \frac{Q/bU}{\left[1 - 1/2 \sqrt{1 - C_p(\pi/2)}\right]} \qquad \text{- - - - - (15)}$$

which can easily be derived from (13). The only restriction here is that $\cos \phi \leq 1$ so that as $C_p(\pi/2)$ approaches -3, the theoretical value for no wake, Q/bU must approach zero faster than the denominator in (15). For the experimental data available, this condition is easily met.

In Figures 69 and 70, two cases are presented in which experimental and potential pressure distributions are compared using the method just outlined. It is seen that the matching, up to the area of separation, is quite good, and that further consideration of the wake simulation by this method is probably justified. Therefore, the general velocity expressions will be worked out, and the corresponding case in the channel considered.

The complex potential for this source flow can be expressed as

$$\frac{F(z)}{2Q} = \ell n \left[\frac{r_1 r_2}{r} e^{i(\theta_1 + \theta_2 - \theta)}\right]$$

where r_1, r_2, θ_1, θ_2 are related as follows (see diagram)

$$r_1^2 = r^2 + b^2 - 2rb \cos(\theta - \phi) \quad ; \quad r/r_1 = \frac{\sin(\theta_1 - \phi)}{\sin(\theta - \phi)}$$

$$r_2^2 = r^2 + b^2 - 2rb \cos(\theta + \phi) \quad ; \quad r/r_2 = \frac{\sin(\theta_2 + \phi)}{\sin(\theta + \phi)}$$

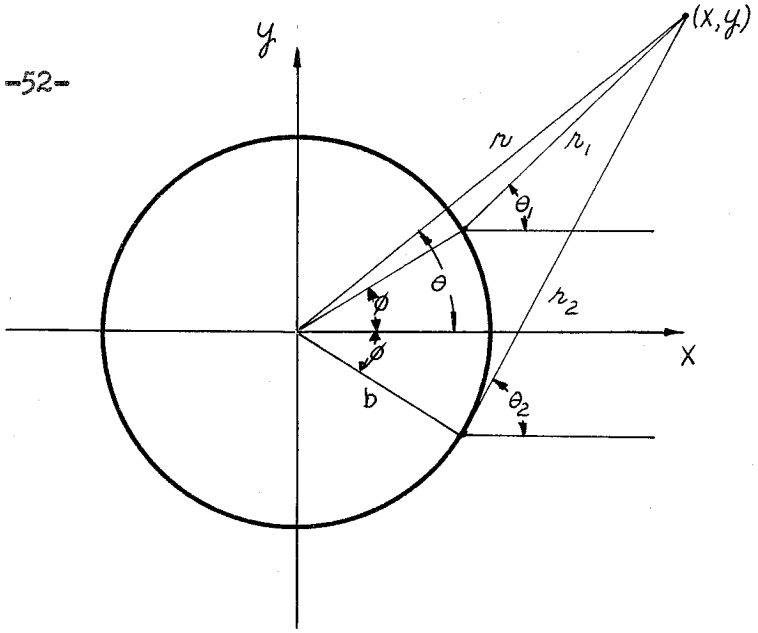

The potential is

$$\frac{\phi}{2Q} = \ell n \frac{r_1 r_2}{r}$$

The stream function is

$$\frac{\psi}{2Q} = \theta_1 + \theta_2 - \theta$$

The velocities can be obtained easily from the transformation of equation (11) letting $r = r'$, $c = b$, $\theta = \theta' - \phi$. First let $c = b$, whereupon u_r/Q and u_θ/Q become

$$\frac{u_r}{Q} = \frac{r^2 - b^2}{r(r^2 + b^2 - 2\,rb\cos\theta)} \quad ; \quad \frac{u_\theta}{Q} = \frac{2\,b\sin\theta}{(r^2 + b^2 - 2\,rb\cos\theta)}$$

then apply the transformation and drop the prime to get

$$\frac{u_r}{Q} = \frac{r^2 - b^2}{r\,r_1^2} \quad ; \quad \frac{u_\theta}{Q} = \frac{2\,b\sin(\theta - \phi)}{r_1^2}$$

Adding this flow to its image in the x-axis and adding the rectilinear flow solution (4), we get the general velocity expressions

$$\left.\begin{aligned} \frac{u_r}{U} &= \left[1 - \left(\frac{b}{r}\right)^2\right]\cos\theta + \frac{2Q}{bU}\left[\frac{\left(\frac{r}{b}\right)^2 - 1}{r/b}\right]\left[\frac{\left(\frac{r}{b}\right)^2 + 1 - 2\,\frac{r}{b}\cos\theta\cos\phi}{\frac{r_1^2\,r_2^2}{b^4}}\right] \\ \frac{u_\theta}{U} &= -\left[1 + \left(\frac{b}{r}\right)^2\right]\sin\theta + \frac{2Q}{bU}\left[2\sin\theta\right]\left[\frac{\left(\left(\frac{r}{b}\right)^2 + 1\right)\cos\phi - 2\,\frac{r}{b}\cos\theta}{\frac{r_1^2\,r_2^2}{b^4}}\right] \end{aligned}\right\} \quad (16)$$

which represent the velocities in free air of the flow proposed to simulate the real flow with wake. The next step is to investigate the similar flow in the channel, after which the two can be compared.

4). Cylinder with wake in a channel of height a.--To determine the flow in the channel, the procedure must be as follows. First, set up a system of sources like that proposed in section 3) with appropriate images. Then the complex potential will be

$$\frac{F(z)}{2Q} = \sum_{n=-\infty}^{\infty} \left\{ \ln \left[(z - b\cos\phi) - i\,(b\sin\phi + na) \right] + \ln \left[(z - b\cos\phi) + i\,(b\sin\phi - na) \right] - \ln \left[z - i\,na \right] \right\}$$

This will give a body in a channel of width a, due to the source flow. Next, another system similar to that of section 2) must be added to cancel out the flow at $x = -\infty$ due to the infinite row of sources, since the disturbance at $-\infty$ must vanish to satisfy the boundary condition. Finally, the solution in section 2) can be added to give the complete solution. The main problem is to adjust the solutions so that the shape of the final body will be as close to the circular cylinder of radius b as possible.

Now consider the complex potential given here. If we let

$$z_1 = z - b\cos\phi - i\,b\sin\phi$$

$$z_2 = z - b\cos\phi + i\,b\sin\phi$$

we can write F(z) as

$$\frac{F(z)}{2Q} = \ln \sinh \frac{\pi z_1}{a} + \ln \sinh \frac{\pi z_2}{a} - \ln \sinh \frac{\pi z}{a} \qquad \text{- - - - - (17)}$$

and writing the real and imaginary parts we get

$$\frac{\phi}{2Q} = \frac{1}{2} \ln \frac{1}{2} \left\{ \cosh \frac{2\pi}{a} (x - b\cos\phi) - \cos \frac{2\pi}{a} (y - b\sin\phi) \right\} + \frac{1}{2} \ln \frac{1}{2} \left\{ \cosh \frac{2\pi}{a} (x - b\cos\phi) - \cos \frac{2\pi}{a} (y + b\sin\phi) \right\} - \frac{1}{2} \ln \frac{1}{2} \left\{ \cosh \frac{2\pi x}{a} - \cos \frac{2\pi y}{a} \right\} \qquad \text{(17a)}$$

and

$$\frac{\psi}{2Q} = \tan^{-1}\left[\frac{\tan\frac{\pi}{a}(y - b\sin\phi)}{\tanh\frac{\pi}{a}(x - b\cos\phi)}\right] + \tan^{-1}\left[\frac{\tan\frac{\pi}{a}(y+b\sin\phi)}{\tanh\frac{\pi}{a}(x - b\cos\phi)}\right] - \tan^{-1}\left[\frac{\tan\frac{\pi y}{a}}{\tanh\frac{\pi x}{a}}\right] \qquad -(17b)$$

The velocities in the x and y directions can be written as

$$\left.\begin{aligned}
\frac{a}{2\pi}\frac{u}{Q} &= \frac{\sinh\frac{2\pi}{a}(x - b\cos\phi)}{\left[\cosh\frac{2\pi}{a}(x-b\cos\phi) - \cos\frac{2\pi}{a}(y-b\sin\phi)\right]} \\
&+ \frac{\sinh\frac{2\pi}{a}(x - b\cos\phi)}{\left[\cosh\frac{2\pi}{a}(x-b\cos\phi) - \cos\frac{2\pi}{a}(y+b\sin\phi)\right]} \\
&- \frac{\sinh\frac{2\pi x}{a}}{\left[\cosh\frac{2\pi x}{a} - \cos\frac{2\pi y}{a}\right]} \\
\frac{a}{2\pi}\frac{v}{Q} &= \frac{\sin\frac{2\pi}{a}(y - b\sin\phi)}{\left[\cosh\frac{2\pi}{a}(x-b\cos\phi) - \cos\frac{2\pi}{a}(y-b\sin\phi)\right]} \\
&+ \frac{\sin\frac{2\pi}{a}(y + b\sin\phi)}{\left[\cosh\frac{2\pi}{a}(x-b\cos\phi) - \cos\frac{2\pi}{a}(y+b\sin\phi)\right]} \\
&- \frac{\sin\frac{2\pi y}{a}}{\left[\cosh\frac{2\pi x}{a} - \cos\frac{2\pi y}{a}\right]}
\end{aligned}\right\} \qquad - - - (18)$$

When $y = \pm\frac{a}{2}$, $\frac{\psi}{2Q} = \mp\frac{\pi}{2}$; and at $y = 0$ and on the cylinder to the source singularities $\frac{\psi}{2Q} = \pi$. To get an equation which represents the shape of the cylinder, we must let $\frac{\psi}{2Q} = \pi$ and combine terms in (17b). When this is done, the following relation is obtained.

$$\tan^2\left(\frac{\pi y}{a}\right) = \frac{\tanh^2 \frac{\pi}{a}(x - b\cos\phi) + \tan^2 \frac{\pi b}{a}\sin\phi)}{1 + \tan^2(\frac{\pi b}{a}\sin\phi)\tanh^2 \frac{\pi}{a}(x - b\cos\phi)}$$

$$- \frac{2\tanh \frac{\pi x}{a}\tanh \frac{\pi}{a}(x - b\cos\phi)\left[1 + \tan^2(\frac{\pi b}{a}\sin\phi)\right]}{1 + \tan^2(\frac{\pi b}{a}\sin\phi)\tanh^2 \frac{\pi}{a}(x - b\cos\phi)} \quad \text{- - - (19)}$$

This gives the relation between x and y on the body in terms of b, ϕ and a. In the strict sense of the derivation it only applies for $x < b\cos\phi$ but it can easily be shown that it actually applies to the whole body. The intersections of the cylinder with the coordinate axes can be obtained from the relations

$$\left[\tan^2\left(\frac{\pi y}{a}\right)\right]_{x=0} = \frac{\eta^2 + \xi^2}{1 + \eta^2\xi^2}$$

and

$$\left[\tanh^3\left(\frac{\pi x}{a}\right)\right]_{y=0} + \left[\frac{1 + \xi^2\eta^2}{2\xi(1+\eta^2)} - \frac{1 + \xi^2}{\xi}\right]\left[\tanh^2\left(\frac{\pi x}{a}\right)\right]_{y=0} + \frac{\xi^2 + \eta^2}{2\xi(1 + \eta^2)} = 0 \quad \text{- - - (19a)}$$

where $\xi^2 = \tanh^2(\pi b/a\cos\phi)$ and $\eta^2 = \tan^2(\pi b/a\sin\phi)$

Two things should be noted here. First, we now have a body symmetrical about the x-axis but not about the y-axis, and second, the size of the body relative to a cannot be adjusted by varying the source strength, since Q does not appear in (19). Since Q is assumed invariant from the free air to the channel case anyway, it does not matter. The cylinder size can be adjusted in the next step, as will soon become apparent. Equation (19a) is plotted on Figure 72 to indicate the body shape.

Once the flow due to the source system is known, the rest of the flow can be constructed. From equation (18) it is seen that, at very large negative values of x, the velocity u approaches $-\frac{2\pi Q}{a}$ while v approaches zero. So the first thing to do is to cancel out this velocity, since the disturbance at $x = -\infty$ must be zero for the final flow. This is done by superimposing a system similar to that of section 2) upon the source system. The velocity of this system at $x = -\infty$ will be $\frac{2\pi Q}{a}$ and the doublet strength in it, μ', will be undetermined. Therefore its complex potential will be

$$F(z) = \frac{2\pi Q}{a} z + \mu' \coth \frac{\pi z}{a} \qquad \text{- - - - - (20)}$$

The shape of the body produced by this potential in the channel will be close to a circular cylinder, but will be unlike the shape from the source system. Therefore, the addition of the two systems will produce a third body of still a different shape which will also be slightly distorted from the circle. On this last cylinder, we would like to have $y = b$ when $x = 0$, and this can be done by picking μ' as follows.

The complex potential for the combined flow is (17) + (20) or

$$\frac{F(z)}{2Q} = \frac{\pi z}{a} + \frac{\mu'}{2Q} \coth \frac{\pi z}{a} + \ln \sinh \frac{\pi z_1}{a} + \ln \sinh \frac{\pi z_2}{a} - \ln \sinh \frac{\pi z}{a} \qquad \text{-(21)}$$

The stream function is

$$\frac{\psi}{2Q} = \frac{\pi y}{a} - \left(\frac{\mu'}{2Q}\right) \frac{\sin \frac{2\pi y}{a}}{\cosh \frac{2\pi x}{a} - \cos \frac{2\pi y}{a}} + \tan^{-1} \left[\frac{\tan \frac{\pi}{a} (y - b \sin \phi)}{\tanh \frac{\pi}{a} (x - b \cos \phi)}\right] \qquad \text{- (21a)}$$

$$+ \tan^{-1} \left[\frac{\tan \frac{\pi}{a} (y + b \sin \phi)}{\tanh \frac{\pi}{a} (x - b \cos \phi)}\right] - \tan^{-1} \left[\frac{\tan \frac{\pi y}{a}}{\tanh \frac{\pi x}{a}}\right]$$

and on the body when $x < b \cos \phi$, $\Psi/2Q = \pi$

Now letting $x = 0$, $y = b$, $\Psi/2Q = \pi$, we can rewrite (21a) as

$$\frac{\mu'}{2Q}\left[\frac{1}{\tan\frac{\pi b}{a}}\right] = -\pi + \tan^{-1}\left[\nu\right] - \tan^{-1}\left[\infty\right] + \tan^{-1}\left[\frac{2\nu(-\xi)(1+\eta^2)}{\xi^2(1-\nu^2\eta^2)\nu^2+\eta^2}\right]$$

where $-\xi = \tanh\left(-\frac{\pi b}{a}\cos\phi\right)$, $\eta^2 = \tan^2\left(\frac{\pi b}{a}\sin\phi\right)$, $\nu = \tan\left(\frac{\pi b}{a}\right)$

Thus, the value of doublet strength which is desired can be written as

$$\frac{\mu'}{2Q} = \tan\frac{\pi b}{a}\left[\frac{\pi b}{a} - \tan^{-1}\left|\frac{\xi^2\left[1-\nu^2\eta^2\right]-\nu^2+\eta^2}{-2\nu\xi\left[1+\eta^2\right]}\right|\right] \qquad \text{- - - - - (22)}$$

Some representative values of $\mu'/2Q$ have been computed and are plotted on Figure 71. Note that for $\phi \neq 90^\circ$, $\mu'/2Q$ has a finite limit as $b/a \to 1/2$. This limit can be expressed simply as

$$\left[\frac{\mu'}{2Q}\right]_{\frac{b}{a}=\frac{1}{2}} = \frac{2\xi\left[1+\eta^2\right]}{\xi^2\eta^2+1} - 1 \qquad \text{- - - - - (22a)}$$

This means that we can construct a flow with a finite doublet strength in which the cylinder actually touches the walls. This naturally cannot be done when the velocity U has been added to the system.

To get the x coordinate of this body for $y = 0$ and $x < 0$ we let $y \to 0$ in the expression for the stream function. Then for very small y the expression becomes

$$\Pi = y\left(\frac{\pi}{a}\right) - y\left[\frac{\frac{2\pi}{a}\,\frac{\mu'}{2Q}}{\cosh\frac{2\pi x}{a}-1}\right] + y\left[\frac{\frac{2\pi}{a}\tanh\frac{\pi}{a}(x-b\cos\phi)\left[1+\tan^2\left(\frac{\pi b}{a}\sin\phi\right)\right]}{\tanh^2\frac{\pi}{a}(x-b\cos\phi)+\tan^2\left(\frac{\pi b}{a}\sin\phi\right)}\right]$$

$$- y\left[\frac{\pi/a}{\tanh\frac{\pi x}{a}}\right]$$

which can also be written as

$$y\left[\frac{\frac{2\pi}{a}\frac{\mu'}{2Q}}{\cosh\frac{2\pi x}{a}-1}\right] = y\left(\frac{\pi}{a}\right) + y\left|\frac{\pi/a}{\tanh\frac{\pi x}{a}}\right|$$

$$- y\left|\frac{\frac{2\pi}{a}\tanh\frac{\pi}{a}(x-b\cos\phi)\left[1+\tan^2(\frac{\pi b}{a}\sin\phi)\right]}{\tanh^2\frac{\pi}{a}(x-b\cos\phi)+\tan^2(\frac{\pi b}{a}\sin\phi)}\right|$$

$$-\pi-\pi+2\pi$$

Finally canceling out the y's we obtain

$$1 = \frac{\left(\frac{\mu'}{2Q}\right)}{\sinh^2\left(\frac{\pi x}{a}\right)} - \left|\frac{1}{\tanh\frac{\pi x}{a}}\right| + \left|\frac{2\tanh\frac{\pi}{a}(x-b\cos\phi)\left[1+\tan^2(\frac{\pi b}{a}\sin\phi)\right]}{\tanh^2\frac{\pi}{a}(x-b\cos\phi)+\tan^2(\frac{\pi b}{a}\sin\phi)}\right| \qquad \text{- - - - - (23)}$$

which gives x/a in terms of b/a, ϕ and $\frac{\mu'}{2Q}$. The resulting value of x is the coordinate of the leading edge of the body.

We now have produced the desired source flow in a channel about a slightly distorted circular cylinder, and must now add the free stream velocity U. This is equivalent to adding in the solution from section 2) and now the complete complex potential becomes

$$F(z) = \left[U + \frac{2\pi Q}{a}\right] z + \left[\mu_1 + \mu'\right]\coth\frac{\pi z}{a} + 2Q\left[\ln\sinh\frac{\pi z_1}{a} + \ln\sinh\frac{\pi z_2}{a} - \ln\sinh\frac{\pi z}{a}\right] \qquad (24)$$

and the stream function becomes

$$\frac{\psi}{Ua} = \left[1+\frac{2\pi Q}{Ua}\right]\frac{y}{a} - \left[\frac{\mu_1}{Ua} + \left(\frac{\mu'}{2\pi Q}\right)\left(\frac{2\pi Q}{Ua}\right)\right]\frac{\sin\frac{2\pi y}{a}}{\cosh\frac{2\pi x}{a}-\cos\frac{2\pi y}{a}}$$

$$+ \frac{1}{\pi}\left(\frac{2\pi Q}{Ua}\right)\left\{\tan^{-1}\left[\frac{\tan\frac{\pi}{a}(y-b\sin\phi)}{\tanh\frac{\pi}{a}(x-b\cos\phi)}\right] + \tan^{-1}\left[\frac{\tan\frac{\pi}{a}(y+b\sin\phi)}{\tanh\frac{\pi}{a}(x-b\cos\phi)}\right]\right.$$

$$\left. - \tan^{-1}\left[\frac{\tan\frac{\pi y}{a}}{\tanh\frac{\pi x}{a}}\right]\right\} \qquad \text{- - (24a)}$$

and on the body when $x < b \cos \phi$, $\frac{\psi}{Ua} = \frac{2\pi Q}{Ua}$.

The ordinates of this final body can be immediately defined. $(y)_{x=0} = b$ by definition since the doublet strengths have been picked with this as a criterion. Noting that (24a) is of exactly the same form as (21a) we can write an equation like (23) by inspection which defines $(x)_{y=0}$ on the body when $x < 0$. This is

$$\left[1 + \frac{2\pi Q}{Ua}\right] = \left[\frac{\mu_1}{Ua} + \left(\frac{\mu'}{2\pi Q}\right)\left(\frac{2\pi Q}{Ua}\right)\right] \frac{\pi}{\sinh^2\left(\frac{\pi x}{a}\right)} - \frac{2\pi Q}{Ua}\left|\frac{1}{\tanh \frac{\pi x}{a}}\right| + \frac{2\pi Q}{Ua}\left|\frac{2 \tanh \frac{\pi}{a}(x - b\cos\phi)\left[1 + \tan^2\left(\frac{\pi b}{a}\sin\phi\right)\right]}{\tanh^2 \frac{\pi}{a}(x - b\cos\phi) + \tan^2\left(\frac{\pi b}{a}\sin\phi\right)}\right| \quad --(25)$$

which gives x/a in terms of b/a, ϕ, and Q. No attempt is made to write the explicit relation x/a (b/a, ϕ, Q) but a typical solution is presented in Figure 73 compared with the solution of equation (8). This indicates that while the body is slightly more distorted than for the case with no wake simulation, the increase is not significant.

The velocities for this final configuration may be most conveniently written as

$$\frac{u}{U} = \left[1 + \frac{2\pi Q}{Ua}\right] + 2\pi\left[\frac{\mu_1}{Ua} + \left(\frac{\mu'}{2\pi Q}\right)\left(\frac{2\pi Q}{Ua}\right)\right] \frac{\cosh \frac{2\pi x}{a} \cos \frac{2\pi y}{a} - 1}{\left[\cosh \frac{2\pi x}{a} - \cos \frac{2\pi y}{a}\right]^2} + \frac{u}{U} \text{ (Eq. 18)}$$

$$\frac{v}{U} = -2\pi\left[\frac{\mu_1}{Ua} + \left(\frac{\mu'}{2\pi Q}\right)\left(\frac{2\pi Q}{Ua}\right)\right] \frac{\sinh \frac{2\pi x}{a} \sin \frac{2\pi y}{a}}{\left[\cosh \frac{2\pi x}{a} - \cos \frac{2\pi y}{a}\right]^2} + \frac{v}{U} \text{ (Eq. 18)}$$

---- (26)

To check experimental data, O and Q must be picked as in the free air case. Q may be computed from the equation

$$\frac{2\pi Q}{Ua} = \frac{1}{2}\left[\sqrt{\frac{q_1}{q_o}} - 1\right]$$

and ϕ must be found by solving $\left[\frac{u}{U}\right]_{\substack{x=0 \\ y=b}}$ using an experimental value of $C_p(\pi/2)$. The doublet strengths for any case may be taken from Figures 64 and 67 or computed from the equations. Once a solution is computed in the channel, it should be compared with the free air case using the same values of Q and ϕ.

Time was not available to include any extensive computations of this sort in this thesis, but they are quite important in testing the validity of the method, and should be carried out to some extent at least. Two short calculations were made and their results are indicated in Figures 74, 75 and 76.

Figure 74 illustrates a typical blockage calculation at x = 0 with wake. Note that the parameter $(a/b)\Delta u/U$ is used rather than $(a/b)^2\Delta u/U$ which was used for case 2. This is done because the latter parameter has a singularity at b/a = 0 due to the wake terms. Notice that here there is a double limit as y/a and b/a approach zero, which can be compared with the double limit in Figure 66. At b/a = 0, $\left(\frac{a}{b}\Delta\frac{u}{U}\right)_{x=0} = \frac{2\pi Q}{Ub}$, and this in conjunction with equation (14) gives the result that

$$\left[\frac{\Delta u}{U}\right]_{\substack{x=0 \\ b/a=0}} = \frac{1}{2}\left[\frac{u_1 - U}{U}\right]$$

where u_1 is the velocity outside the wake downstream of the cylinder. However, if $\frac{b}{a}$ and $\frac{y}{a}$ approach zero at the same rate $\left(\frac{a}{b}\Delta\frac{u}{U}\right)_{x=0} \longrightarrow \frac{4\pi Q}{Ub}$ or twice the above value. More calculations of this nature should be made to illustrate the general effects of wake size on the rest of the flow.

Figures 75 and 76 illustrate two comparisons between the measured pressure distribution at the channel wall and the theoretical value computed from equation (26). The correlation is reasonably good although not perfect by any means. It was found in computing such examples from the data that the quantity q_1/q_o is often not well defined numerically, and this fact contributes to the differences on the Figures to a large degree. It would be well to make similar computations on the remainder of the data available to further check the correlation.

A Check on the Importance of Cylinder Distortion

Since the circular cylinder is distorted slightly in the channel by the analysis given here, the effect of distortion on velocity should be checked. This may be done by considering the flow over an elliptic cylinder.

Using elliptic coordinates, the potential flow about an elliptic cylinder in a rectilinear flow can easily be derived. On the surface of the cylinder, the velocity can be expressed as

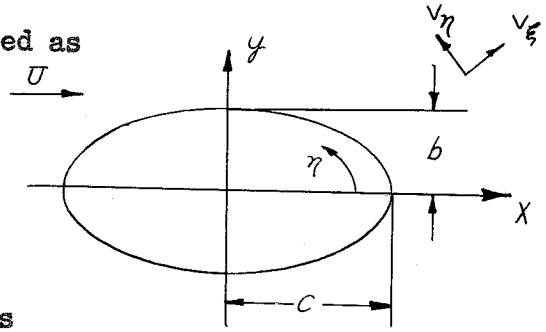

$$\frac{v_\eta}{U} = \frac{-(b+c)\sin\eta}{\sqrt{b^2\cos^2\eta + c^2\sin^2\eta}}$$

where c = the semi major axis

b = the semi minor axis

η = coordinate perpendicular to the cylinder surface

$x = c\cos$, $y = b\sin$

For our purpose it is sufficient to check the velocity at $x = 0$, $y = b$, $\eta = \pi/2$. Here, the velocity becomes

$$\left[-\frac{v_\eta}{U}\right]_{\eta=\frac{\pi}{2}} = \frac{b+c}{c}$$

and to check the distortion effect, let $c = b(1+\tau)$ where $\tau \ll 1$.

Under this condition the velocity becomes, with higher terms neglected

$$\left[-\frac{v_\eta}{U}\right]_{\eta=\frac{\pi}{2}} = (2 - \tau + \tau^2)$$

and the pressure coefficient is

$$C_p\left(\frac{\pi}{2}\right) = -3 + 4\tau - 5\tau^2$$

Thus a 1% distortion in shape will create about 0.5% velocity distortion on the surface and a 1.5% C_p distortion. For our case a 1% shape distortion occurs when $b/a \stackrel{\circ}{=} 0.2$, and for such a size the change in velocity due to the blockage is about 30%. Therefore, it is clear that the amount of distortion introduced is quite negligible.

BIBLIOGRAPHY

1. Description of the GALCIT 10' Wind Tunnel, The Model Suspension System, General Facilities and Model Specifications, Revised September 10, 1942 (Unpublished)

2. GALCIT Two-Dimensional Tunnel Installation and Test Procedures (Unpublished)

3. Prandtl, L. and Tietjens, O.G., "Applied Hydro- and Aeromechanics", McGraw-Hill, 1934

4. Thom, A., "Blockage Corrections in a Closed High-Speed Tunnel", R.& M.No. 2033, Nov. 1943

5. Streeter, V.L., "Fluid Dynamics", McGraw-Hill, 1948

6. Goldstein, S., "Modern Developments in Fluid Mechanics", Oxford, 1938

7. Thom, A., "An Investigation of Fluid Flow in Two Dimensions", R. & M. No. 1194, Nov. 1928

8. Lock, C.N.H., "The Interference of a Wind Tunnel on a Symmetrical Body", R. & M. No. 1275, Oct. 1929

9. Allen, H.J. and Vincenti, W.G., "Wall Interference in a Two-Dimensional Flow Wind Tunnel with Consideration of the Effect of Compressibility", A.R.R. No. 4K03, Dec. 1944

Cylinder	θ° Separation Wire	C_{D_1}	C_{D_W}	at x/d
$C_1 + T_1$	65	.759		
$C_1 + T_2$	65	.764	.635 .607	3.108 5.837
$C_1 + T_3$	85	.603	.433 .419	3.108 5.837
$C_1 + T_4$	65 and 85	.907	.904 .848	3.108 5.837
$C_2 + T_{11}$	65	.714	.911 .642	1.626 3.053
$C_2 + T_{12}$	65 and 85	1.243	1.690 1.377	1.626 3.053
$C_3 + T_5$	65	.747		
$C_3 + T_6$	55	.805		
$C_3 + T_7$	85	.632		

C_{D_1} = pressure drag coefficient (equation (1))

C_{D_W} = wake drag coefficient (equation (1a))

Figure 63

TABLE OF PRESSURE AND WAKE DRAG COEFFICIENTS FOR TWO-DIMENSIONAL WAKE CONFIGURATIONS

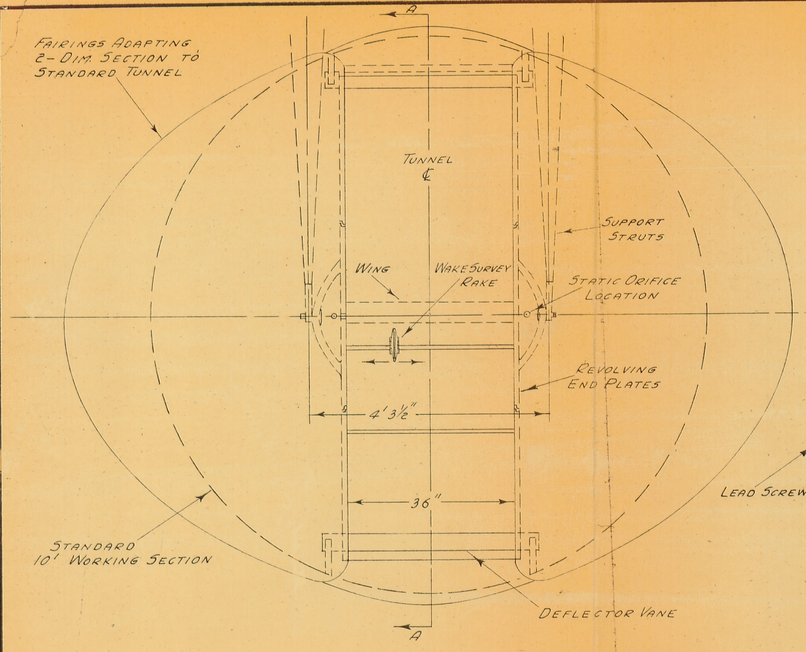

DOWNSTREAM VIEW

SKETCH SHOWING TWO-DIMENSIONAL WORKING SECTION

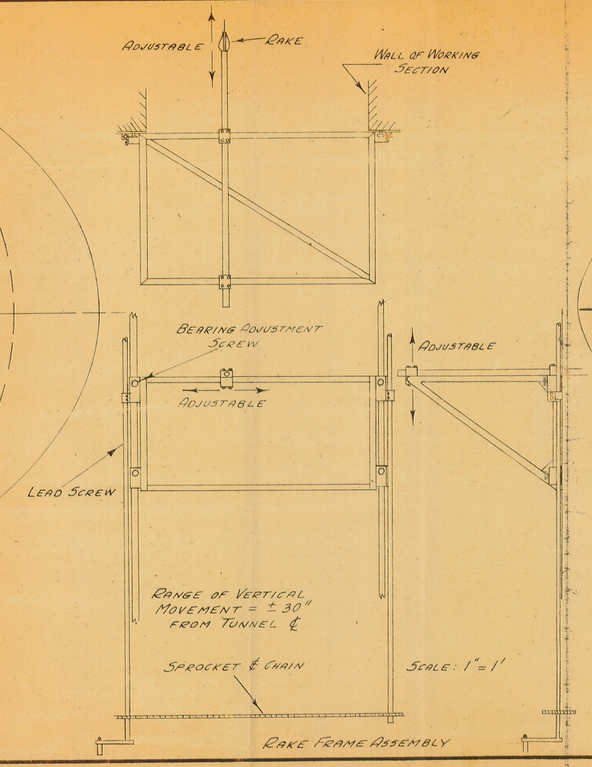

SCALE: 1" = 1'

RAKE FRAME ASSEMBLY

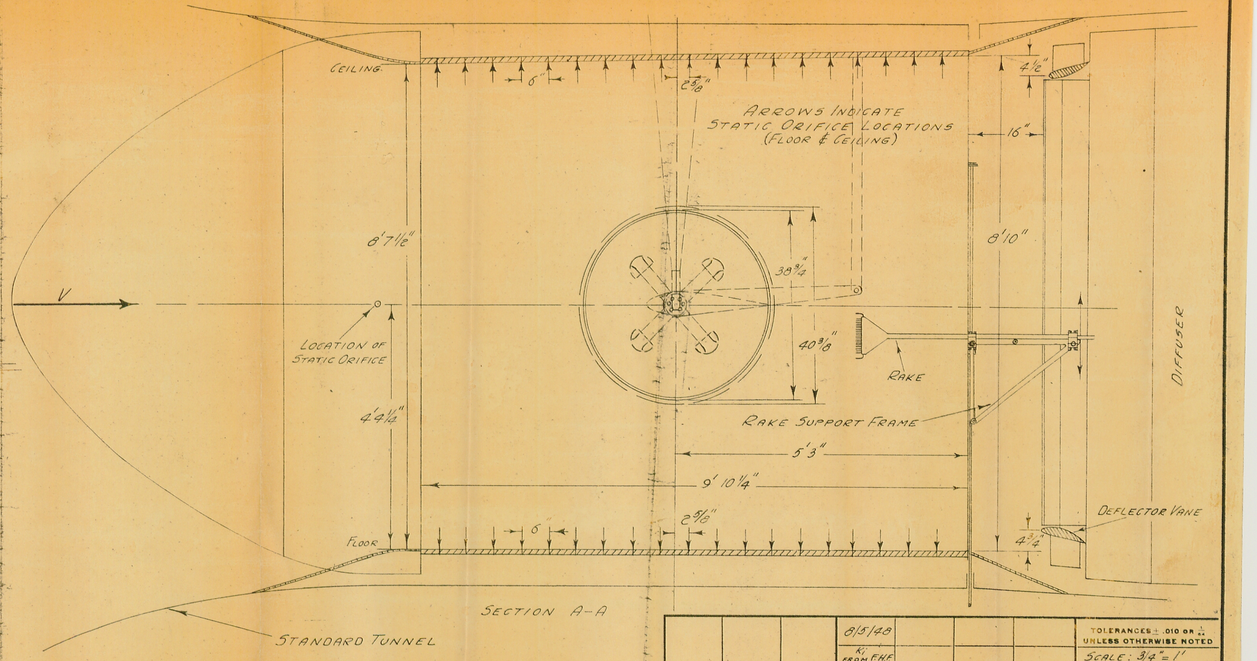

SECTION A-A

STANDARD TUNNEL

REF. GALCIT DWG. 5-253-4 -6

MATERIAL	FINISH	HEAT TREAT	DRAFTSMAN	CHECKED	APPROVED	ENGINEER
			8/5/40 K. FROM THE BIGGIE			

TOLERANCES ± .010 OR ± UNLESS OTHERWISE NOTED

SCALE: 3/4" = 1" AND NOTED

GUGGENHEIM AERONAUTICAL LABORATORY
CALIFORNIA INSTITUTE OF TECHNOLOGY

NAME: GALCIT TWO-DIMENSIONAL TUNNEL

DRAWING NO.

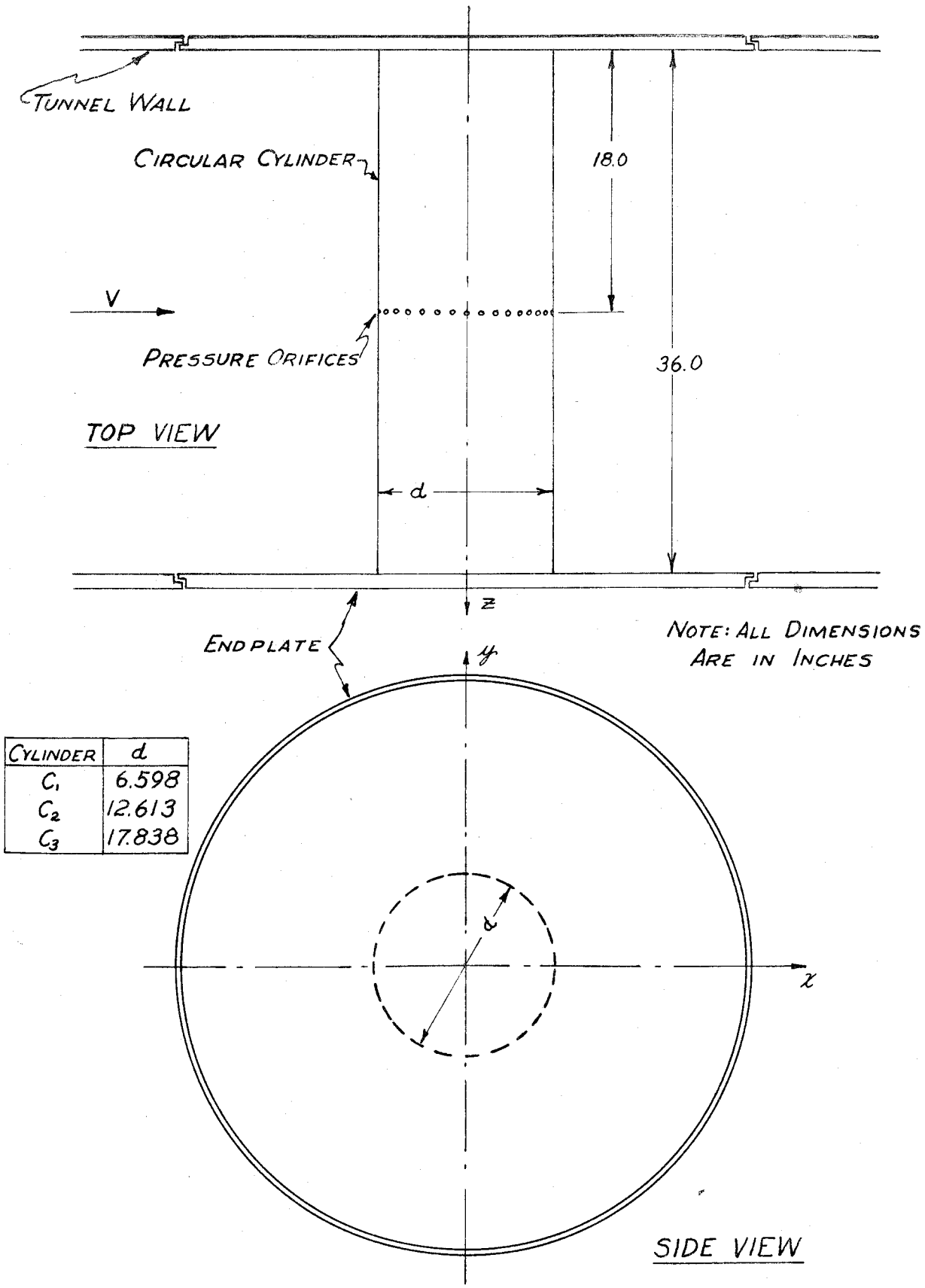

CYLINDER	d
C_1	6.598
C_2	12.613
C_3	17.838

Fig. 2 Sketch of Circular Cylinders

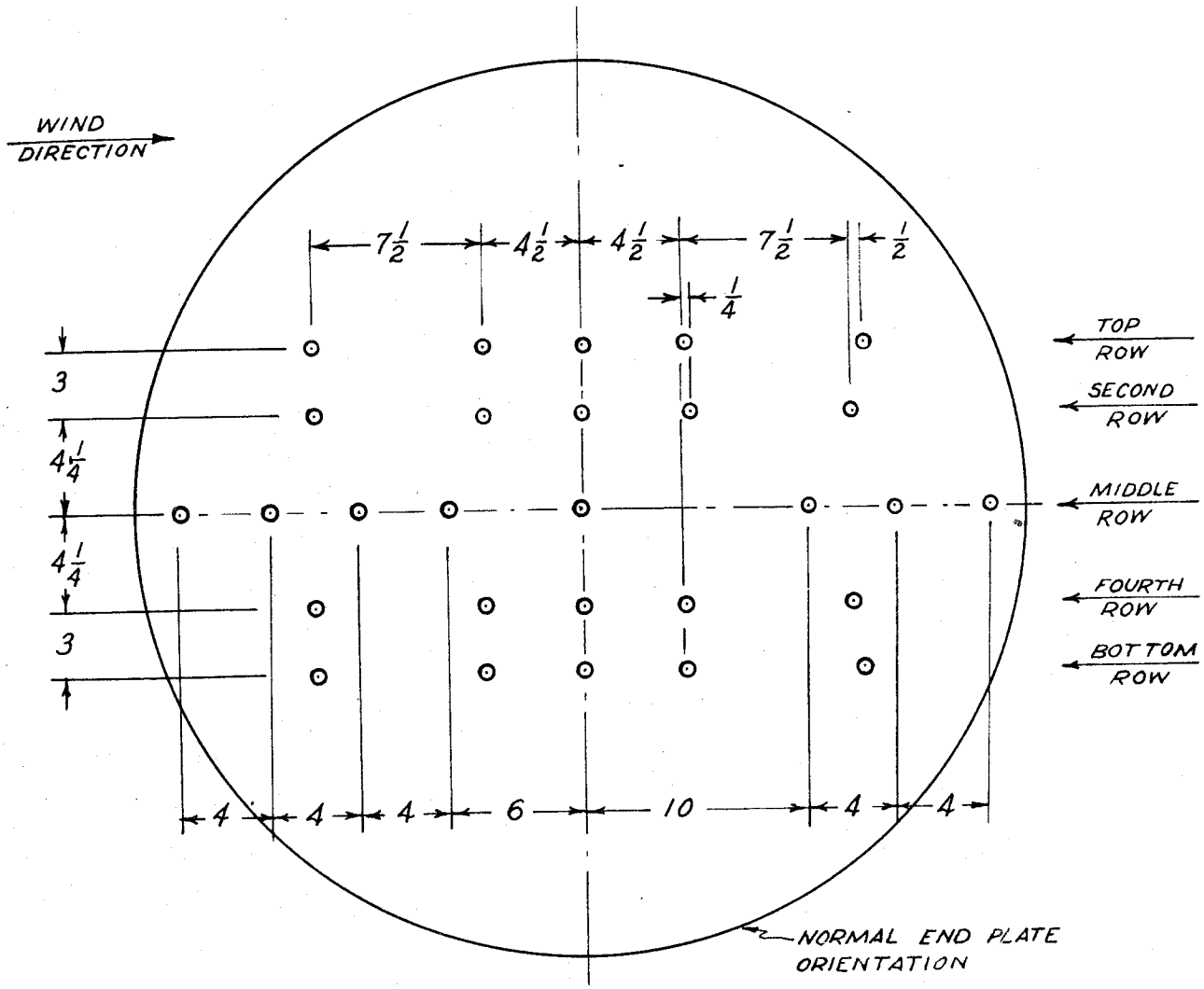

DIMENSIONS IN INCHES

⊙ ~ ORIFICE

Fig. 3 Sketch Showing Endplate Orifice Locations

PAGE
FIG

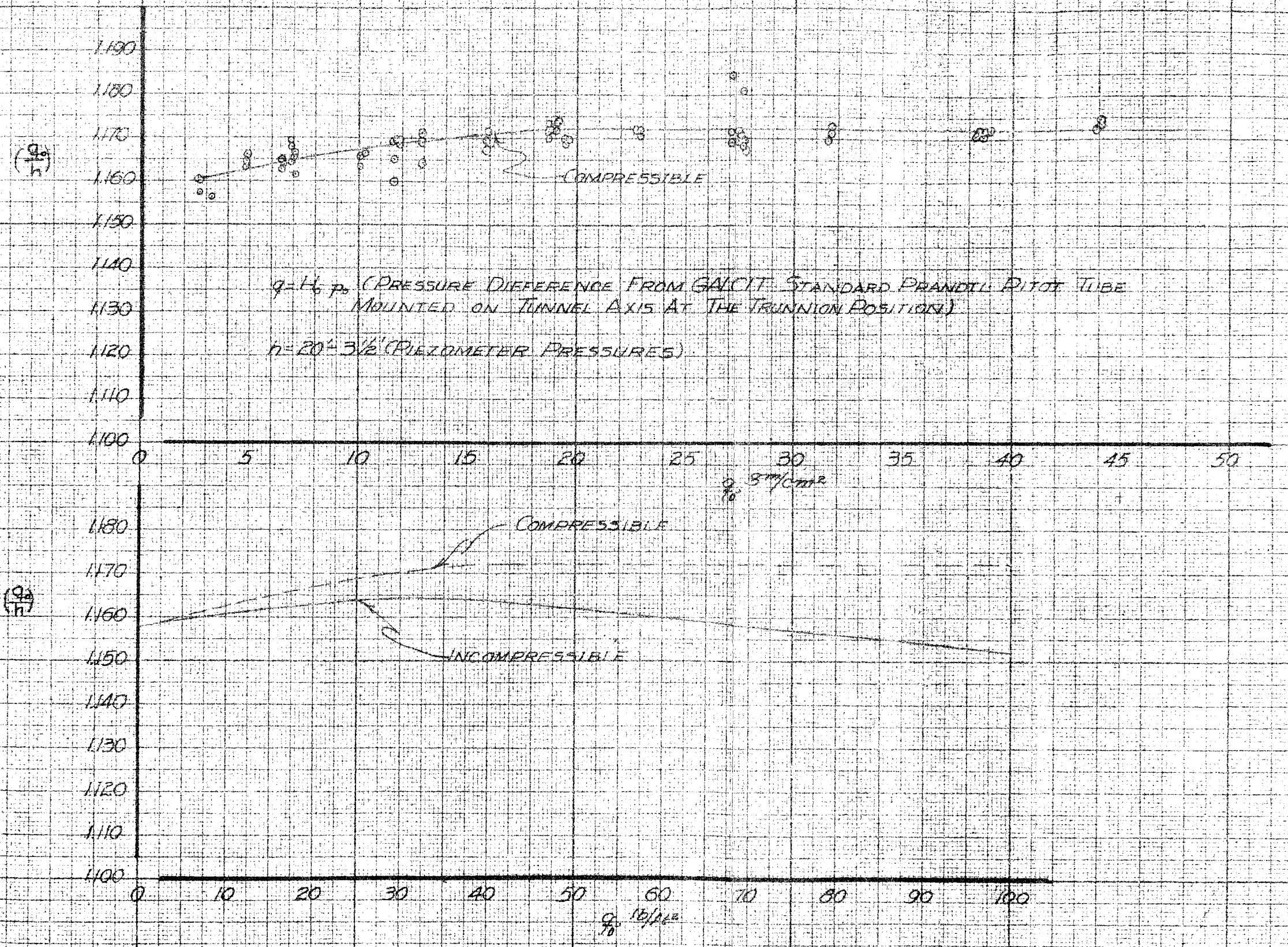

FIG 4

6-BLADED FAN, LONG DIFFUSER, TUNNEL WIDTH = 36.0", HEIGHT = 8.5'

TWO-DIMENSIONAL TUNNEL VELOCITY CALIBRATION
CALIBRATED 2-26-48

H_0 & P_0 = PITOT TUBE PRESSURES, PITOT ON TUNNEL AXIS AT TRUNNIONS

$\frac{Q}{P_{INC}} = \frac{H_0 - P_0}{1+\delta}$ WHERE $1+\delta$ IS COMPRESSIBILITY CORRECTION

P_{ℓ} = STATIC PRESSURE ALONG TUNNEL AXIS

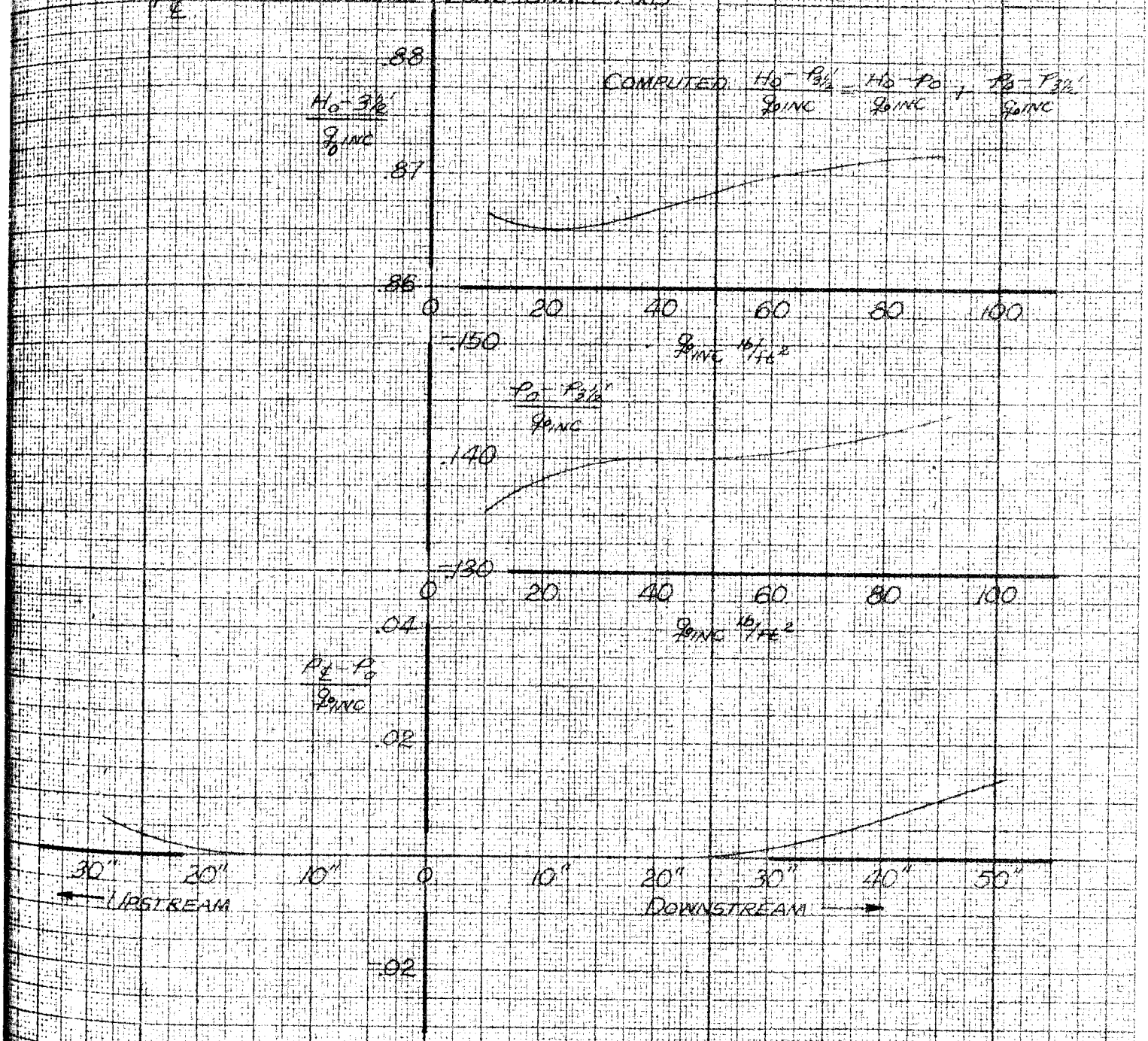

FIG. 5

TWO DIMENSIONAL TUNNEL REFERENCE PRESSURES
CALIBRATED 1948

GALCIT REP 534

○ CLEAR TUNNEL, q_o = 40 LB/FT.² RUN 6

STATIC PRESSURE TRAVERSE USING GALCIT STANDARD PRANDTL PITOT TUBE MOUNTED ON TRAVERSE FRAME

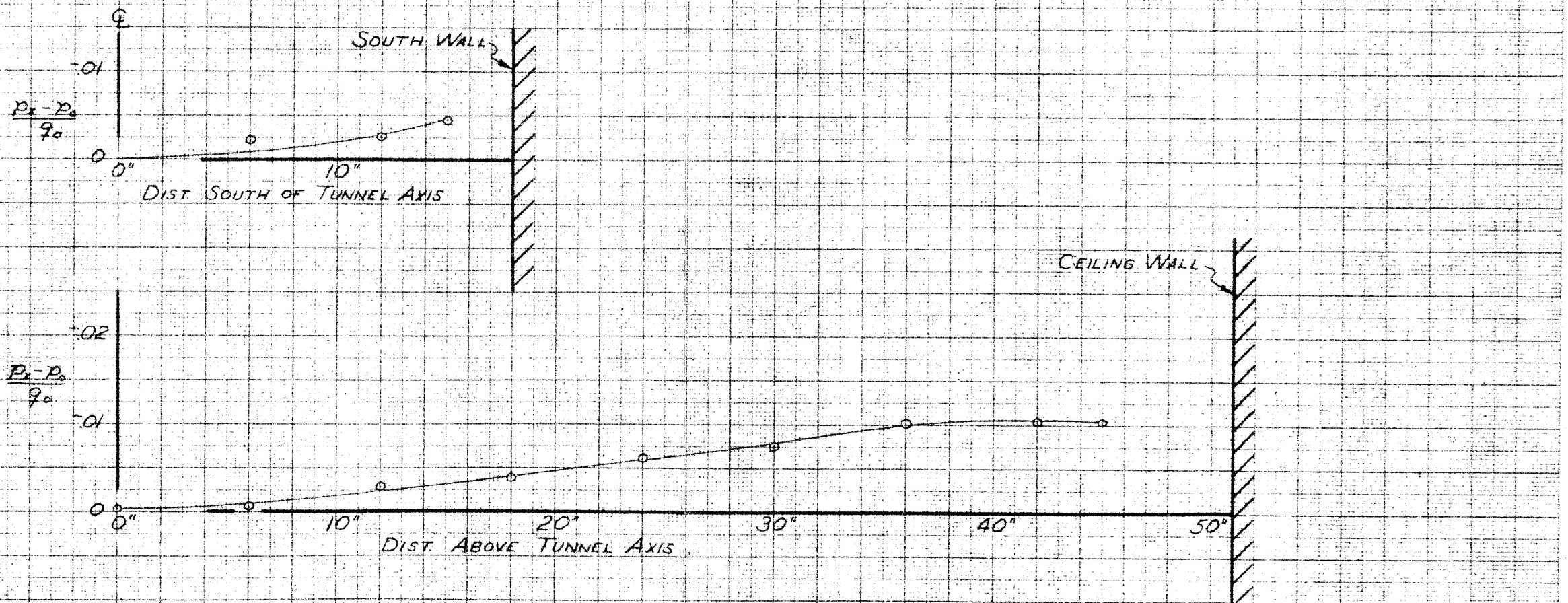

Fig -6 Static Pressure Survey Across Tunnel

GALCIT REP. 534

PAGE
FIG

AVERAGE OF FLOOR & CEILING AXIAL STATIC PRESSURES (CLEAR TUNNEL)

- ○ q_o=10 LB/FT², RUNS 1,27
- △ q_o=20 LB/FT², " 2,27
- □ q_o=80 LB/FT², " 4,27

p_{w_o} = STATIC PRESSURE AT FLOOR & CEILING, CLEAR TUNNEL
p_o = " " " INTERSECTION OF TRUNNION AND TUNNEL AXES, CLEAR TUNNEL
q_o = DYNAMIC PRESSURE AT INTERSECTION OF TRUNNION AND TUNNEL AXES, CLEAR TUNNEL

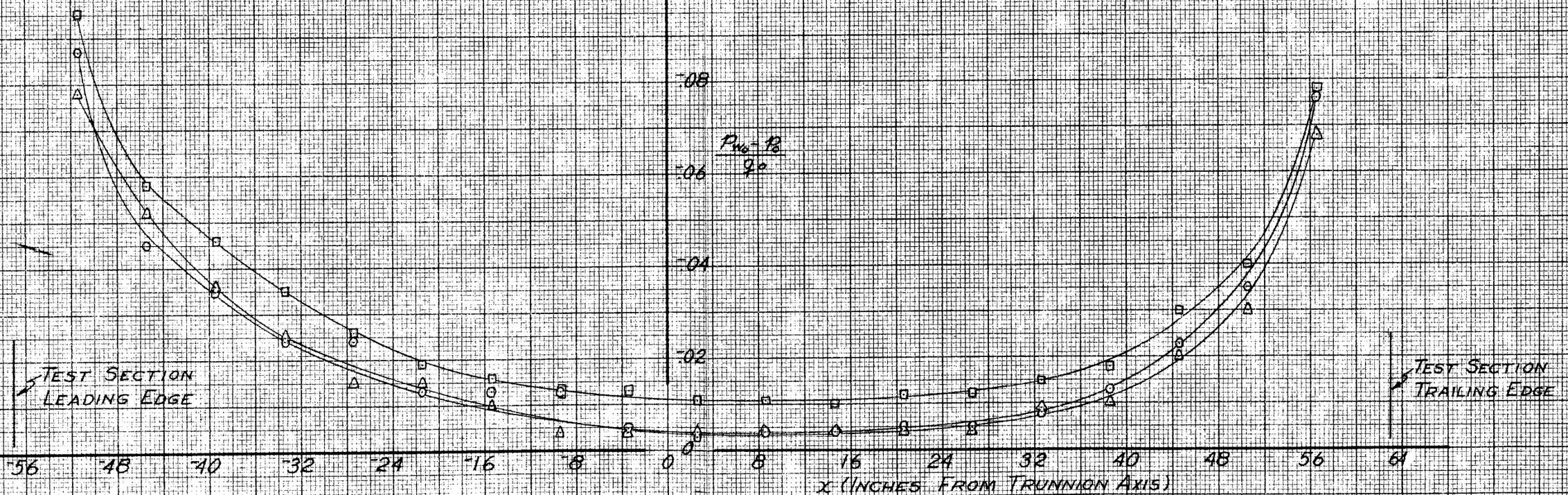

FIG. 7
STATIC PRESSURE SURVEY ALONG TUNNEL FLOOR AND CEILING

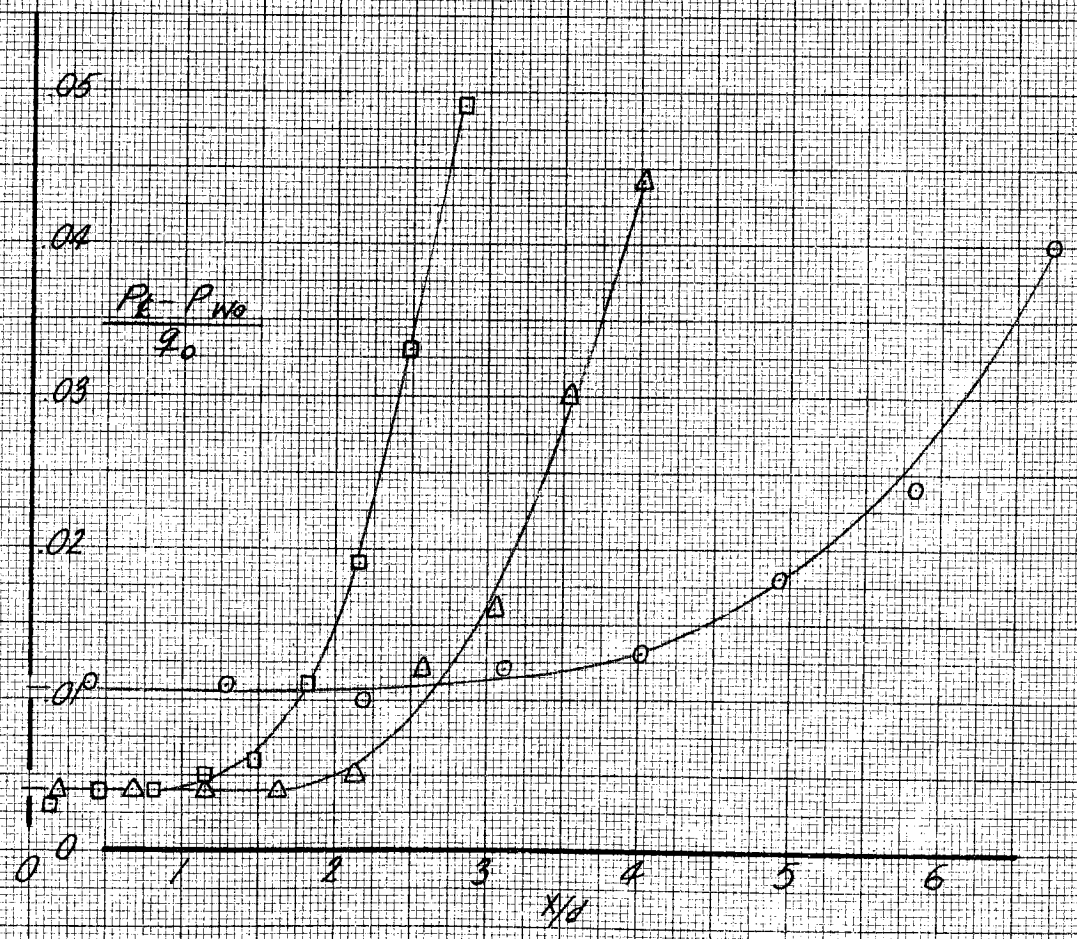

FIGURE 8
VARIATIONS BETWEEN WALL AND CENTERLINE REFERENCE PRESSURES

GALCIT REP. 534

WAKE RAKE STATIC PRESSURE ORIFICE CALIBRATION (RUN 39)

$\Delta p = p_x - p_{TRUE}$

p_x = RAKE STATIC PRESSURE READING

p_{TRUE} = TRUE " " ON TUNNEL AXIS

q_o = DYNAMIC PRESSURE (CLEAR TUNNEL)

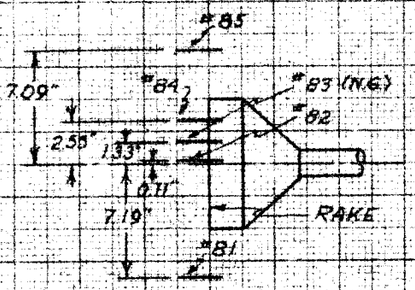

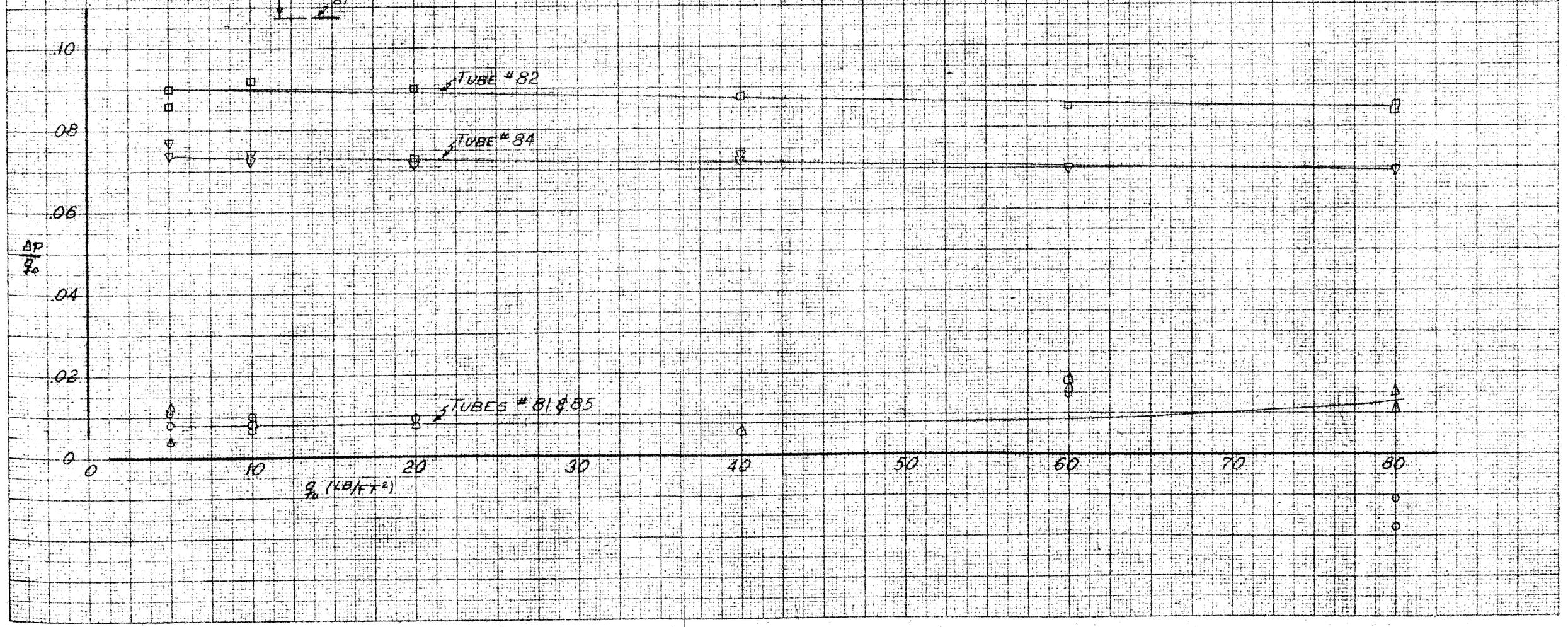

Fig 9 Calibration of Rake Static Pressure Tubes

GALCIT RER 534

PAGE
FIG.

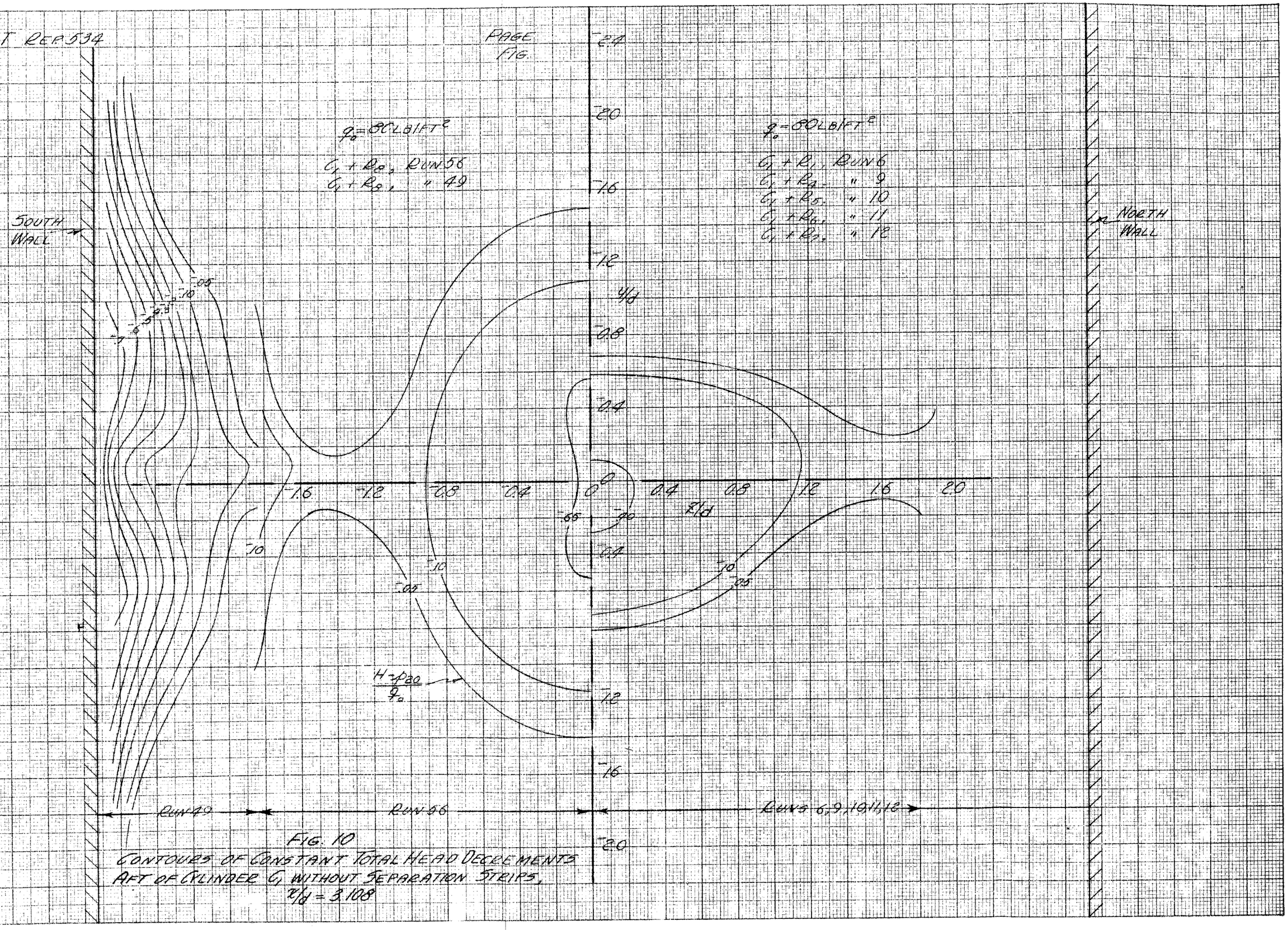

FIG. 10
CONTOURS OF CONSTANT TOTAL HEAD DECREMENTS AFT OF CYLINDER G, WITHOUT SEPARATION STRIPS, $z/b = 3.108$

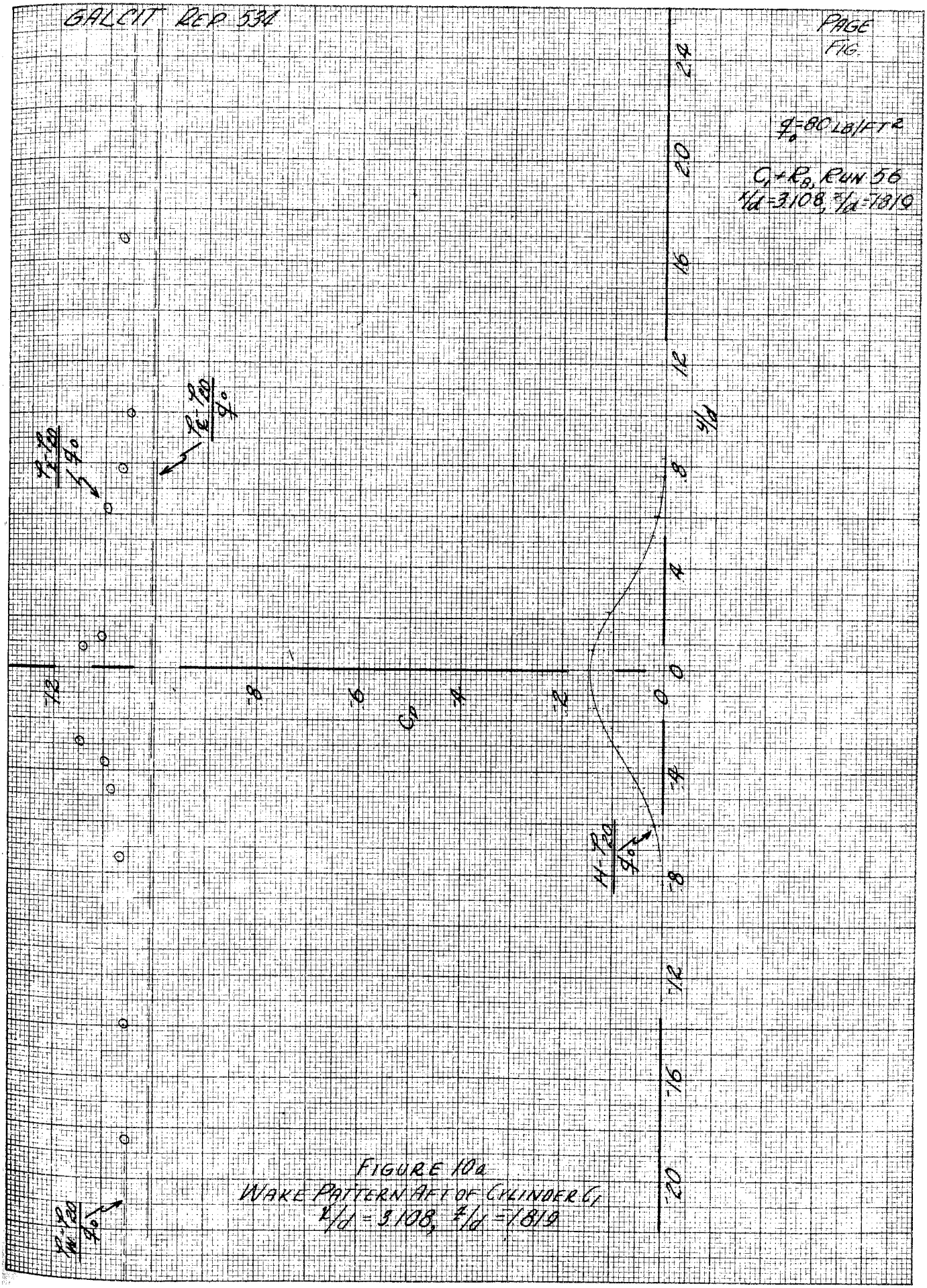

FIGURE 10a
WAKE PATTERN AFT OF CYLINDER C_1
x/d = 3.108, z/d = .7819

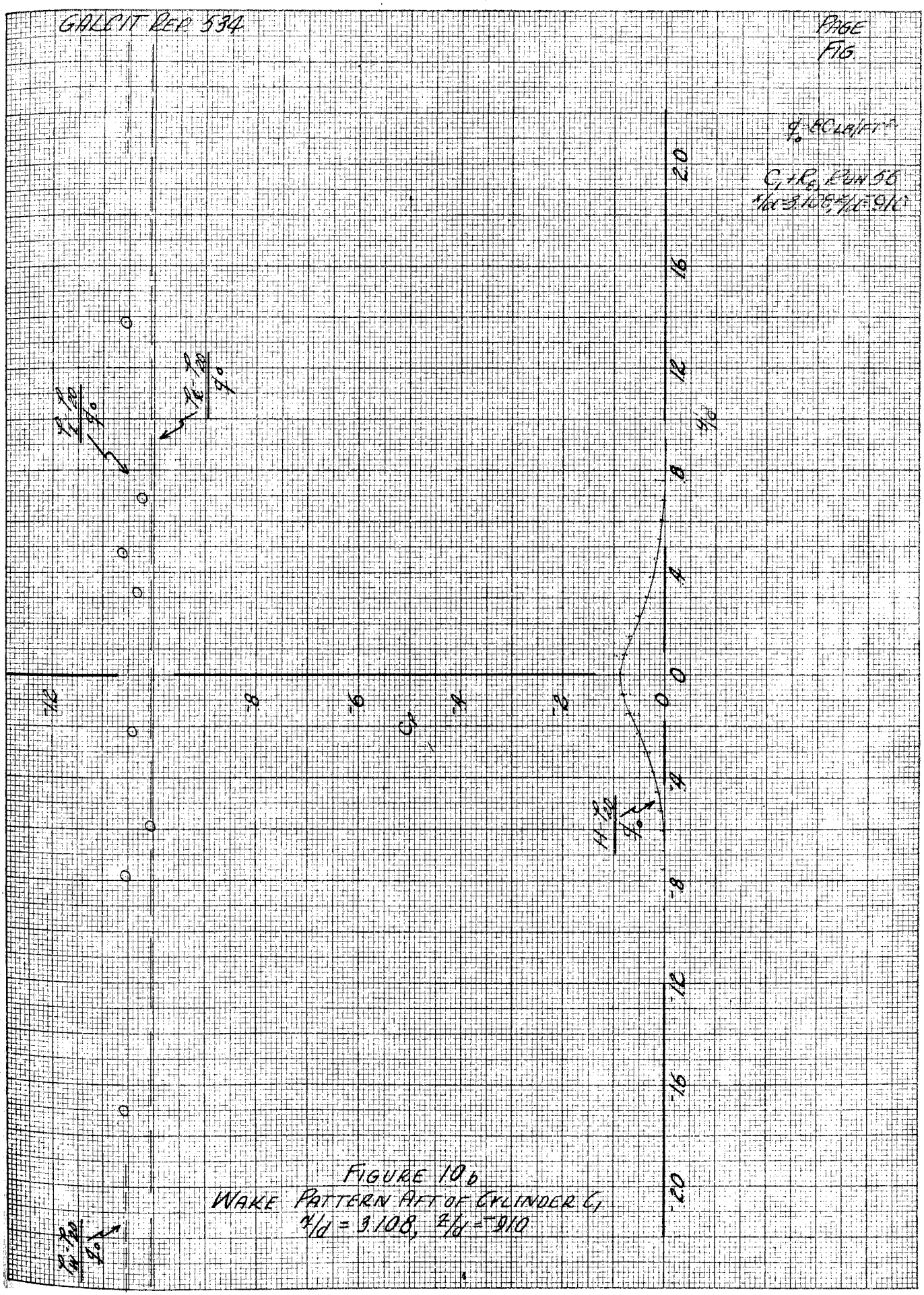

FIGURE 10b
WAKE PATTERN AFT OF CYLINDER C_1
$x/d = 3.108$, $z/d = 0.910$

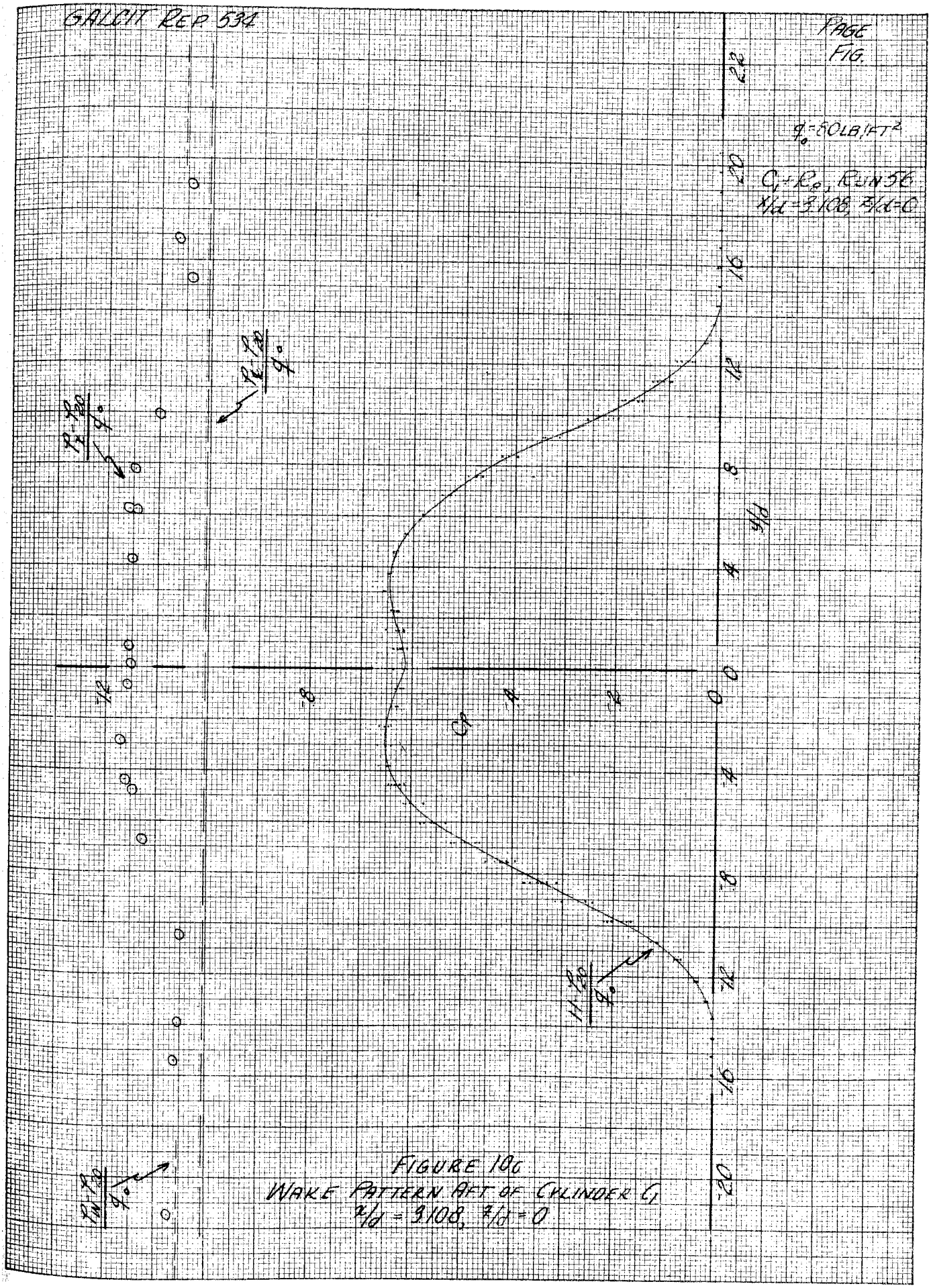

FIGURE 10c
WAKE PATTERN AFT OF CYLINDER C
x/d = 3.108, z/d = 0

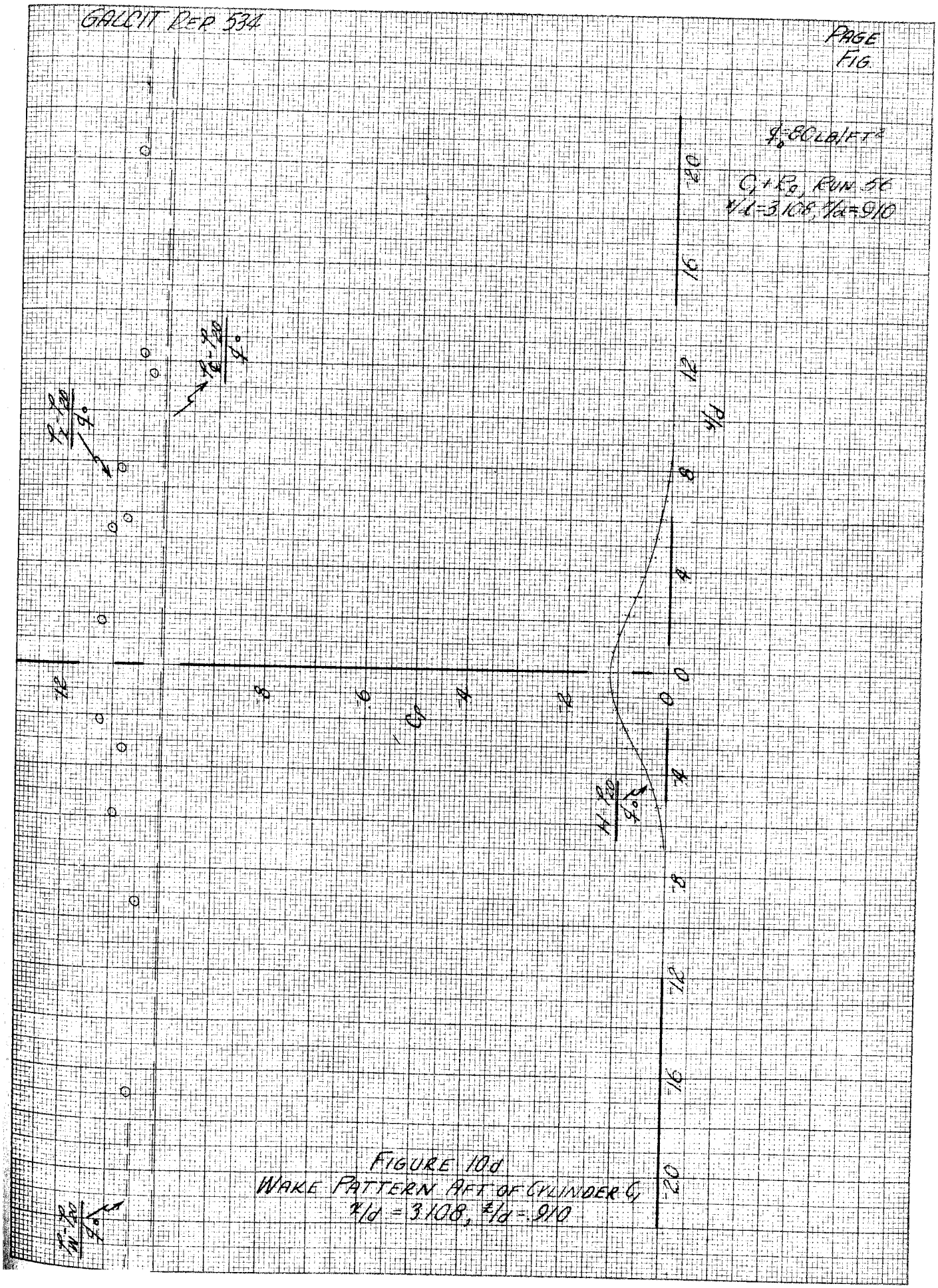

FIGURE 10d
WAKE PATTERN AFT OF CYLINDER 6
Y/d = 3.108, Z/d = .910

GALCIT REP 534

PAGE
FIG.

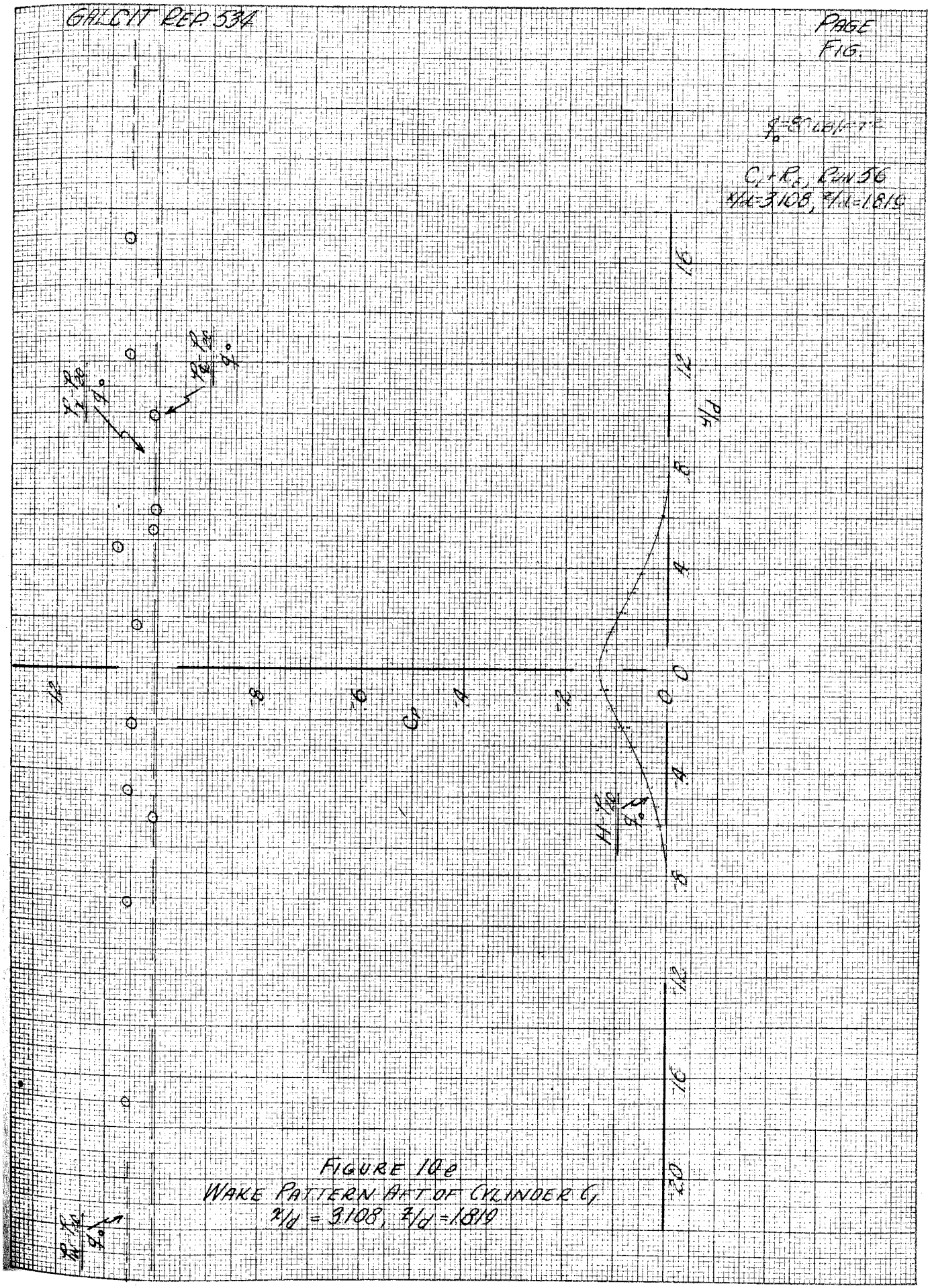

FIGURE 10e
WAKE PATTERN AFT OF CYLINDER 6,
$x/d = 3108$, $z/d = 1819$

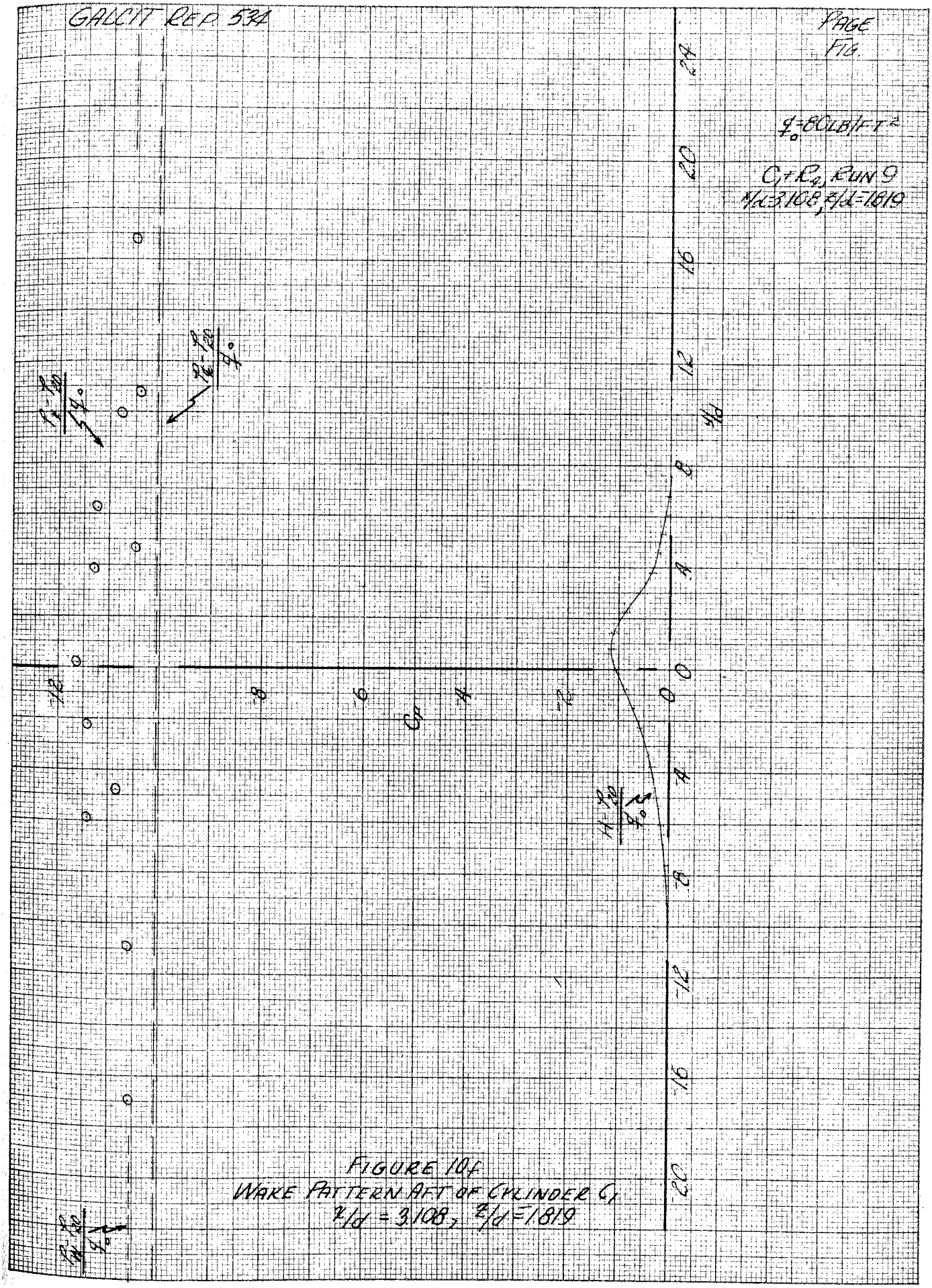

FIGURE 10f
WAKE PATTERN AFT OF CYLINDER C_1
$x/d = 3.108$, $z/d = 1.819$

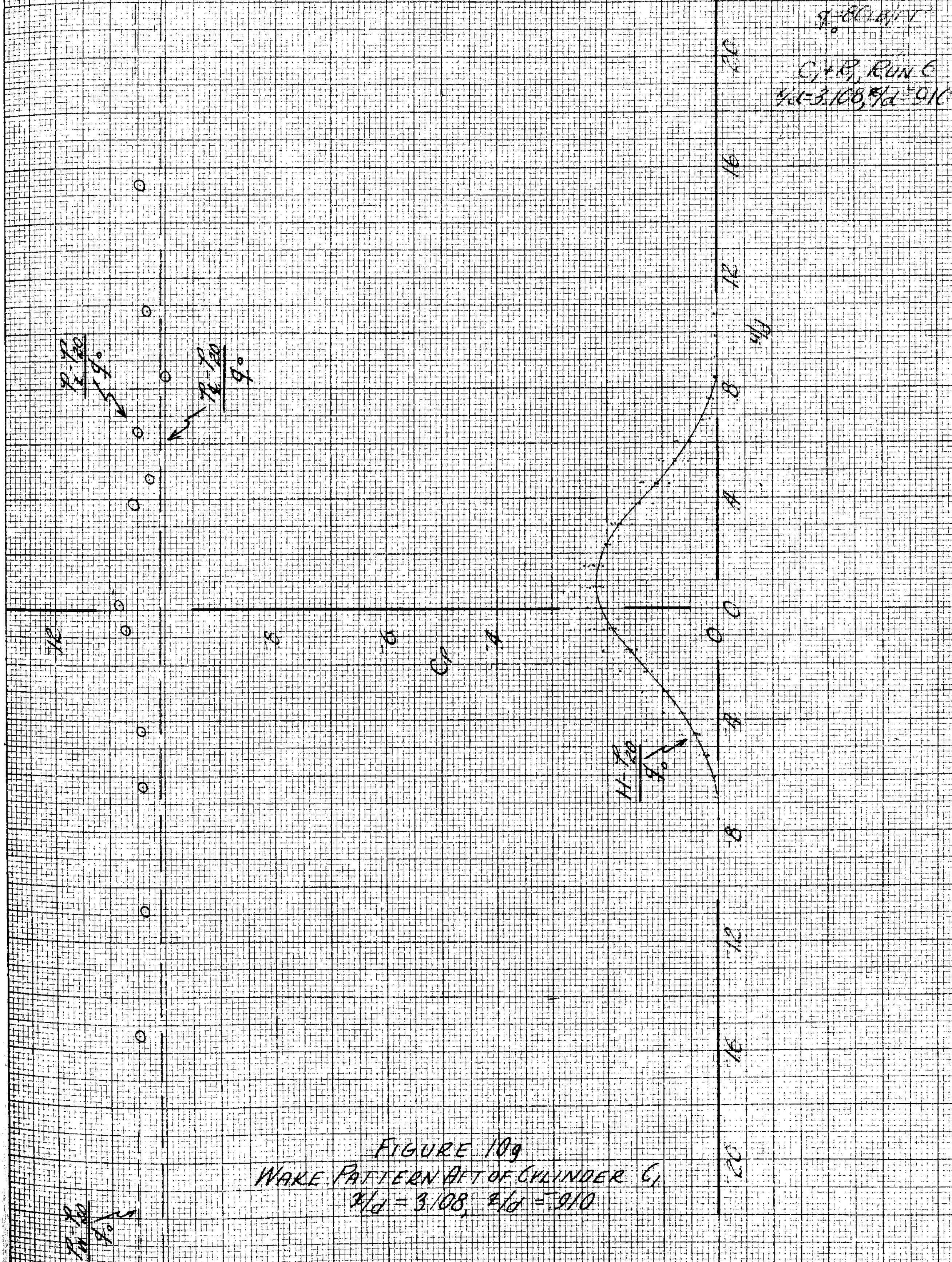

FIGURE 10g
WAKE PATTERN AFT OF CYLINDER C_1
$x/d = 3.108$, $z/d = .910$

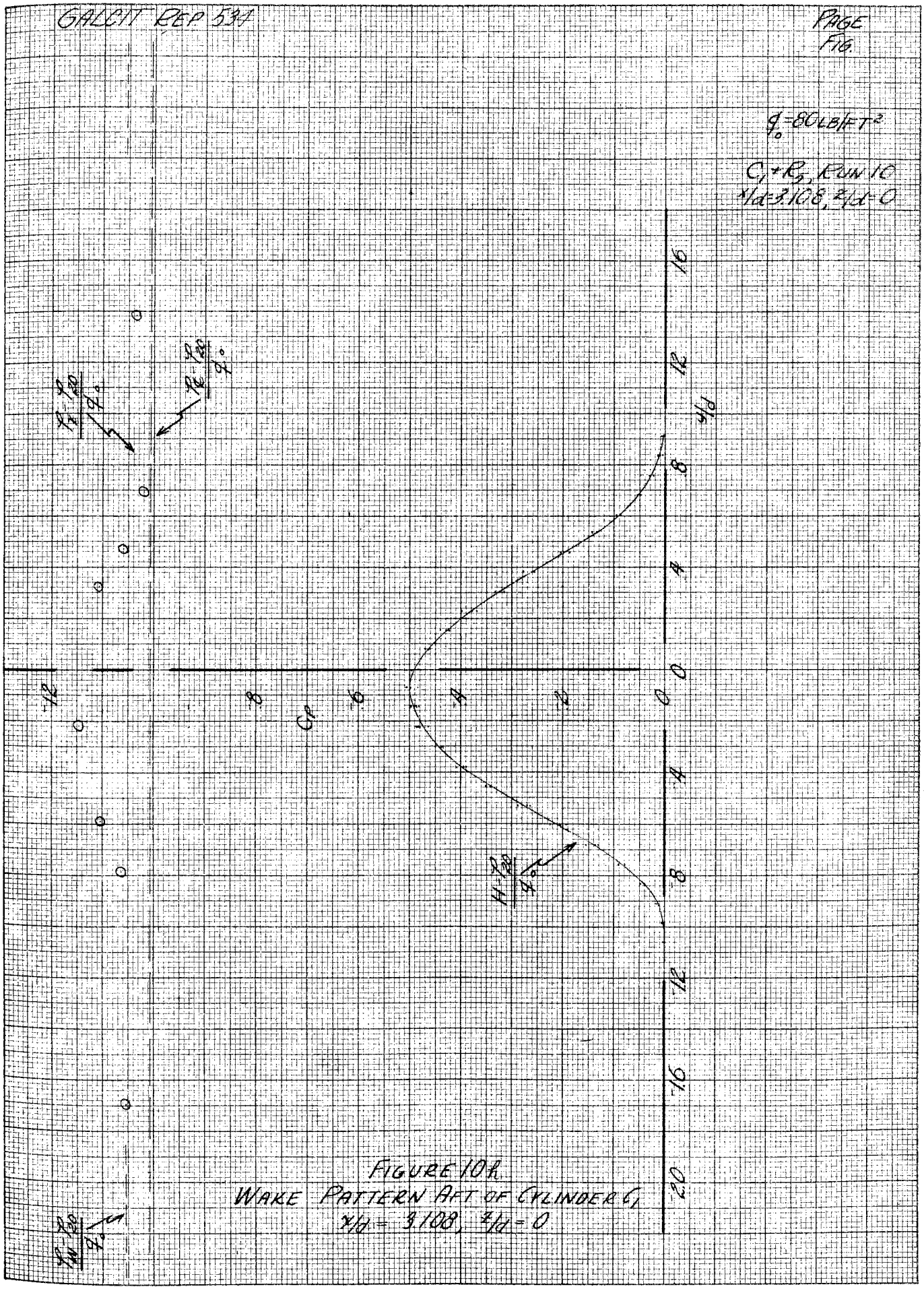

FIGURE 10R
WAKE PATTERN AFT OF CYLINDER 6,
x/d = 3.108, z/d = 0

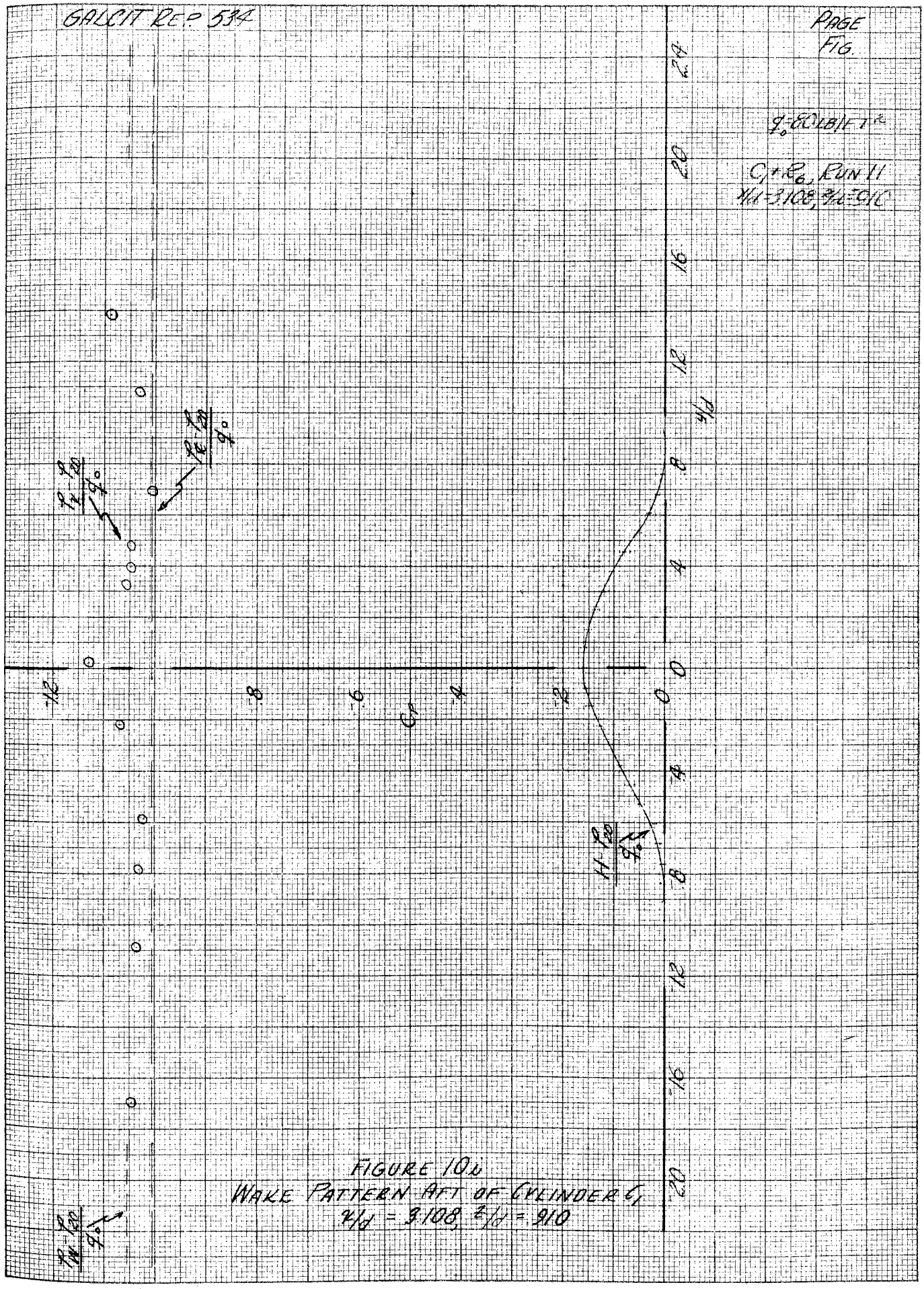

FIGURE 10b
WAKE PATTERN AFT OF CYLINDER C_1
x/d = 3.108, z/d = 910

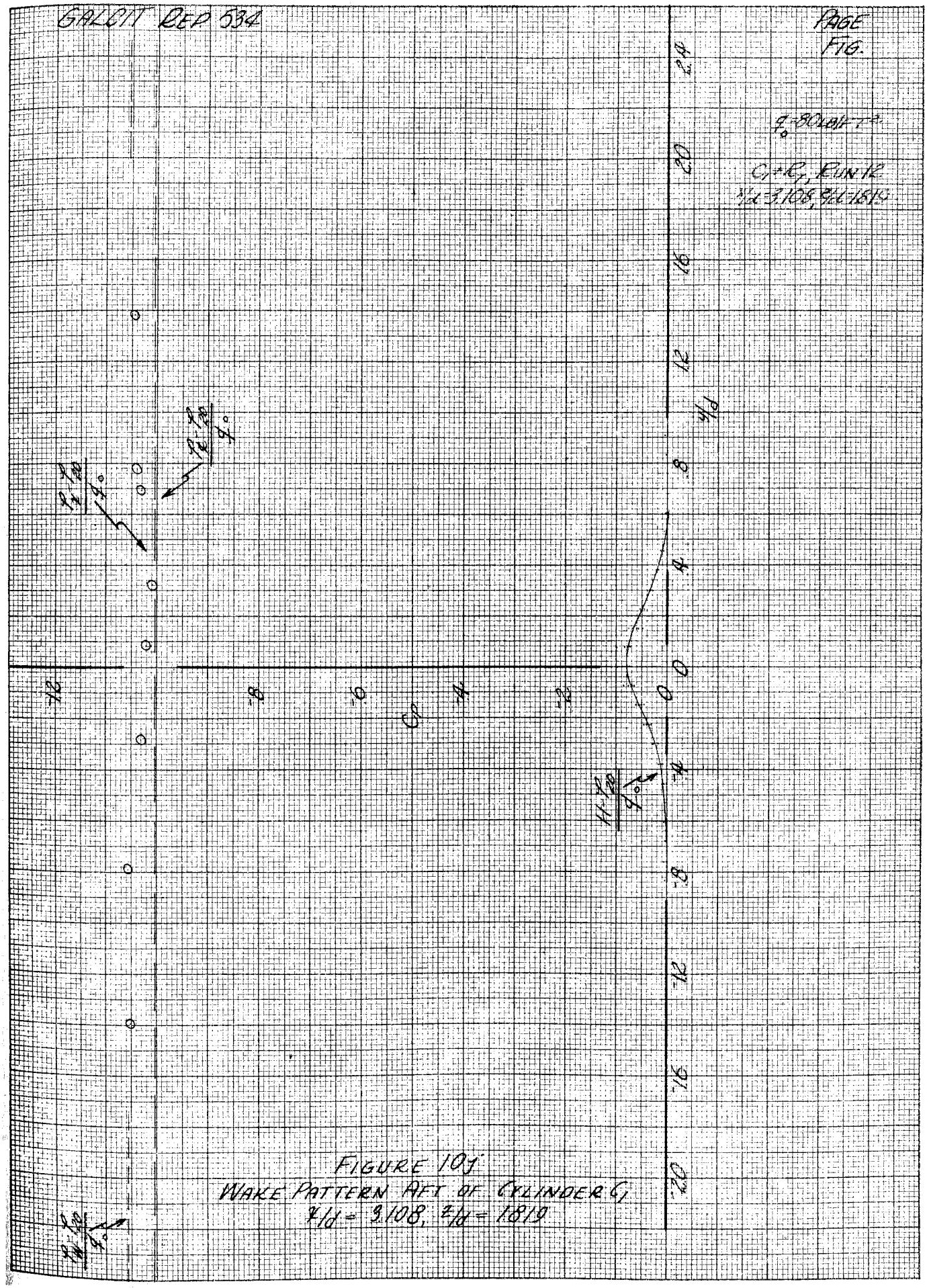

FIGURE 107
WAKE PATTERN AFT OF CYLINDER C,
x/d = 3.108, z/d = 1.819

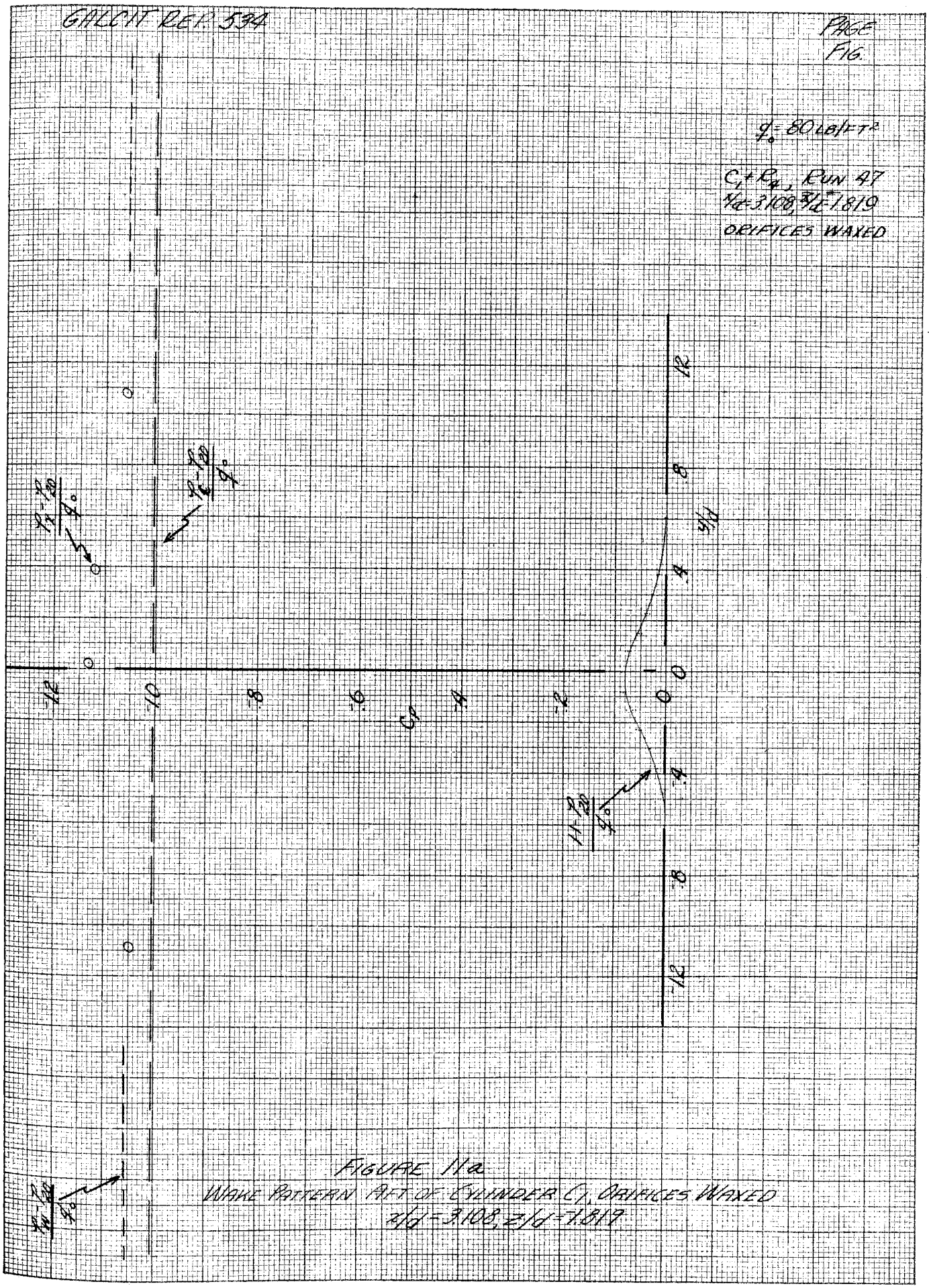

FIGURE 11a

WAKE PATTERN AFT OF CYLINDER C_1, ORIFICES WAXED

R/ℓ = 3108, R/ℓ = 1819

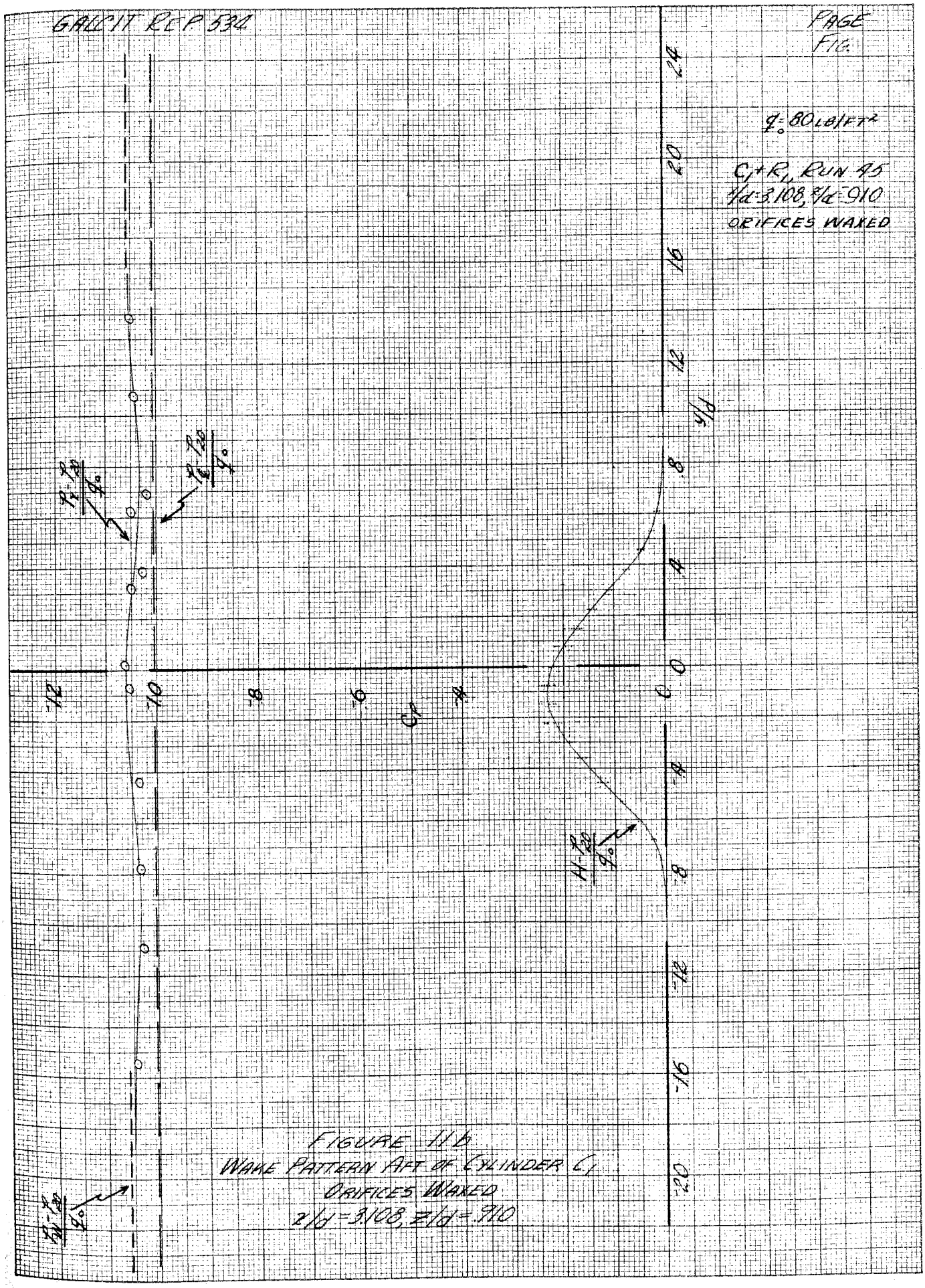

FIGURE 11b
WAKE PATTERN AFT OF CYLINDER C_f
ORIFICES WAKED
$x/d = 3.108$, $z/d = .910$

GALCIT REP 534

PAGE
FIG.

$q_o = 80$ LB/FT^2

C_1+R5, RUN 46
$x/d = 3.108$, $z/d = 0$
ORIFICES WAXED

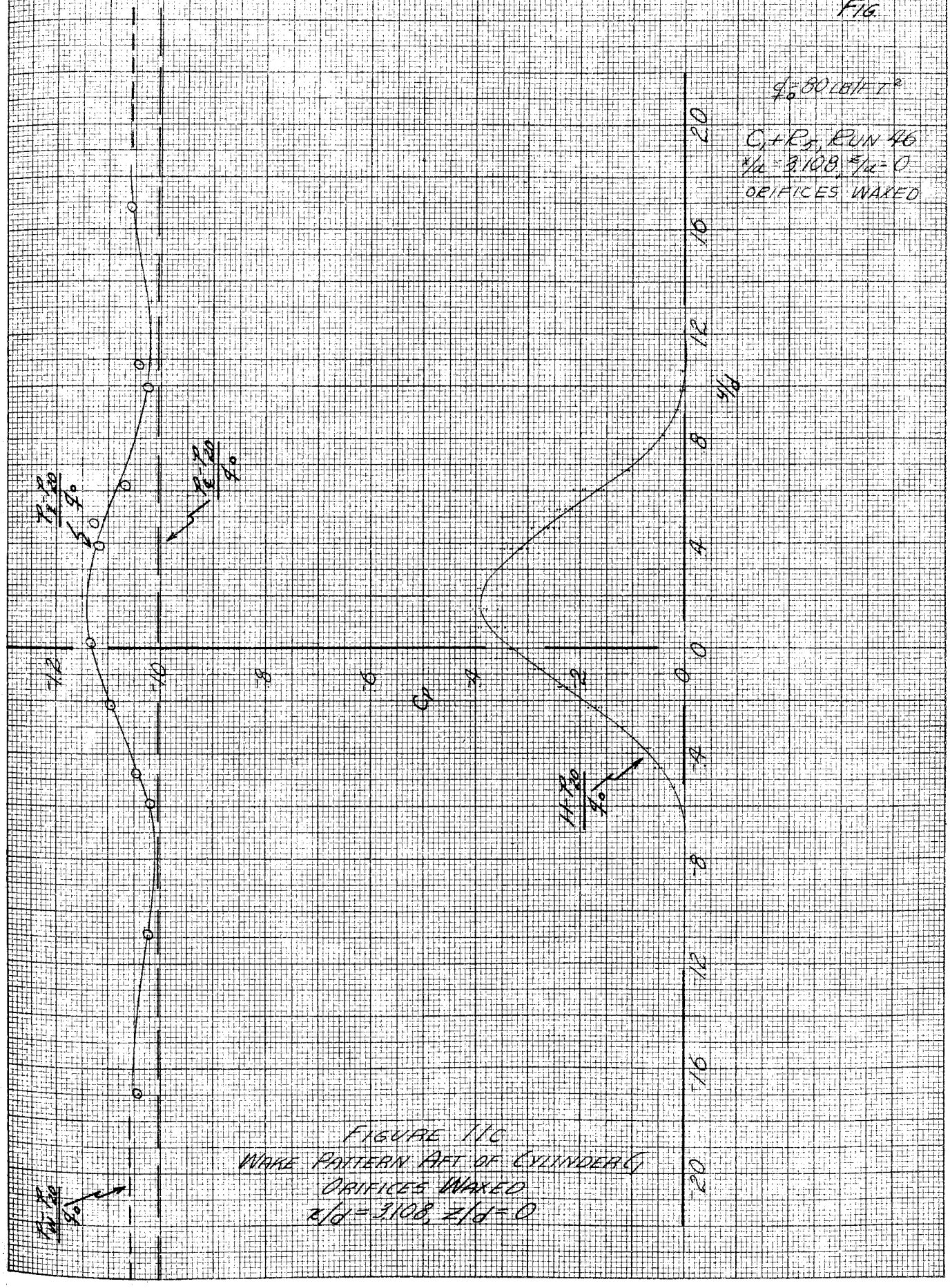

FIGURE 11C
WAKE PATTERN AFT OF CYLINDER G
ORIFICES WAXED
$x/d = 3.108$, $z/d = 0$

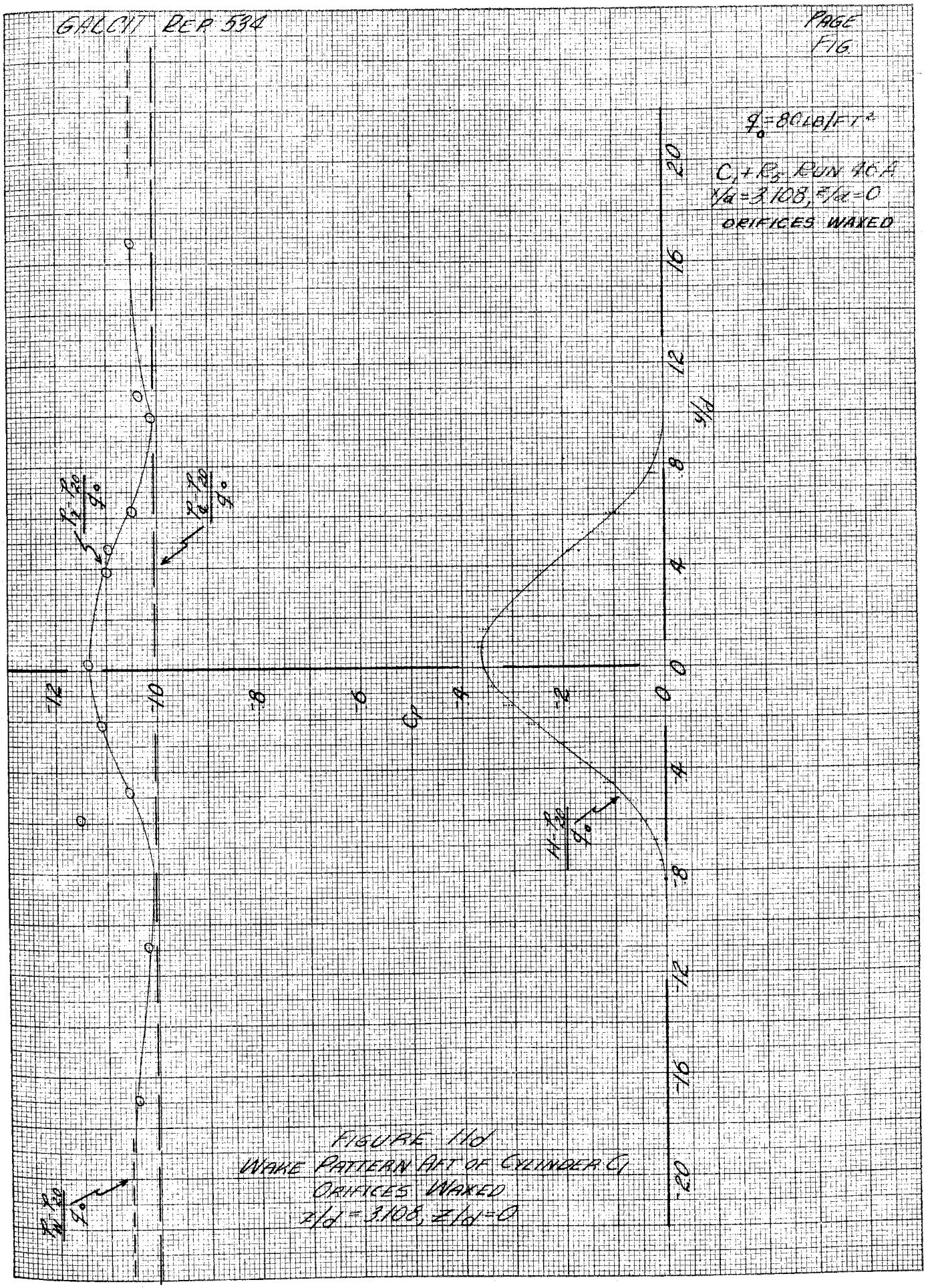

FIGURE 110
WAKE PATTERN AFT OF CYLINDER C
ORIFICES WAXED
x/d = 3.108, z/d = 0

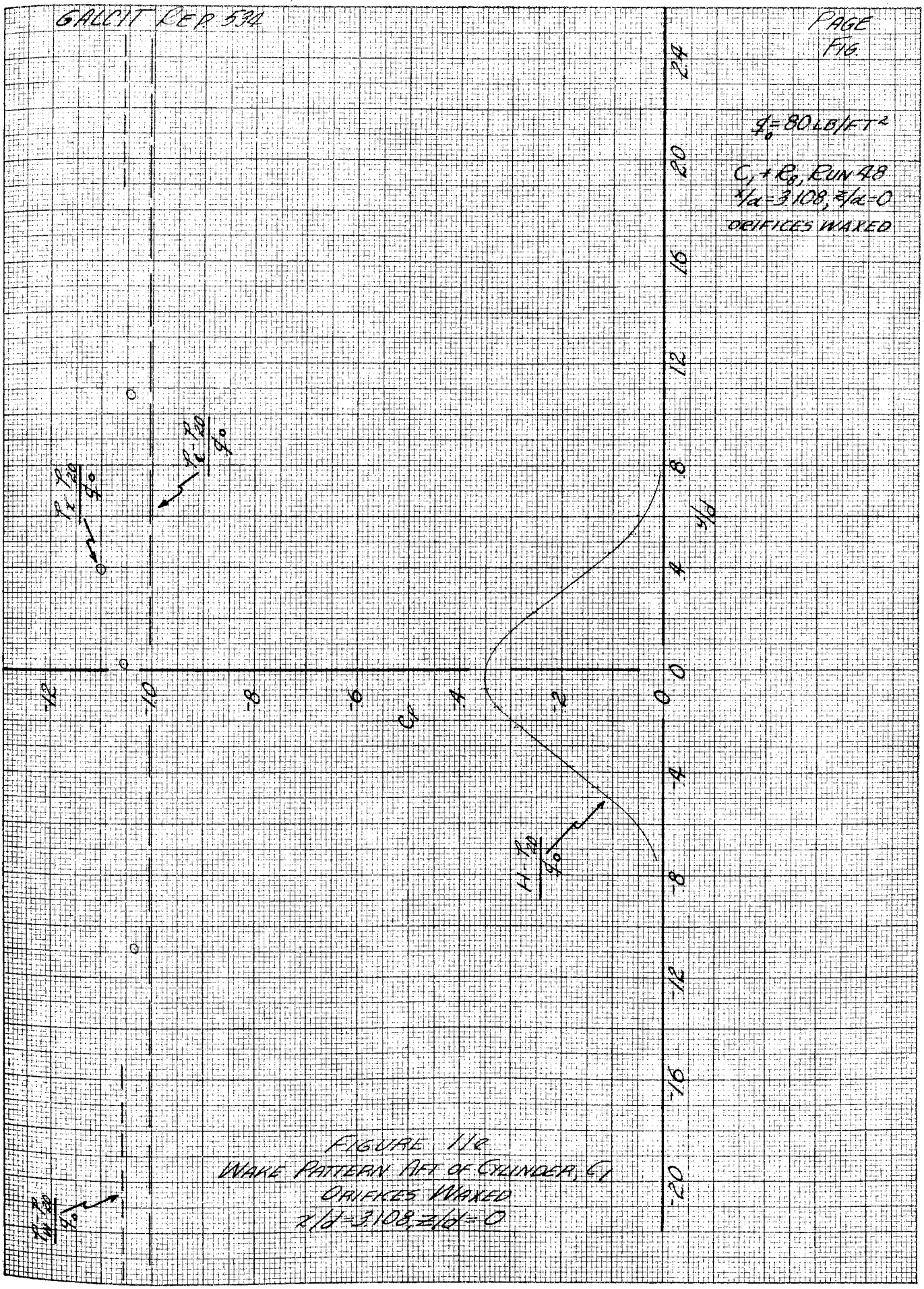

FIGURE 116
WAKE PATTERN AFT OF CYLINDER, 6"
ORIFICES WAXED
$x/d = 3108$, $z/d = 0$

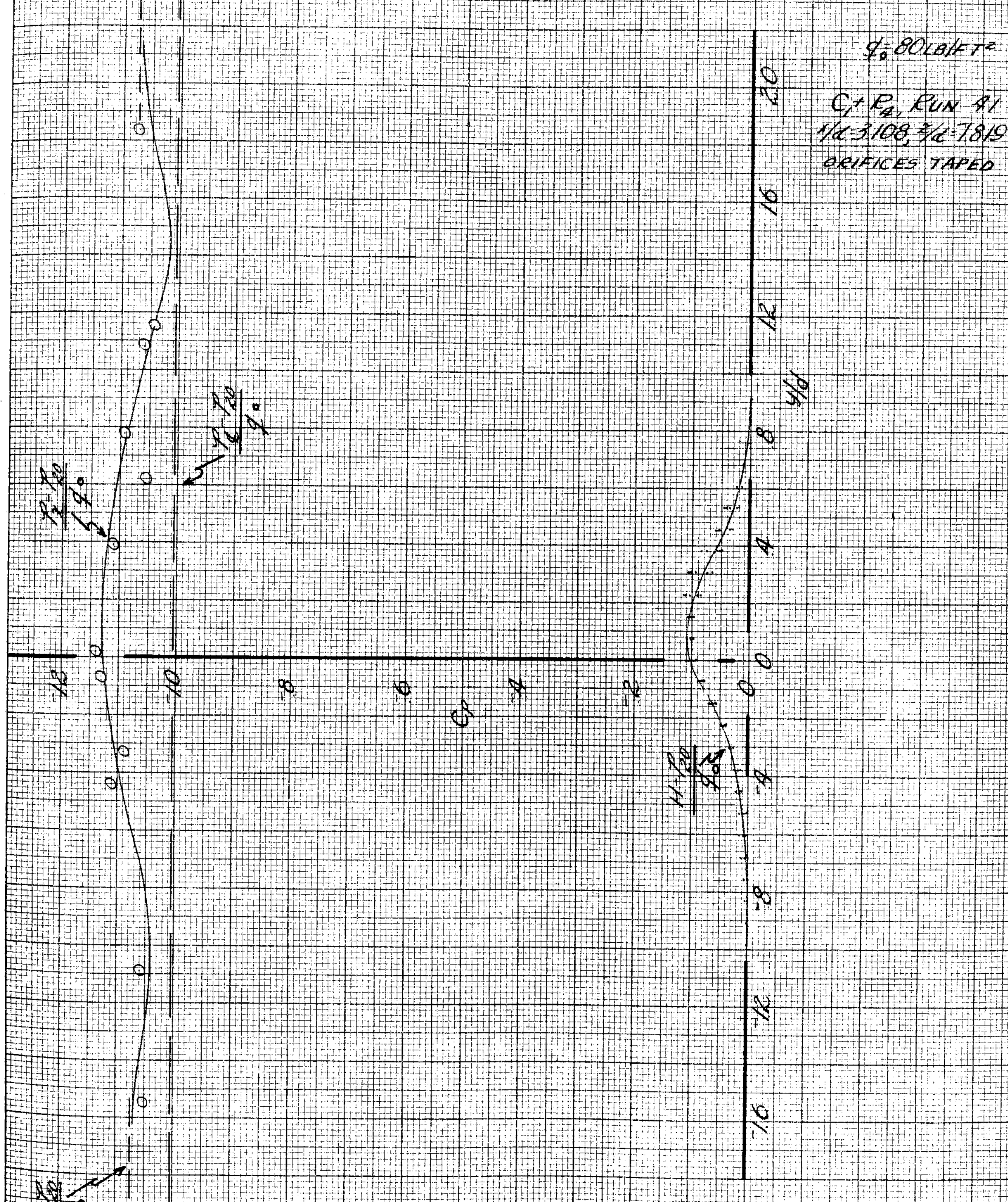

FIGURE 12a
WAKE PATTERN AFT OF CYLINDER C_1, ORIFICES TAPED
$y/d = 3.108$, $z/d = 1.819$

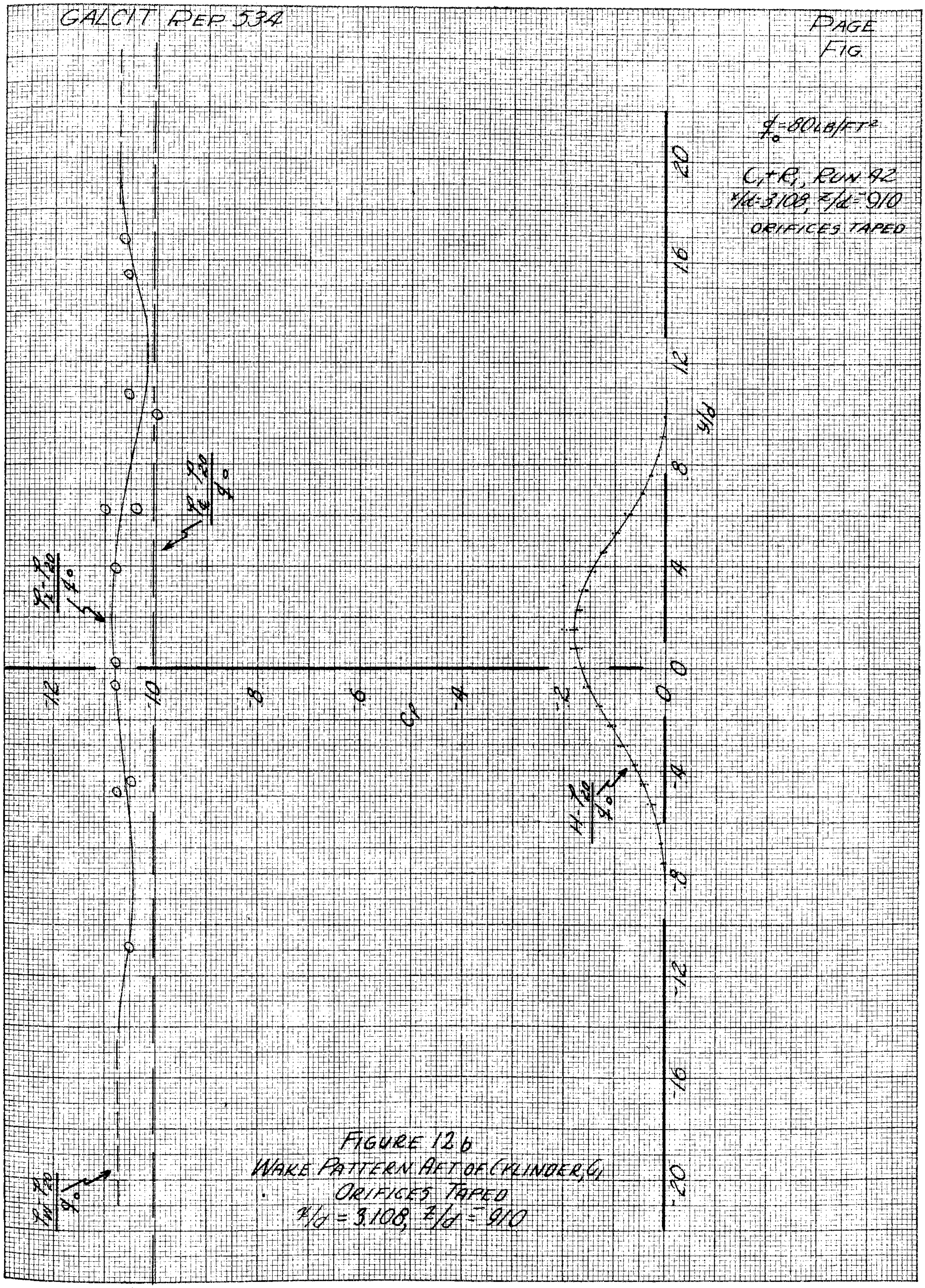

FIGURE 12b
WAKE PATTERN AFT OF CYLINDER, C_1
ORIFICES TAPED
$x/d = 3.108$, $z/d = .910$

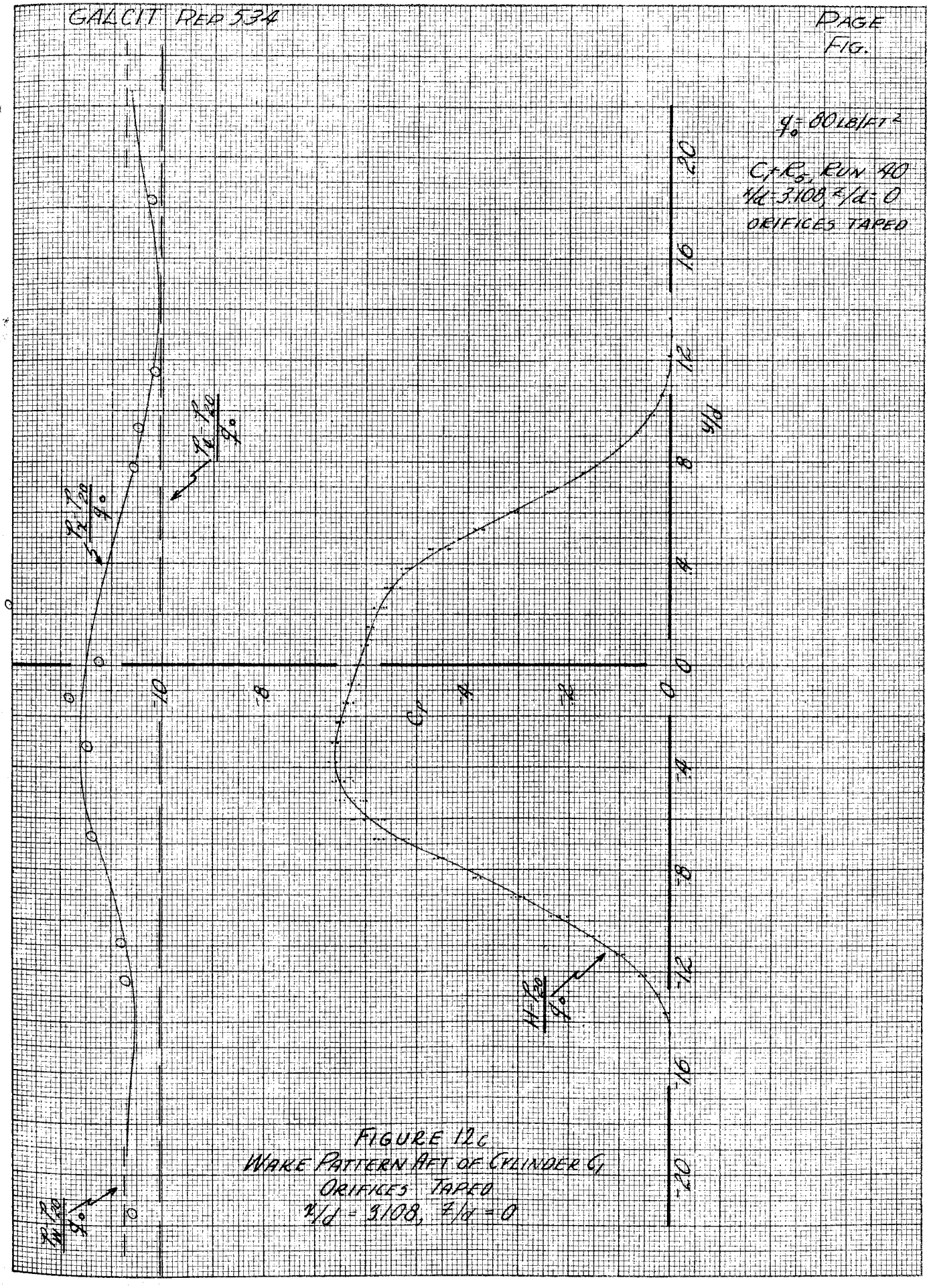

FIGURE 12c
WAKE PATTERN AFT OF CYLINDER C_1
ORIFICES TAPED
$x/d = 3.108$, $z/d = 0$

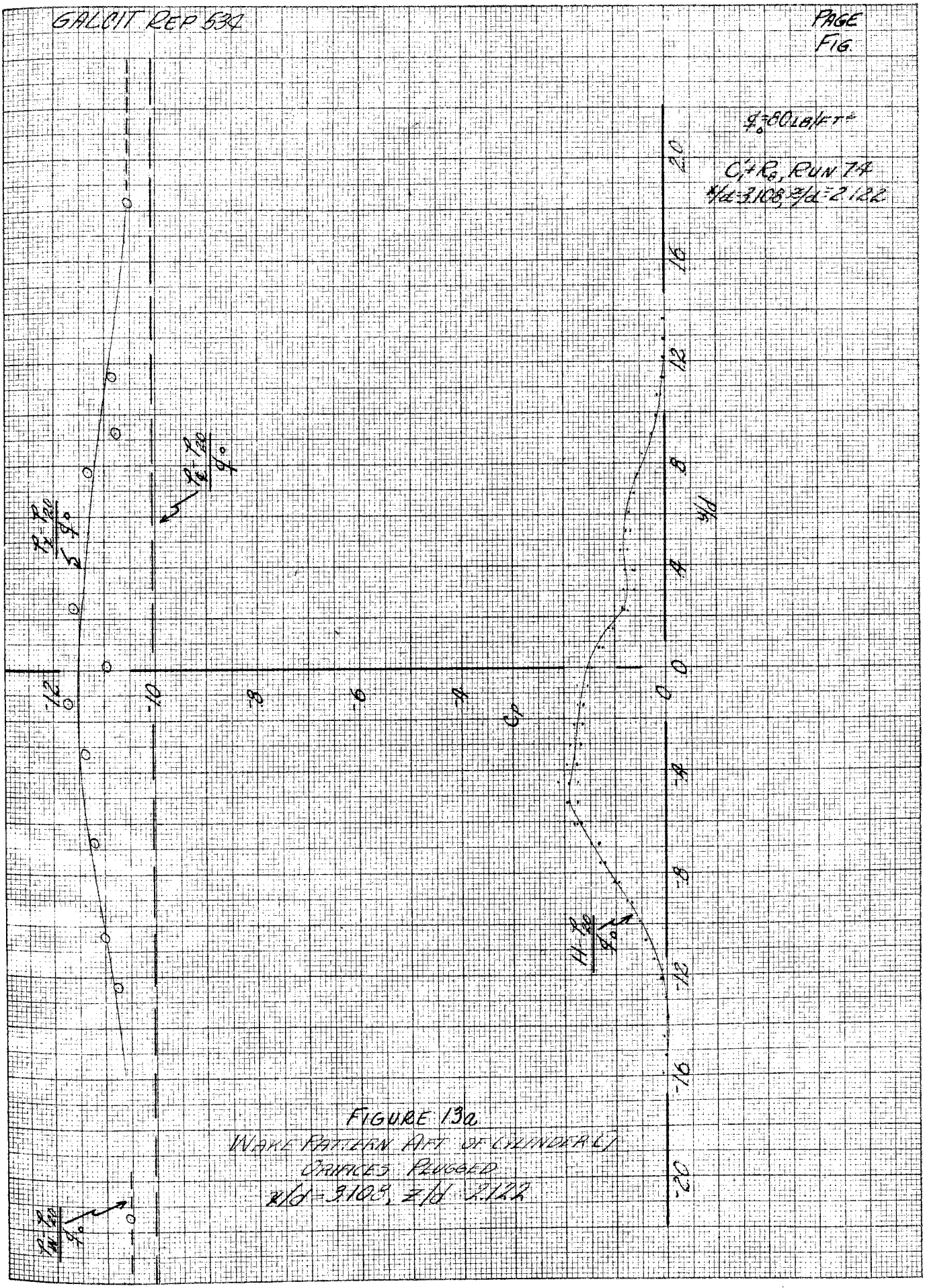

FIGURE 13a
WAKE PATTERN AFT OF CYLINDER (3 INCHES DIAMETER)
R/d=3.108, z/d=2.122

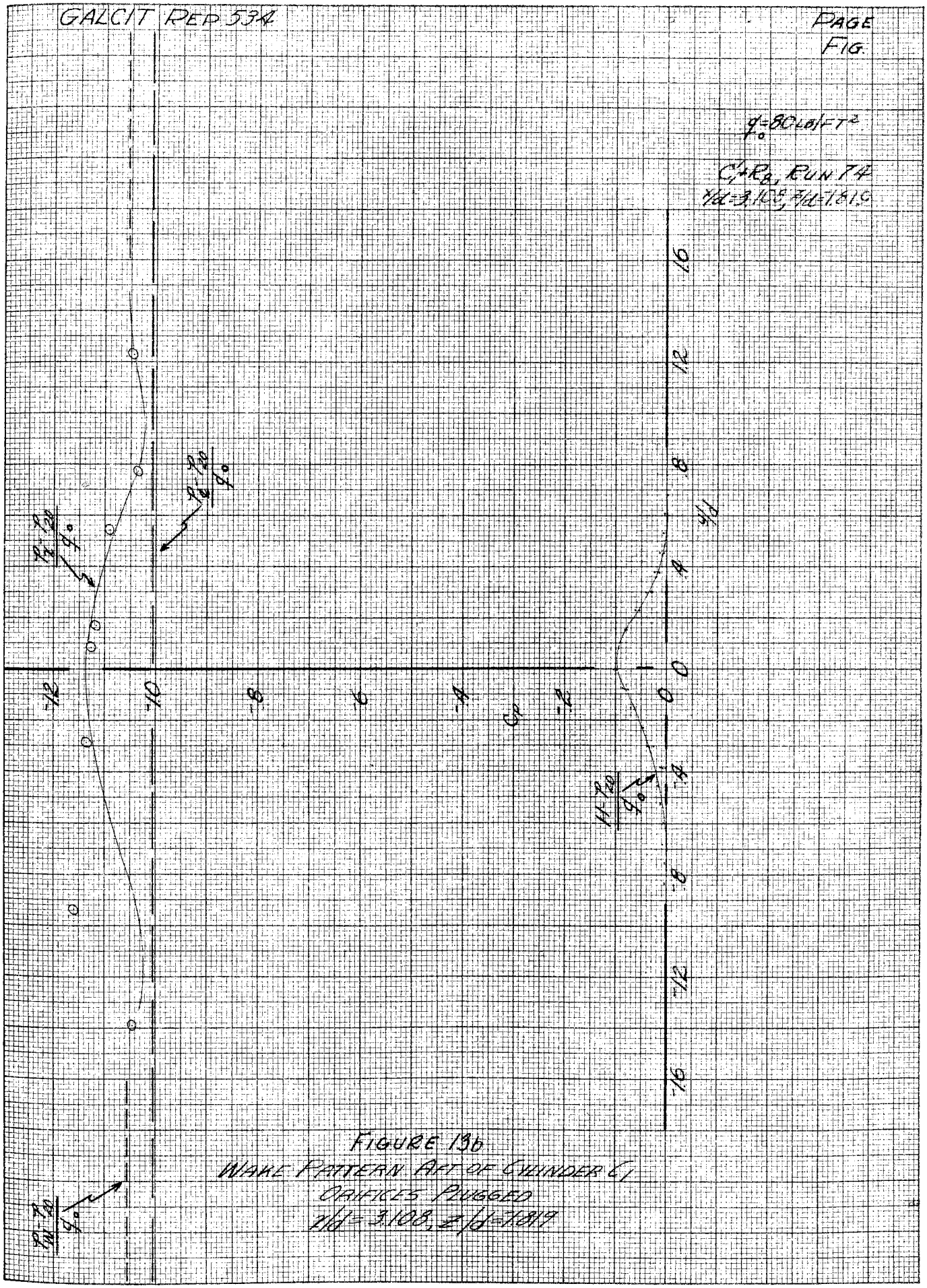

FIGURE 13b
WAKE PATTERN AFT OF CYLINDER 6,
ORIFICES PLUGGED
R_d=3.10⁵, F_d=7.81

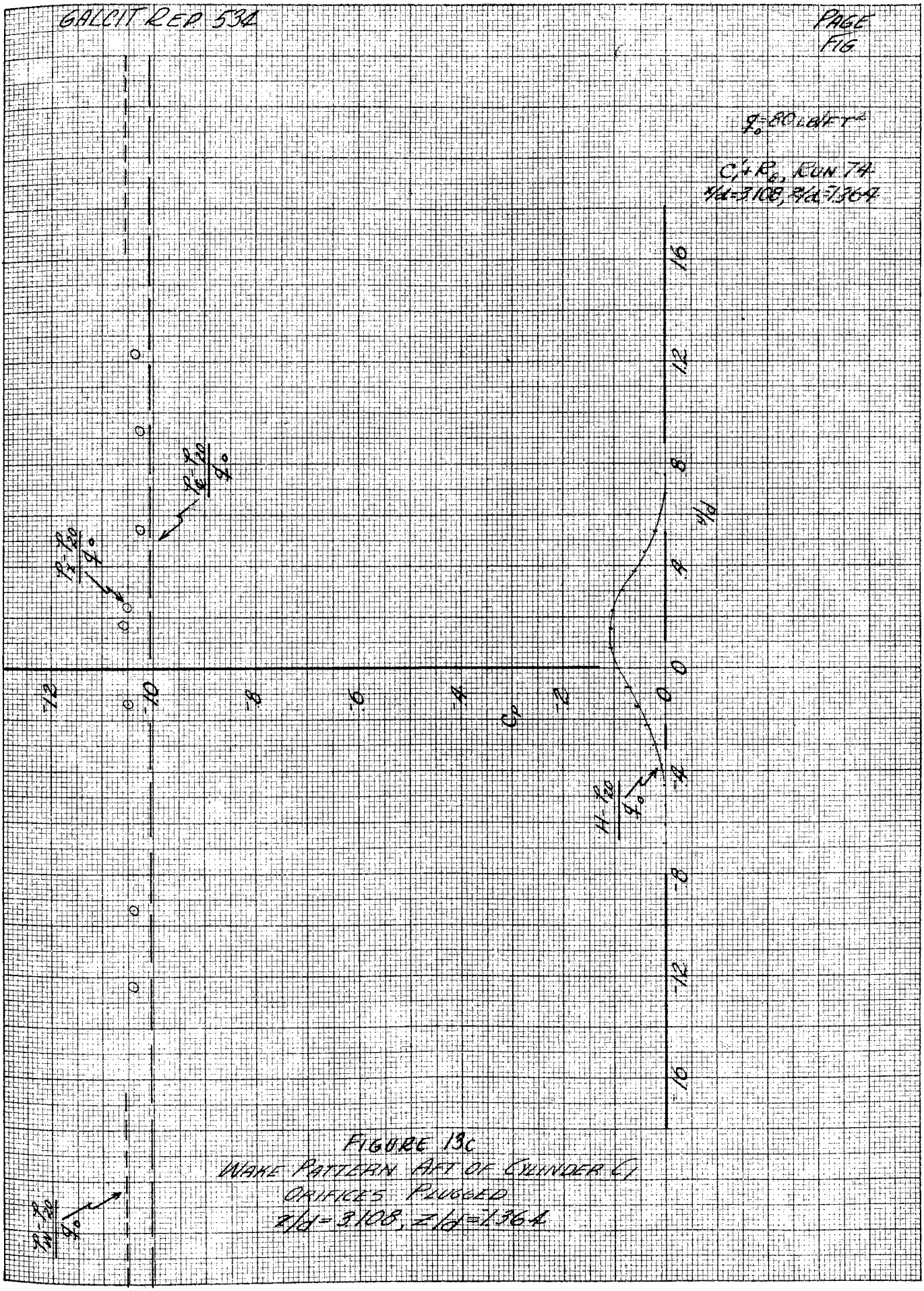

FIGURE 13c
WAKE PATTERN AFT OF CYLINDER C₄
ORIFICES PLUGGED
x/d=3.108, z/d=1.364

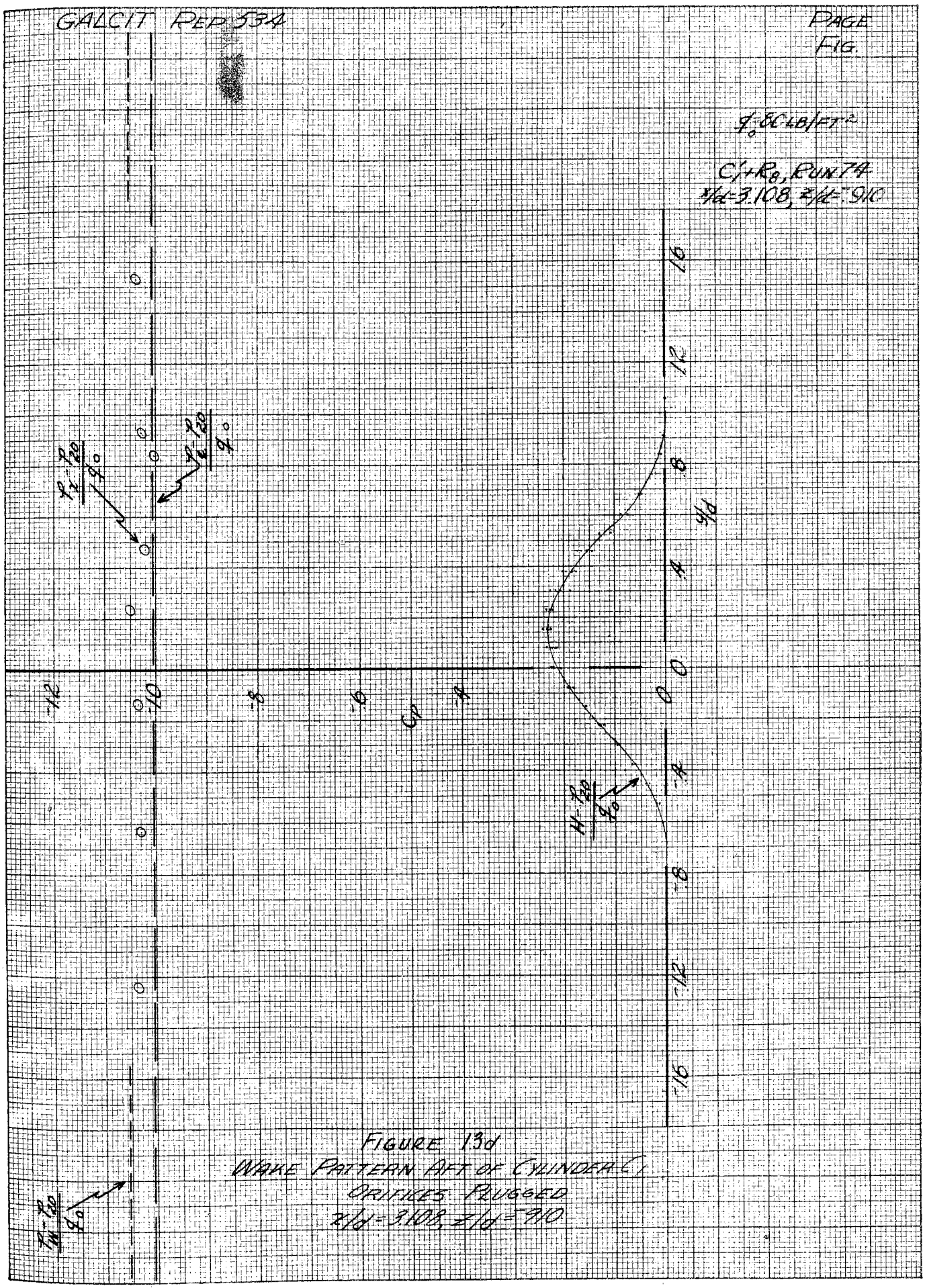

FIGURE 13d
WAKE PATTERN AFT OF CYLINDER C_1
ORIFICES PLUGGED
x/d = 3.108, z/d = .910

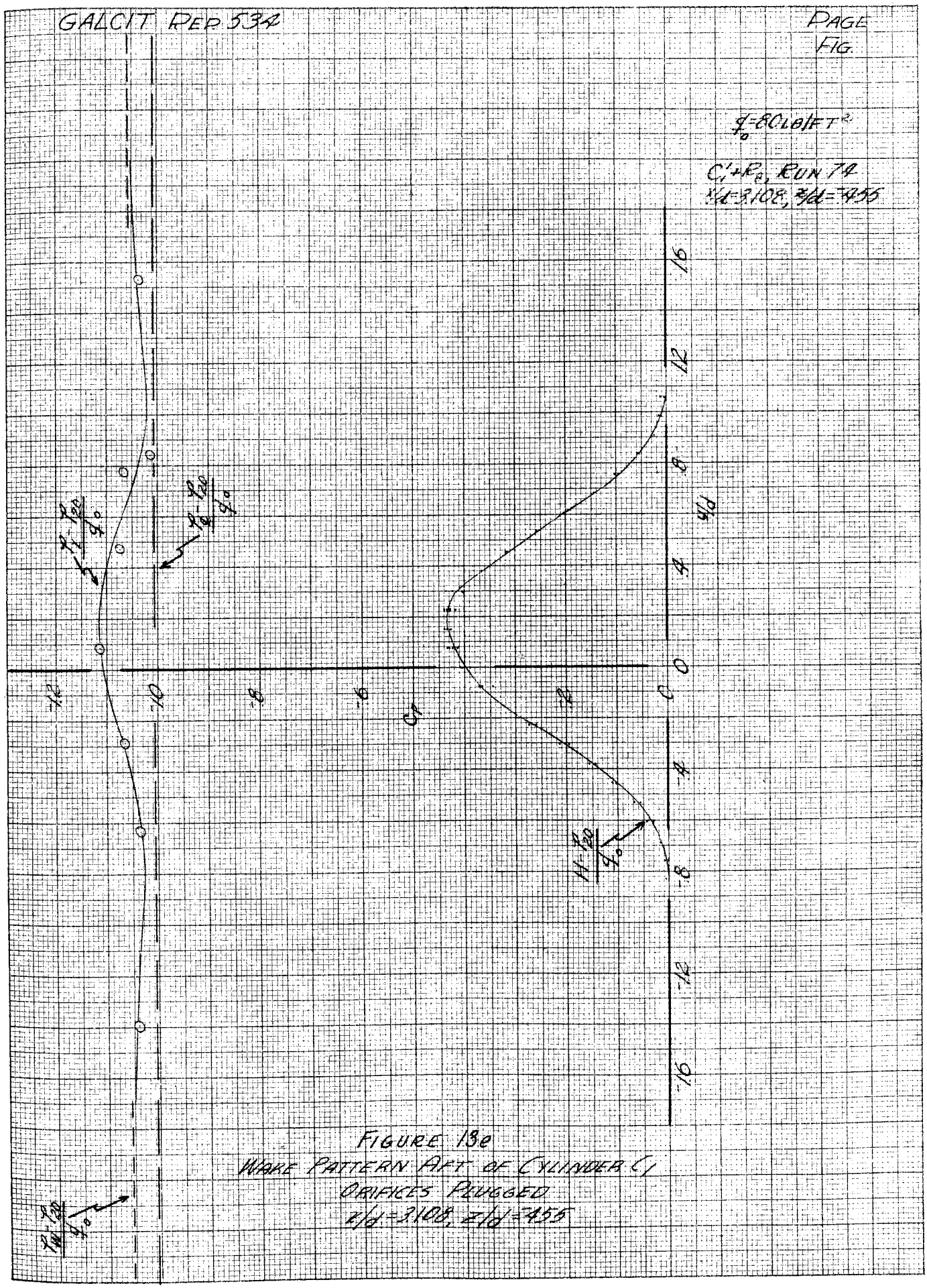

FIGURE 13e
WAKE PATTERN AFT OF CYLINDER C,
ORIFICES PLUGGED
x/d=3.108, z/d=.455

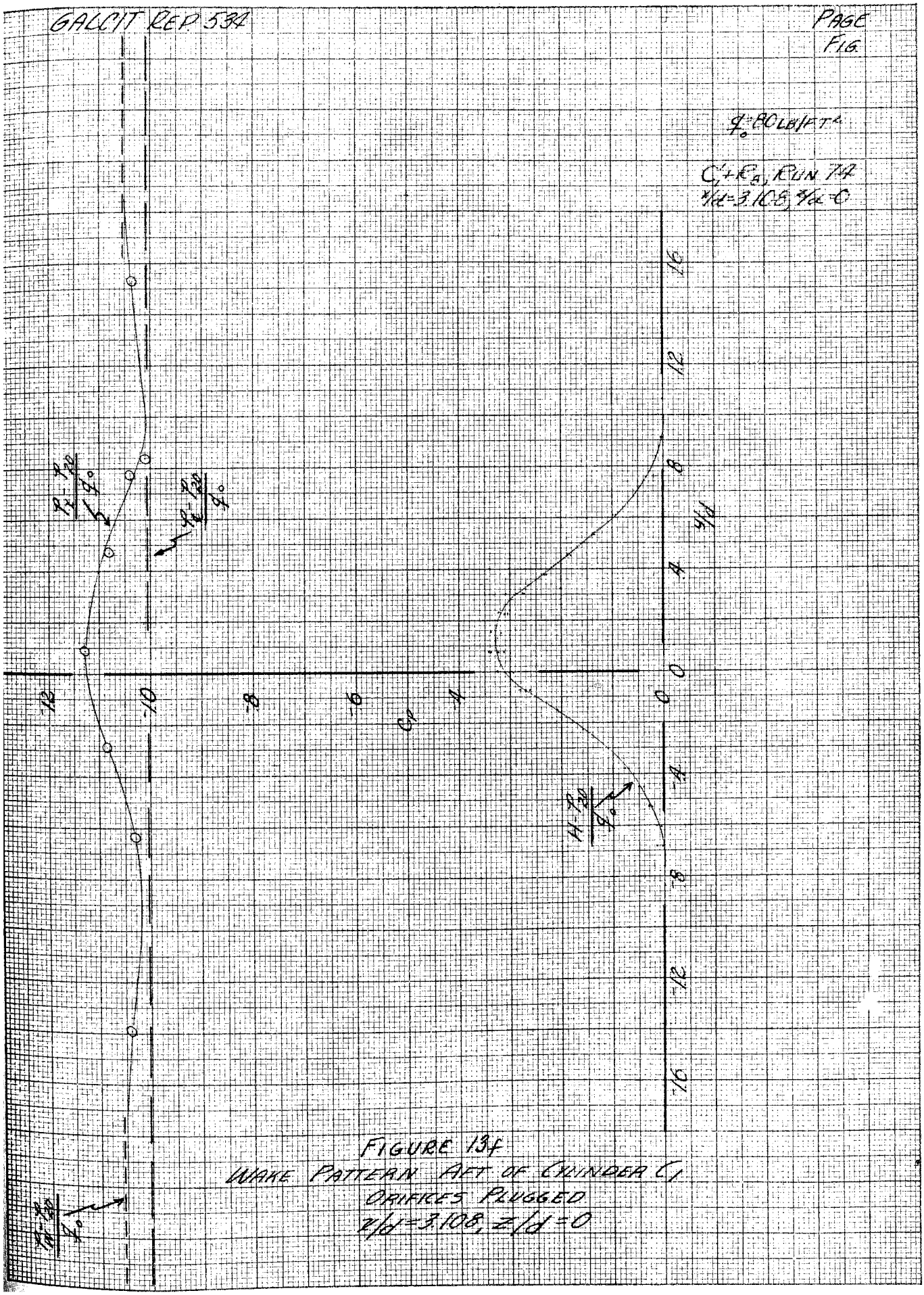

FIGURE 13f
WAKE PATTERN AFT OF CYLINDER C,
ORIFICES PLUGGED
x/d = 3.108, z/d = 0

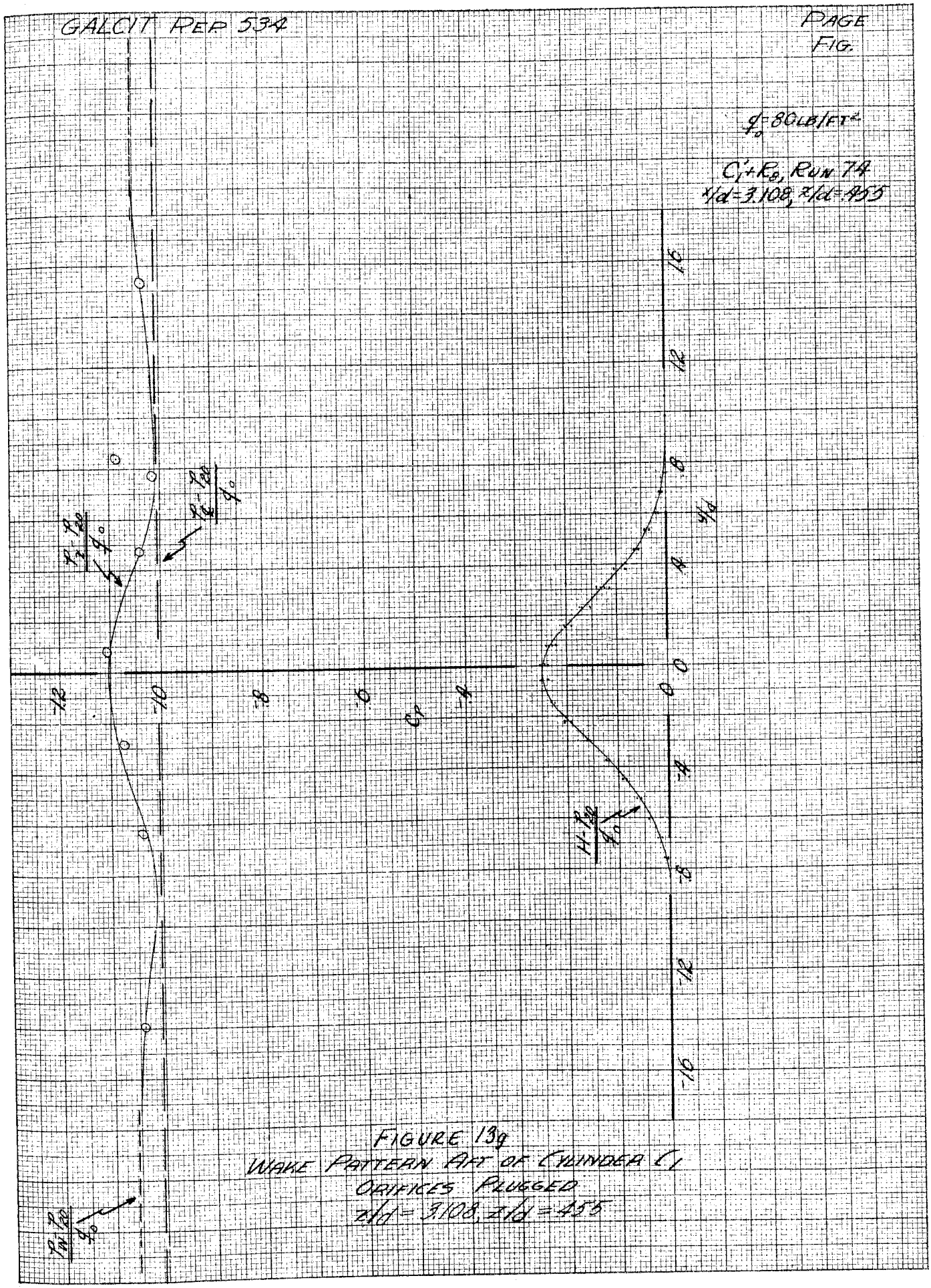

FIGURE 13g
WAKE PATTERN AFT OF CYLINDER C,
ORIFICES PLUGGED
x/d=3.108, z/d=.455

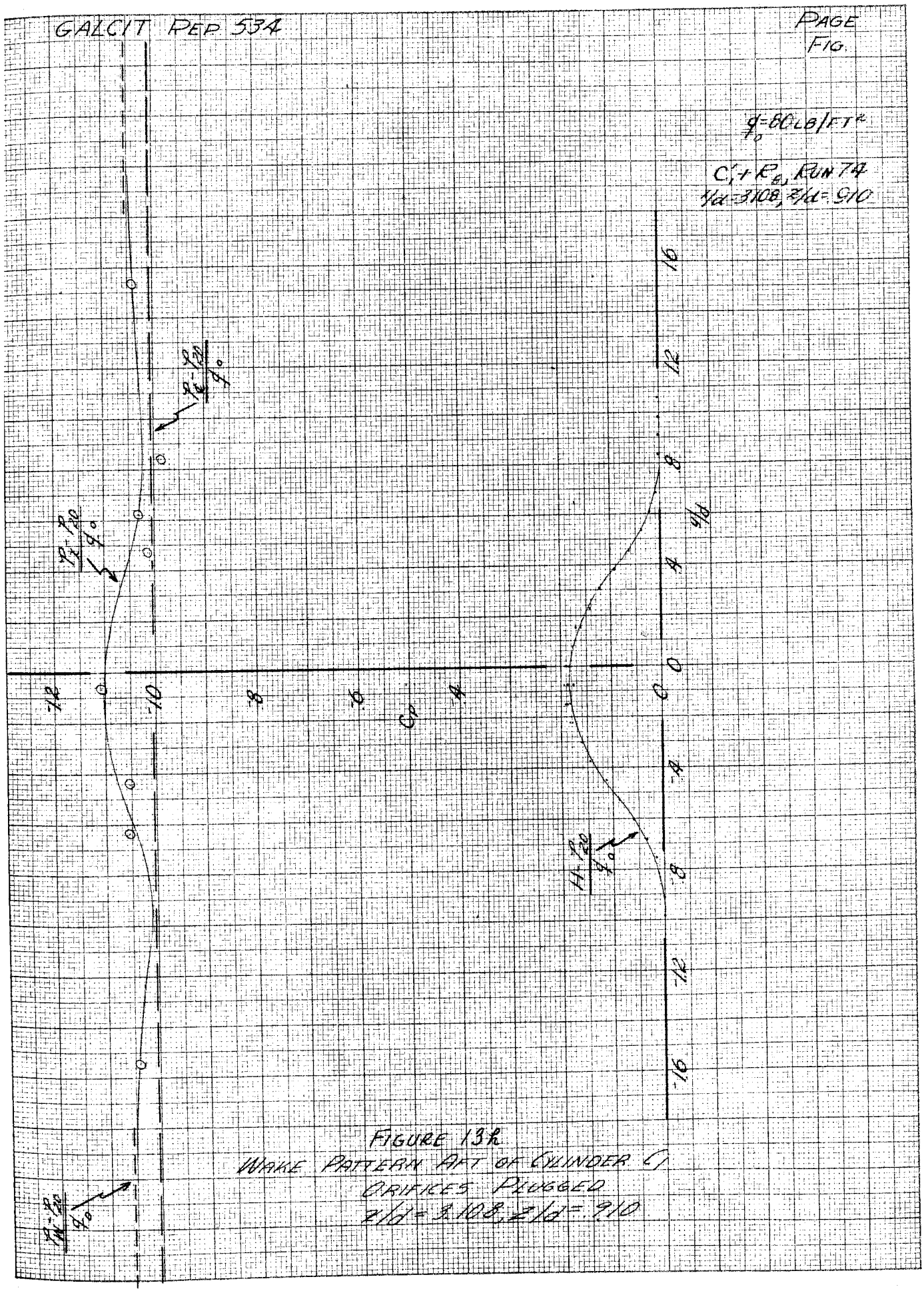

FIGURE 13k
WAKE PATTERN AFT OF CYLINDER C'
ORIFICES PLUGGED
R/d=3108, z/d=.910

$q_o = 80 \text{ LB/FT}^2$

$C_1 + R_8$, RUN 74
$x/d = 3.108$, $y/d = 1.364$

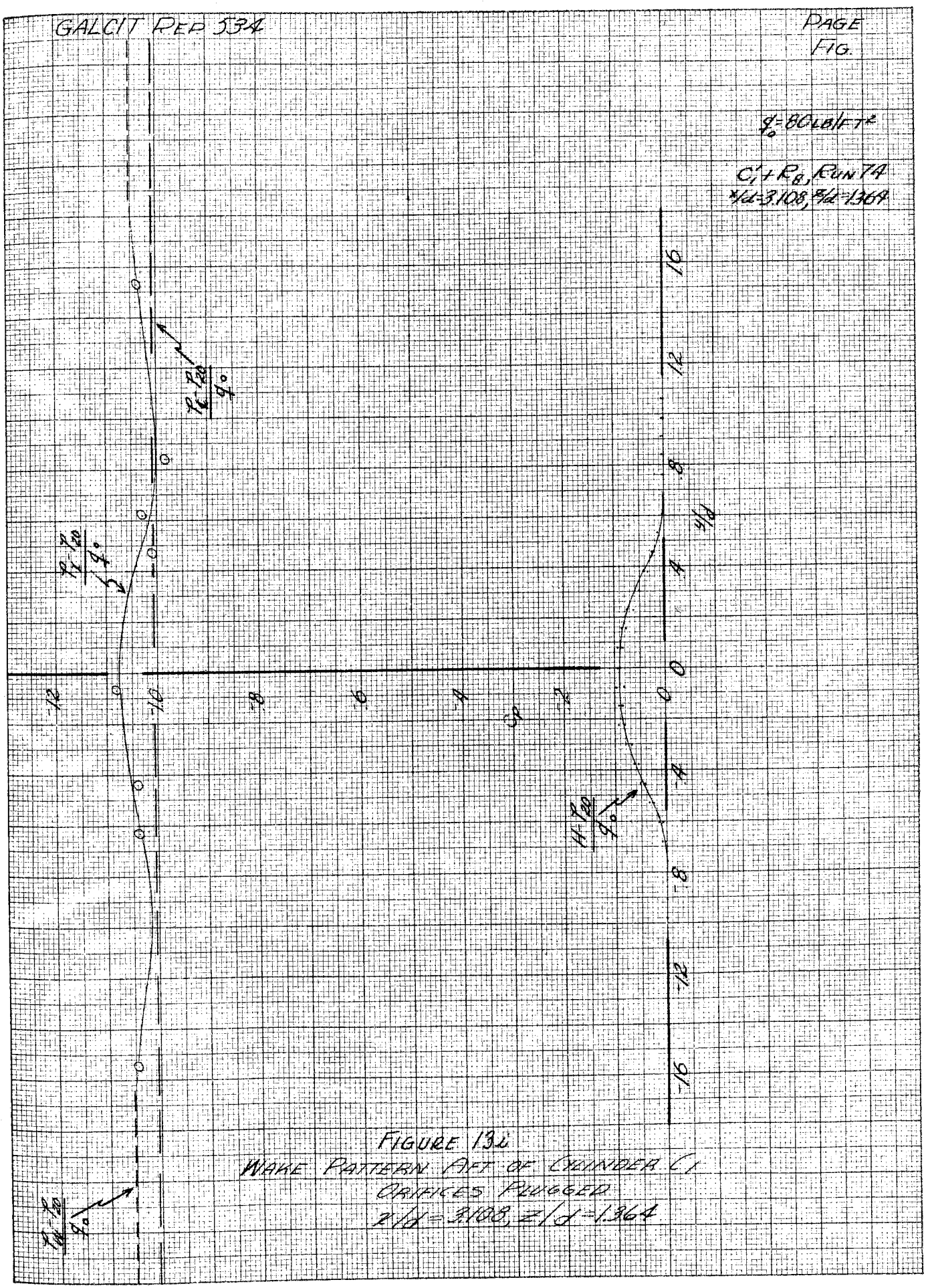

FIGURE 13.2
WAKE PATTERN AFT OF CYLINDER C1
ORIFICES PLUGGED
$x/d = 3.108$, $z/d = 1.364$

GALCIT REP 534

PAGE
FIG.

$q_0 = 60$ LB/FT^2

C'+R$_B$, RUN 74
$x/d = 3.108$, $z/d = 1.819$

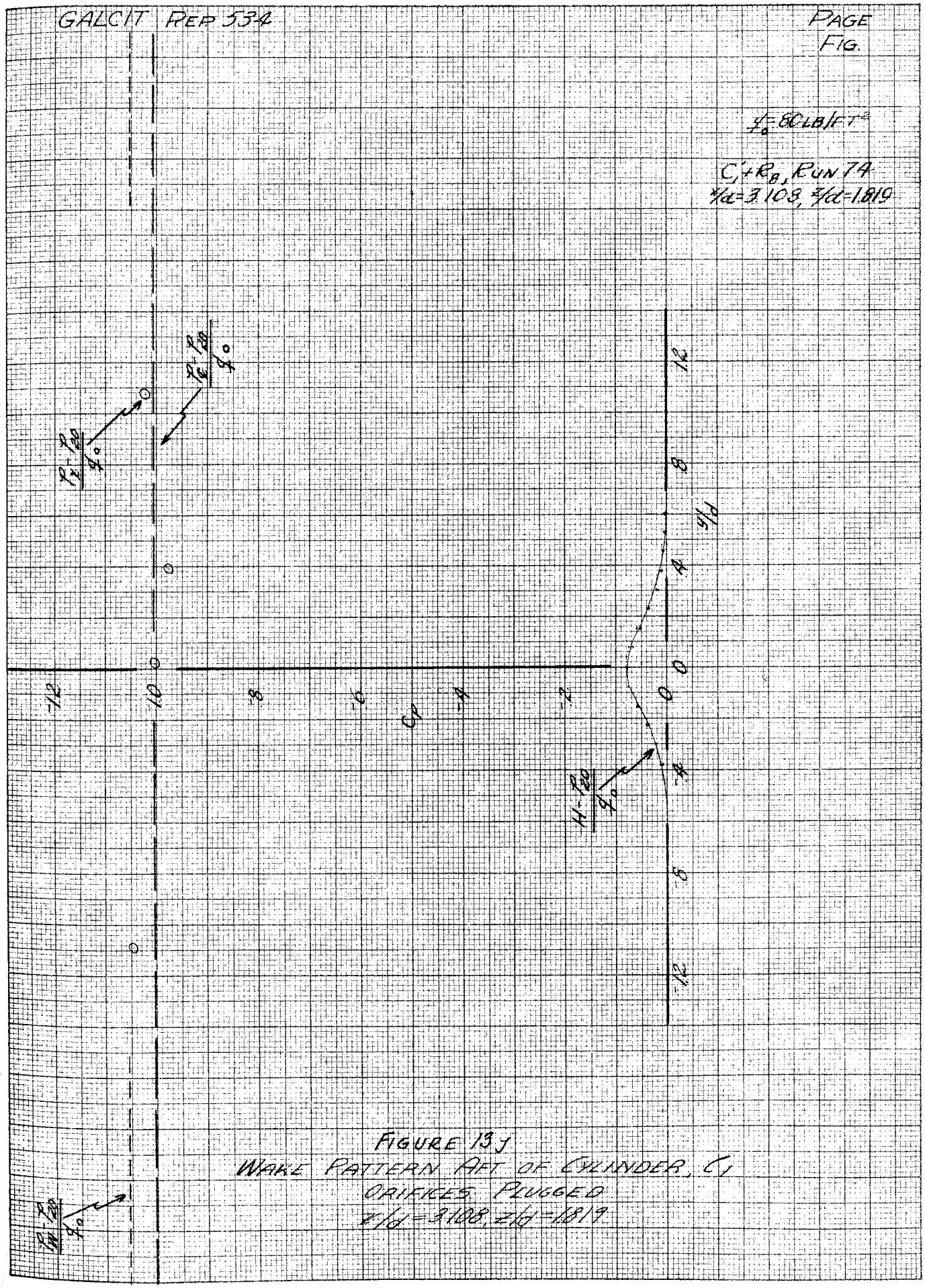

FIGURE 13j
WAKE PATTERN AFT OF CYLINDER, C'
ORIFICES PLUGGED
$x/d = 3.108$, $z/d = 1.819$

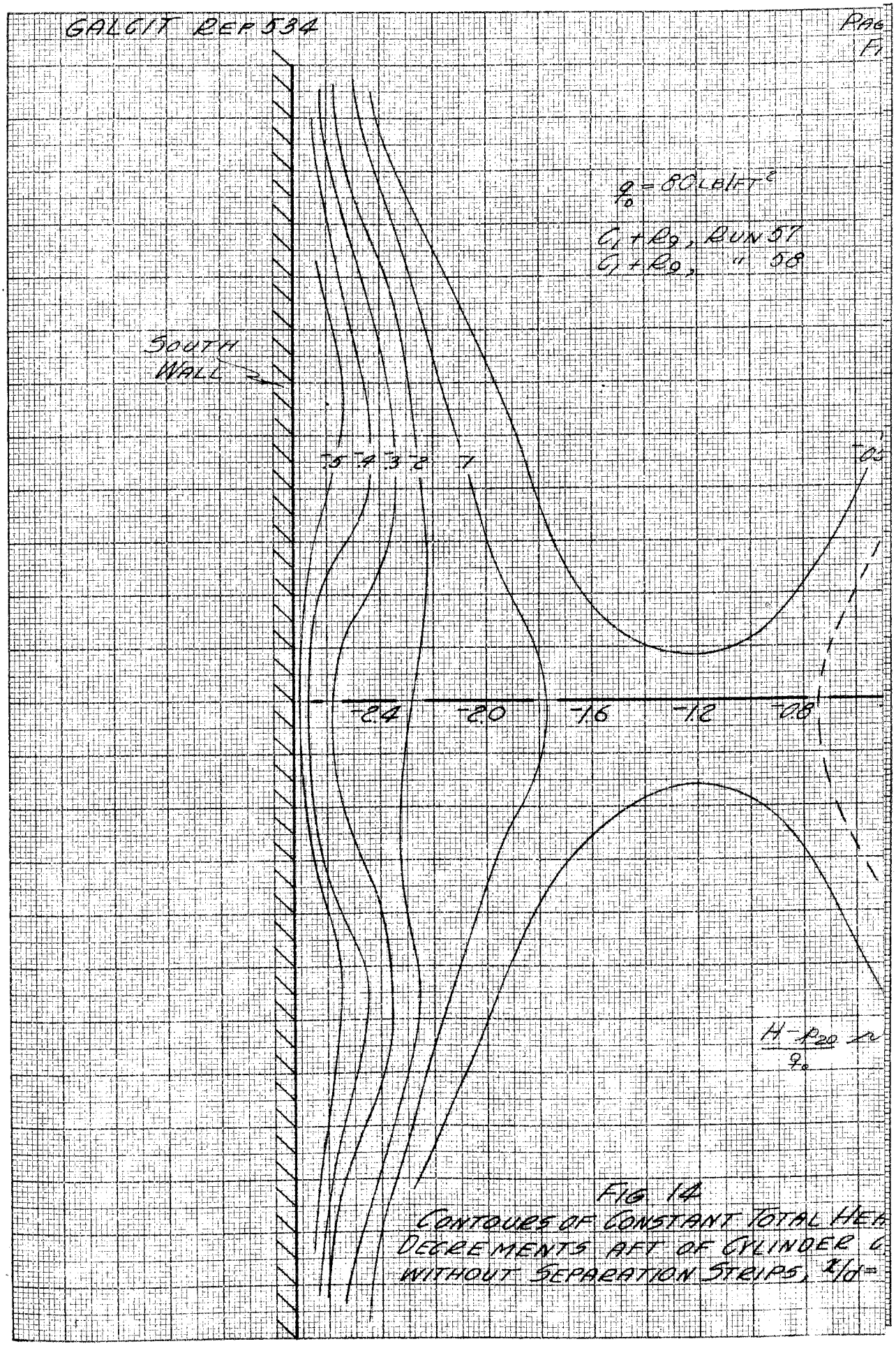

FIG 14
CONTOURS OF CONSTANT TOTAL HEA
DECREMENTS AFT OF CYLINDER C
WITHOUT SEPARATION STRIPS, x/d=

GALCIT REF 534

PAGE
FIG.

$q_0 = 80$ LBS/FT^2
$G_1 + R_9$, RUN 57
$G_1 + R_9$, " 58

SOUTH WALL

NORTH WALL

-5 -4 -3 -2 -1

-.05 -.10

-.35

-.33

$\frac{H - p_{20}}{q_0}$

FIG 14
CONTOURS OF CONSTANT TOTAL HEAD
DOWNSTREAM OF AFT OF CYLINDER G_1
WITHOUT SEPARATION STRIPS, $x/d = 5.837$

GALCIT REP 538

PAGE
FIG

$q_0 = 80 \text{ lb/ft}^2$

C₁-C₂ RUN 7
$x/d = 4.927$, $z/d = 9.16$

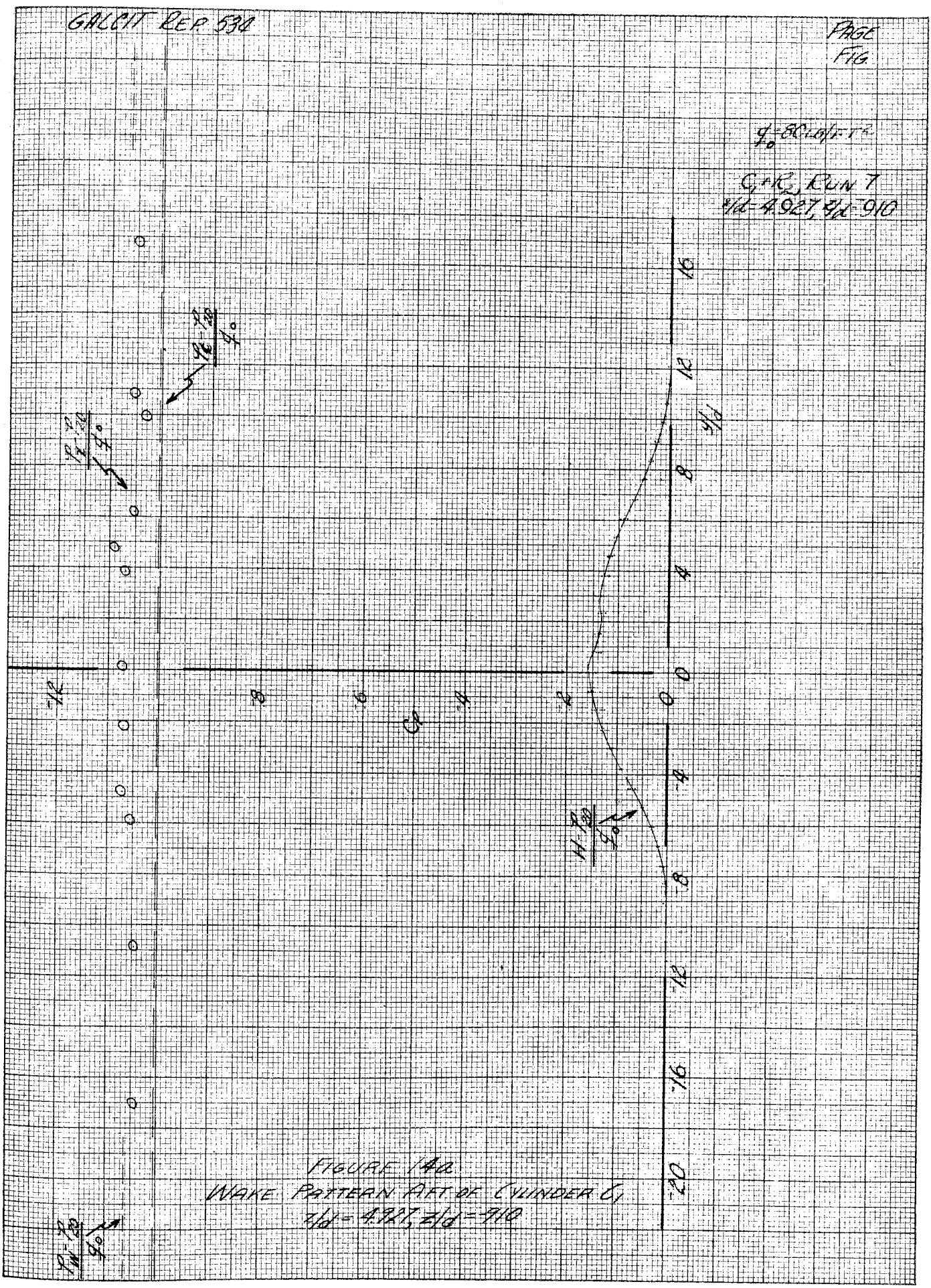

FIGURE 14a
WAKE PATTERN AT OF CYLINDER C_1
$x/d = 4.927$, $z/d = 9.16$

GALCIT REP 534

PAGE
FIG.

$q_0 = 80 \text{ LB/FT}^2$

$C_1 + R_2$, RUN 57
$x/d = 5.837$, $z/d = 7.819$

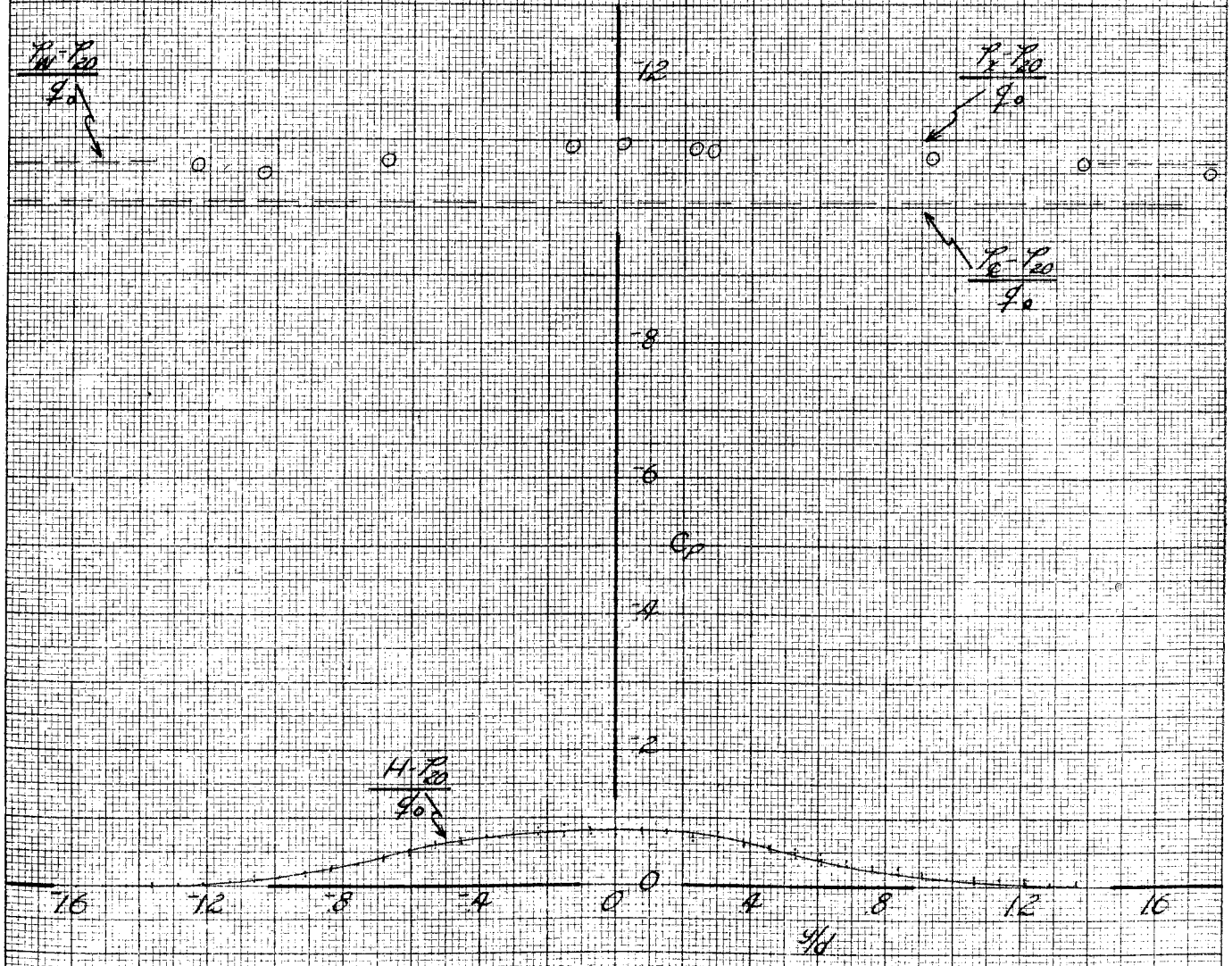

FIGURE 146
WAKE PATTERN AFT OF CYLINDER C
$z/d = 5.837$, $z/d = 7.819$

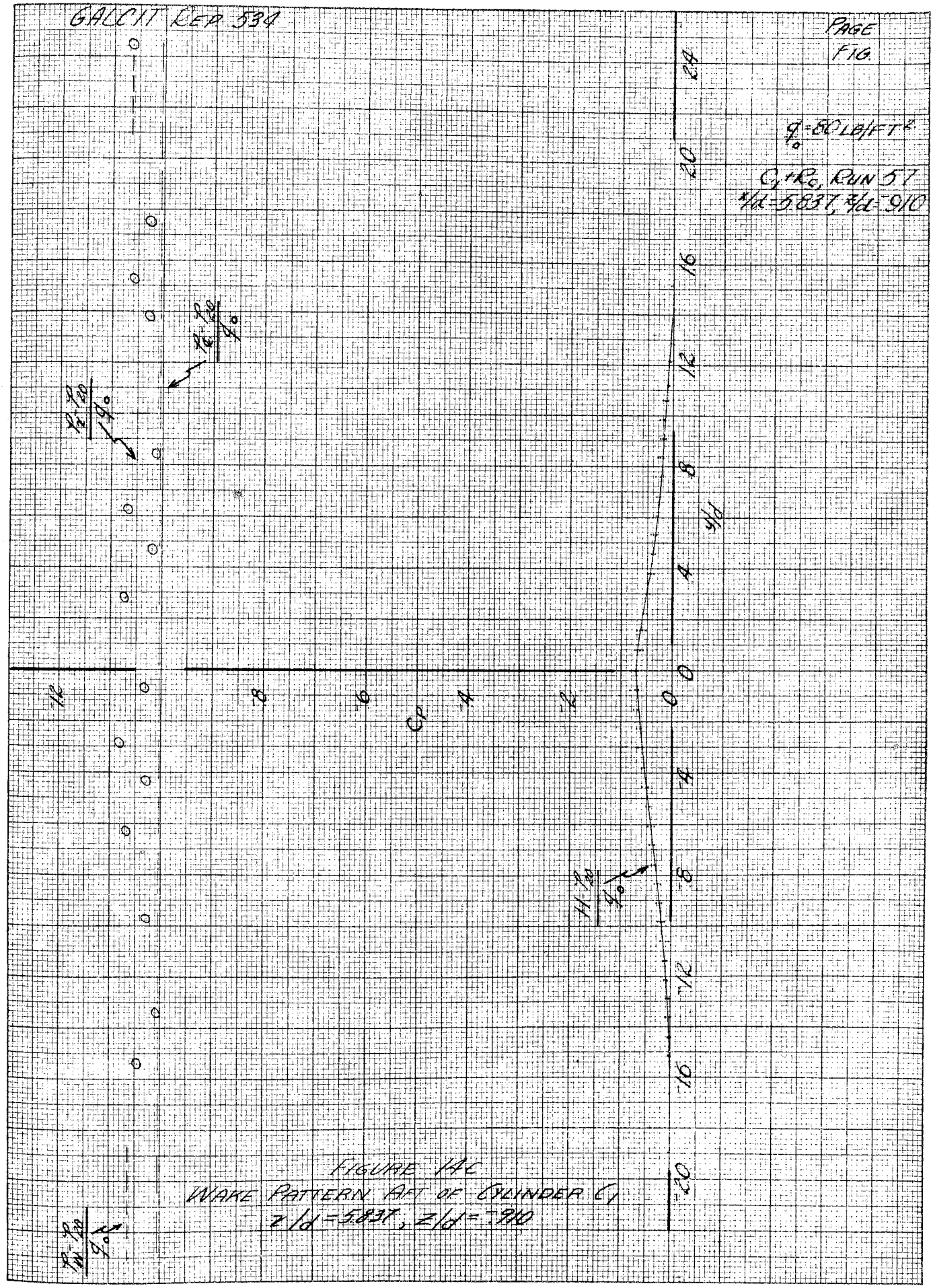

FIGURE 14C
WAKE PATTERN AFT OF CYLINDER C_1
x/d = 5.837, z/d = 7.80

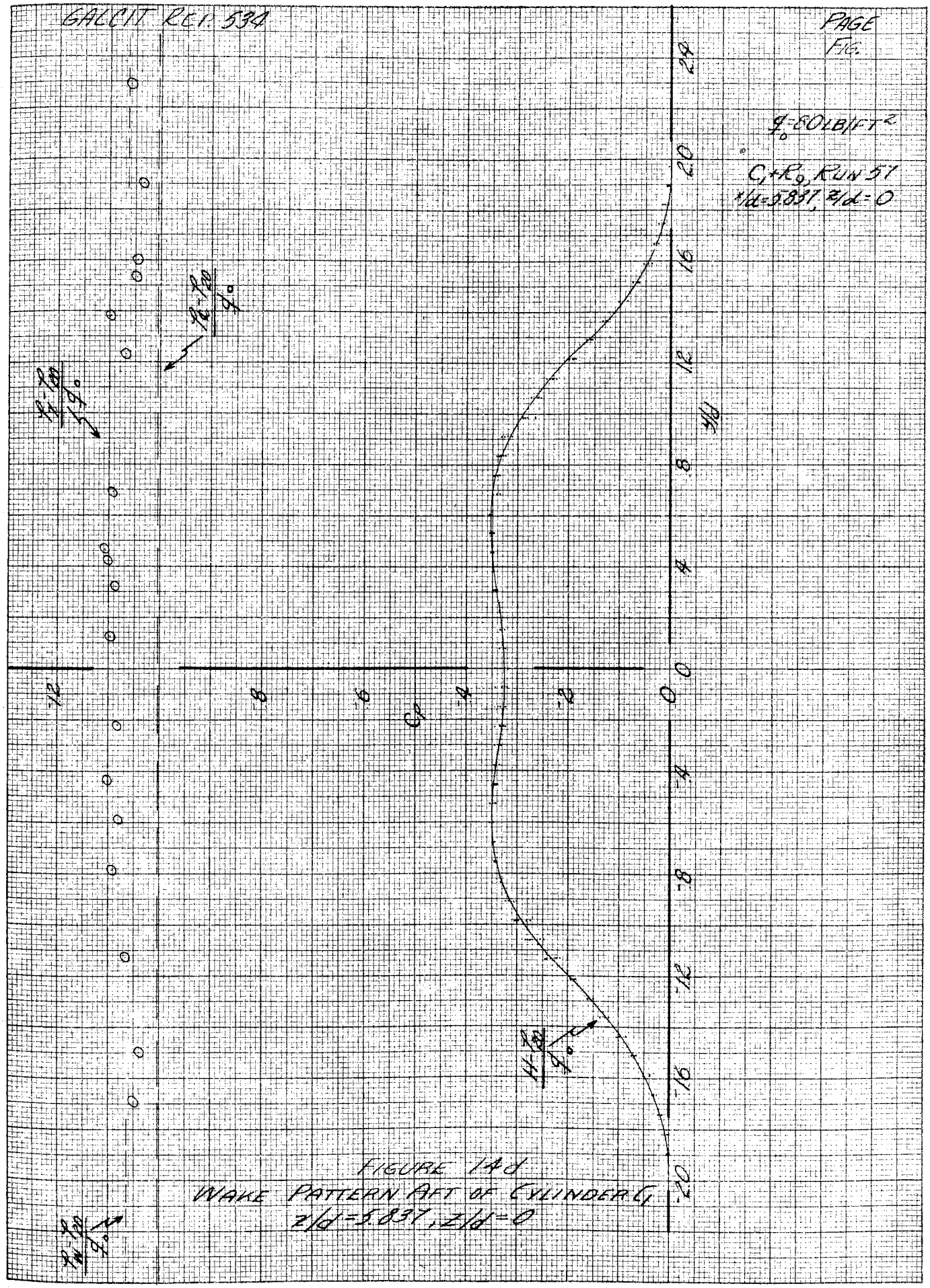

FIGURE 140
WAKE PATTERN AFT OF CYLINDER C₁
z/d = 0.837, z/d = 0

GALCIT REP 534

PAGE
FIG.

$q_0 = 80$ LBS/FT^2

C_1 AC$_0$, RUN 57
$x/d = 5.83$T, $z/d = .91$C

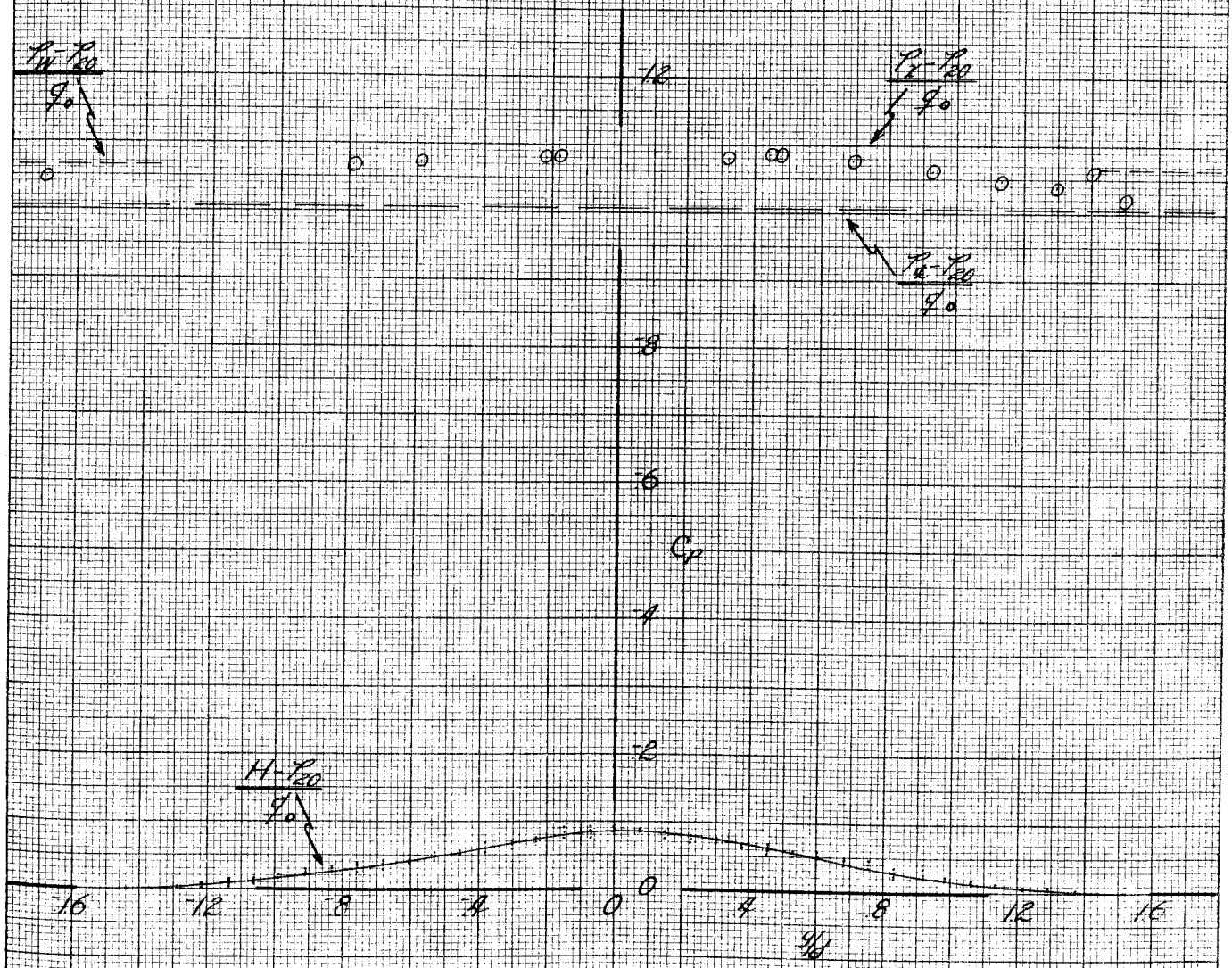

FIGURE 14e
WAKE PATTERN AFT OF CYLINDER C$_1$
$z/d = 5.83$T, $z/d = .910$

GALCIT REP 534

PAGE
F16

$q_o = 80$ LB/FT^2

C_1 + R_0, RUN 57
$x/d = .5831$, $z/d = .1819$

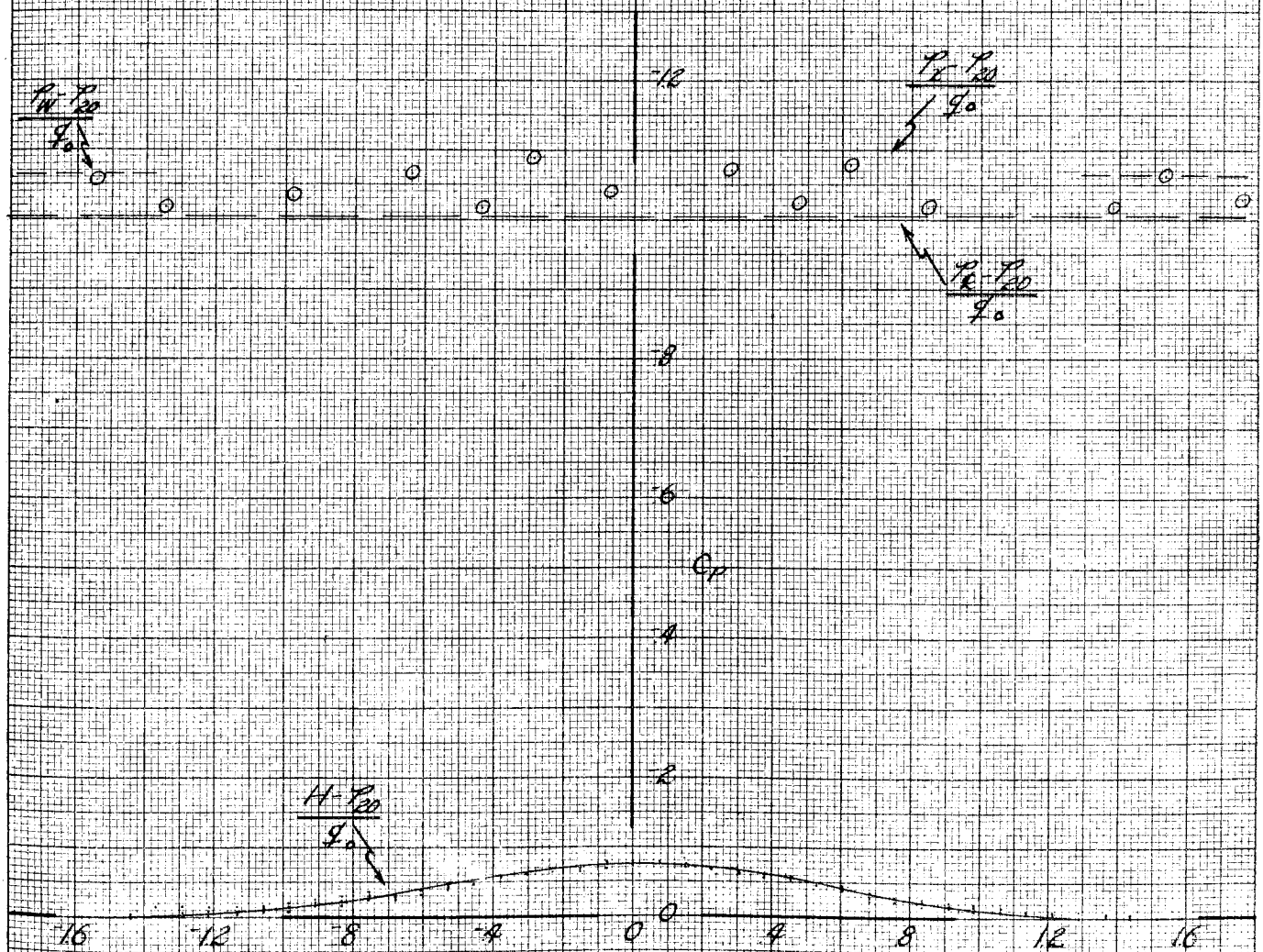

FIGURE 14F
WAKE PATTERN AFT OF CYLINDER C_1
$x/d = .5831$, $z/d = .1819$

GALCIT REP 534

PAGE
FIG.

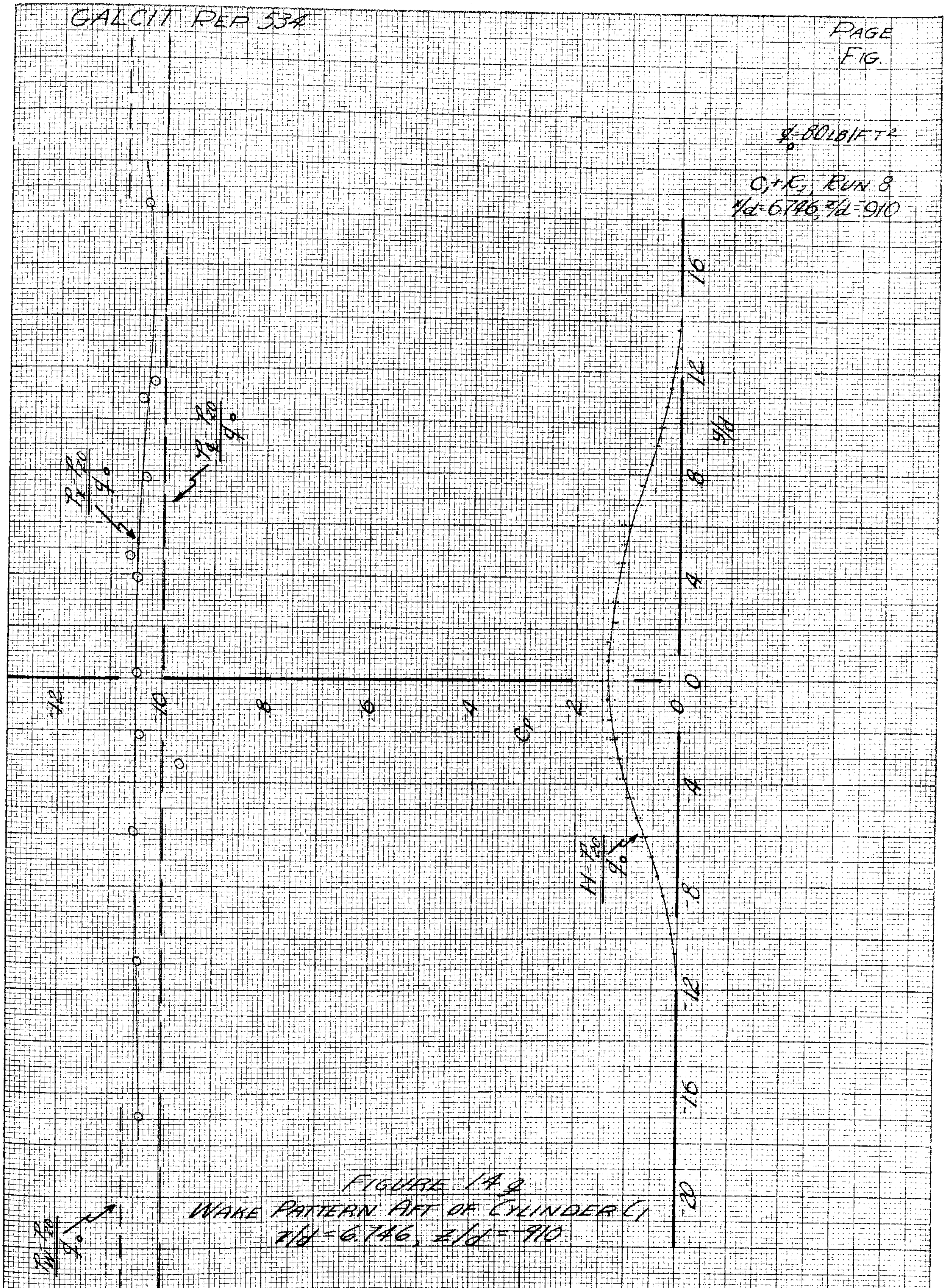

FIGURE 14a
WAKE PATTERN AFT OF CYLINDER C1
y/d = 6.746, z/d = .910

GALCIT REP 534

PAGE
FIG.

$q_0 = 80$ LB/FT²

C, T, & R, RUN 14
$x/d = 3.108$, $z/d = .910$

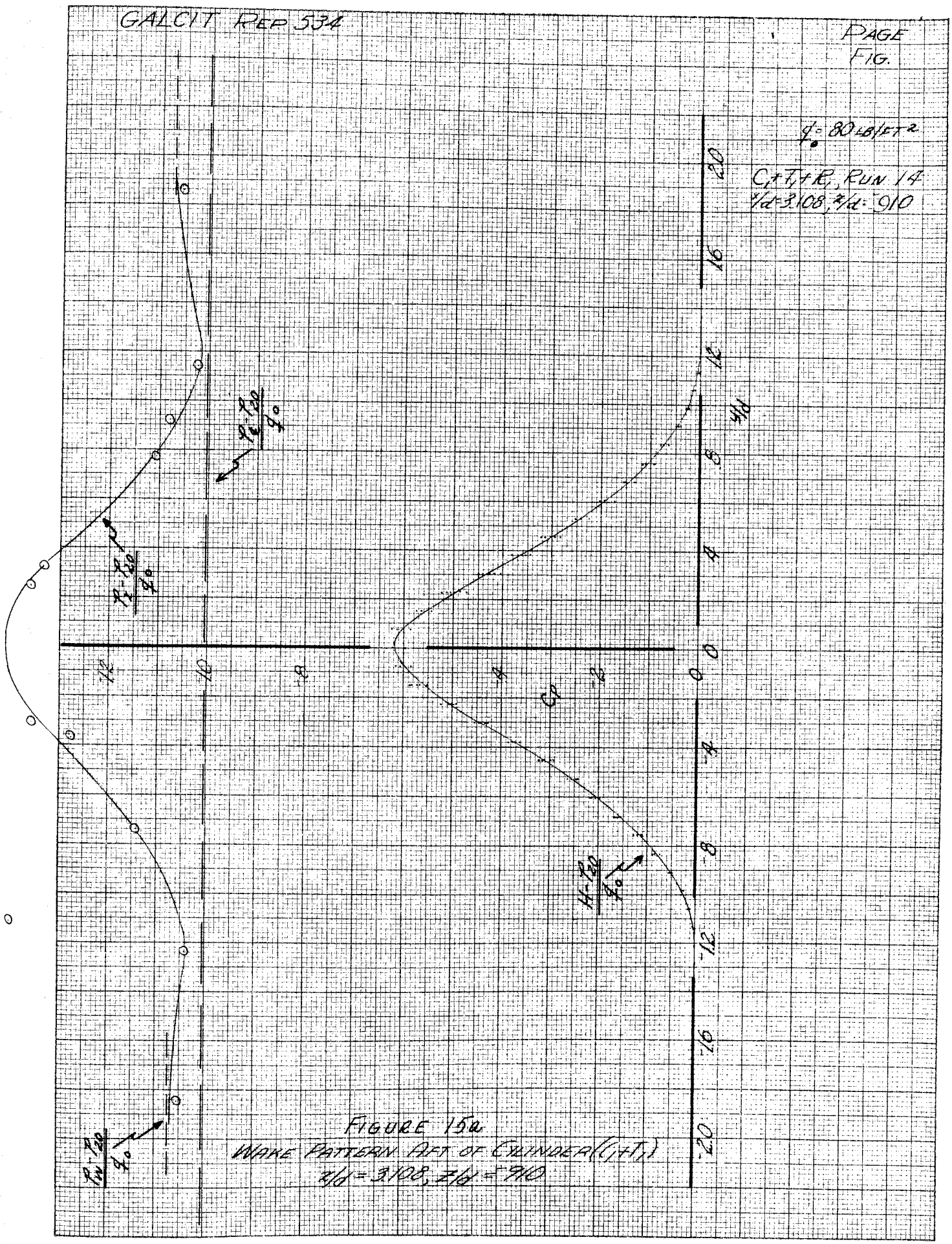

FIGURE 15a
WAKE PATTERN AT 0° OF CYLINDER (C, T, R)
$x/d = 3.108$, $z/d = .910$

GALCIT REP 534

PAGE
FIG.

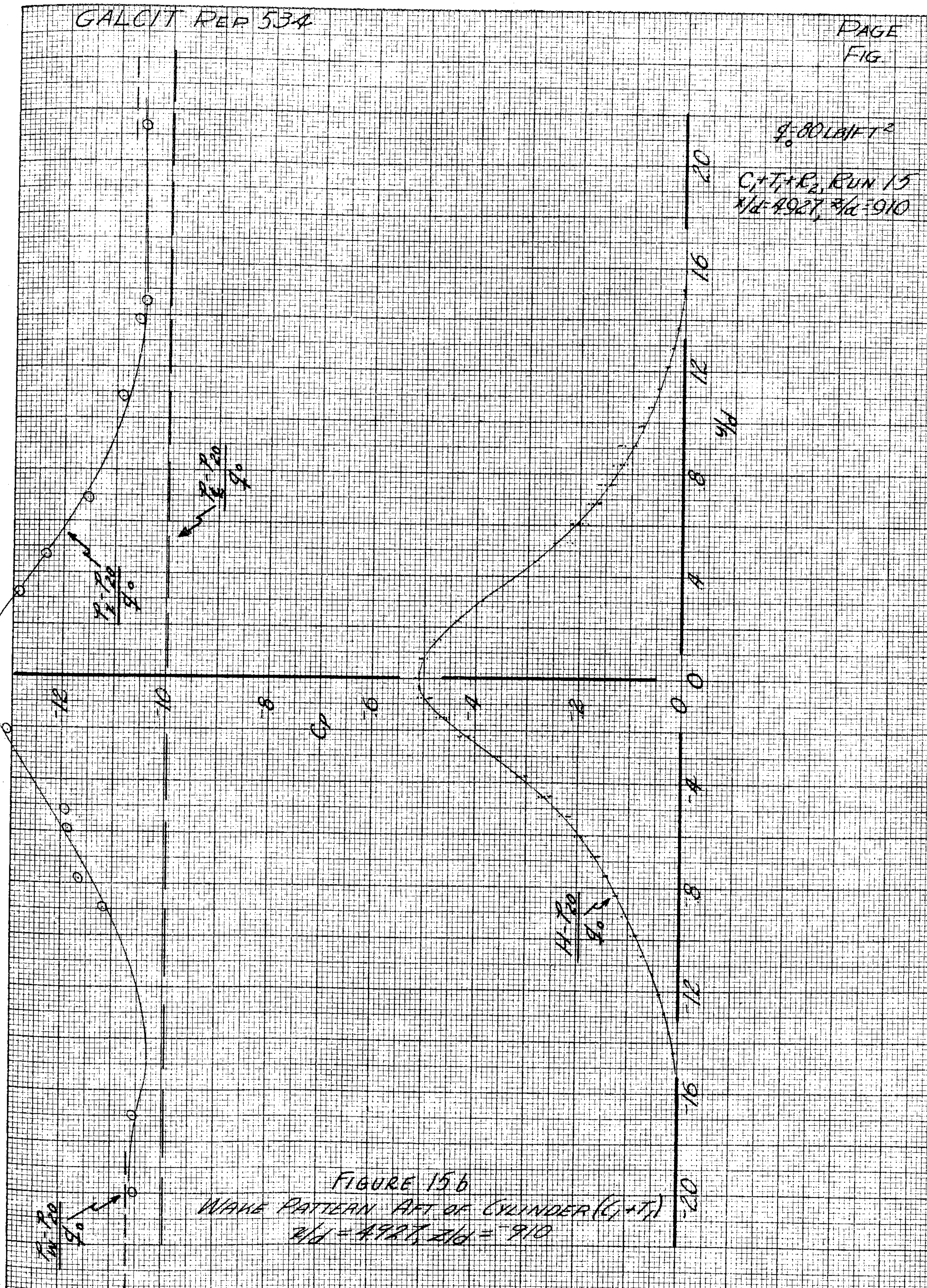

FIGURE 15b
WAKE PATTERN AFT OF CYLINDER (C_1+T_1)
x/d = 4.927, z/d = -.910

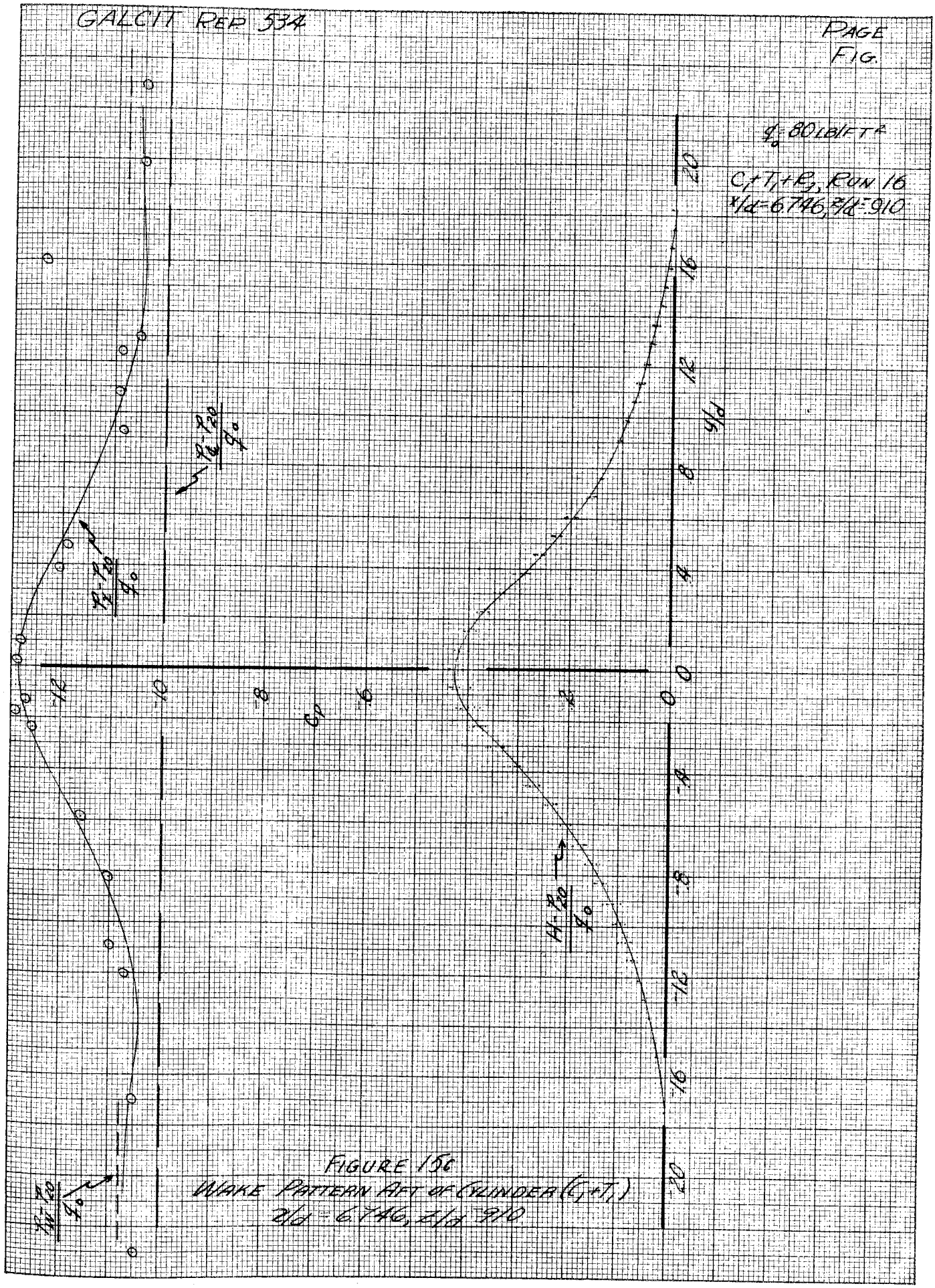

FIGURE 156
WAKE PATTERN AFT OF CYLINDER ($C_1 + T_1$)
z/d = 6.746, z/d = .910

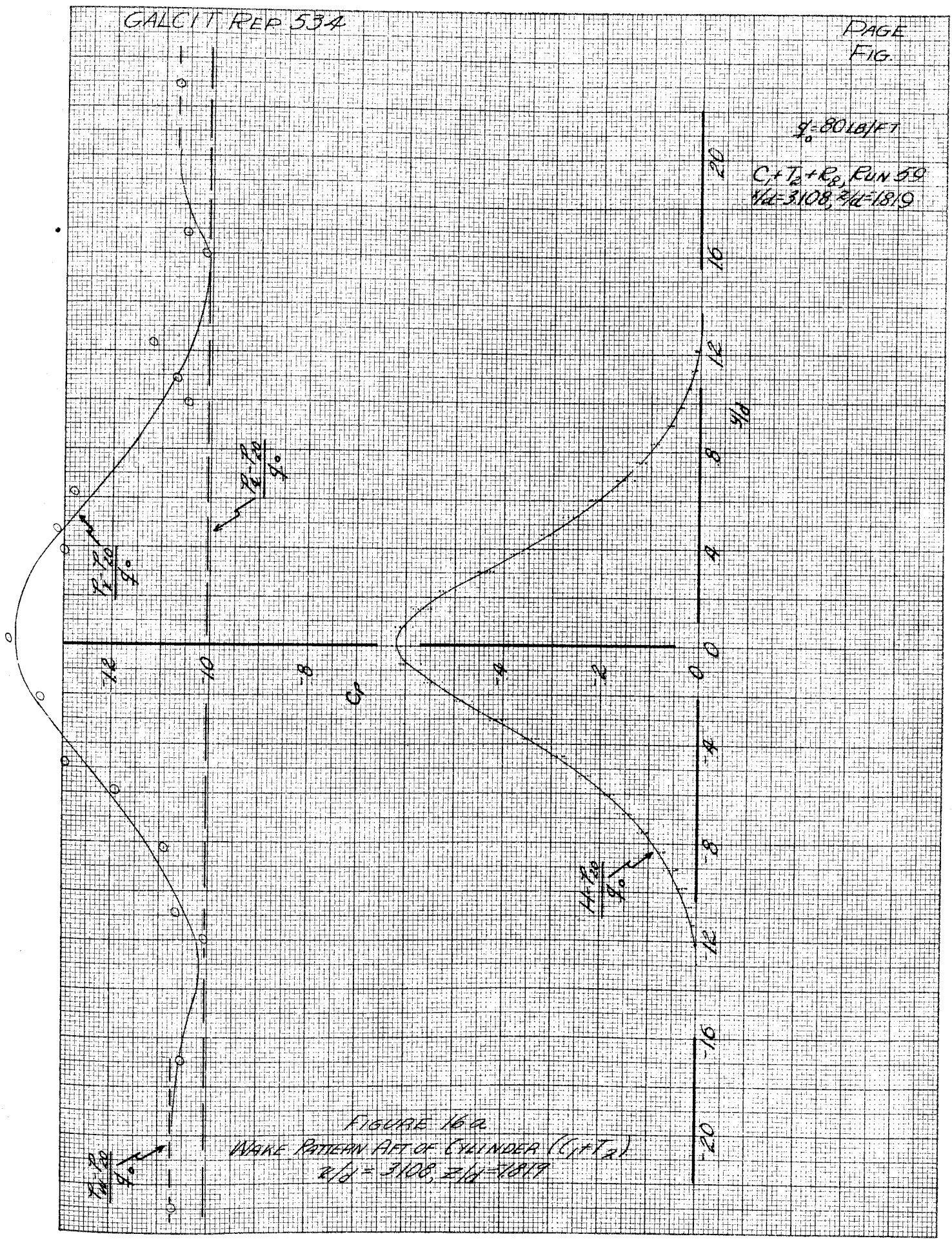

FIGURE 16a.
WAKE PATTERN AFT OF CYLINDER (C_1+T_2)
x/d = 3.108, z/d = 1.819

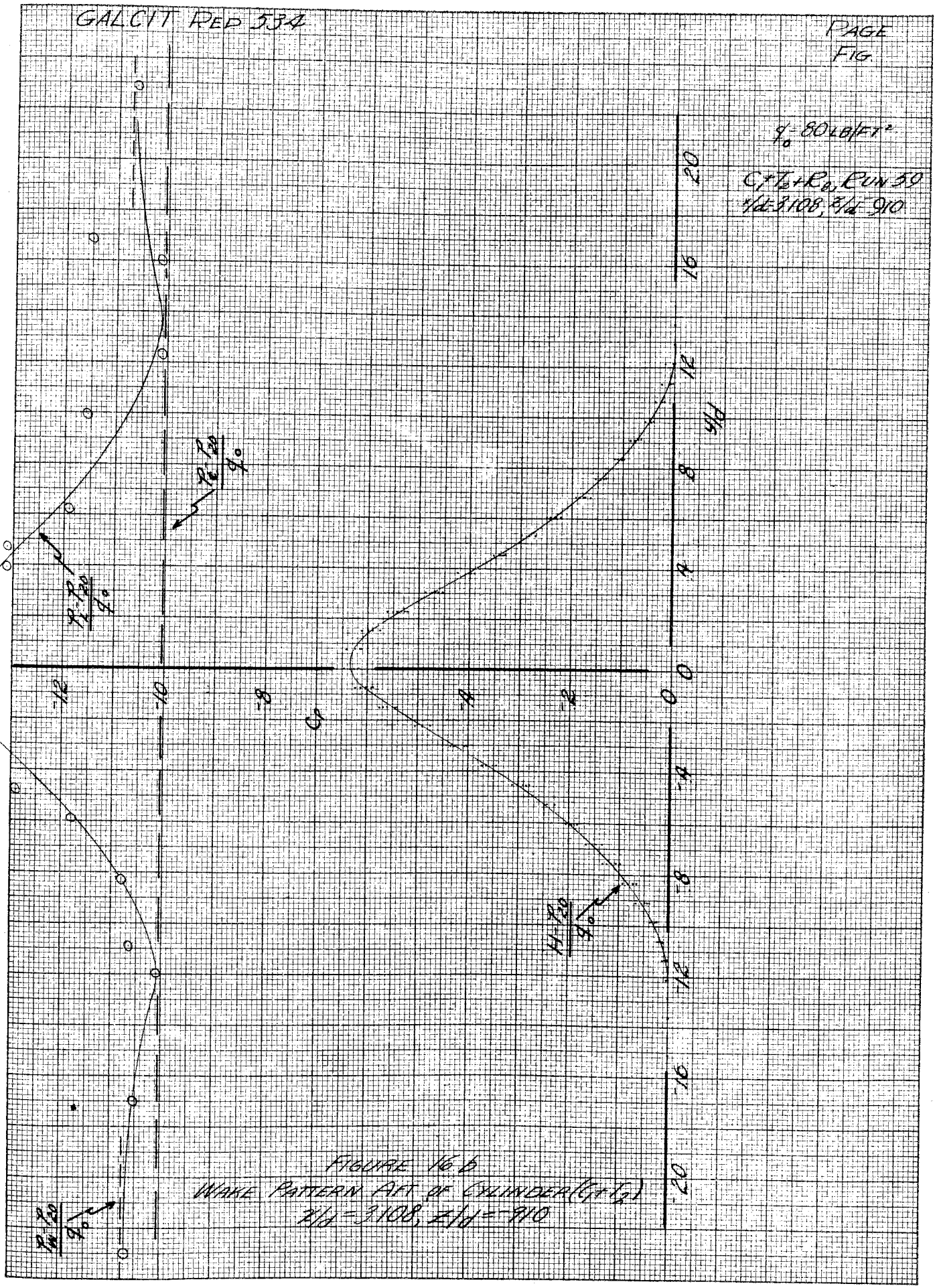

FIGURE 16.b
WAKE PATTERN AFT OF CYLINDER ($C_1 T_0 + C_2$)
x/d = 3.108, z/d = .910

GALCIT REP 534

PAGE
FIG.

q_0 80 LB/FT²

$C_1 + T_2 + R_0$, RUN 59
$x/d = 3.108$, $z/d = 0$

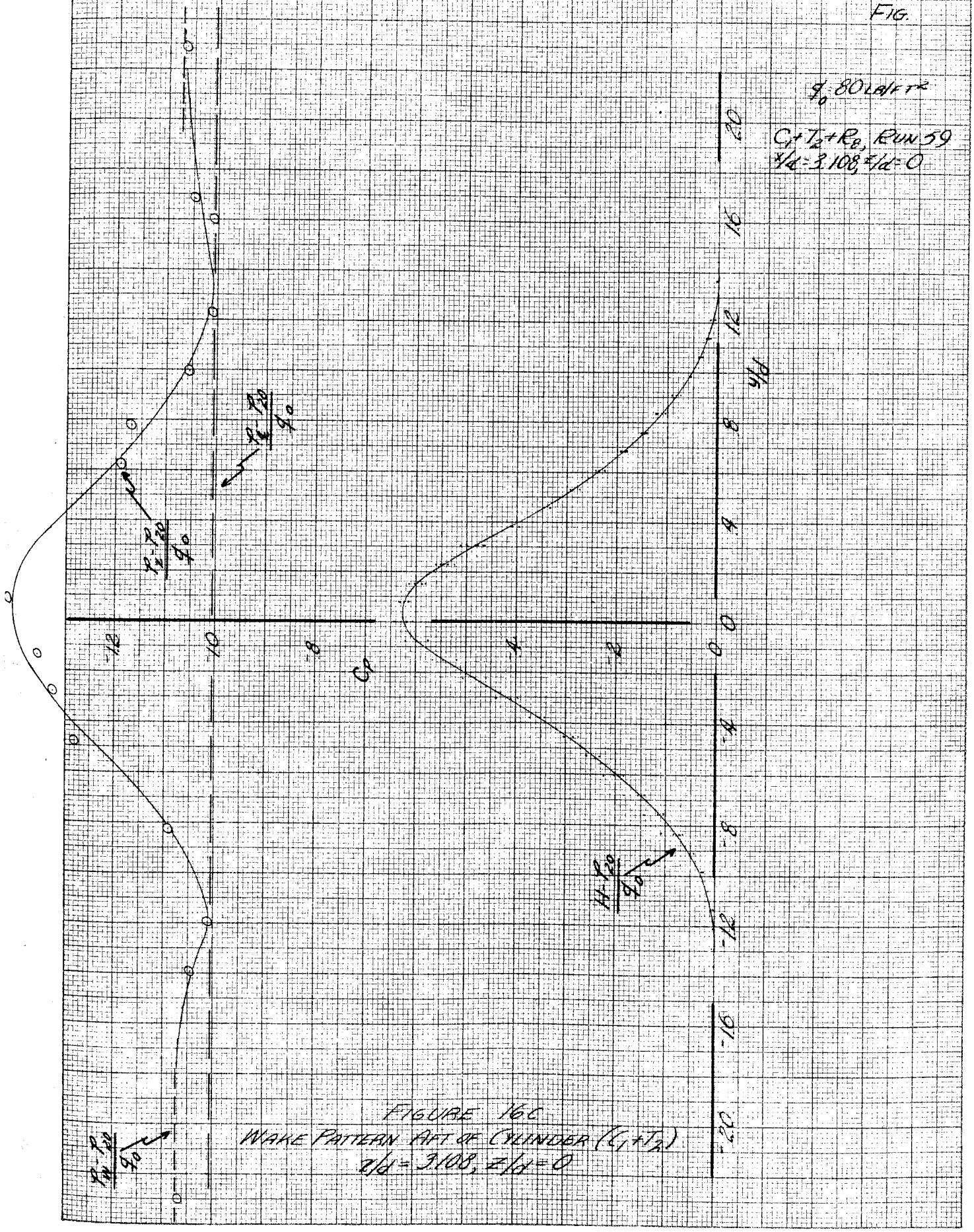

FIGURE 16C
WAKE PATTERN AFT OF CYLINDER ($C_1 + T_2$)
$x/d = 3.108$, $z/d = 0$

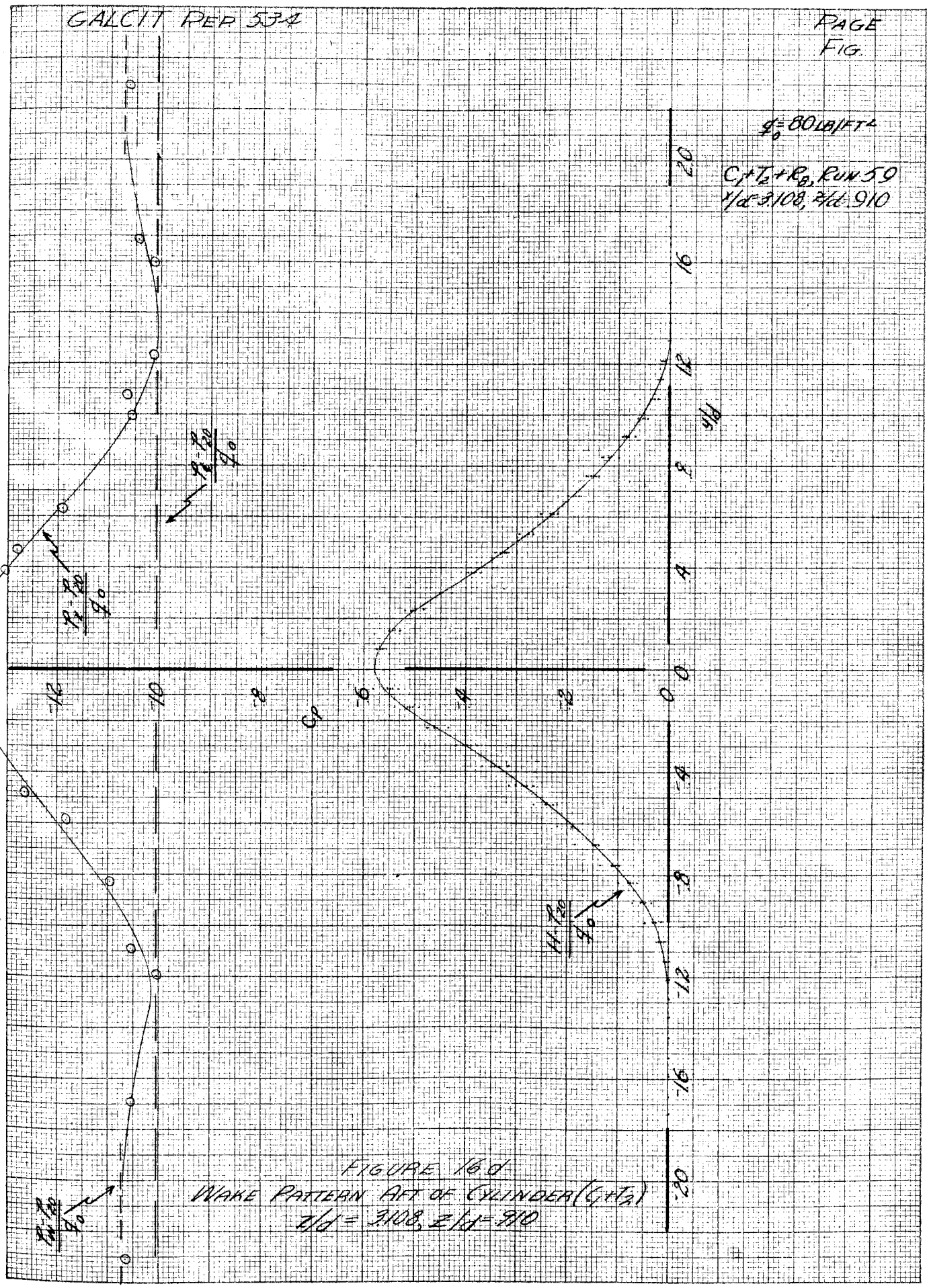

FIGURE 16.0
WAKE PATTERN AFT OF CYLINDER ($C_1 + T_2$)
$x/d = 3.108$, $z/d = .910$

GALCIT REP 534

PAGE
FIG.

$q_0 = 80 \text{ LB/FT}^2$

$C_p = T_2 + R_2$, Run 59
$x/d = 3.108$, $z/d = 1.819$

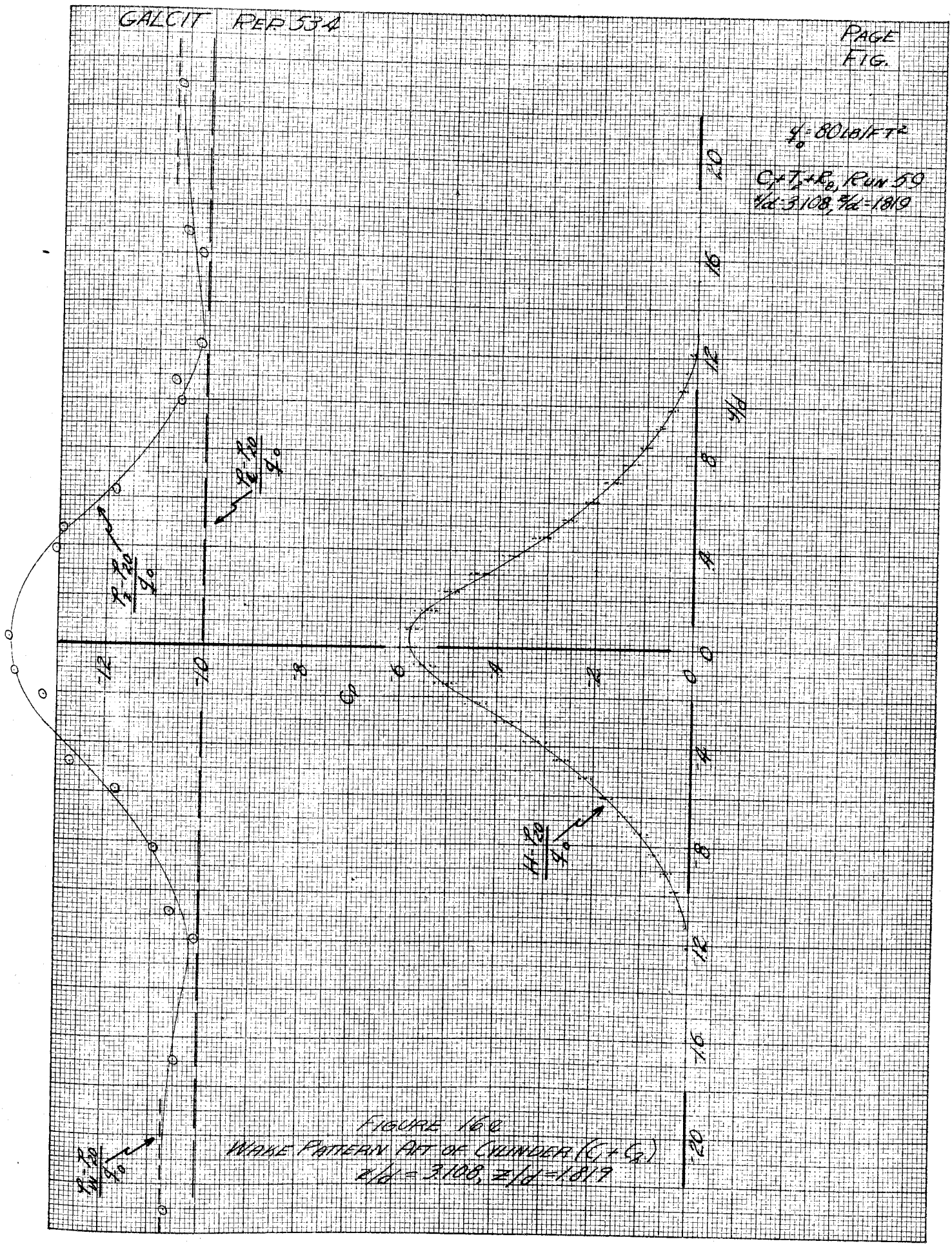

FIGURE 16 C
WAKE PATTERN AT OF CYLINDER ($C_p + C_q$)
$x/d = 3.108$, $z/d = 1.819$

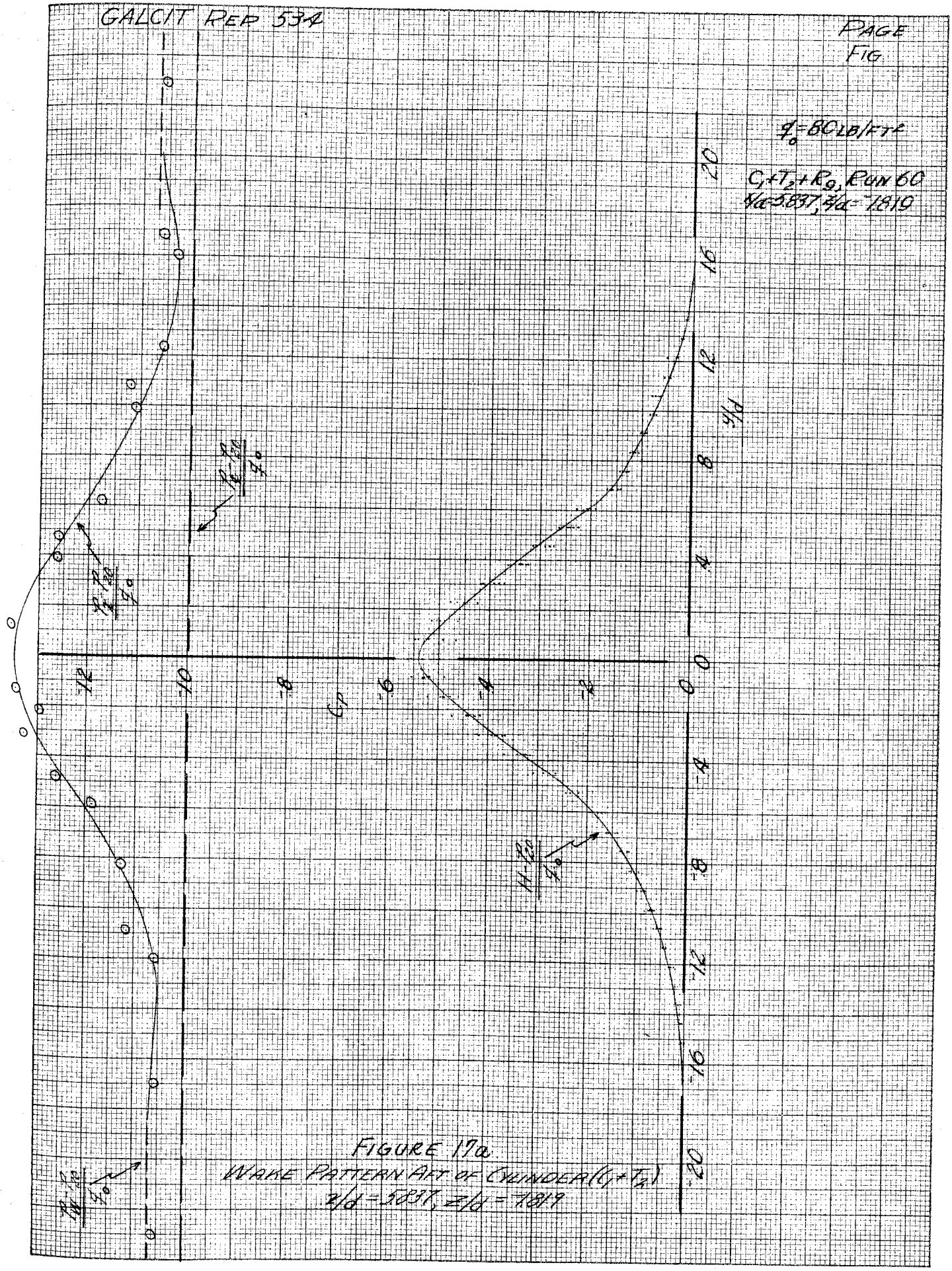

FIGURE 17a
WAKE PATTERN AFT OF CYLINDER (C_1+T_2)
x/a=.3837, z/a=.7819

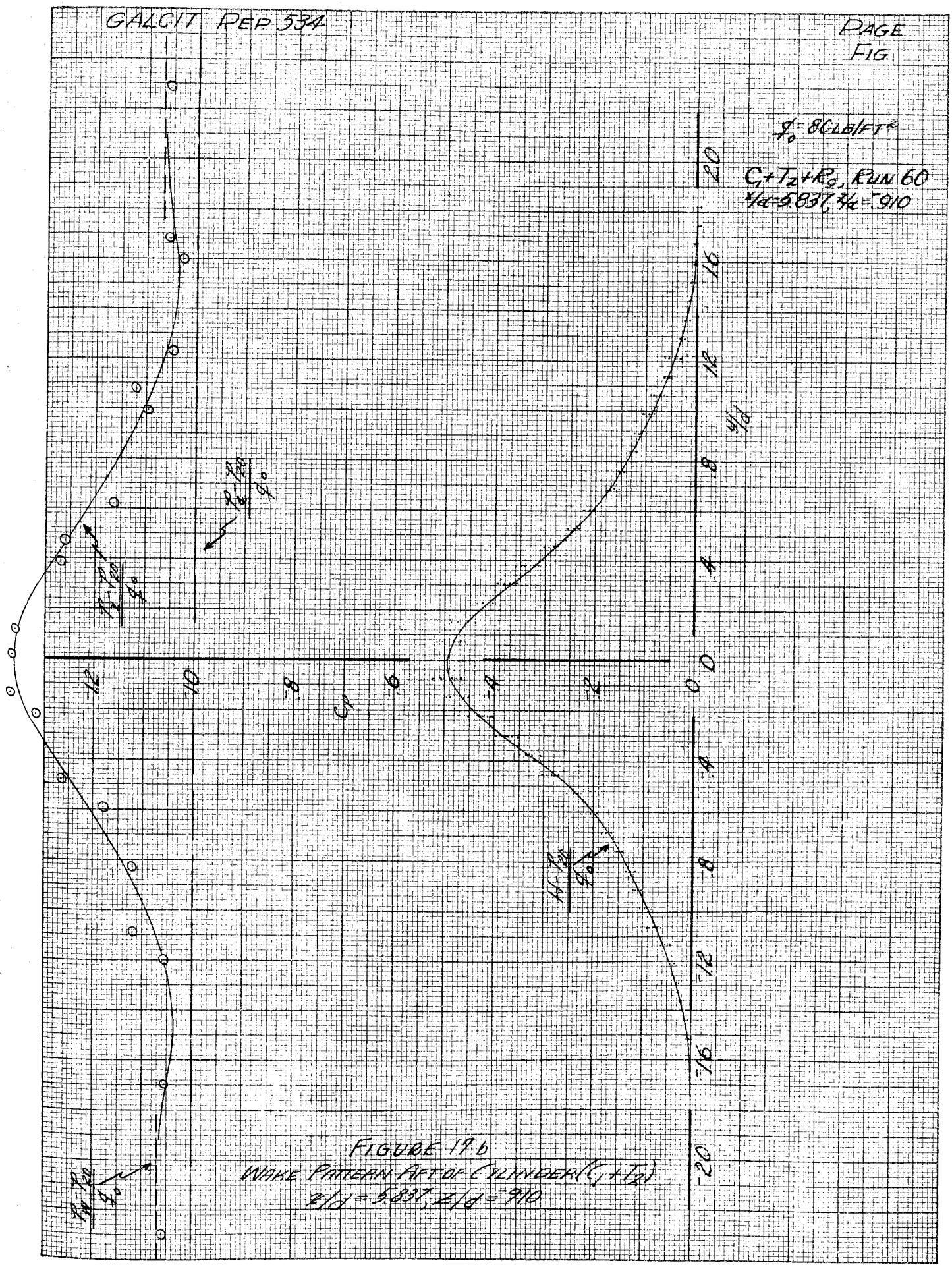

FIGURE 19.b
WAKE PATTERN AFT OF CYLINDER (C_1+T_2)
x/d = 5.837, z/d = .910

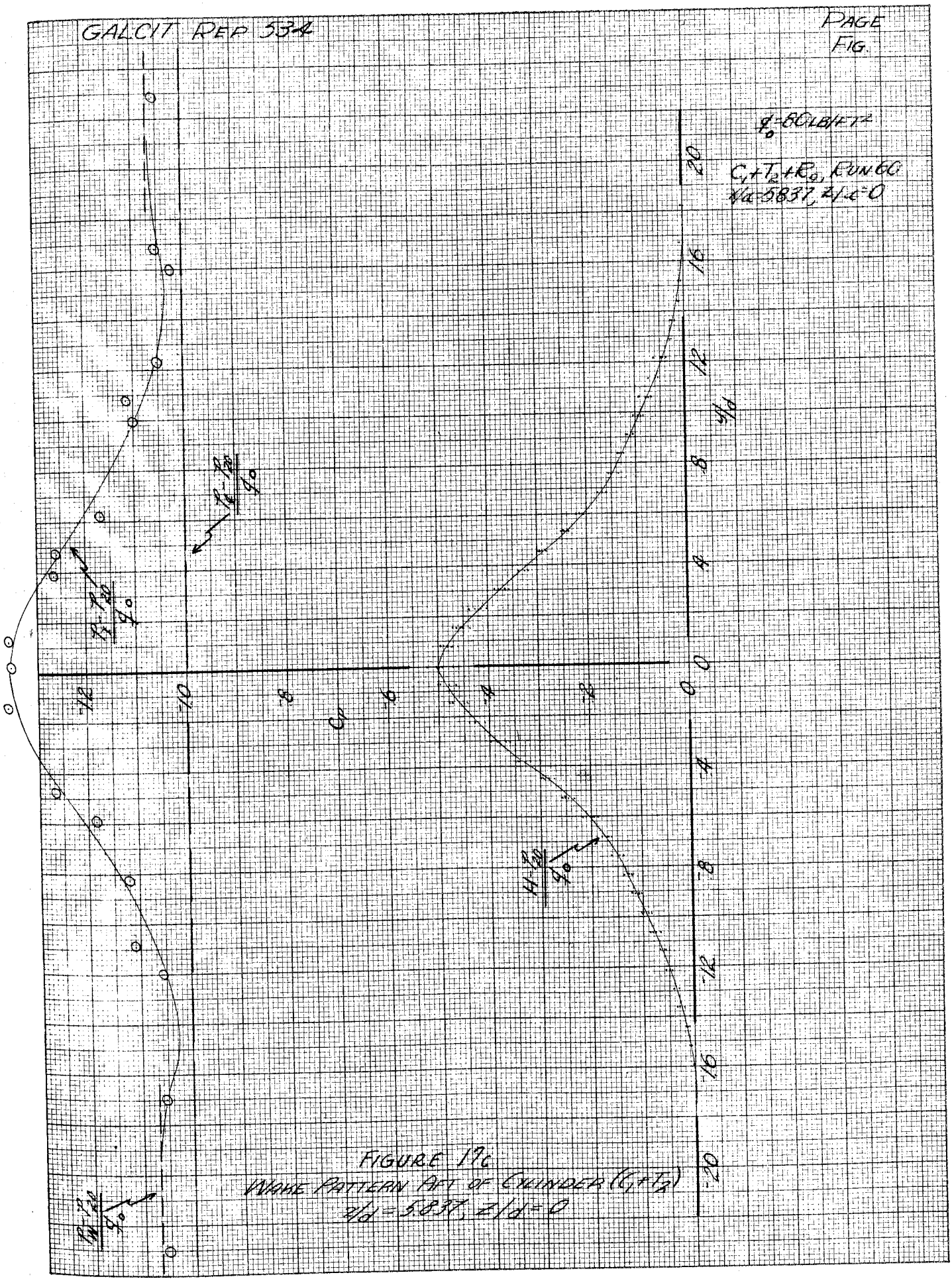

FIGURE 17c
WAKE PATTERN AFT OF CYLINDER (C_1+T_2)
V/d = 5837, Z/d = 0

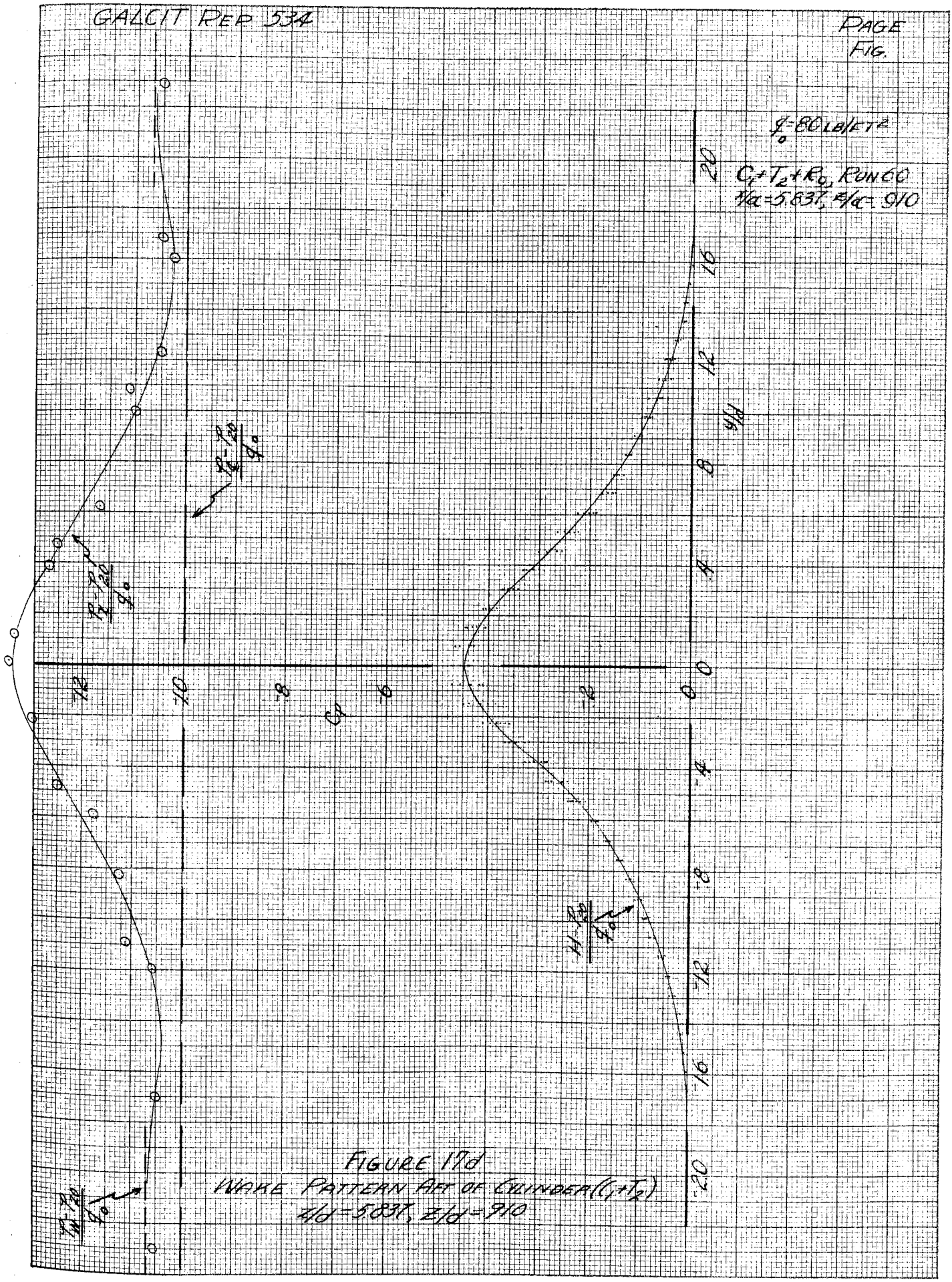

FIGURE 17d
WAKE PATTERN AFT OF CYLINDER (C_1+T_2)
x/d=5.83T, z/d=.910

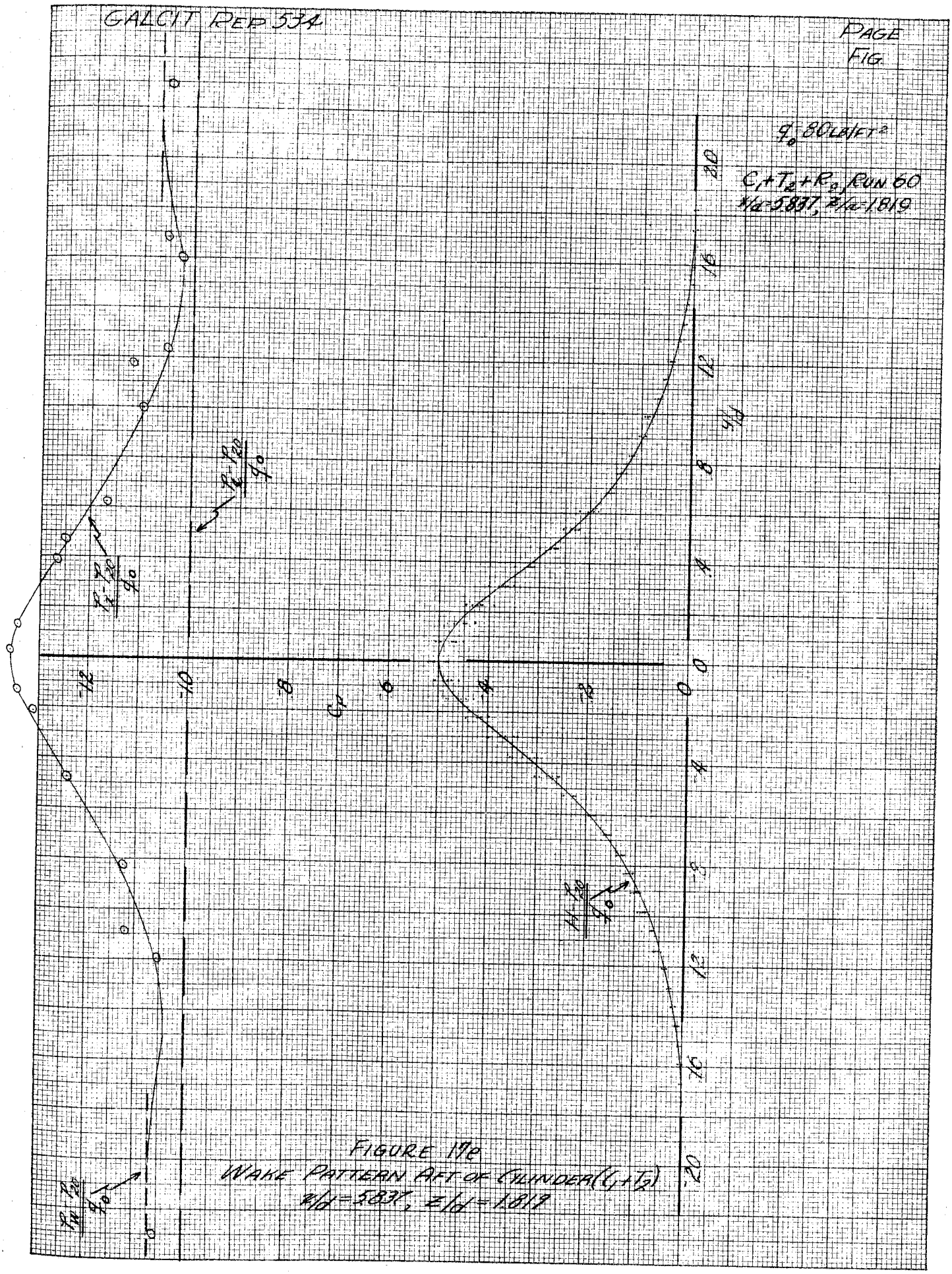

FIGURE 19e
WAKE PATTERN AFT OF CYLINDER(C_1+T_2)
x/d=.5837, z/d=.1819

GALCIT REP 534

PAGE
FIG.

$q_o = 80 LB/FT^2$

$C_1 + T_1 + R_2$, RUN 63
$Y/d = 3.108$, $Z/d = -1.819$

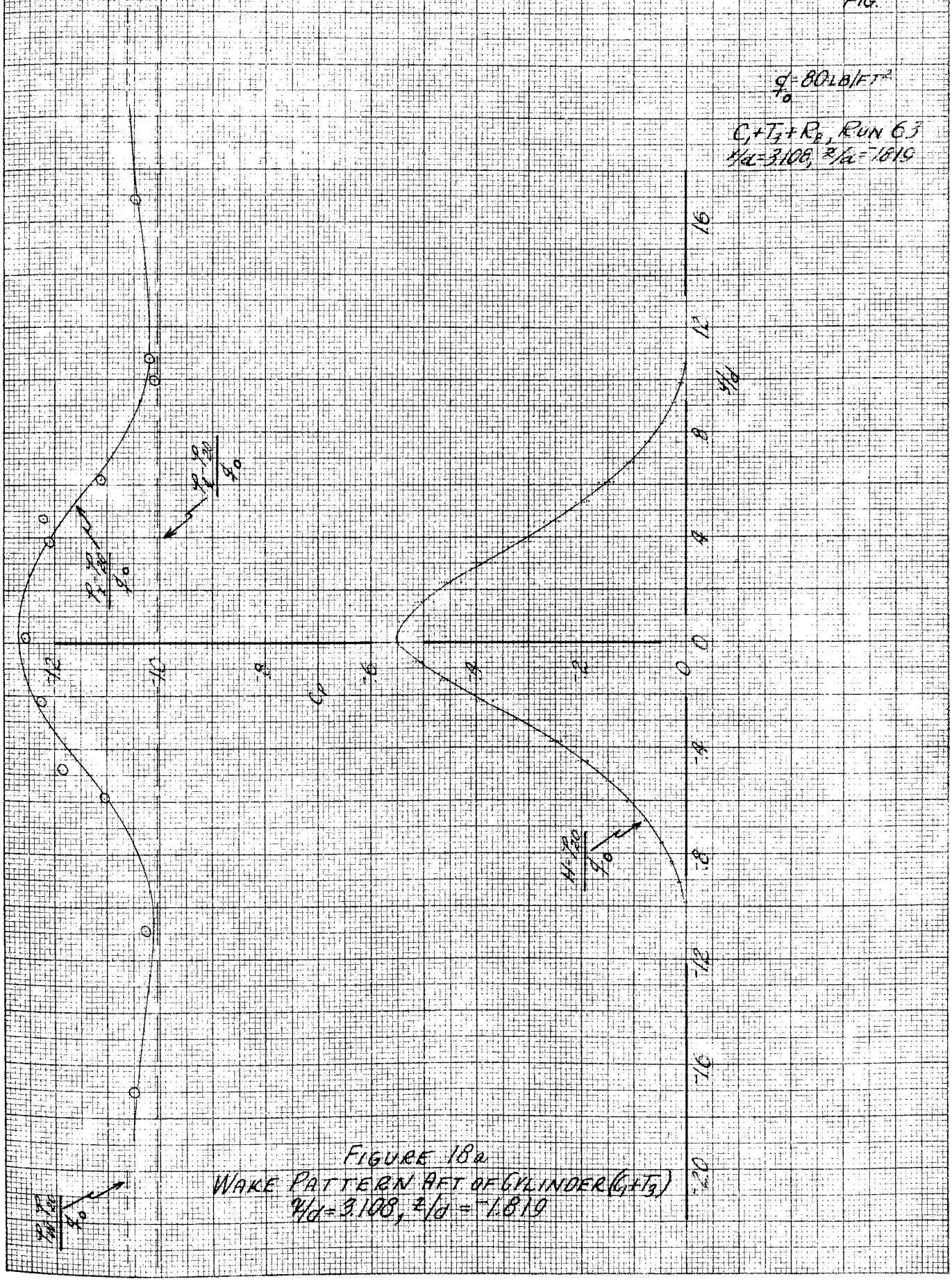

FIGURE 18a
WAKE PATTERN AFT OF CYLINDER ($C_1 + T_1$)
$Y/d = 3.108$, $Z/d = -1.819$

GALCIT REP 534

PAGE
FIG.

$q_0 = 80$ LB/FT²

$C_1 + T_3 + R_8$, RUN 68
$x/d = 3.108$, $z/d = -0.910$

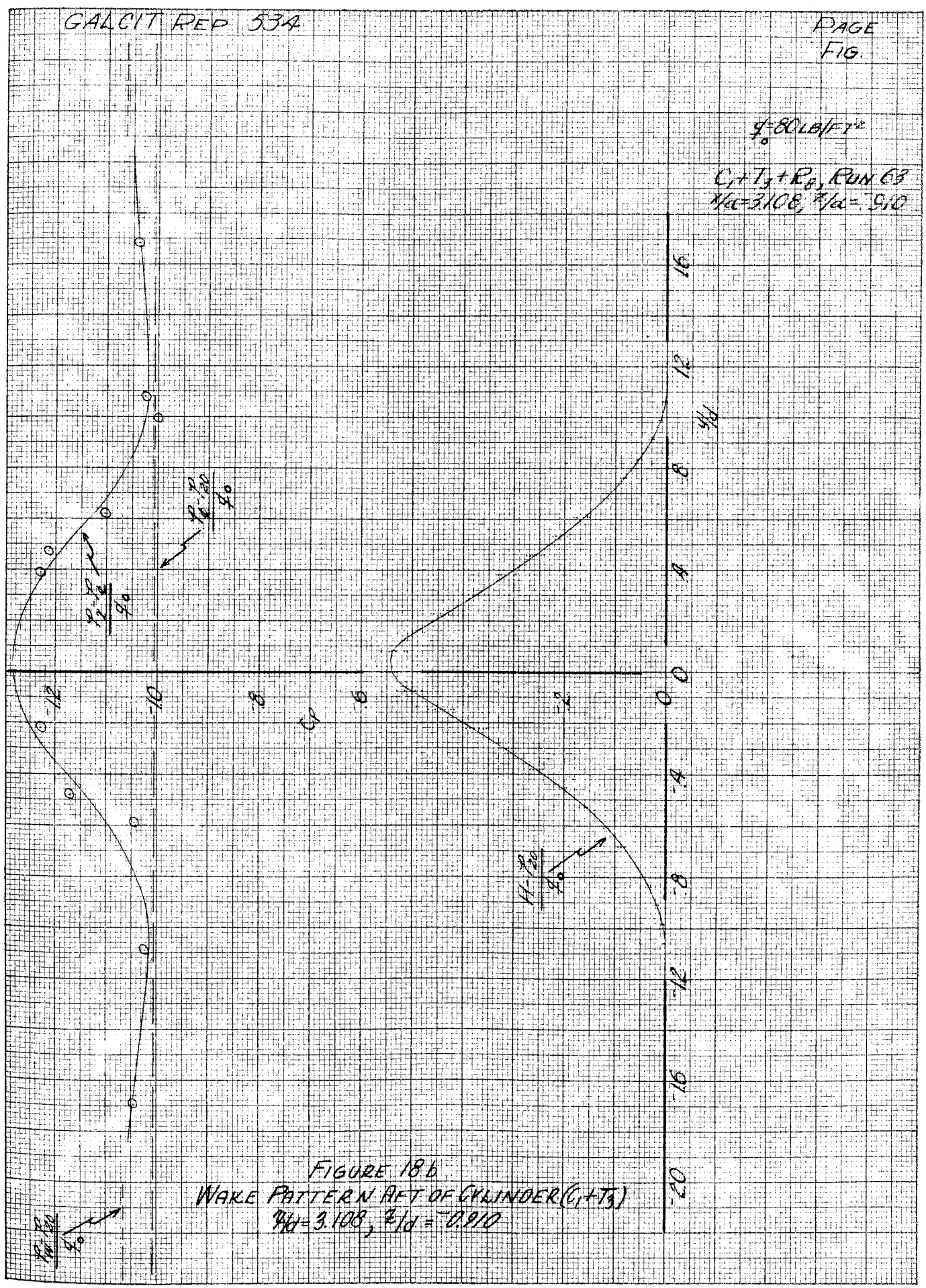

FIGURE 18.b
WAKE PATTERN AFT OF CYLINDER ($C_1 + T_3$)
$x/d = 3.108$, $z/d = -0.910$

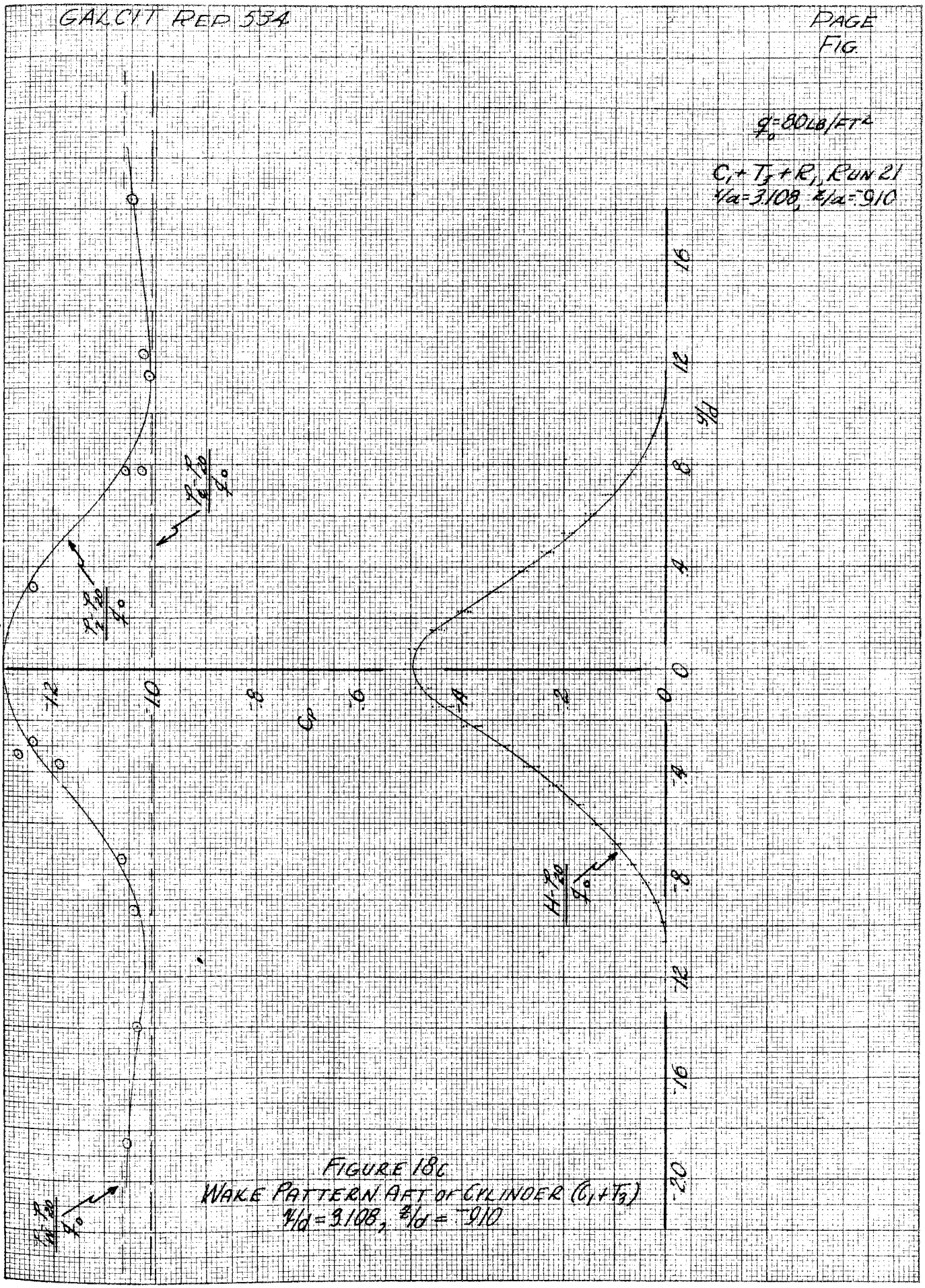

FIGURE 18c
WAKE PATTERN AFT OF CYLINDER (C_1+T_2)
x/d=3.108, z/d=-.910

GALCIT REP 534

PAGE
FIG.

$q_o = 80$ LB/FT^2

$C_1+T_3+R_6$, RUN 63
$x/d = 3.108$, $z/d = 0$

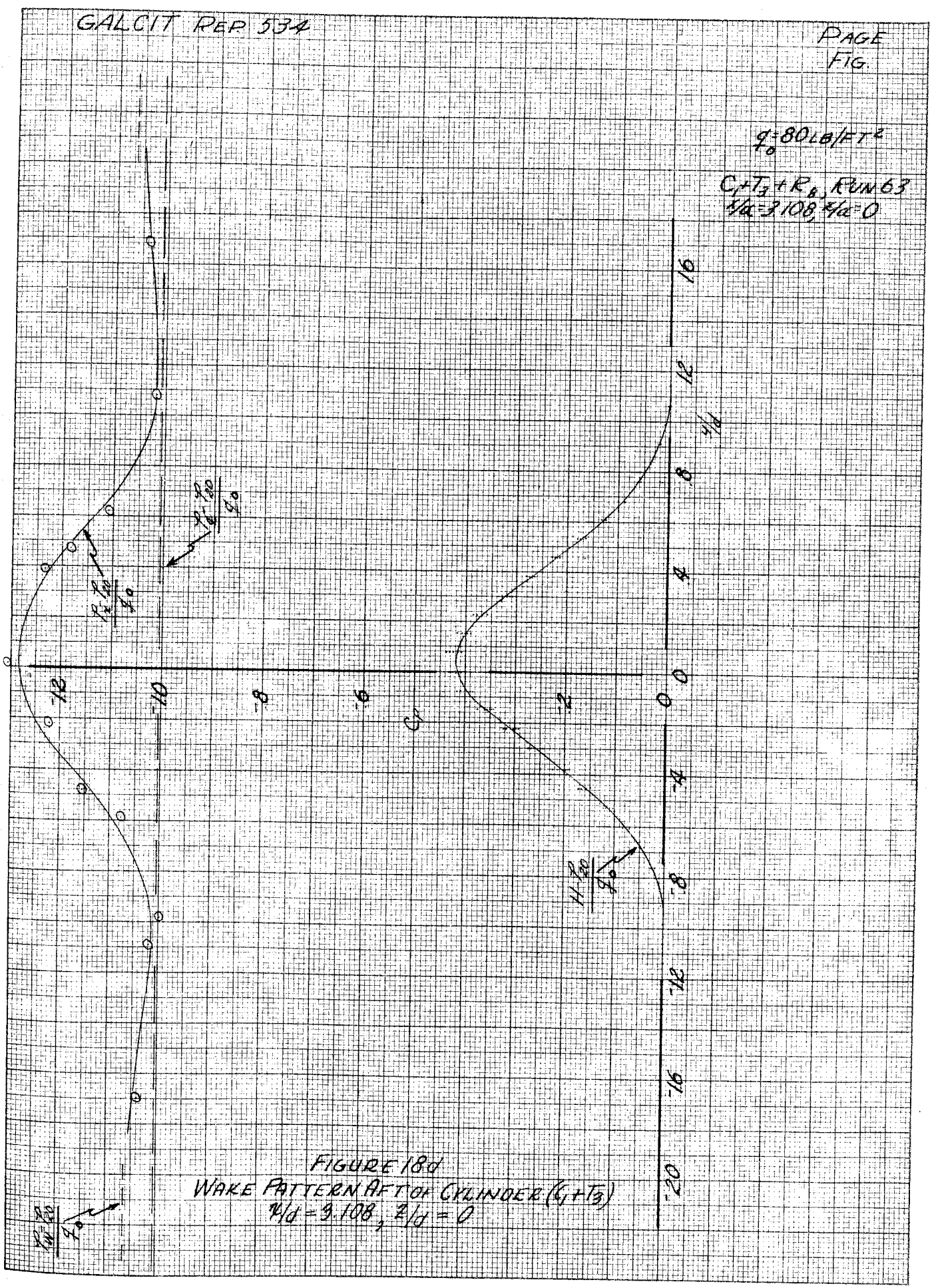

FIGURE 18d
WAKE PATTERN AFT OF CYLINDER (C_1+T_3)
$x/d = 3.108$, $z/d = 0$

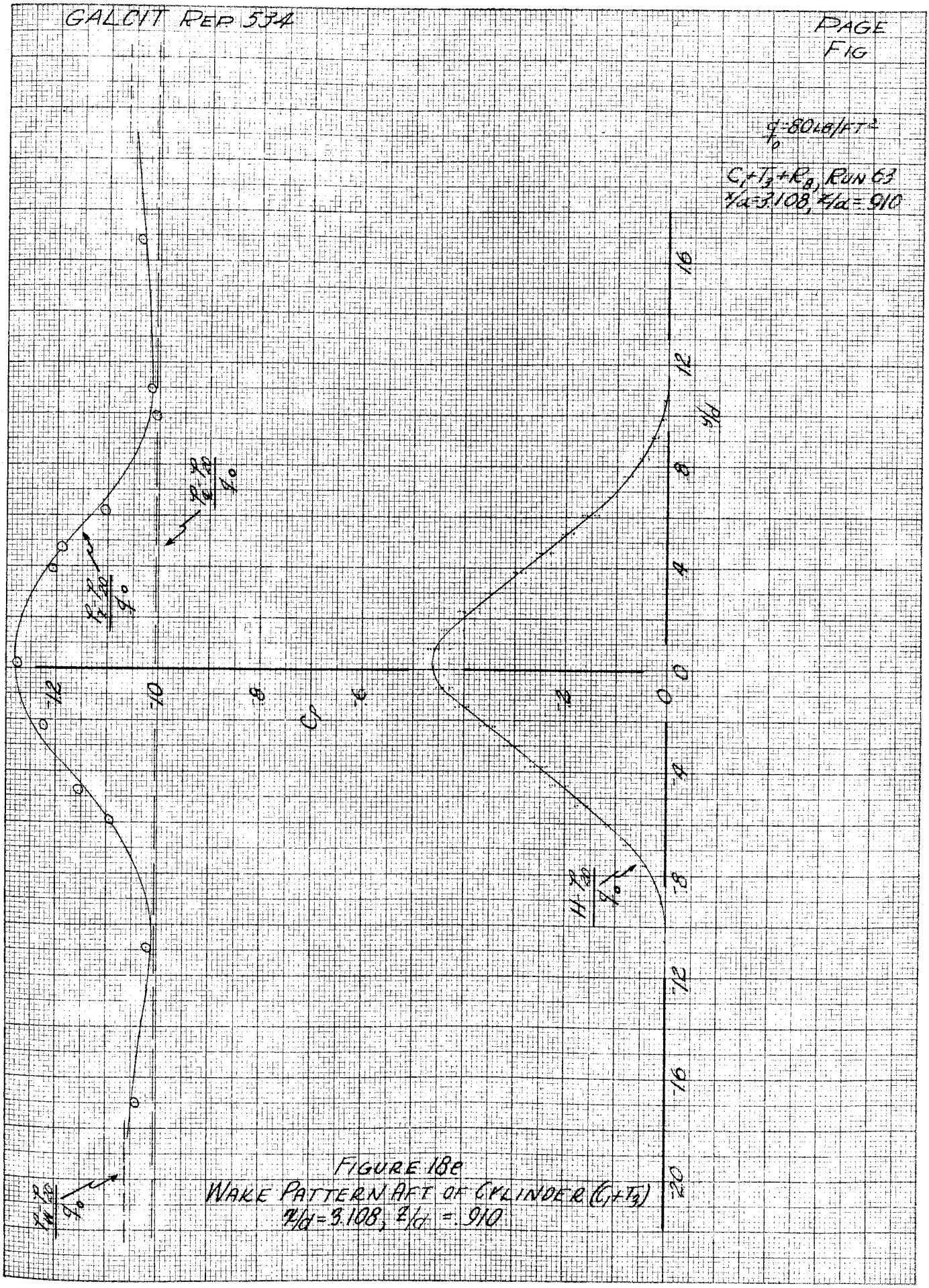

FIGURE 18e
WAKE PATTERN AFT OF CYLINDER (C_1+T_3)
x/d=3.108, z/d = .910

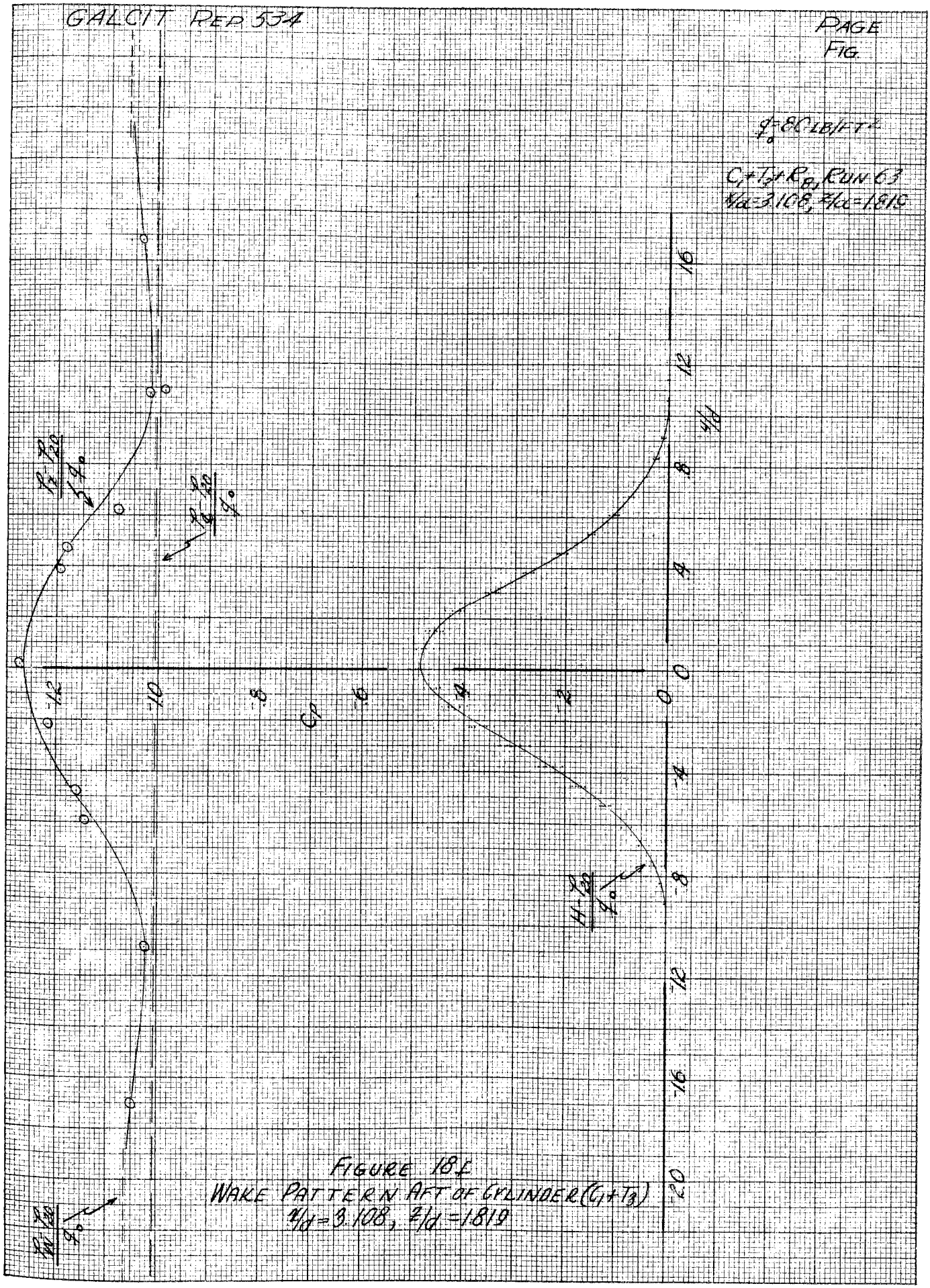

FIGURE 18f
WAKE PATTERN AFT OF CYLINDER (C_f+T_3)
x/a=3.108, z/c=1.819

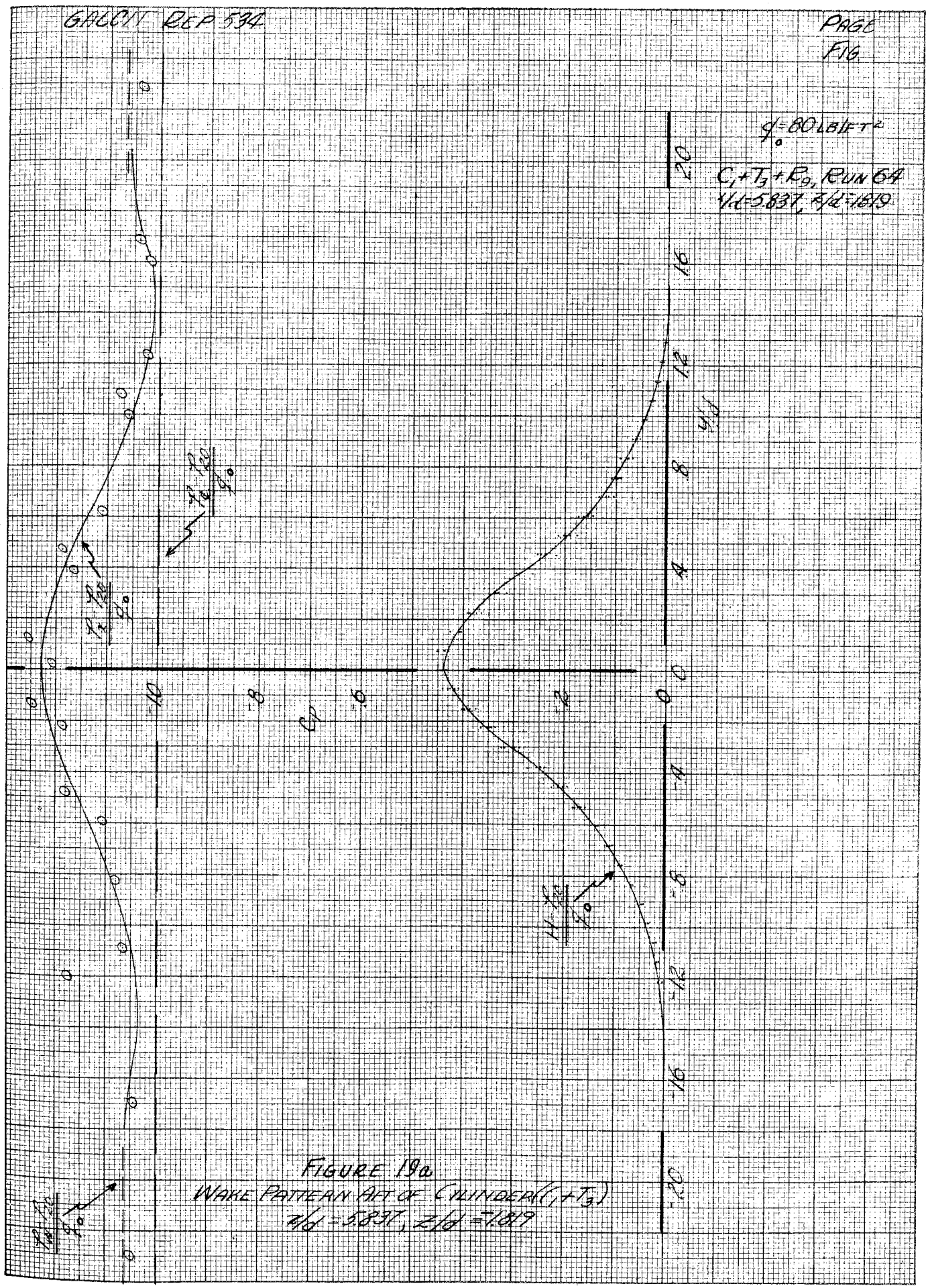

FIGURE 19a
WAKE PROFILE AT 6 DIAMETERS ($C_1 + T_3$)
$Y/d = 5.837$, $Z/d = 7.819$

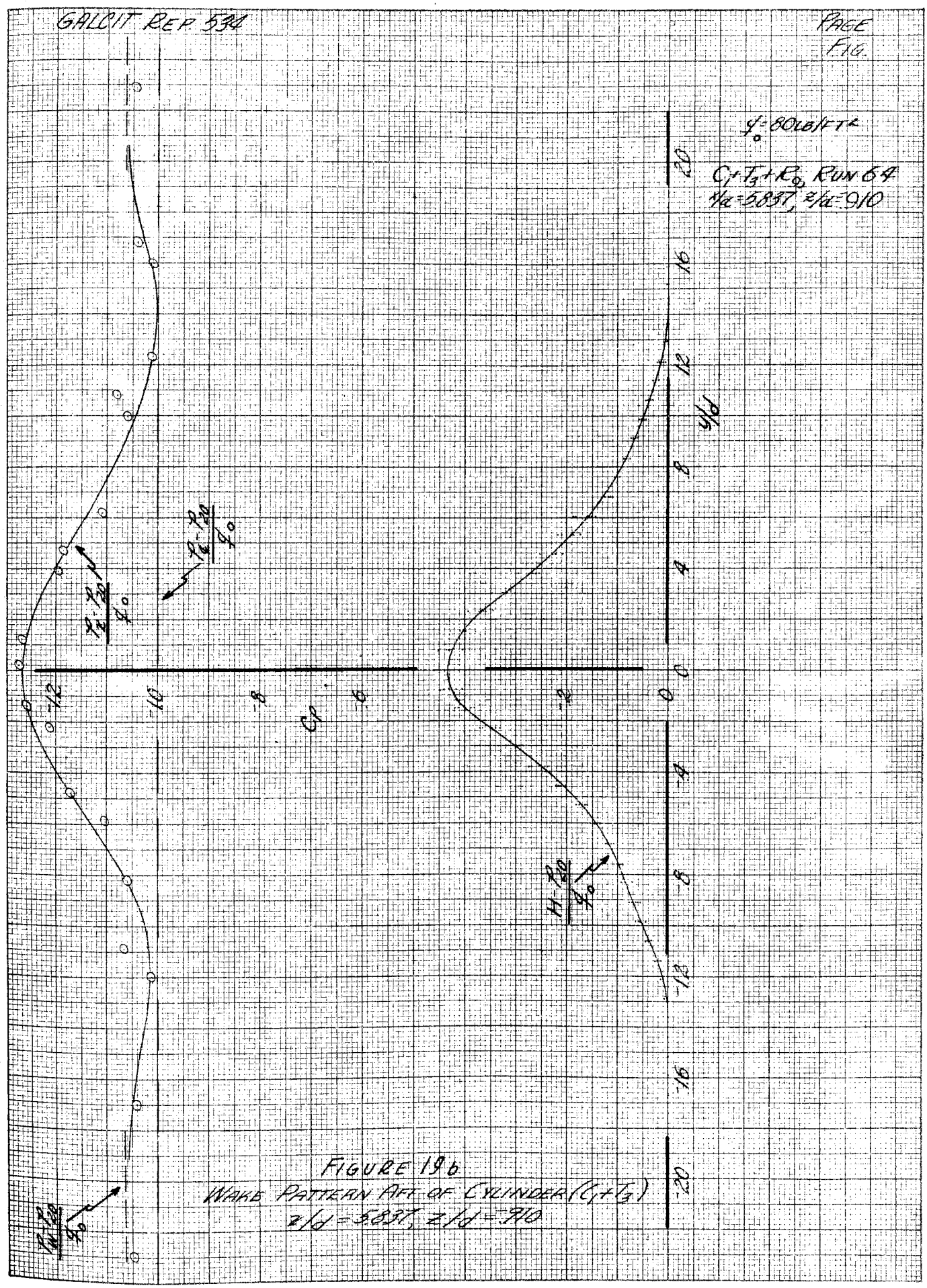

FIGURE 19b
WAKE PATTERN AFT OF CYLINDER ($C_1 + T_3$)
$x/d = 5.83T$, $z/d = 9.10$

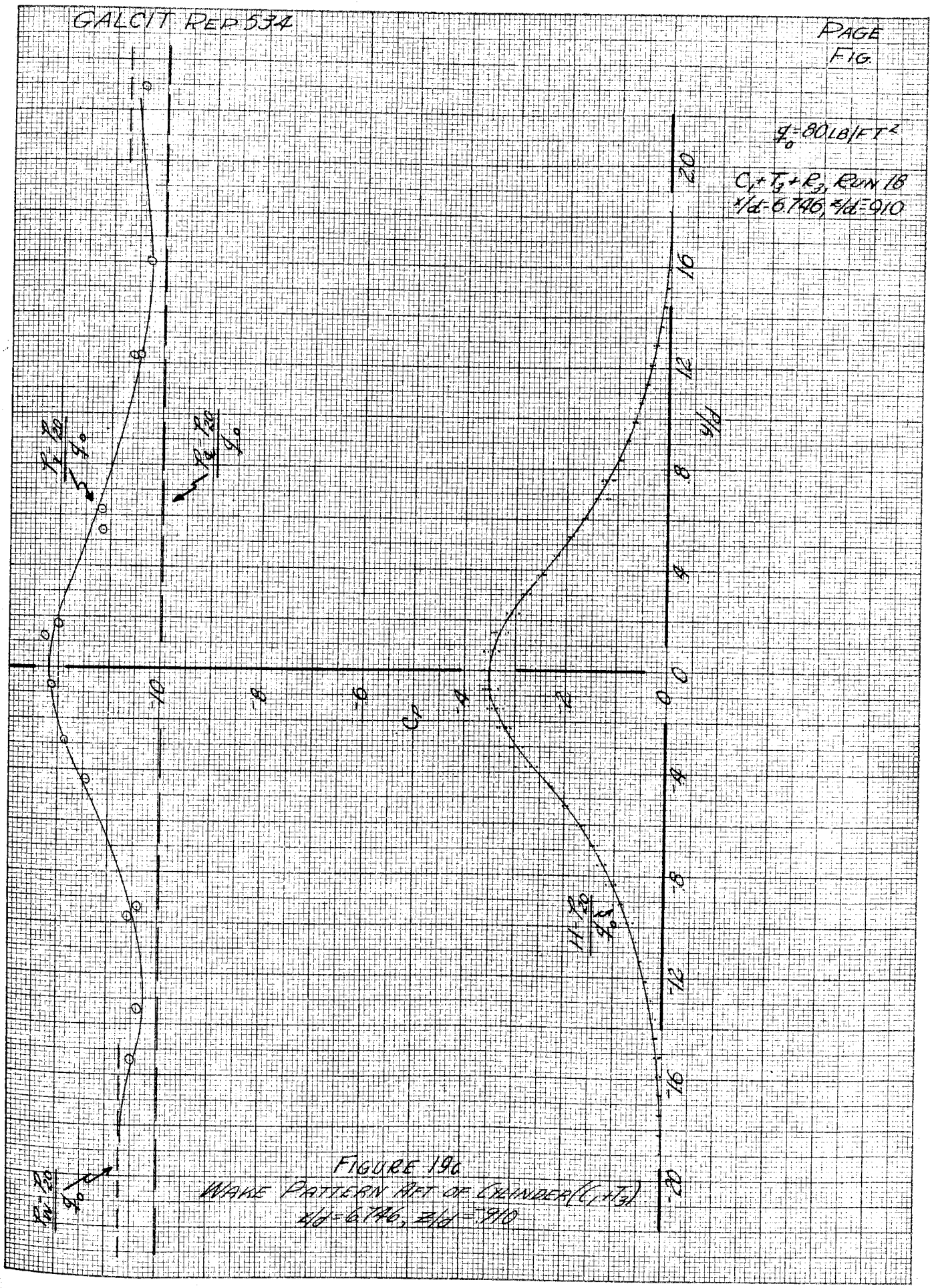

FIGURE 19c
WAKE PATTERN BEHIND CYLINDER ($C_1 + T_3$)
x/d = 6.746, z/d = 9.10

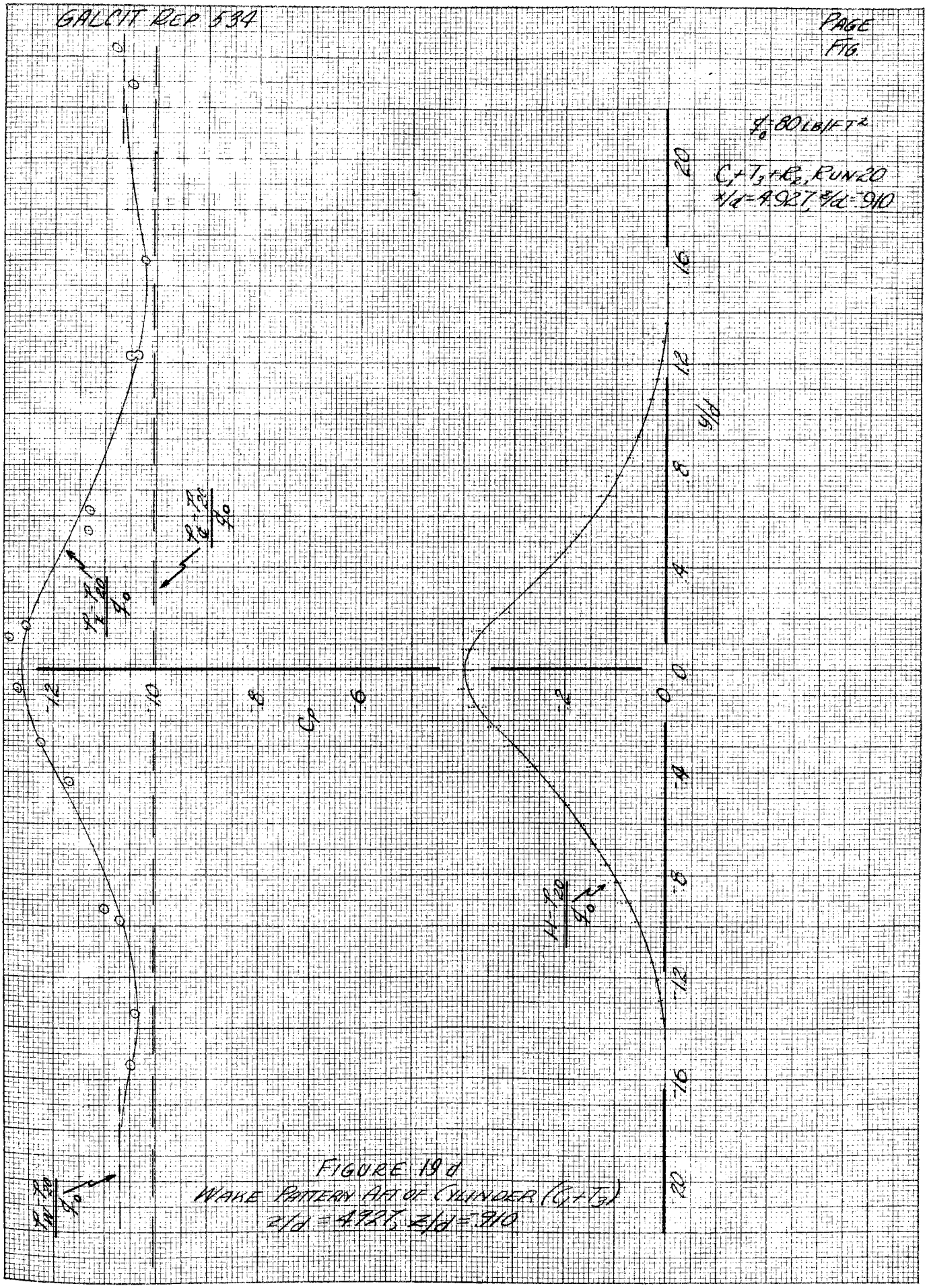

FIGURE 19 d
WAKE PATTERN AFT OF CYLINDER (C_1+T_3)
x/d = .927, z/d = .910

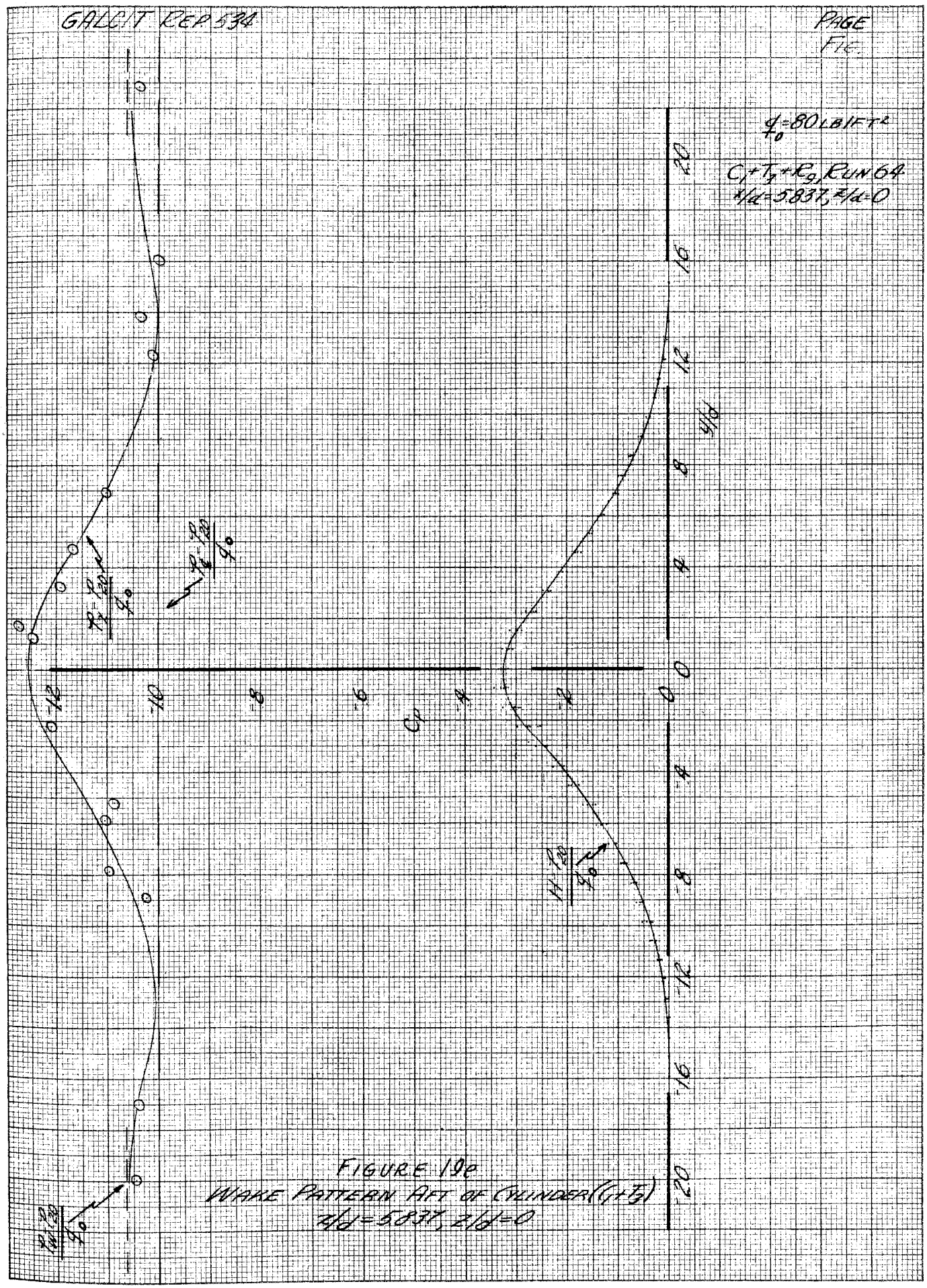

FIGURE 19e
WAKE PATTERN AFT OF CYLINDER (C_1+T_3)
R/a=5.837, Z/a=0

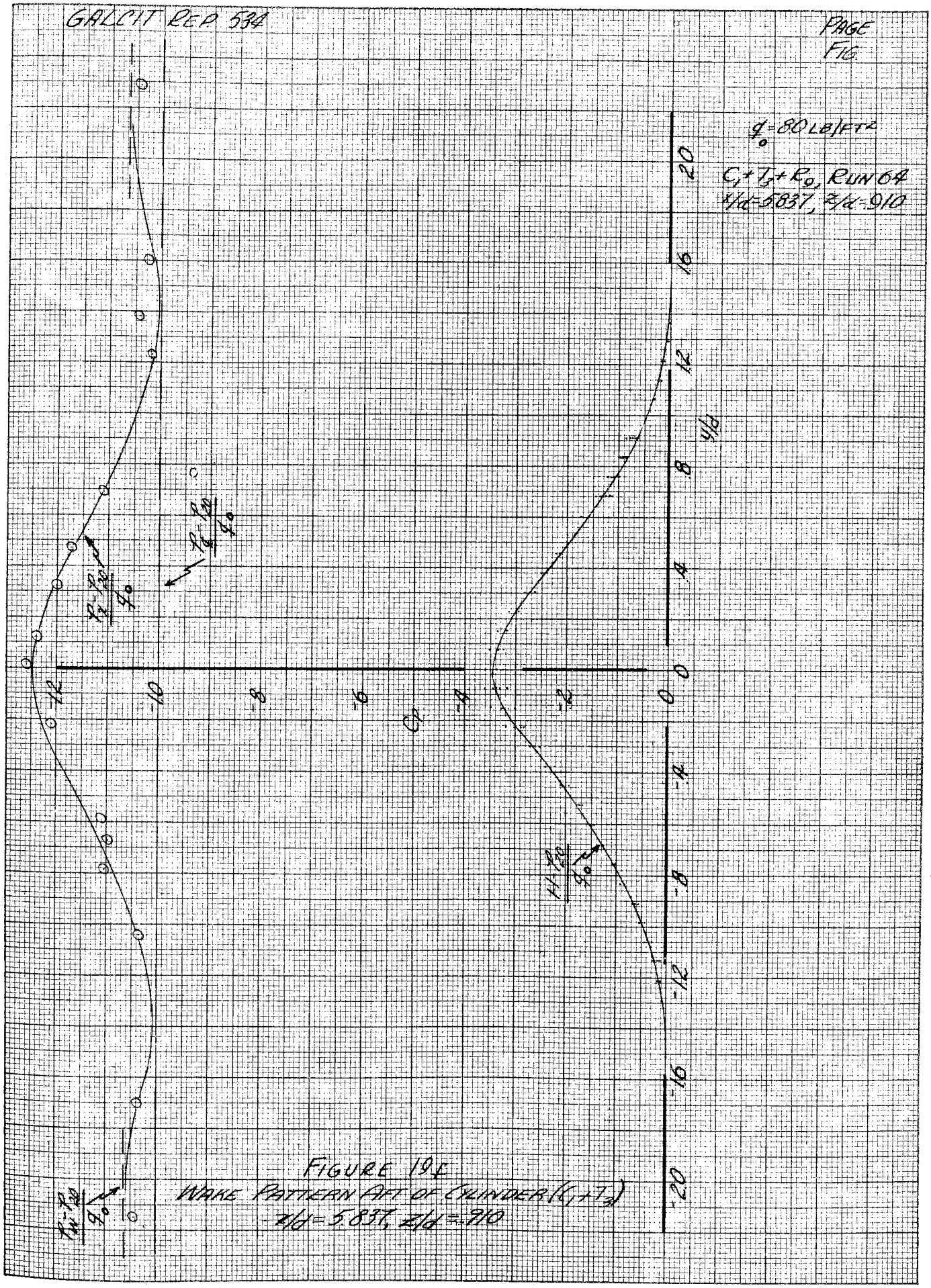

FIGURE 19.f
WAKE PATTERN AFT OF CYLINDER ($C_1 + T_2$)
$x/d = 5.837$, $z/d = .910$

GALCIT REP 539

PAGE
FIG.

$q_0 = 80$ LB/FT²

$C_1 + T_3 + R_9$, RUN 68
$x/d = 5.837$, $r/d = 1.819$

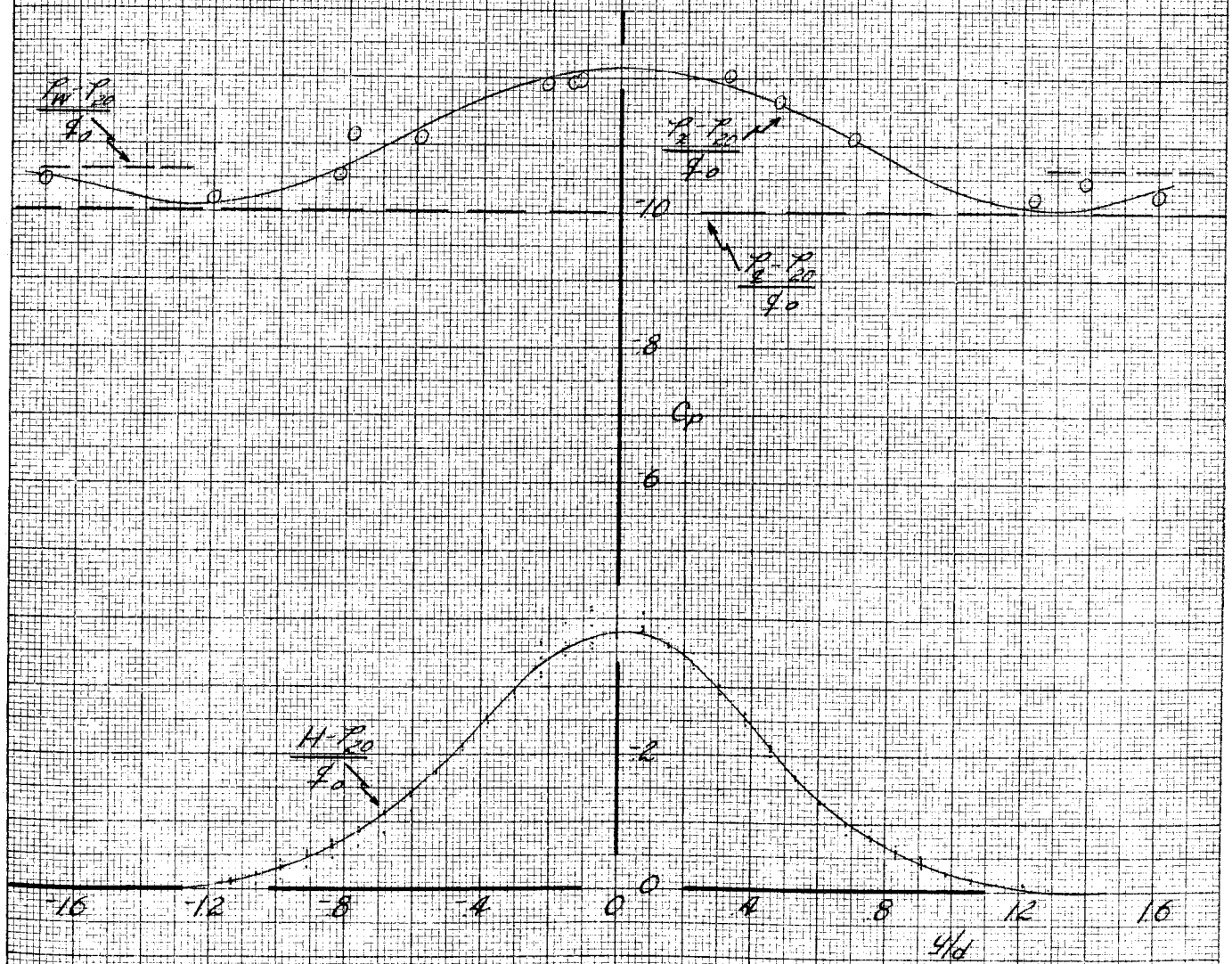

FIGURE 19g
WAKE PATTERN AFT OF CYLINDER ($C_1 + T_3$)
$x/d = 5.837$, $r/d = 1.819$

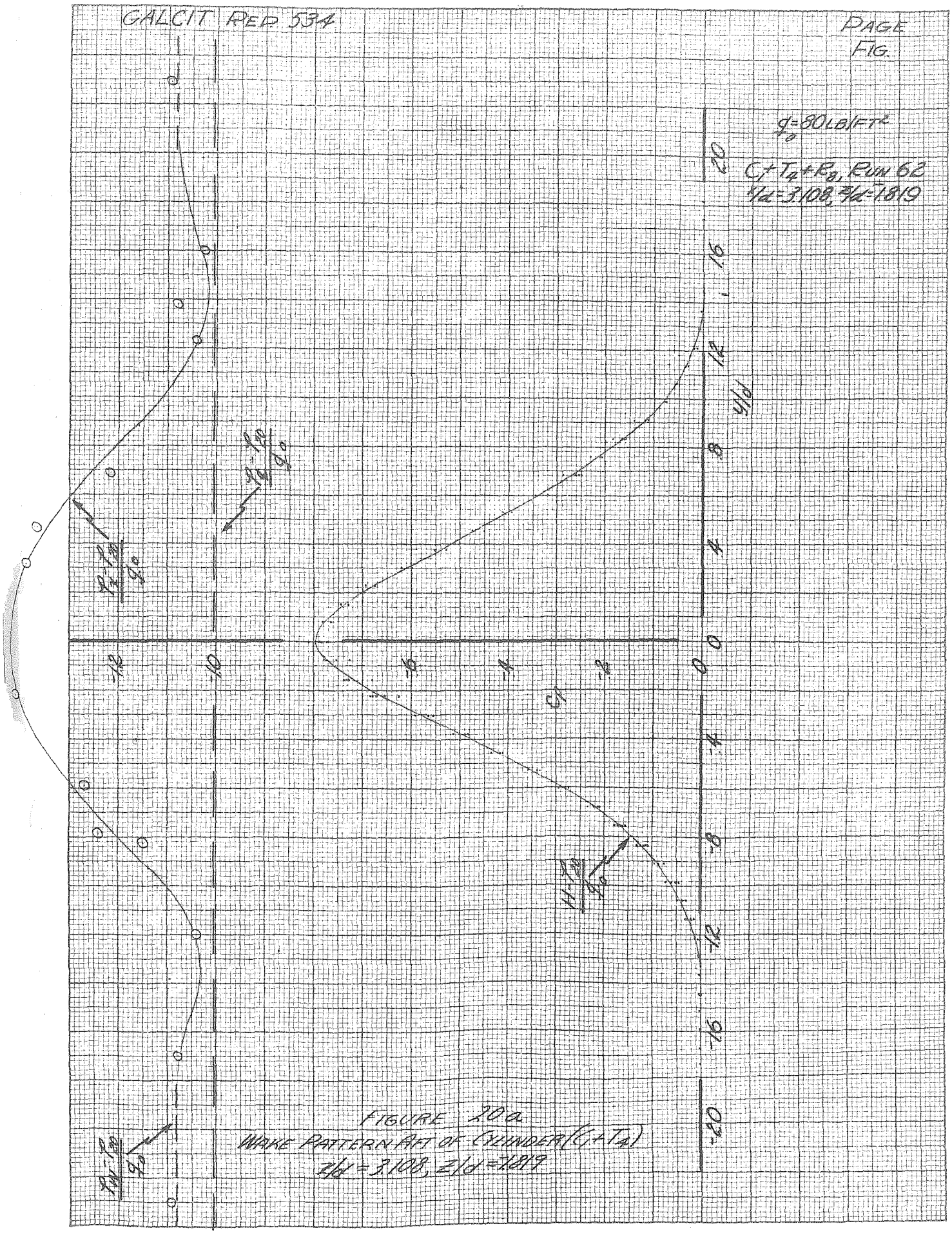

FIGURE 20a
WAKE PATTERN AFT OF CYLINDER (C_f + T_a)
y/d = 3.108, z/d = 7.819

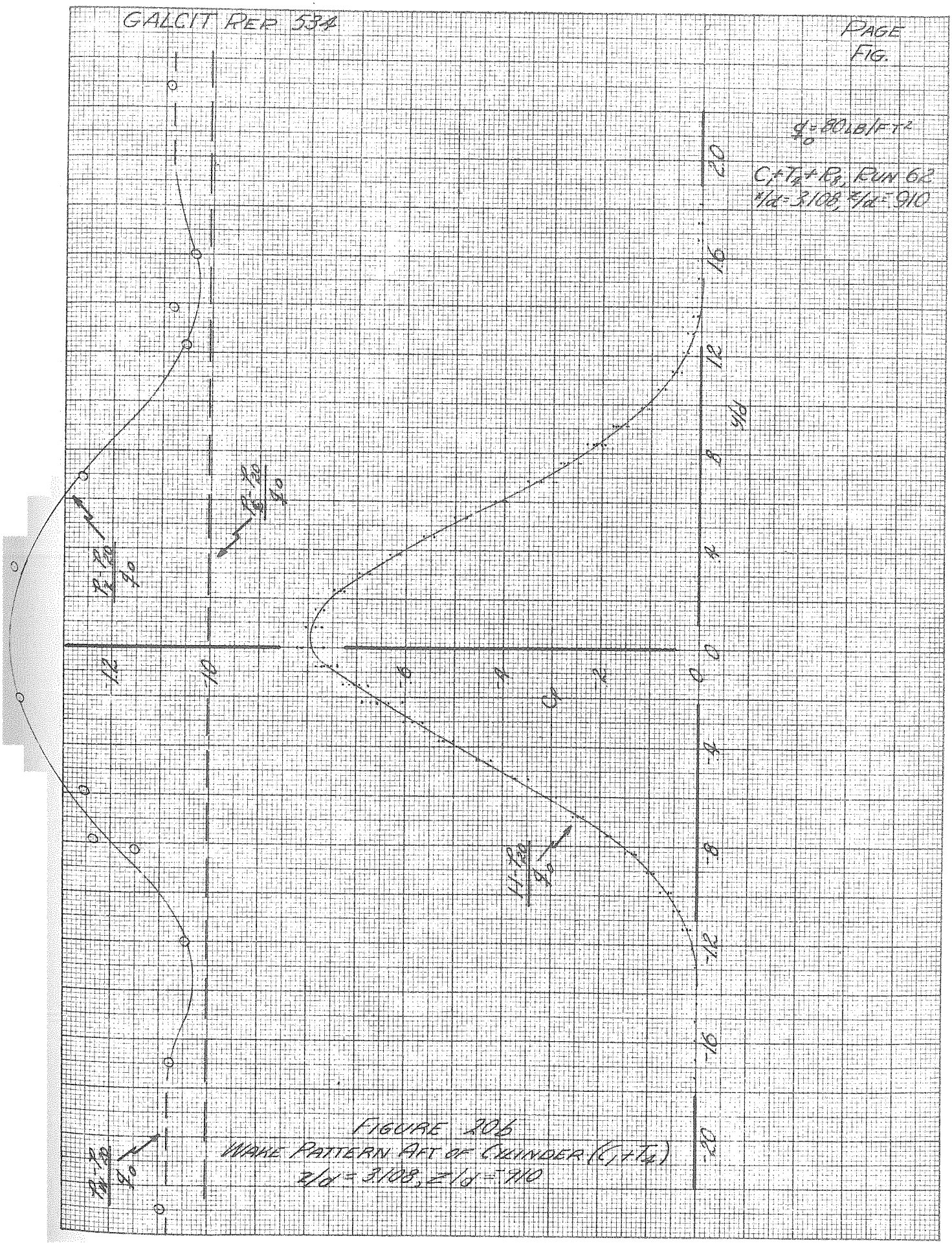

FIGURE 206
WAKE PATTERN AFT OF CYLINDER ($C_1 + T_2$)
$x/d = 3108$, $z/d = 910$

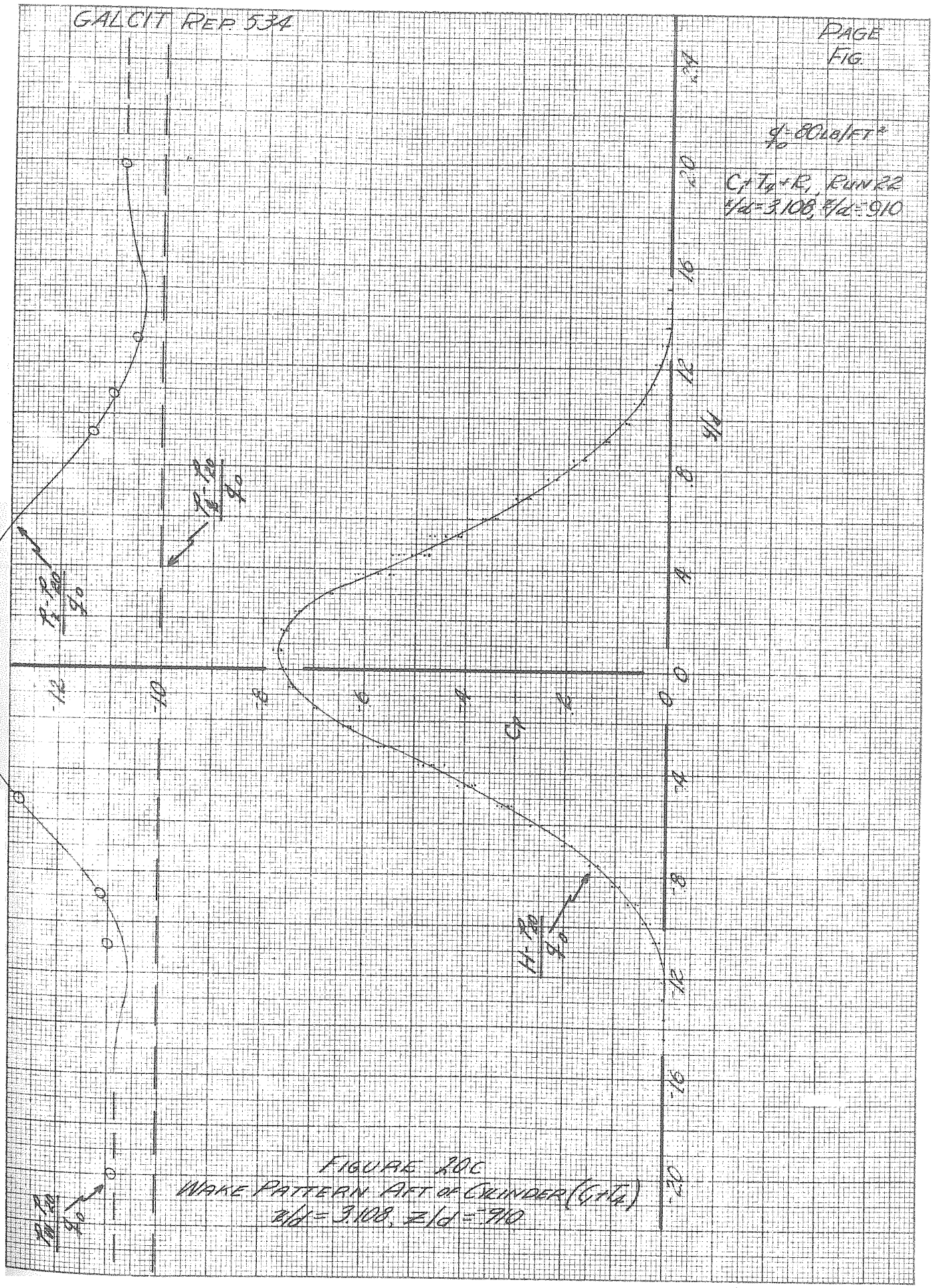

FIGURE 20C
WAKE PATTERN AFT OF CYLINDER (C_f T_g)
x/d = 3.108, r/d = .910

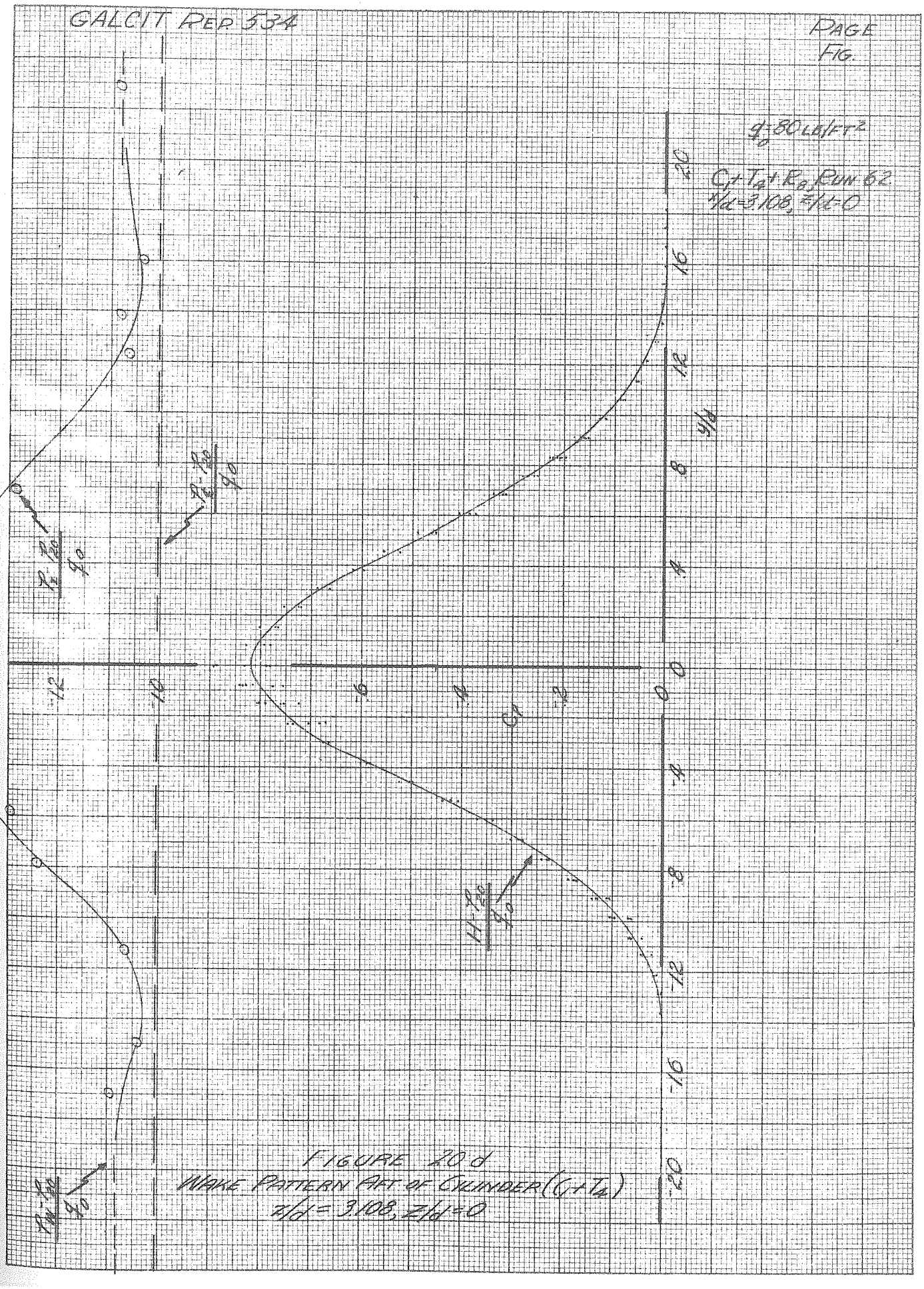

FIGURE 20d
WAKE PATTERN AFT OF SKIMMER (C+T₄)
X/d=3.108, Z/d=0

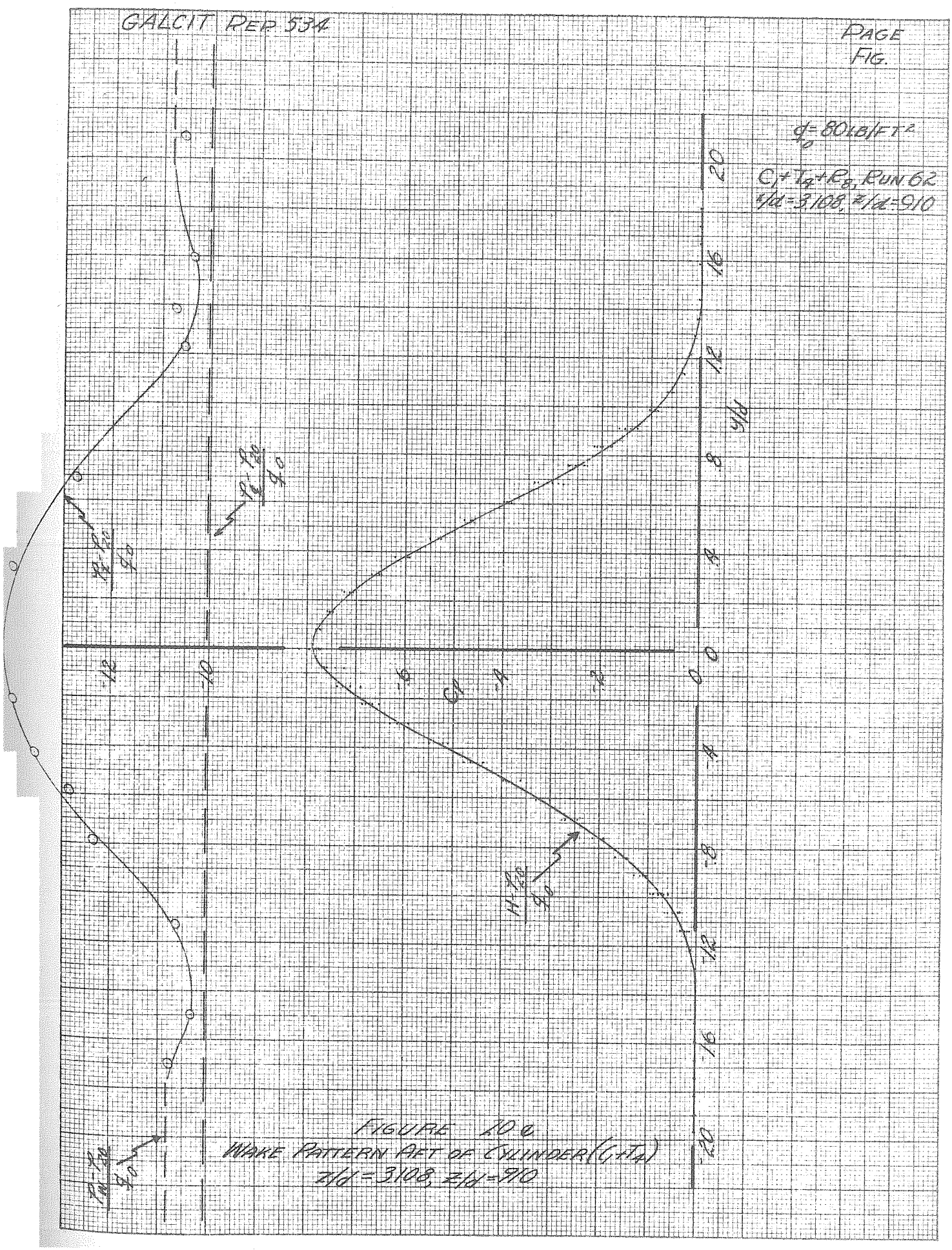

FIGURE 20 e
WAKE PATTERN AFT OF CYLINDER ($C_1 + T_{12}$)
$R_d = 3108$, $R_d = 910$

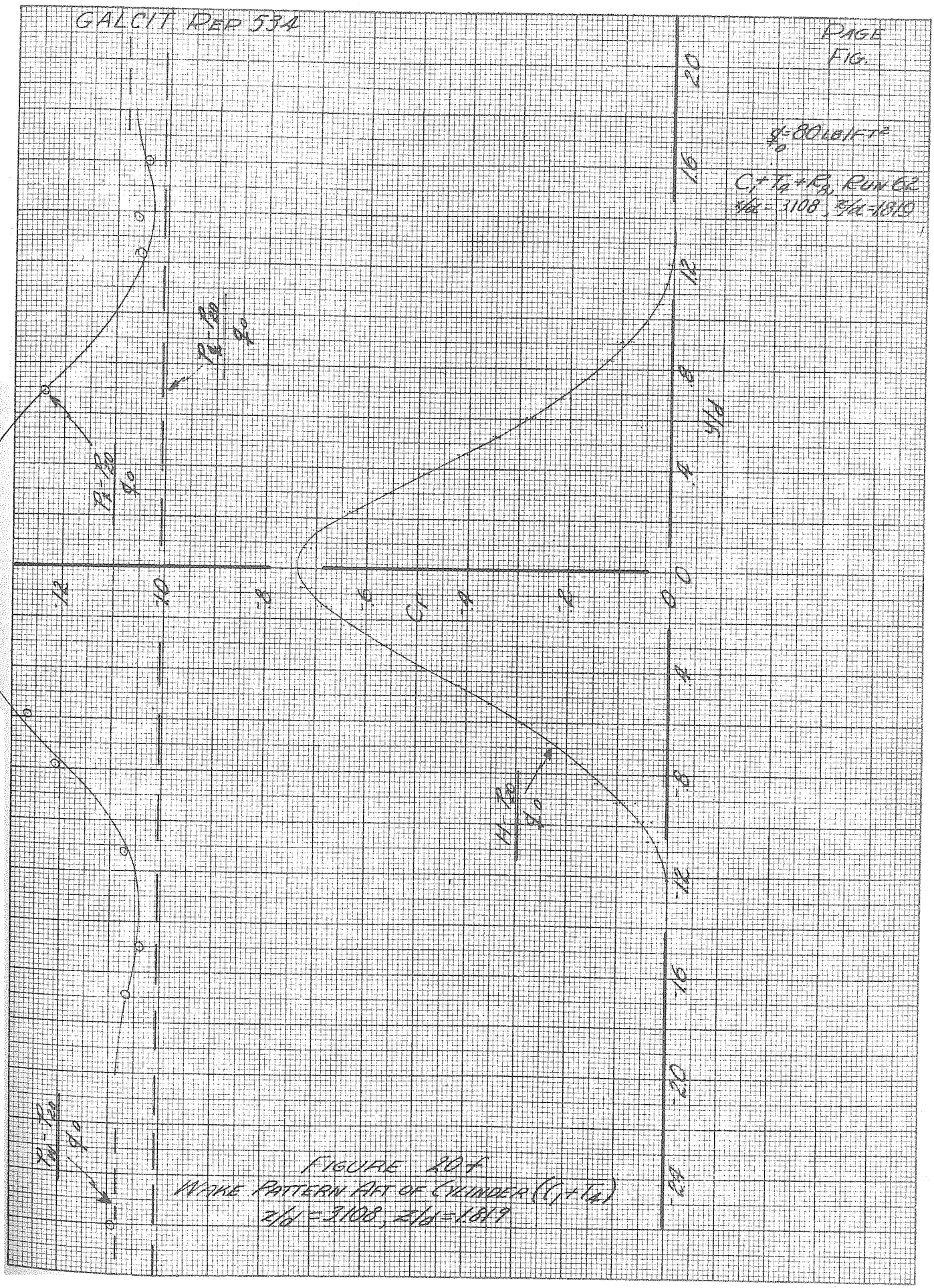

FIGUARE 20A
WAKE PATTERN AFT OF CYLINDER (C_1 + T_{12})
x/c = .3108, z/c = .1819

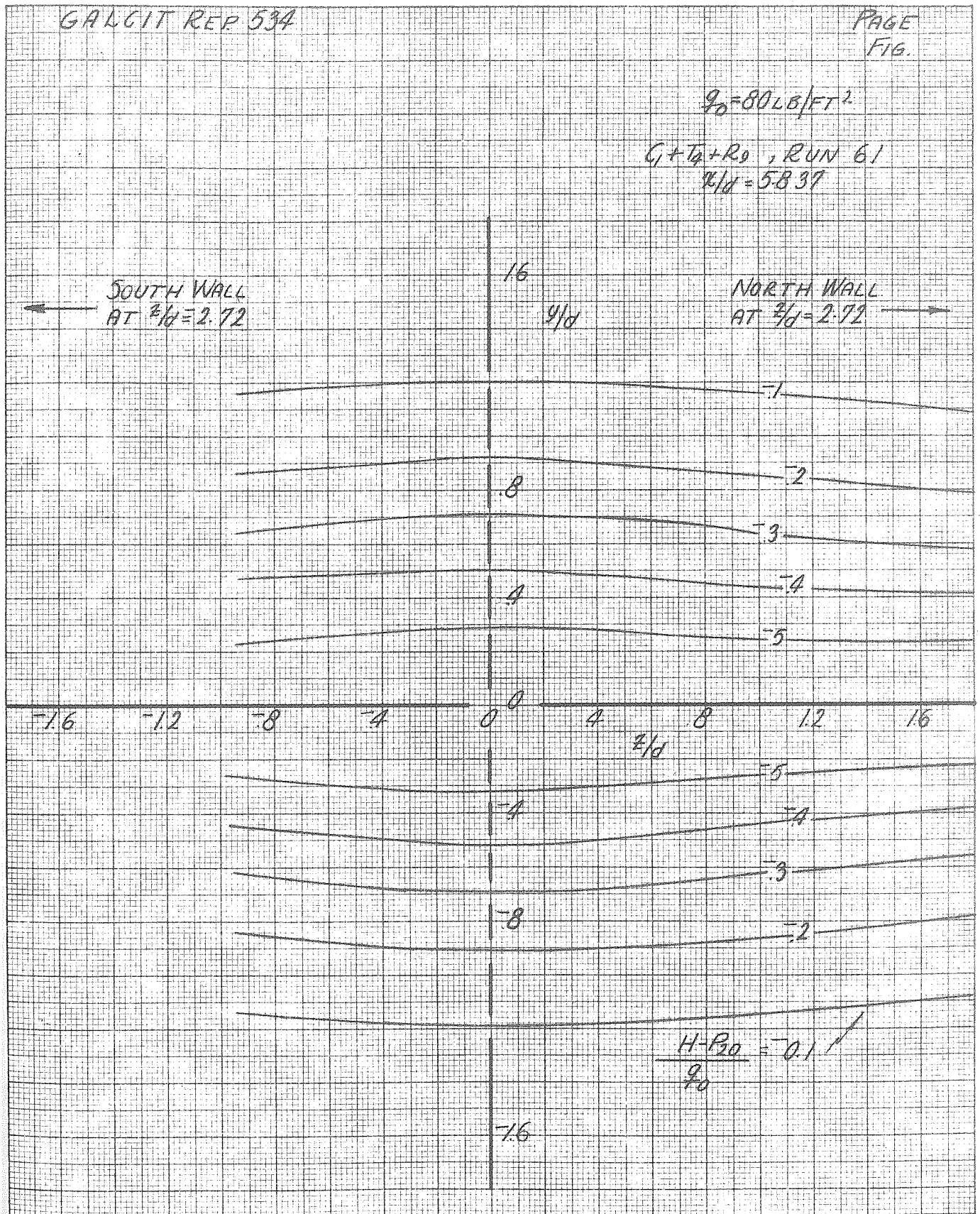

FIGURE 21
CONTOURS OF CONSTANT TOTAL HEAD DECREMENTS
AFT OF CYLINDER ($C_1 + T_4$)
$x/d = 5.837$

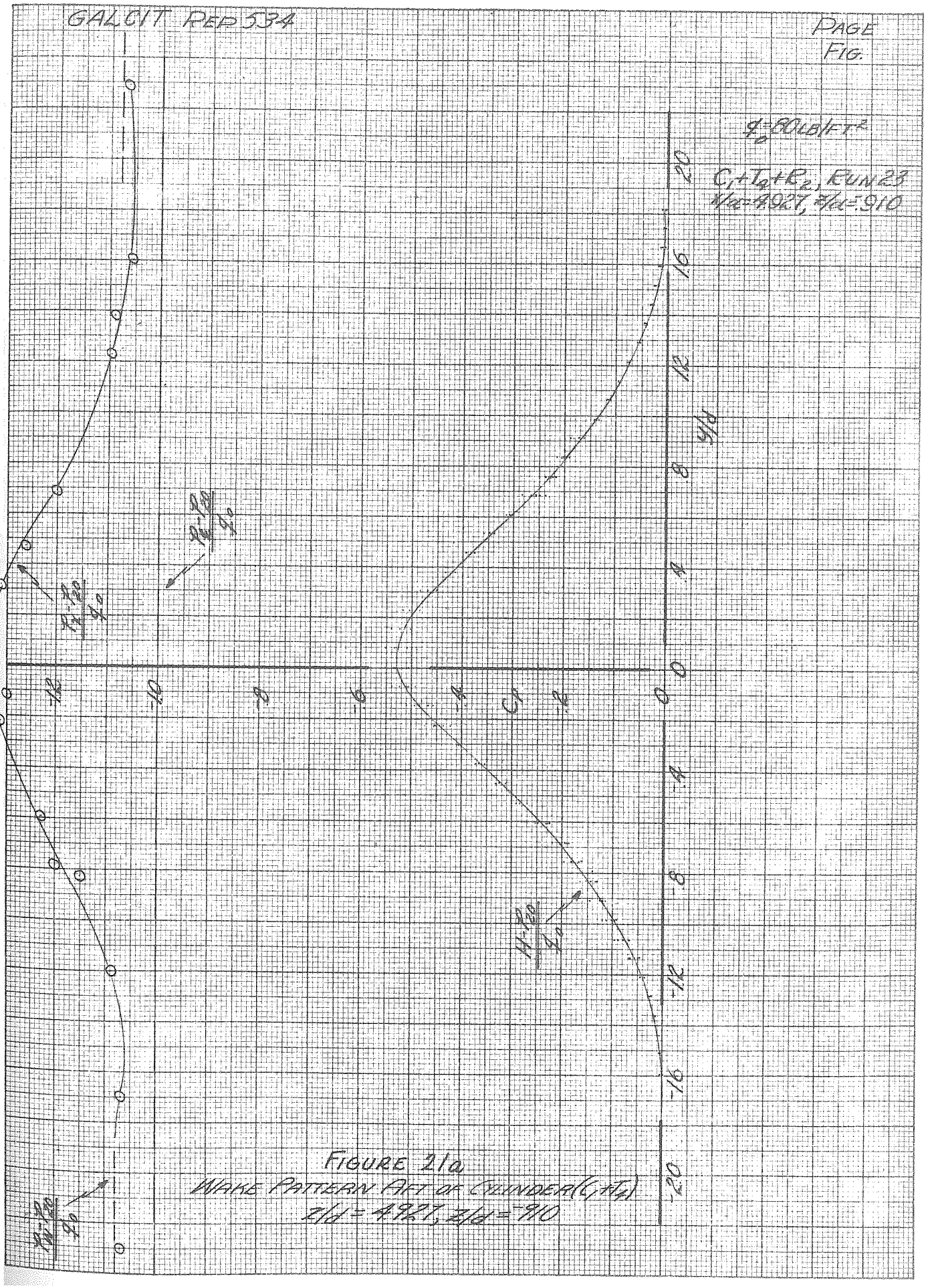

FIGURE 21a
WAKE PATTERN AFT OF CYLINDER (C_1+T_2)
X/d = 4.927, Z/d = .910

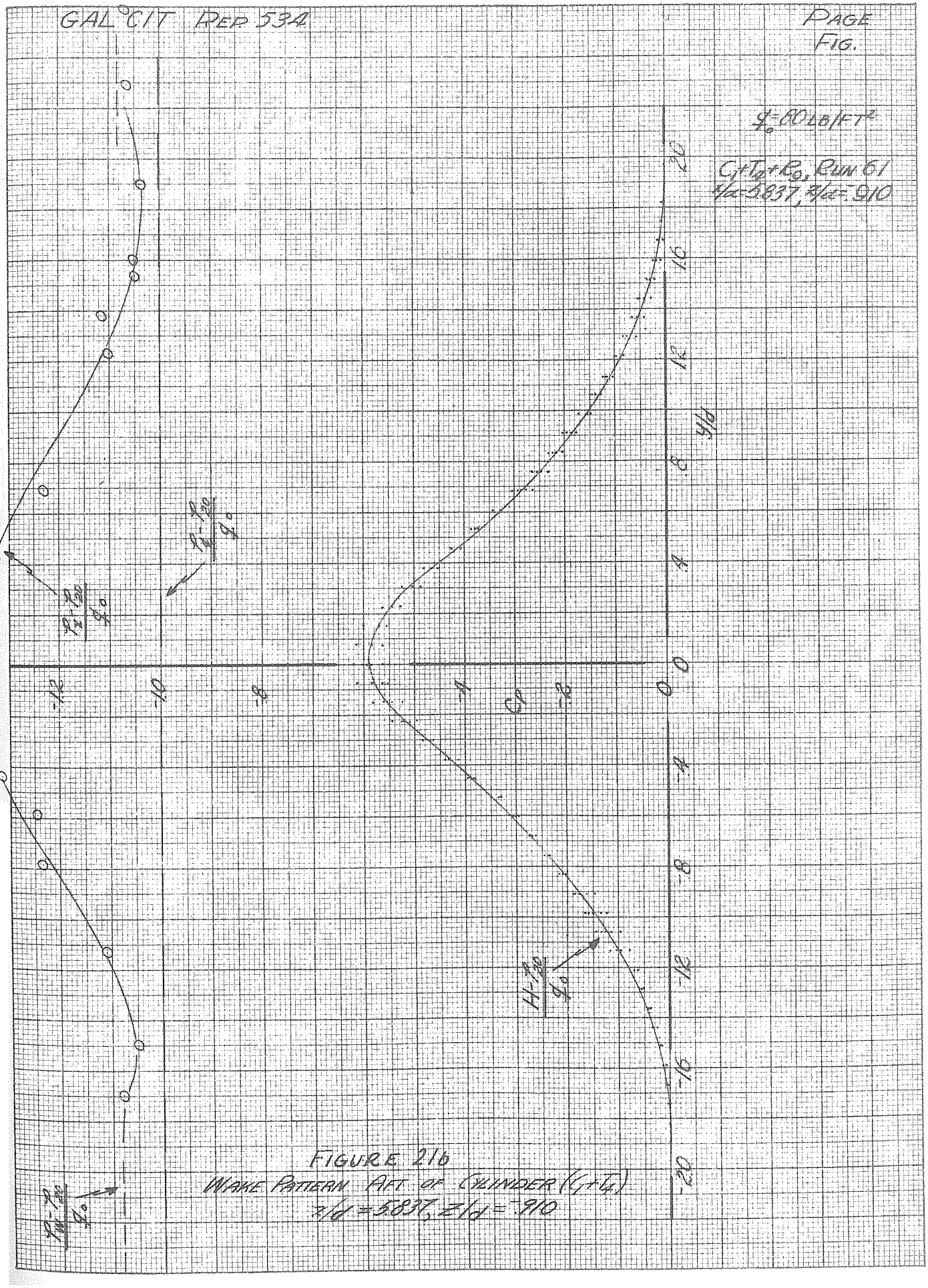

FIGURE 216
WAKE PATTERN AFT OF CYLINDER (C_1+C_4)
x/d = 3.837, z/d = .910

GALCIT REP 534

PAGE
FIG.

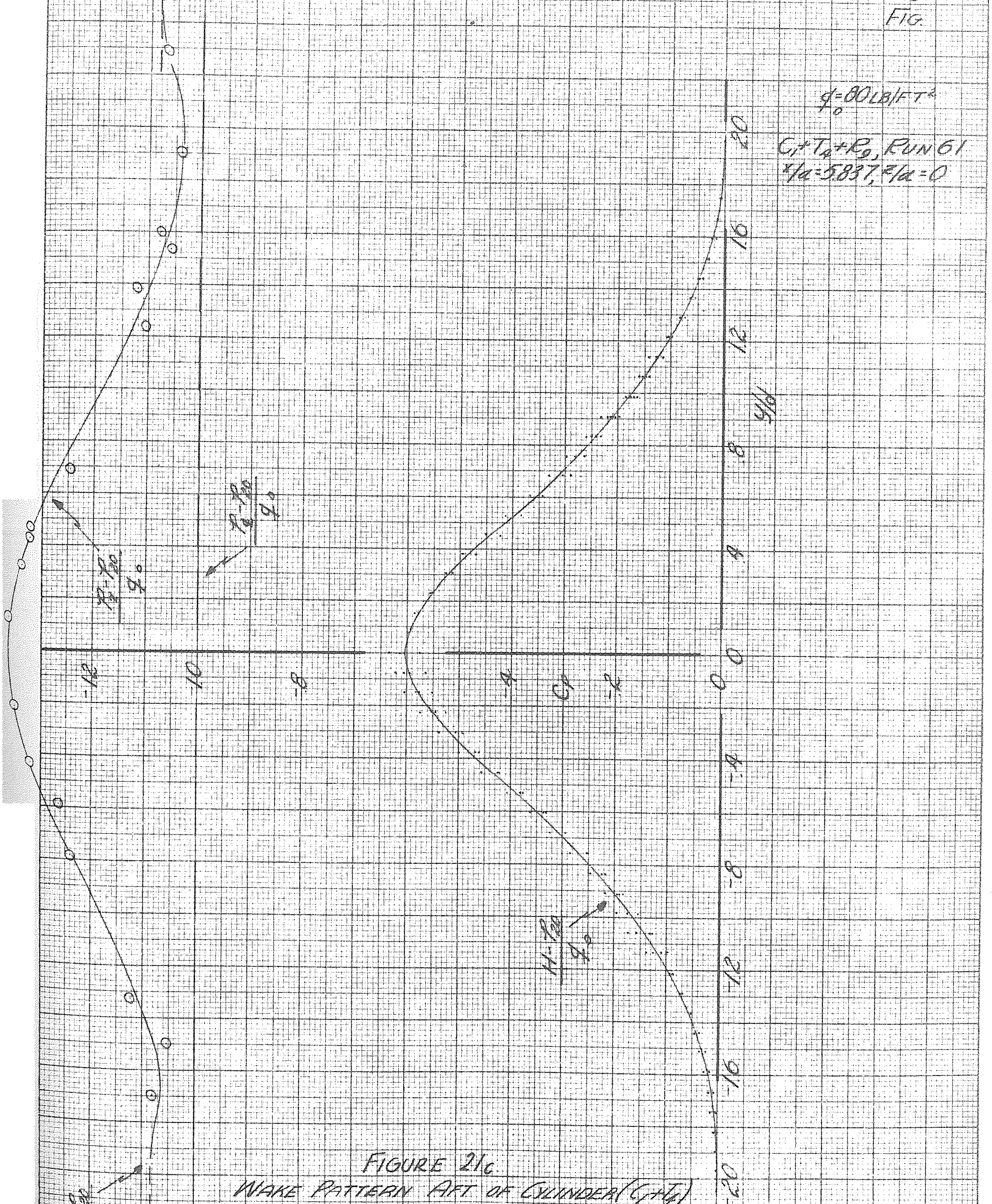

FIGURE 21c
WAKE PATTERN AFT OF CYLINDER (C_1+T_4)
$x/d = 5.837$, $z/d = 0$

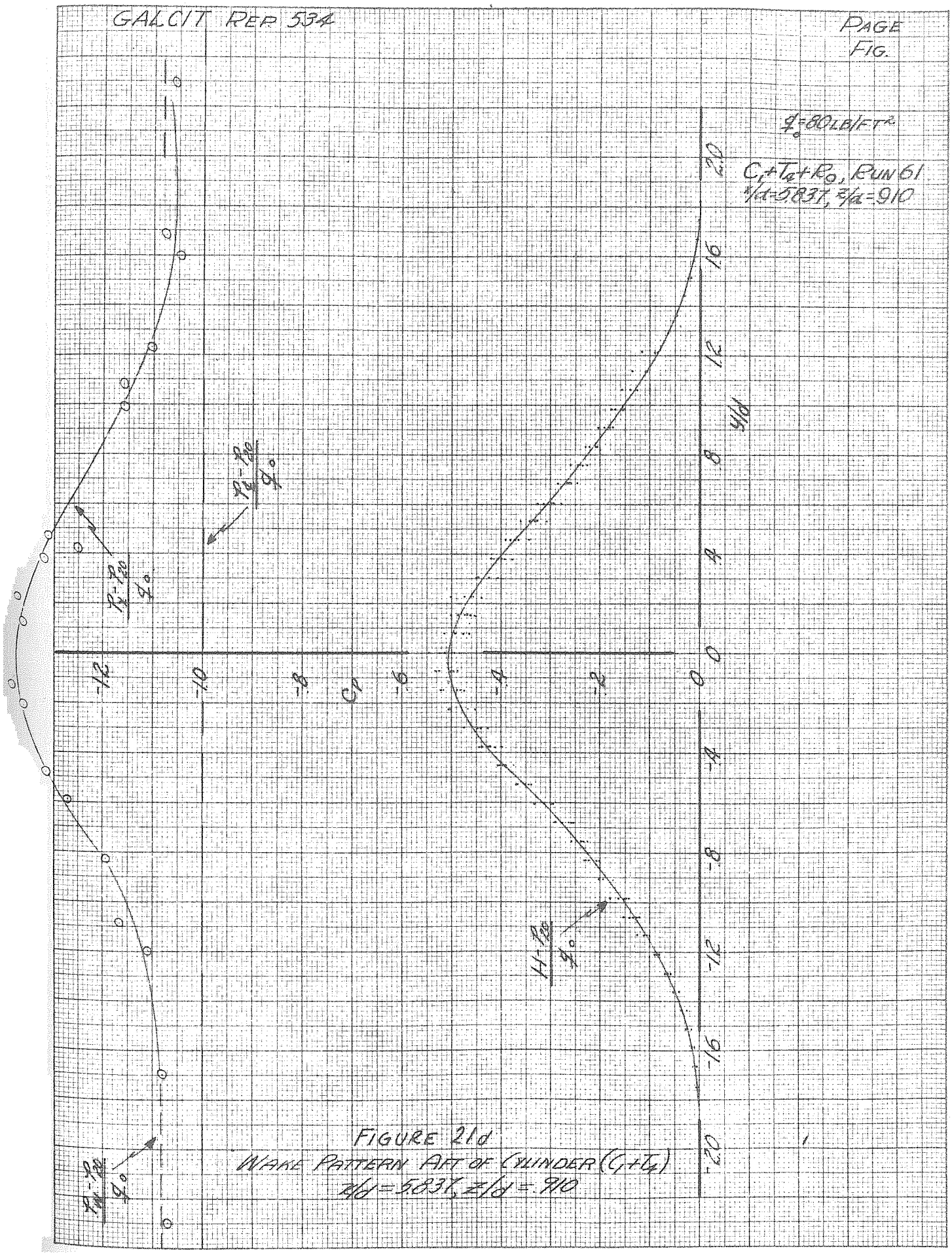

FIGURE 21d
WAKE PATTERN AFT OF CYLINDER (C+T₂)
x/a = 5.83, z/a = .910

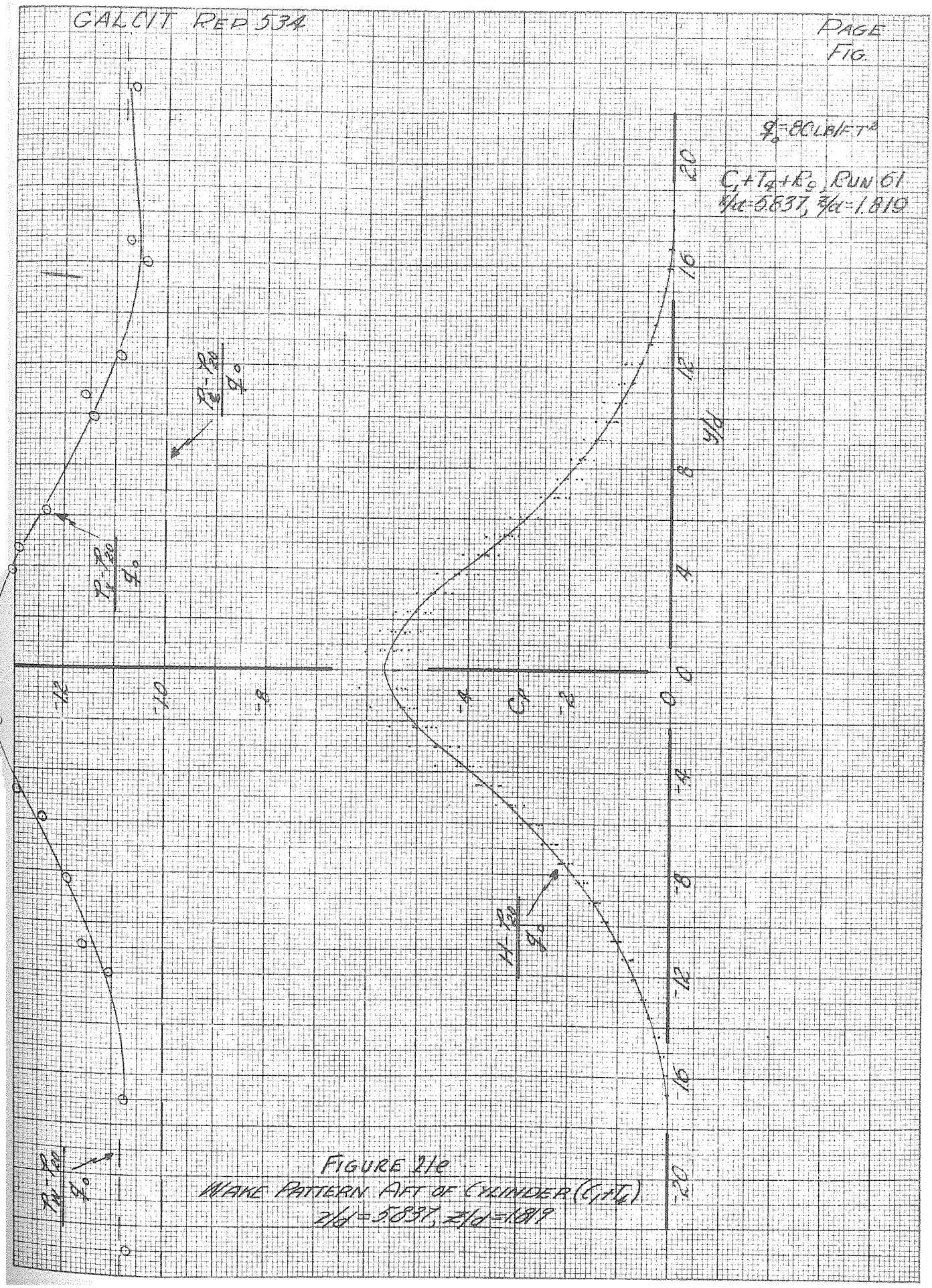

FIGURE 21e
WAKE PATTERN AFT OF CYLINDER (C₁AT₂)
y/d=.5837, z/d=1.819

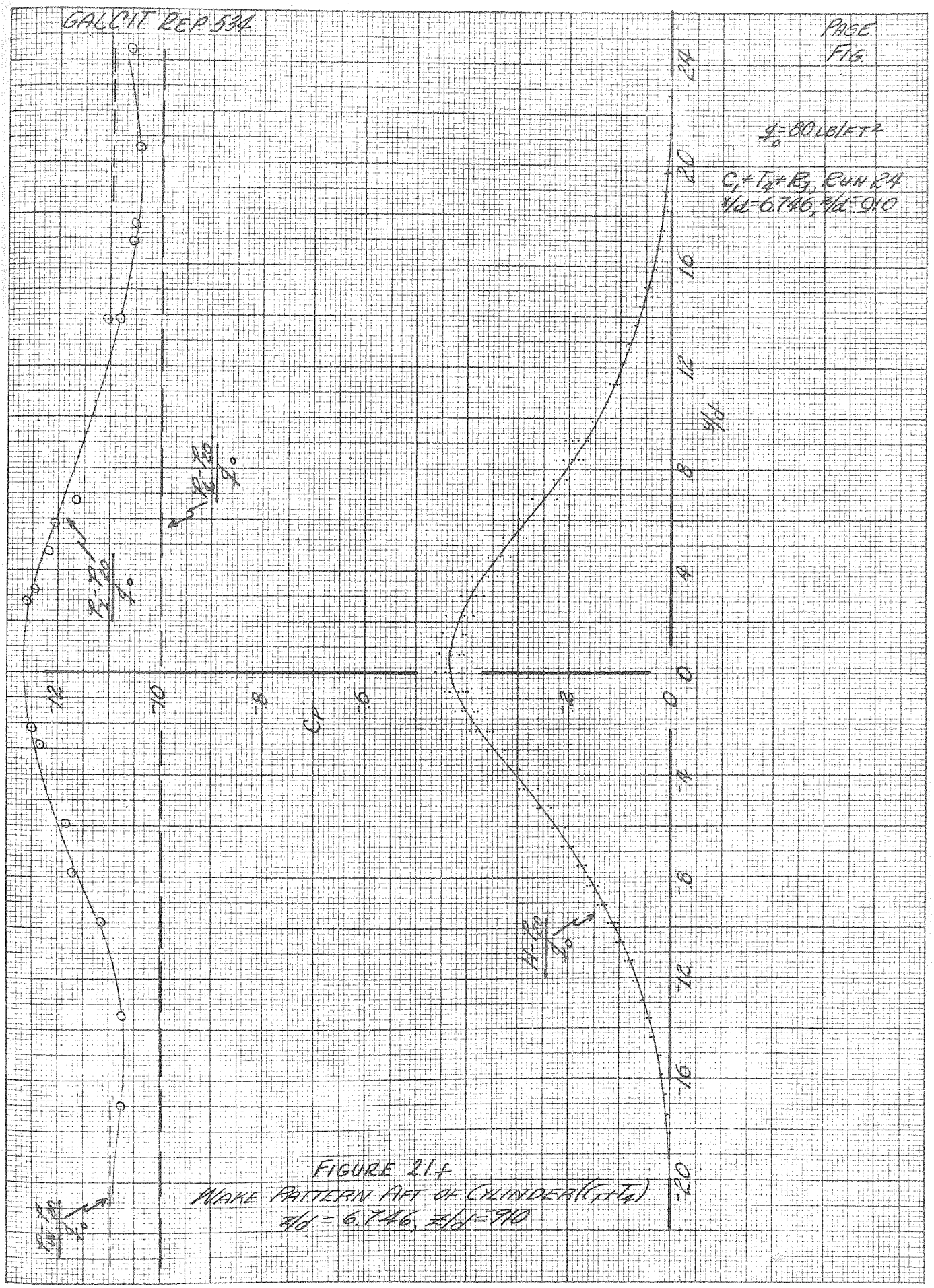

FIGURE 21f
WAKE PATTERN AFT OF CYLINDER (C_1+T_4)
x/d = 6.746, z/d = 9.10

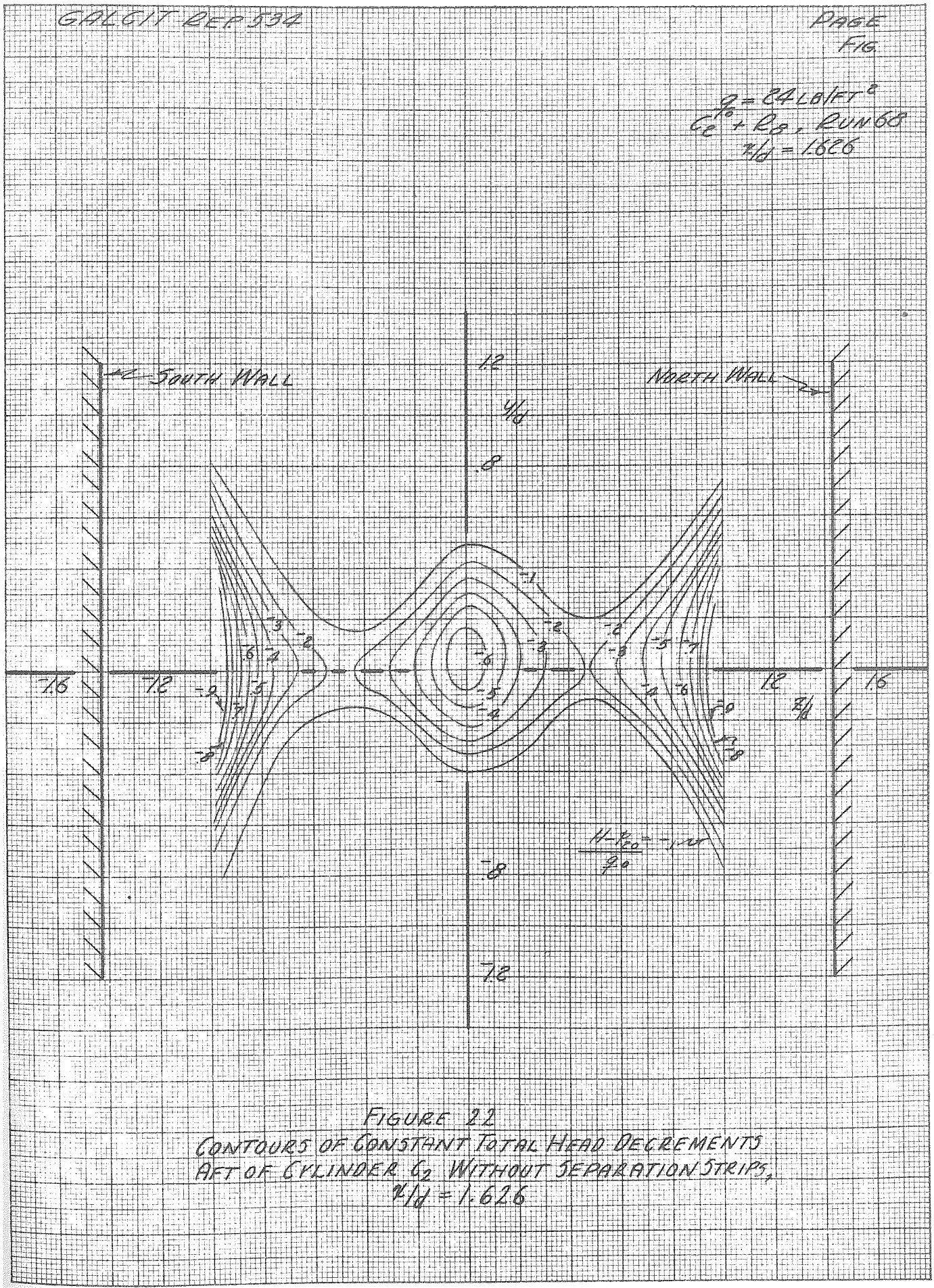

FIGURE 22
CONTOURS OF CONSTANT TOTAL HEAD DECREMENTS
AFT OF CYLINDER C_2 WITHOUT SEPARATION STRIPS,
$x/d = 1.626$

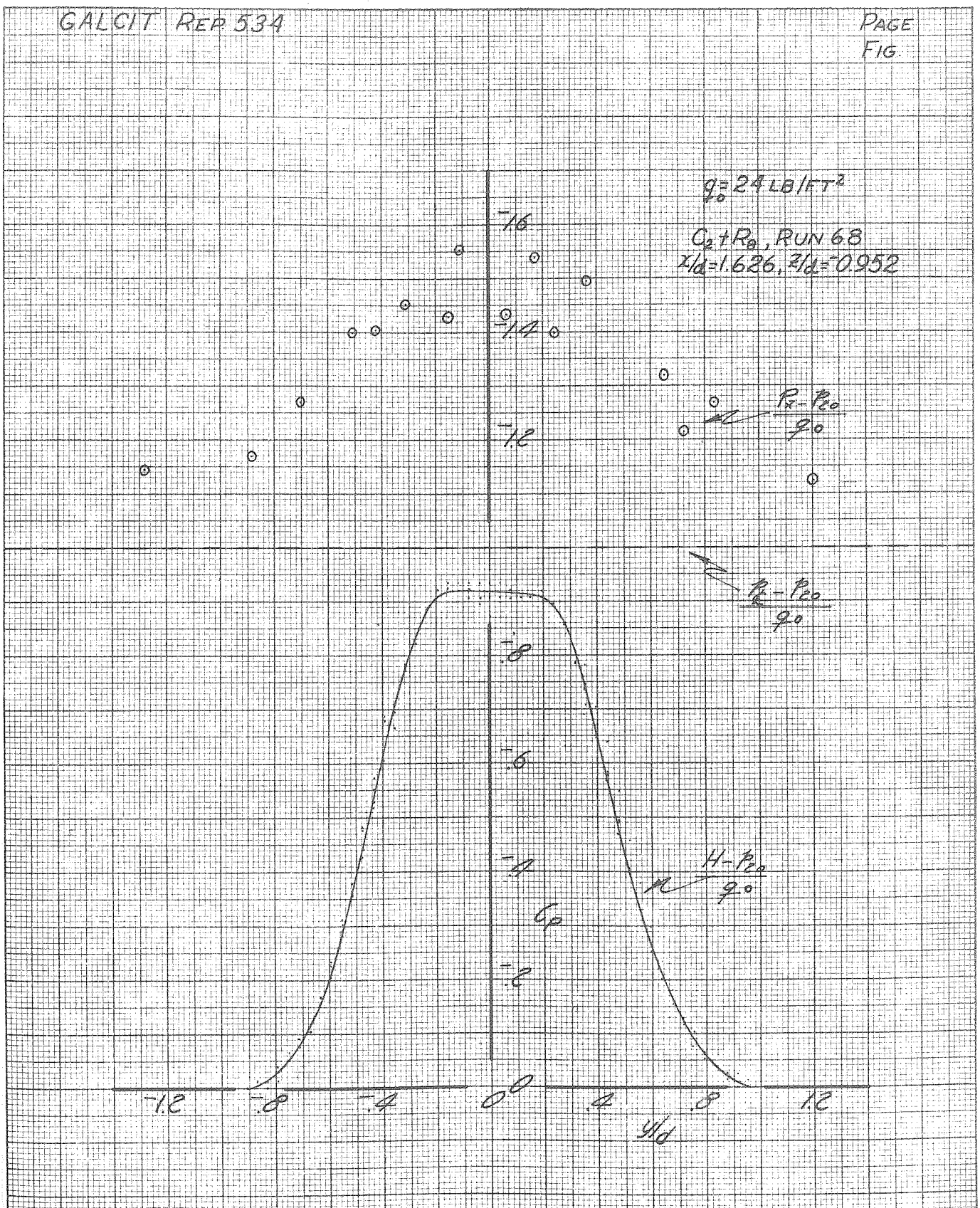

FIGURE 22a
WAKE PATTERN AFT OF CYLINDER C_2
$y/d = 1.626$, $z/d = -0.952$

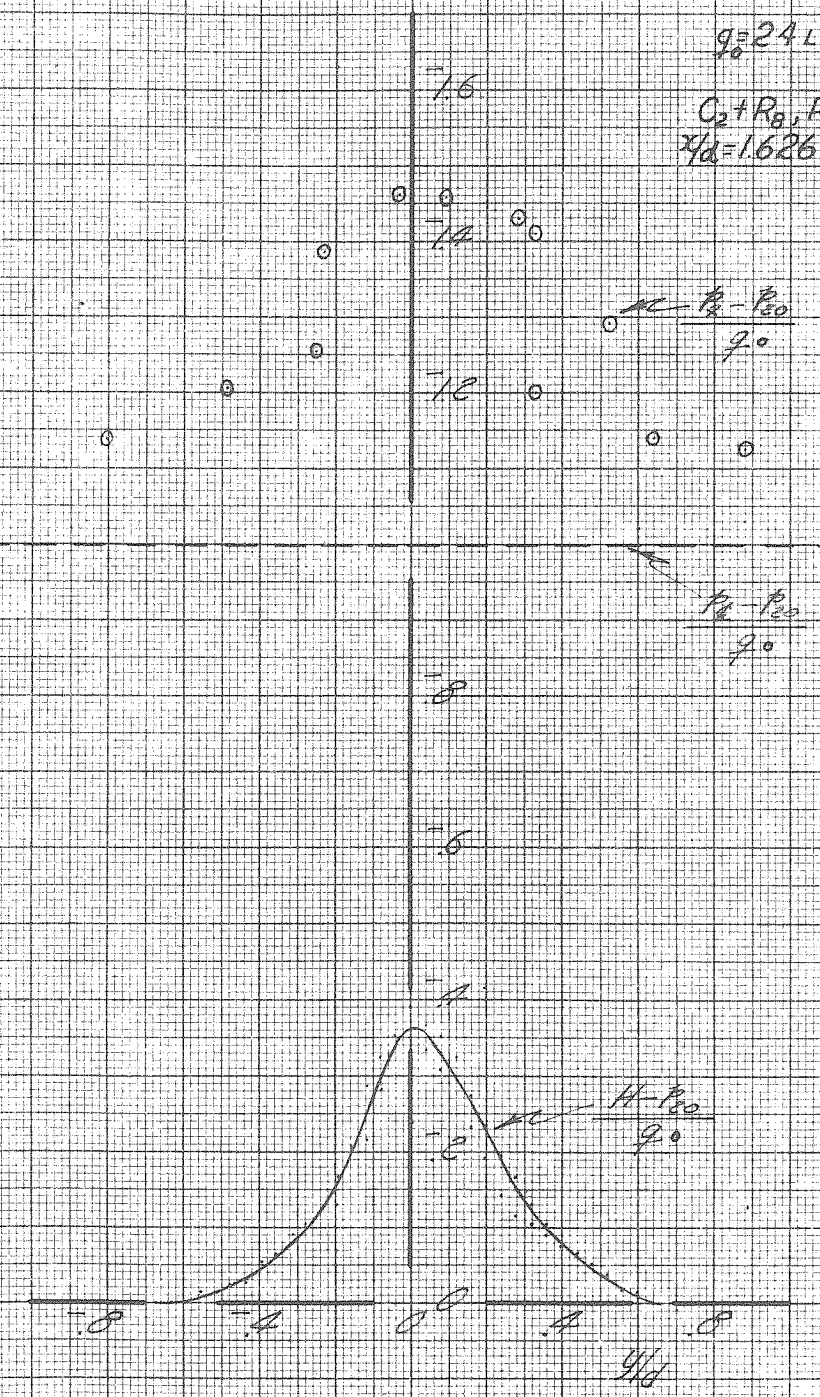

FIGURE 22 b
WAKE PATTERN AFT OF CYLINDER C_2
$x/d = 1.626$, $z/d = -0.714$

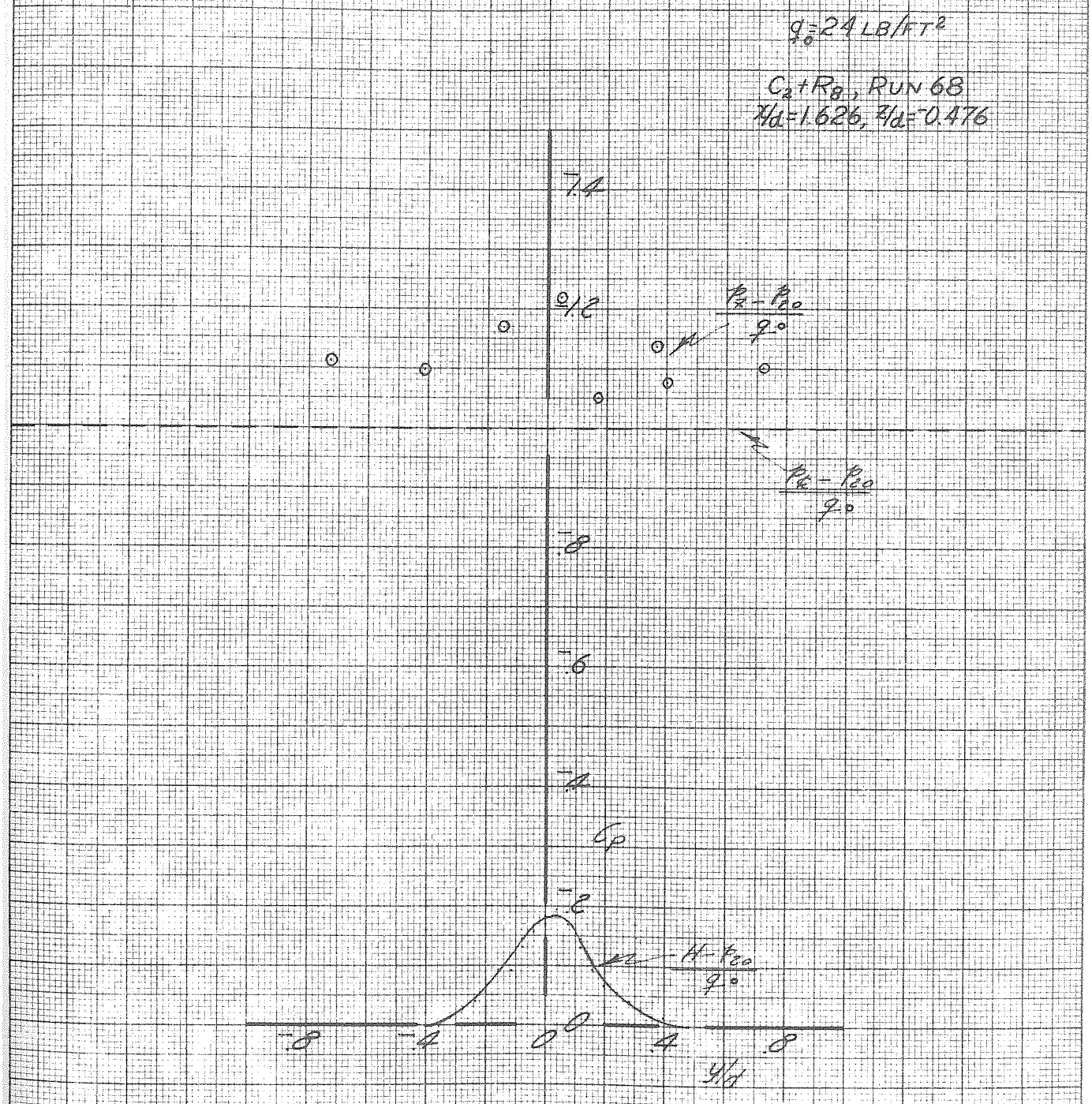

FIGURE 22c
WAKE PATTERN AFT OF CYLINDER C_2
$x/d = 1.626$, $z/d = -0.476$

GALCIT REP. 534

PAGE
FIG.

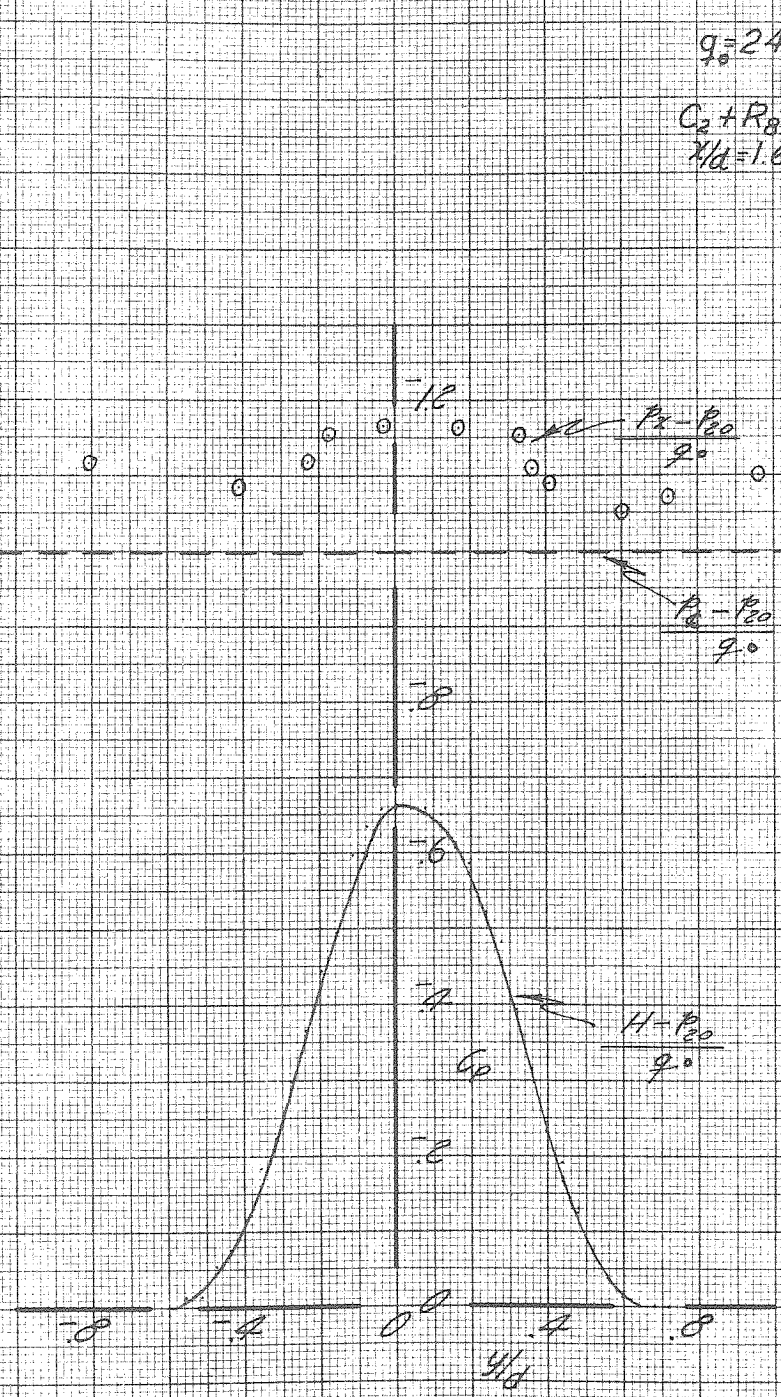

FIGURE 22 d
WAKE PATTERN AFT OF CYLINDER C_2
$x/d = 1.626$, $z/d = 0$

$q_o = 24$ LB/FT²

$C_2 + R_8$, RUN 68
$x/d = 1.626$, $z/d = 0.476$

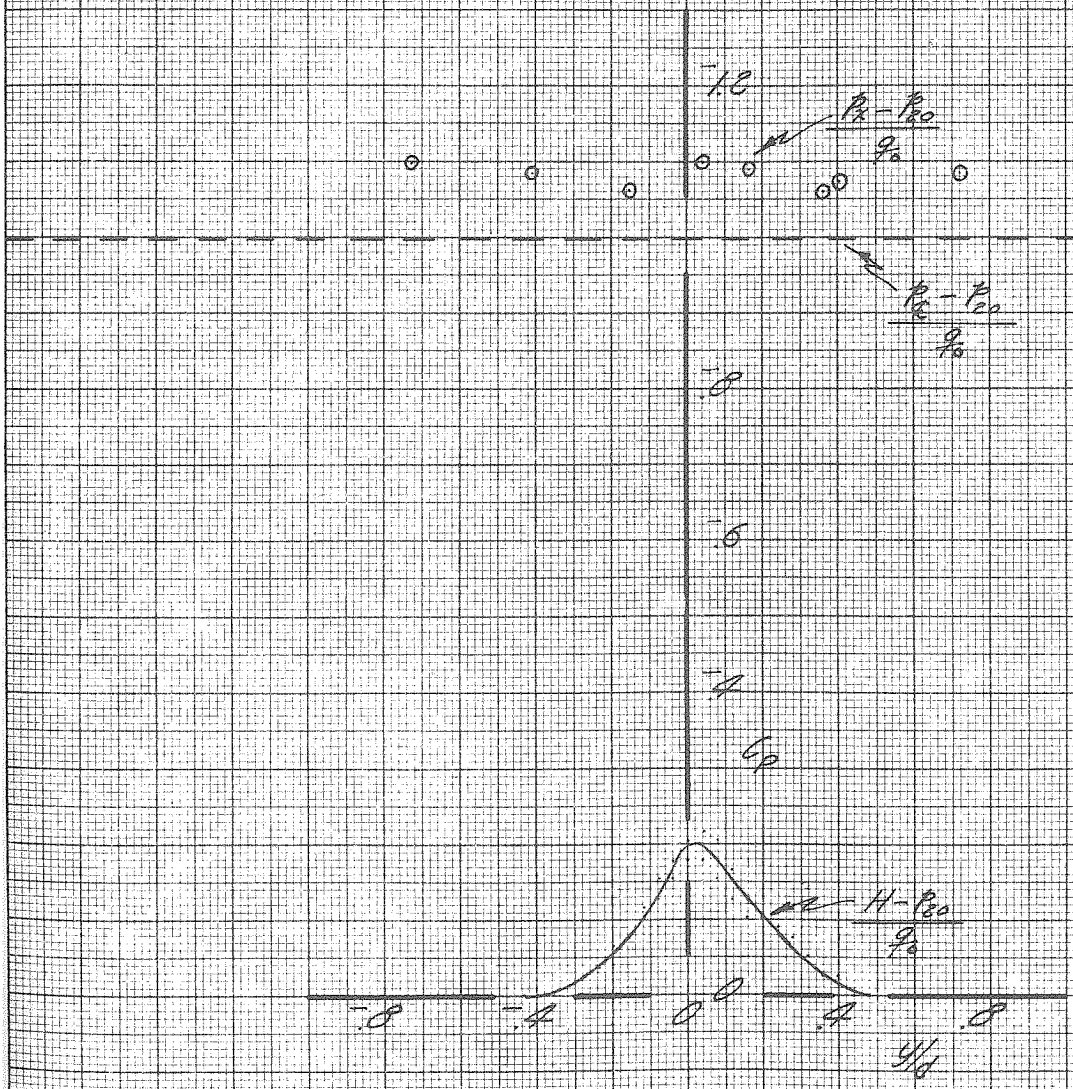

FIGURE 22 a
WAKE PATTERN AFT OF CYLINDER C_2
$x/d = 1.626$, $z/d = 0.476$

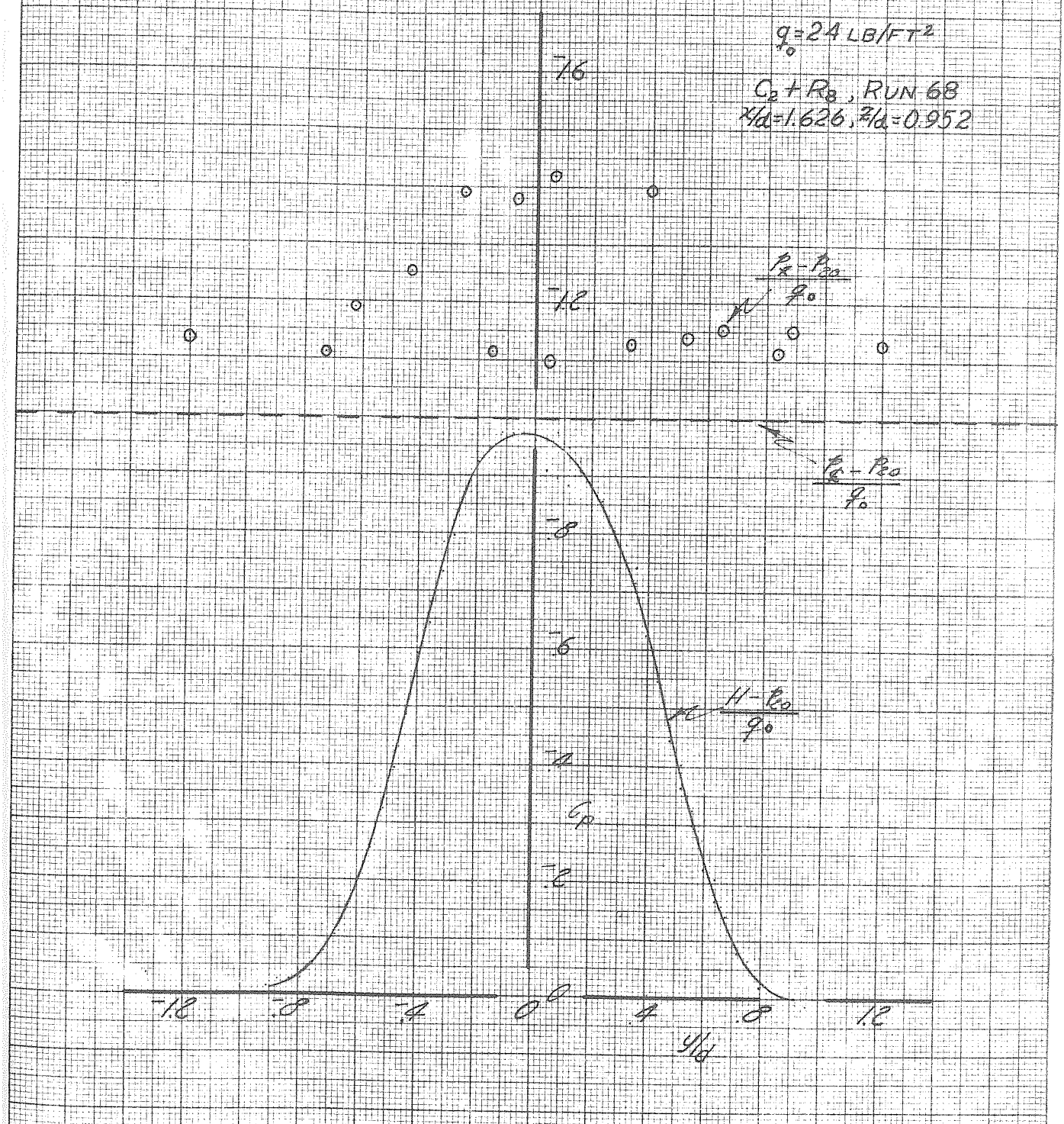

FIGURE 22f
WAKE PATTERN AFT OF CYLINDER C_2
$x/d = 1.626$, $z/d = 0.952$

GALCIT Rep. 534

PAGE FIG.

$q_0 = 22.6 \text{ LB/FT}^2$

$C_2 + R_2$, RUN 66

$Y/d = 3.053$

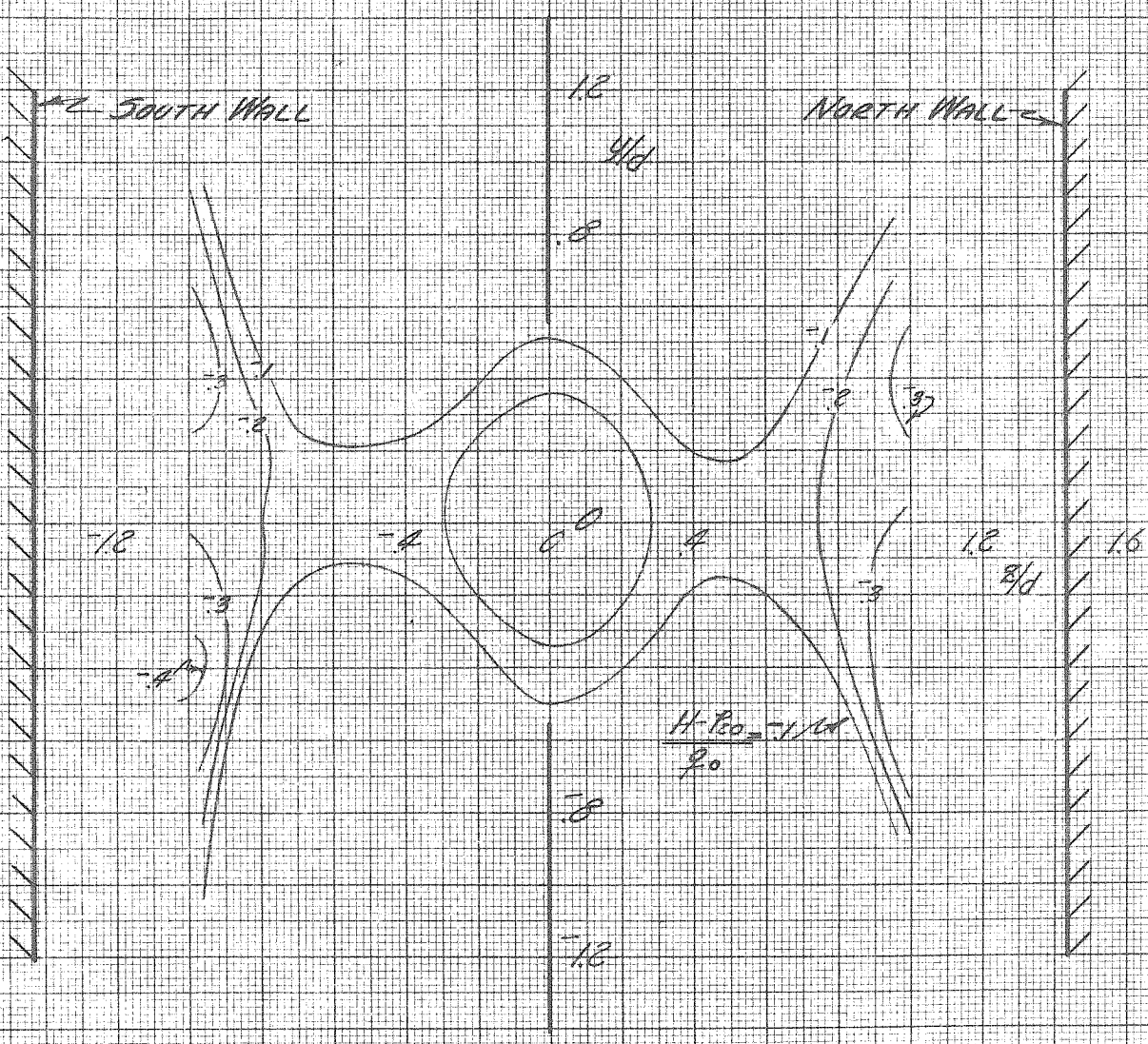

FIGURE 23
CONTOURS OF CONSTANT TOTAL HEAD DECREMENTS AFT OF CYLINDER C_2 WITHOUT SEPARATION STRIPS, $Y/d = 3.053$

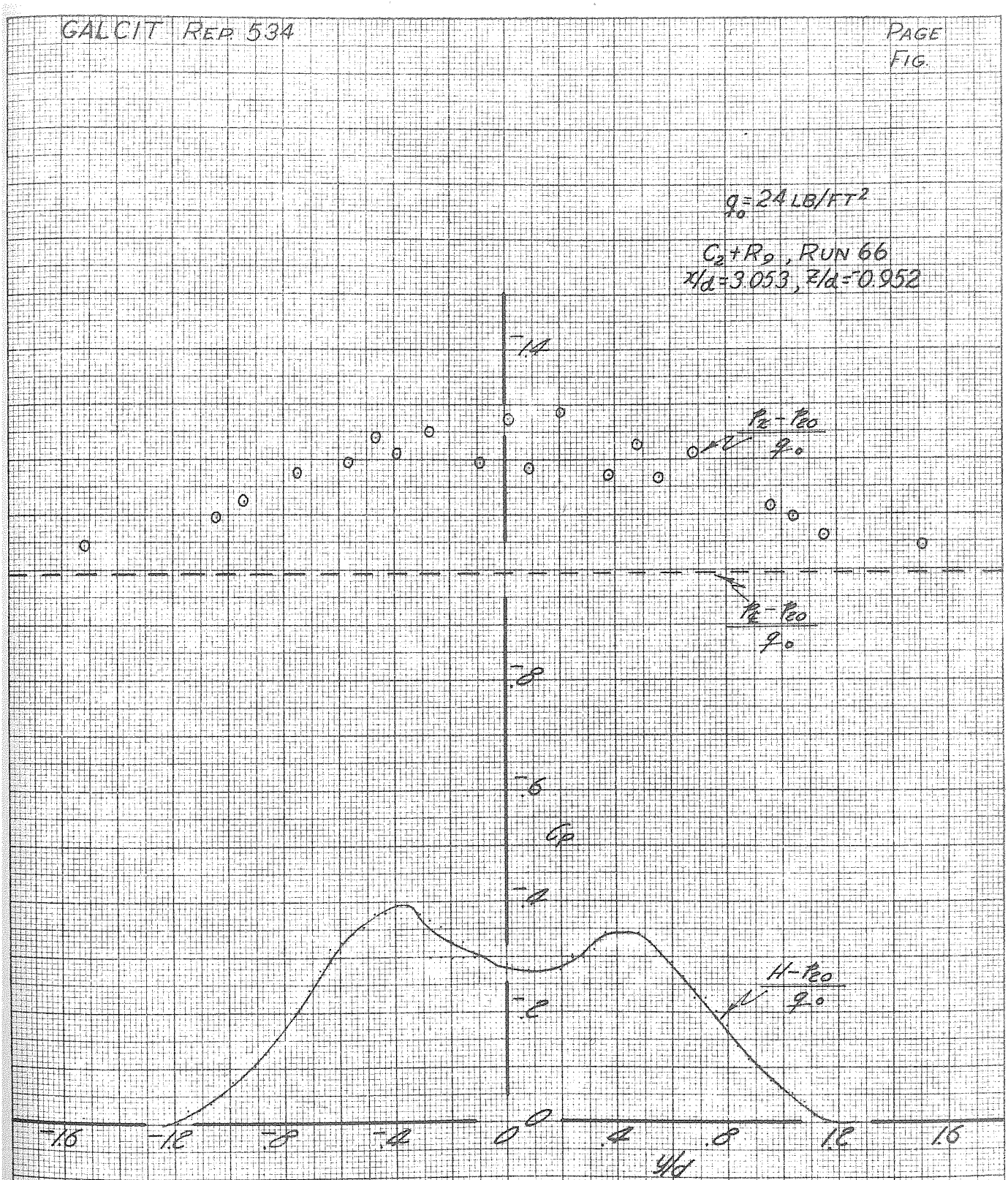

FIGURE 23a
WAKE PATTERN AFT OF CYLINDER C_2
$x/d = 3.053$, $z/d = -0.952$

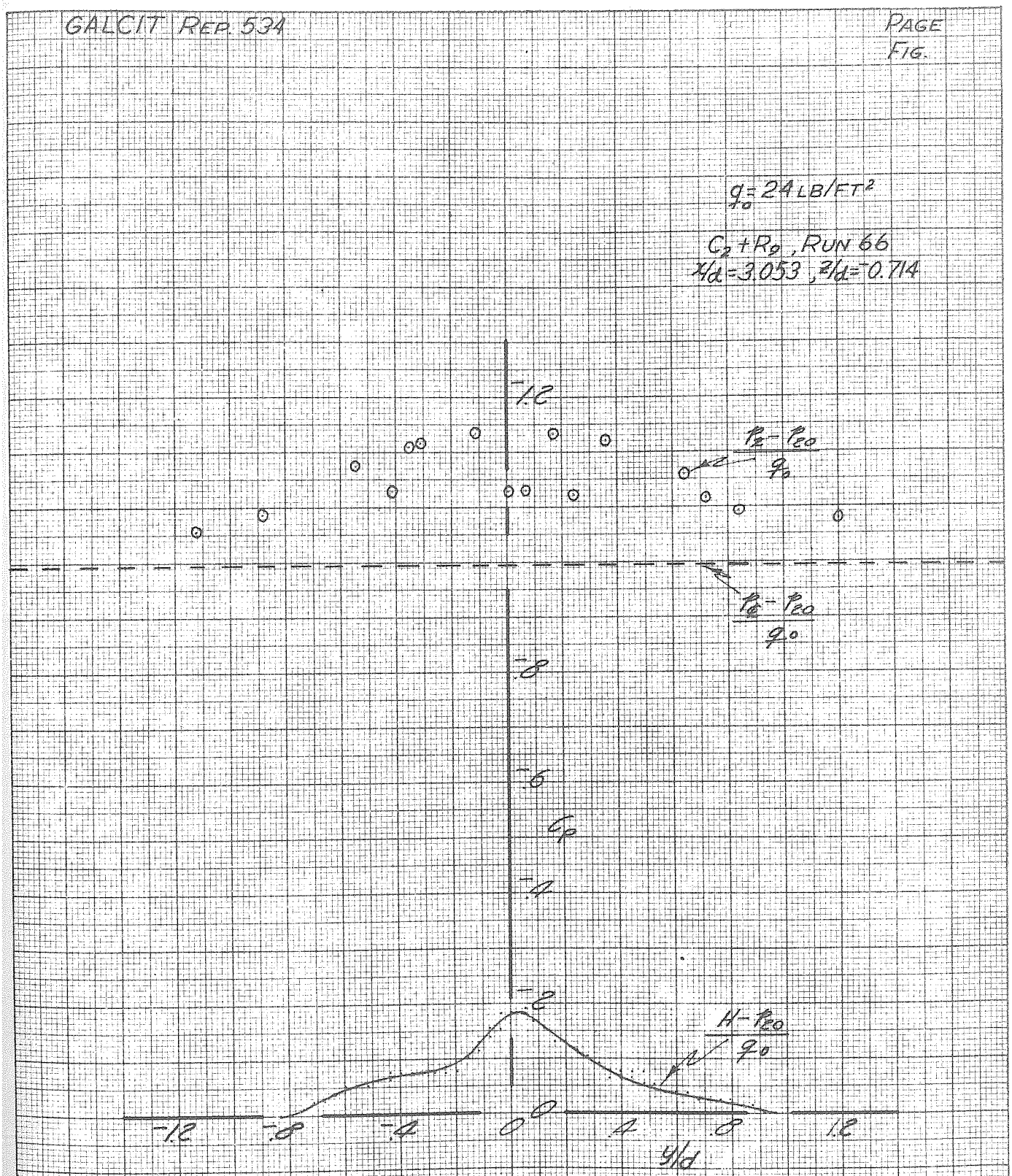

FIGURE 23b
WAKE PATTERN AFT OF CYLINDER C_2
$x/d = 3.053$, $z/d = 0.714$

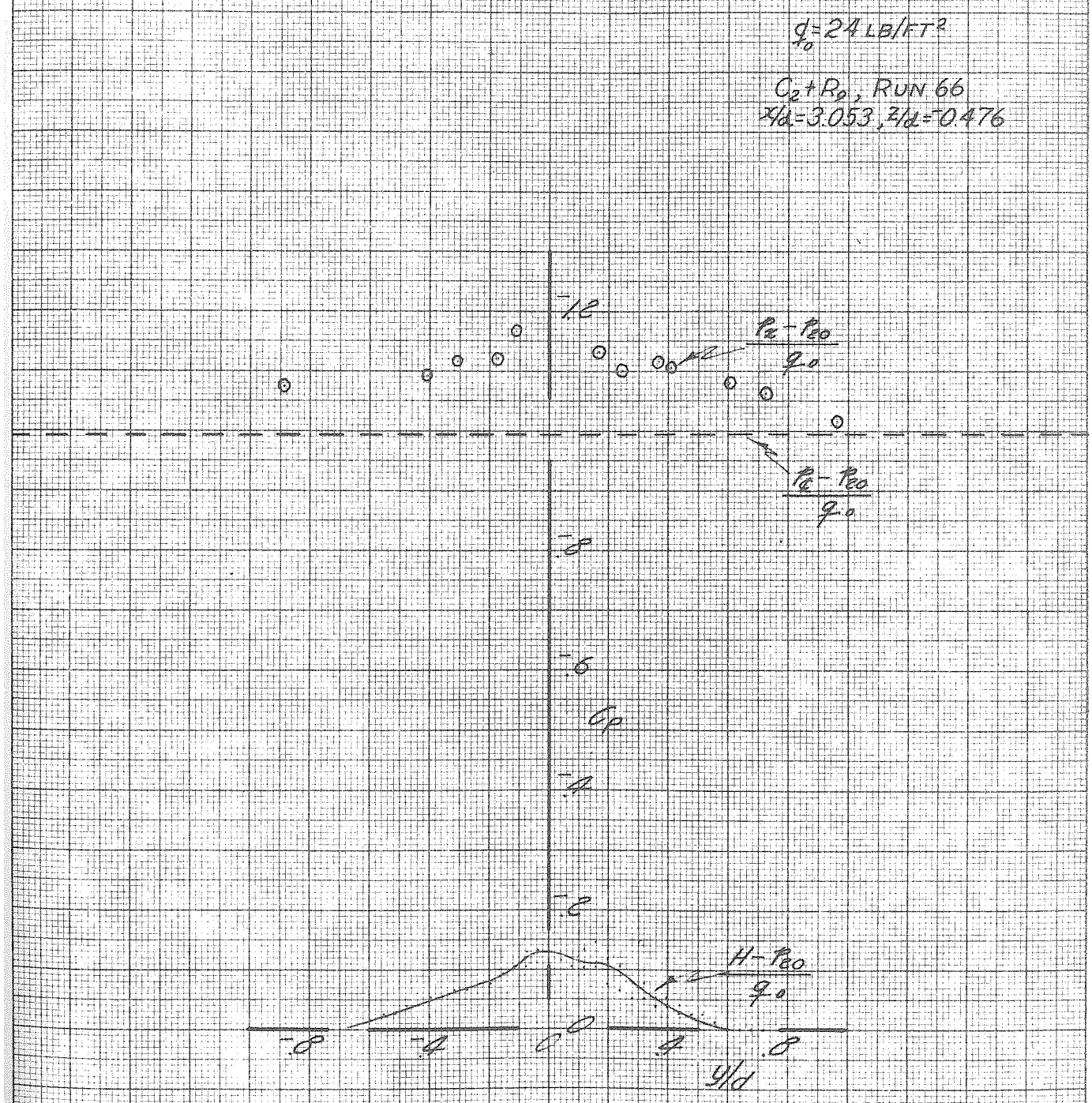

FIGURE 23 c
WAKE PATTERN AFT OF CYLINDER C_2
$x/d = 3.053$, $z/d = 0.476$

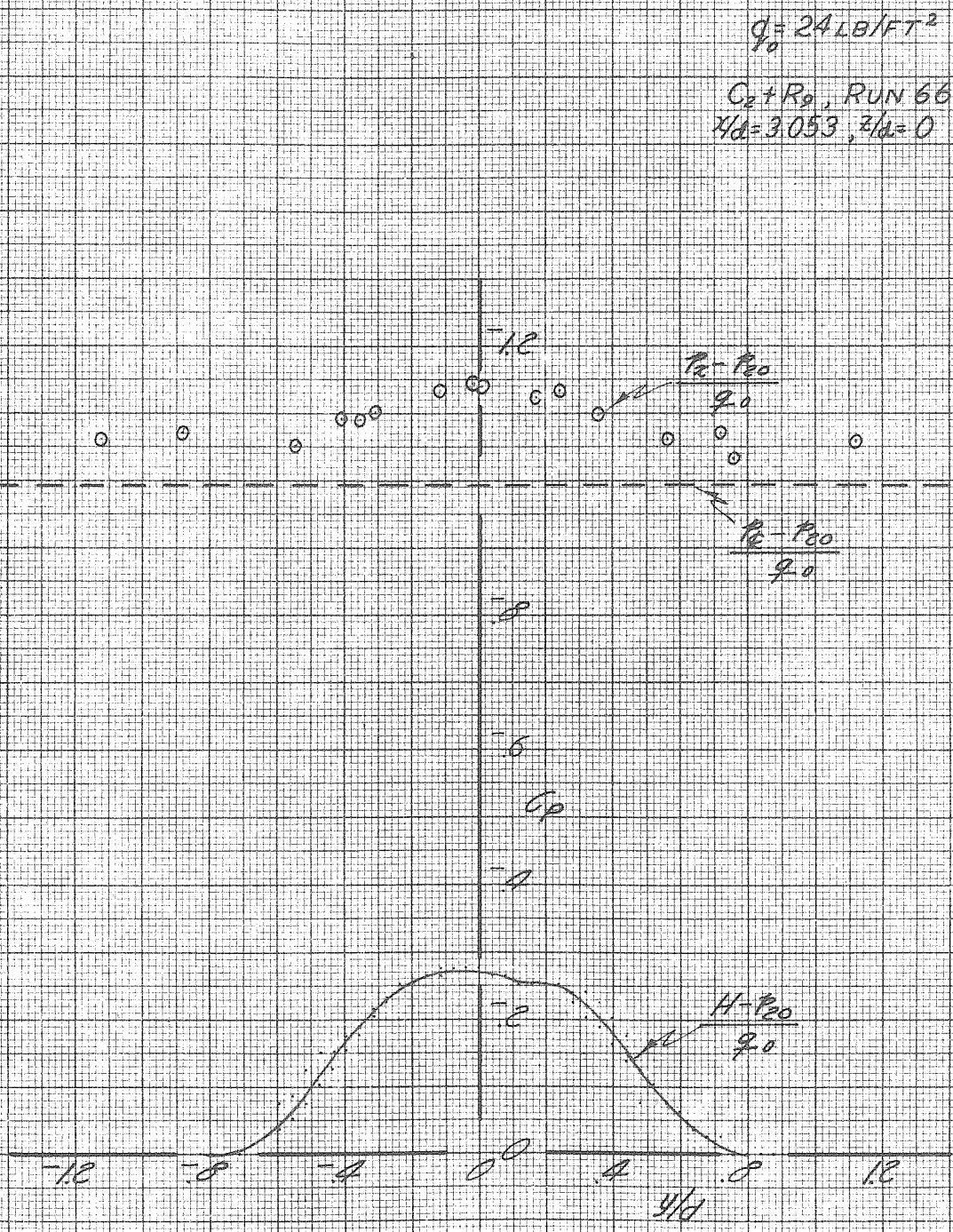

FIGURE 23d
WAKE PATTERN AFT OF CYLINDER C_2
$x/d = 3.053$, $z/d = 0$

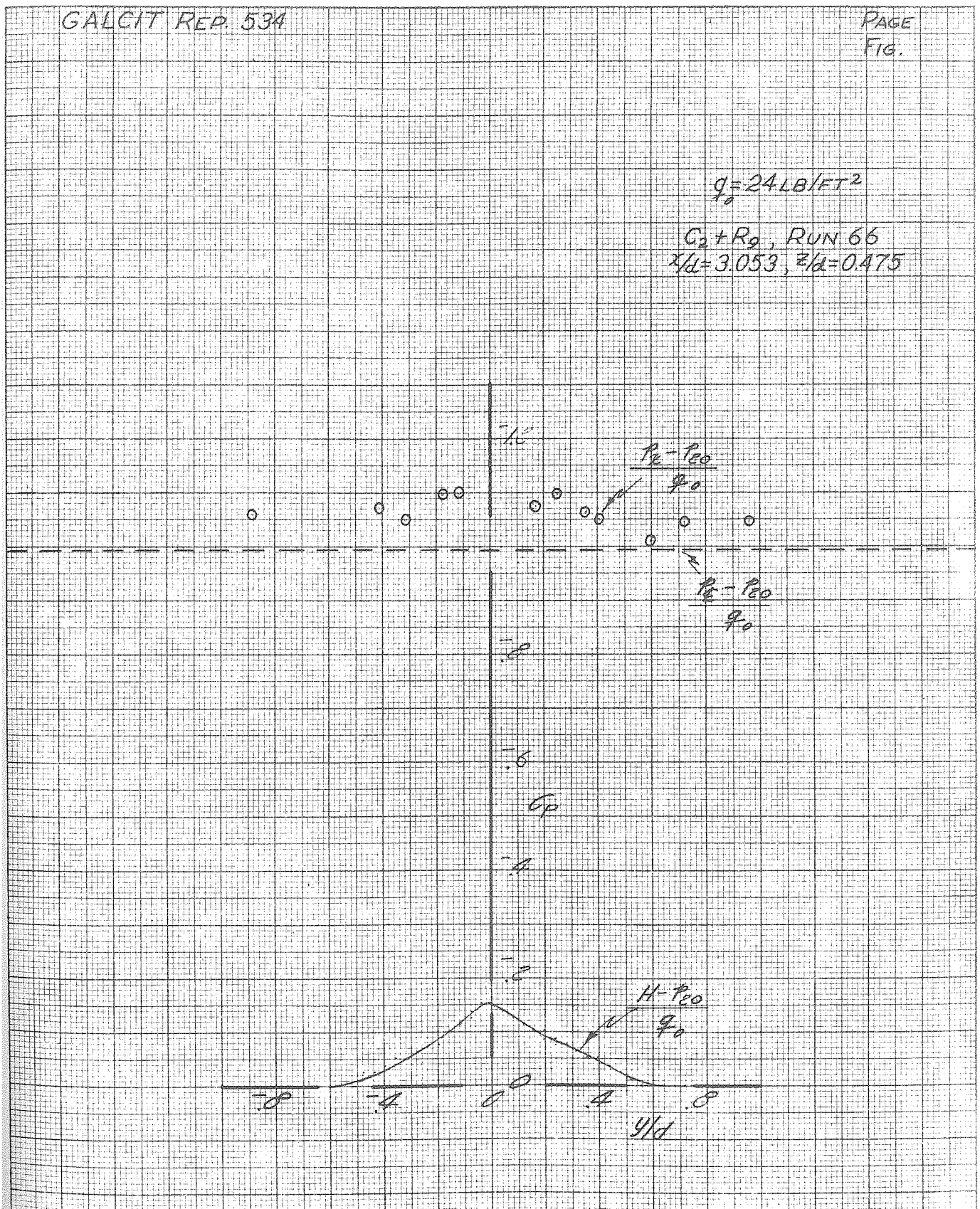

FIGURE 23a
WAKE PATTERN AFT OF CYLINDER C_2
$x/d = 3.053$, $z/d = 0.475$

GALCIT REP. 534

PAGE
FIG.

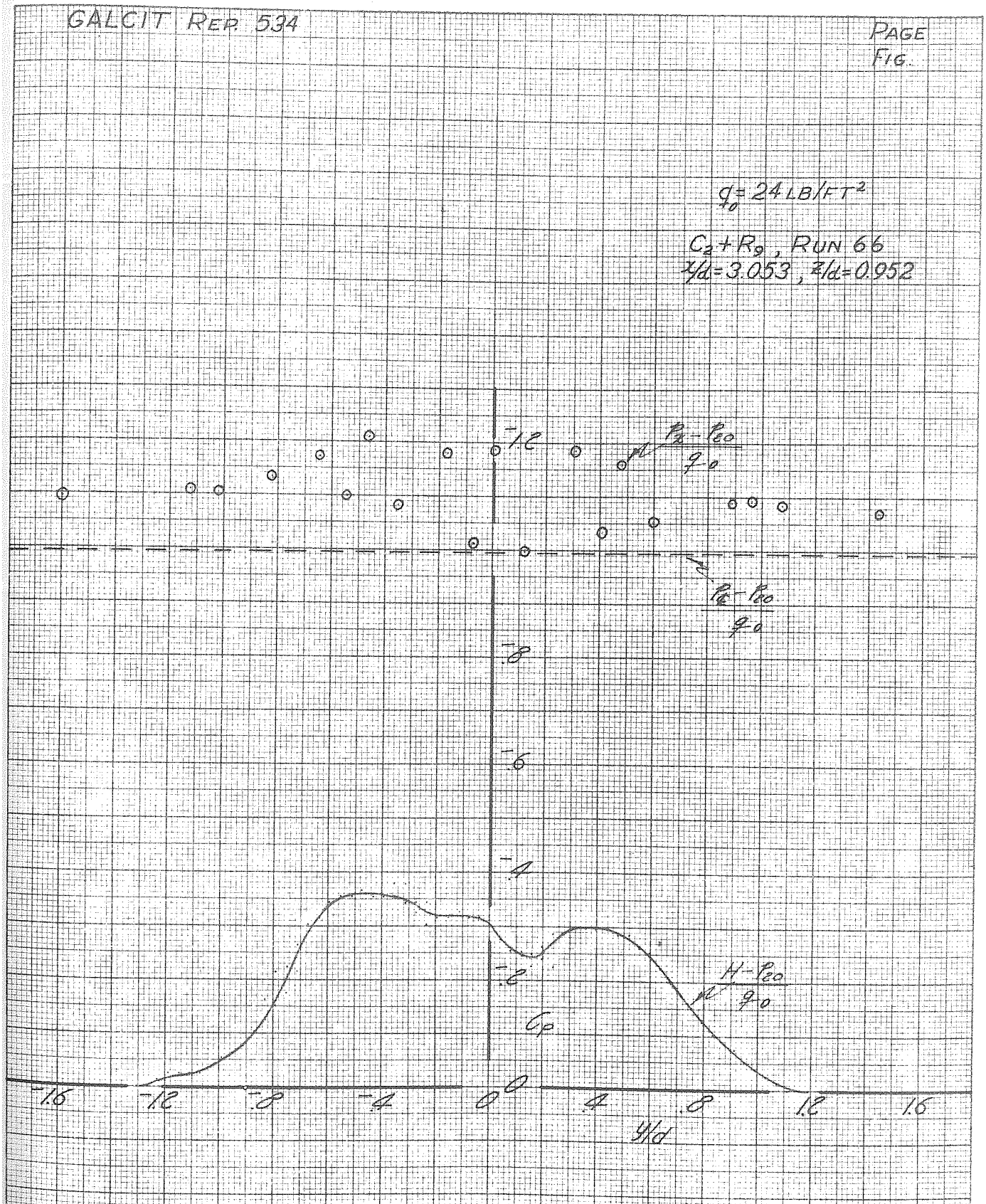

FIGURE 23f
WAKE PATTERN AFT OF CYLINDER C_2
$x/d = 3.053$, $z/d = 0.952$

GALCIT REP 338 PAGE FIG

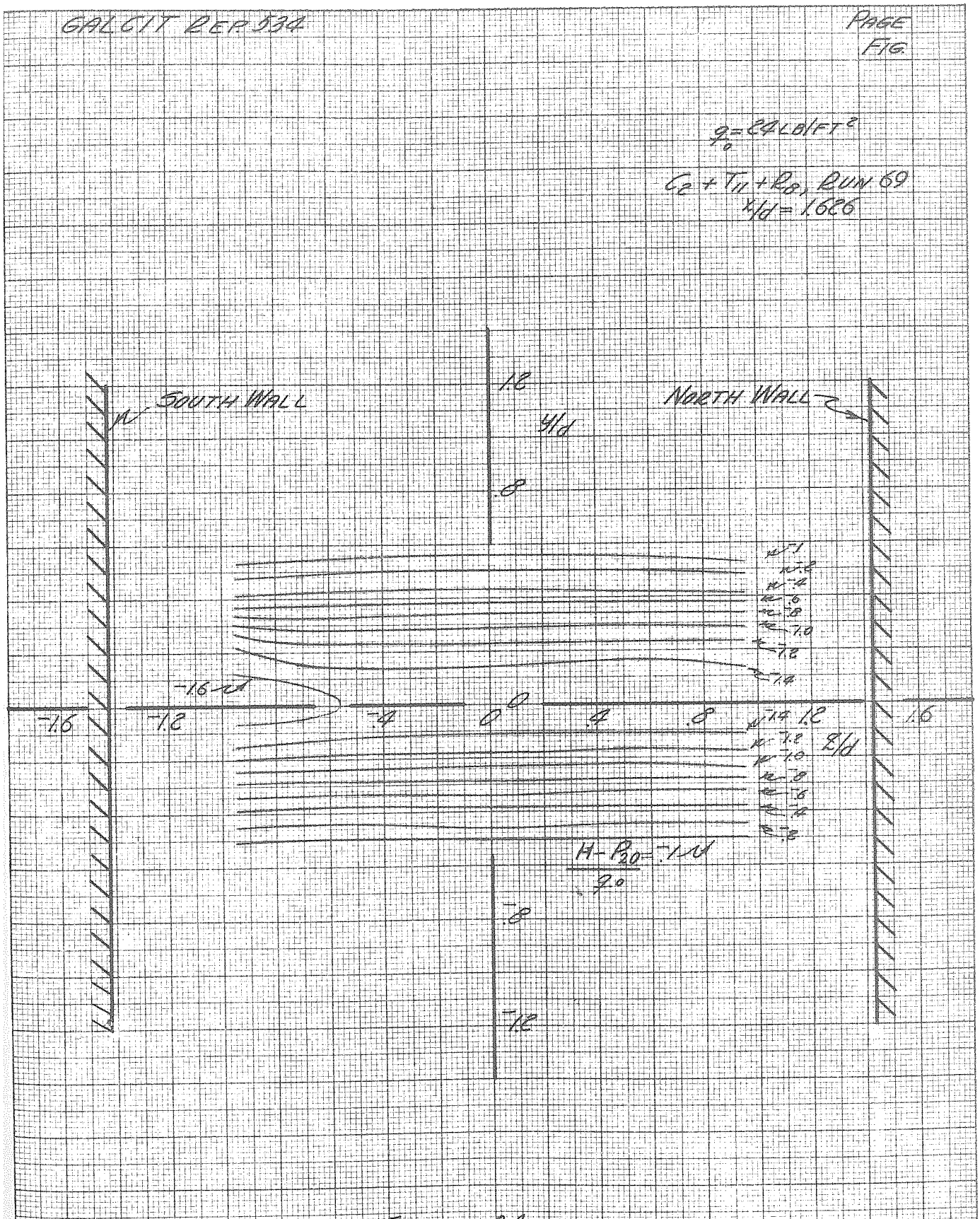

FIGURE 24
CONTOURS OF CONSTANT TOTAL HEAD DECREMENTS AFT OF CYLINDER ($C_2 + T_{11}$)
X/d = 1.626

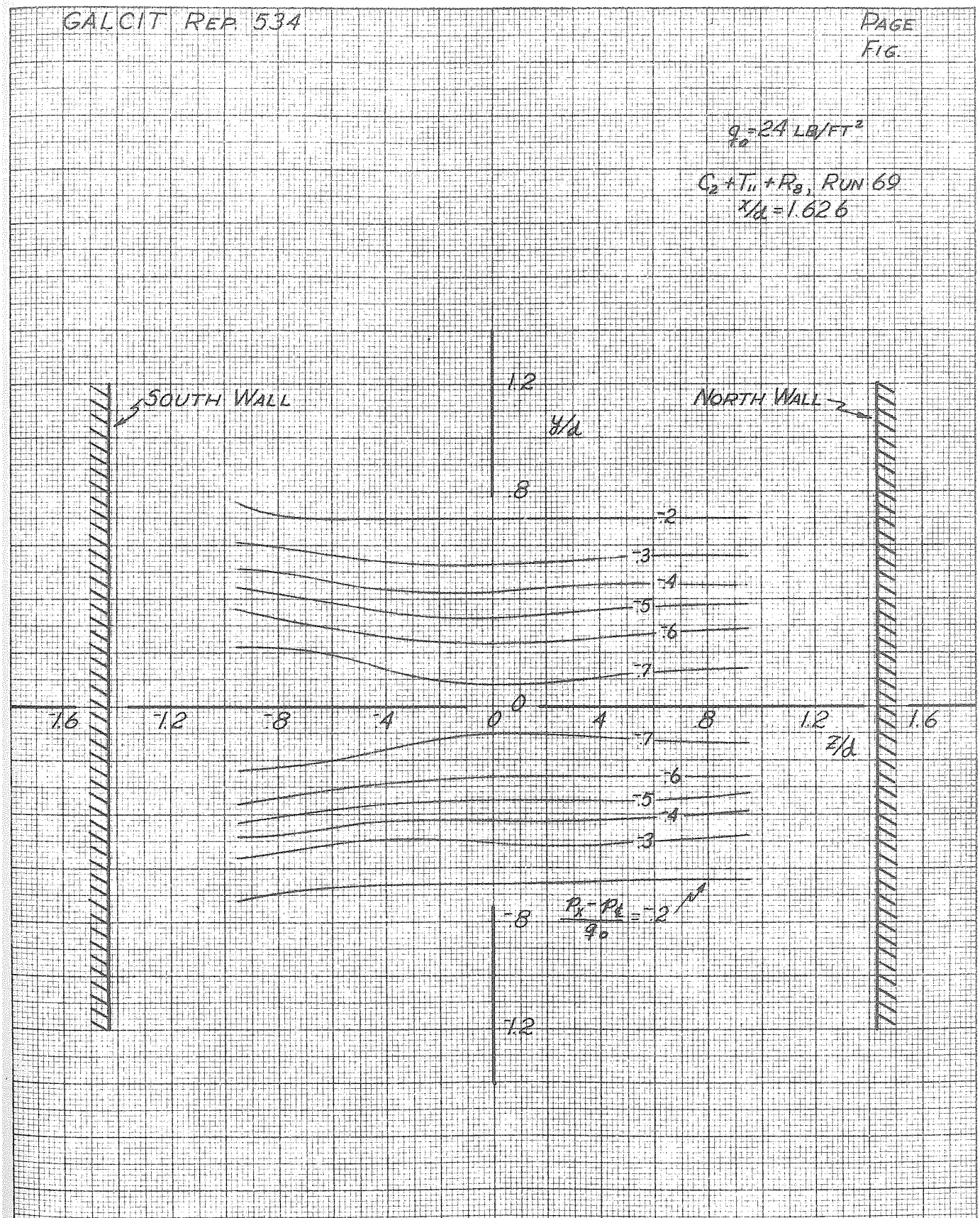

FIGURE 24-1
CONTOURS OF CONSTANT STATIC PRESSURE DECREMENTS AFT OF CYLINDER ($C_2 + T_{11}$)
x/d = 1.626

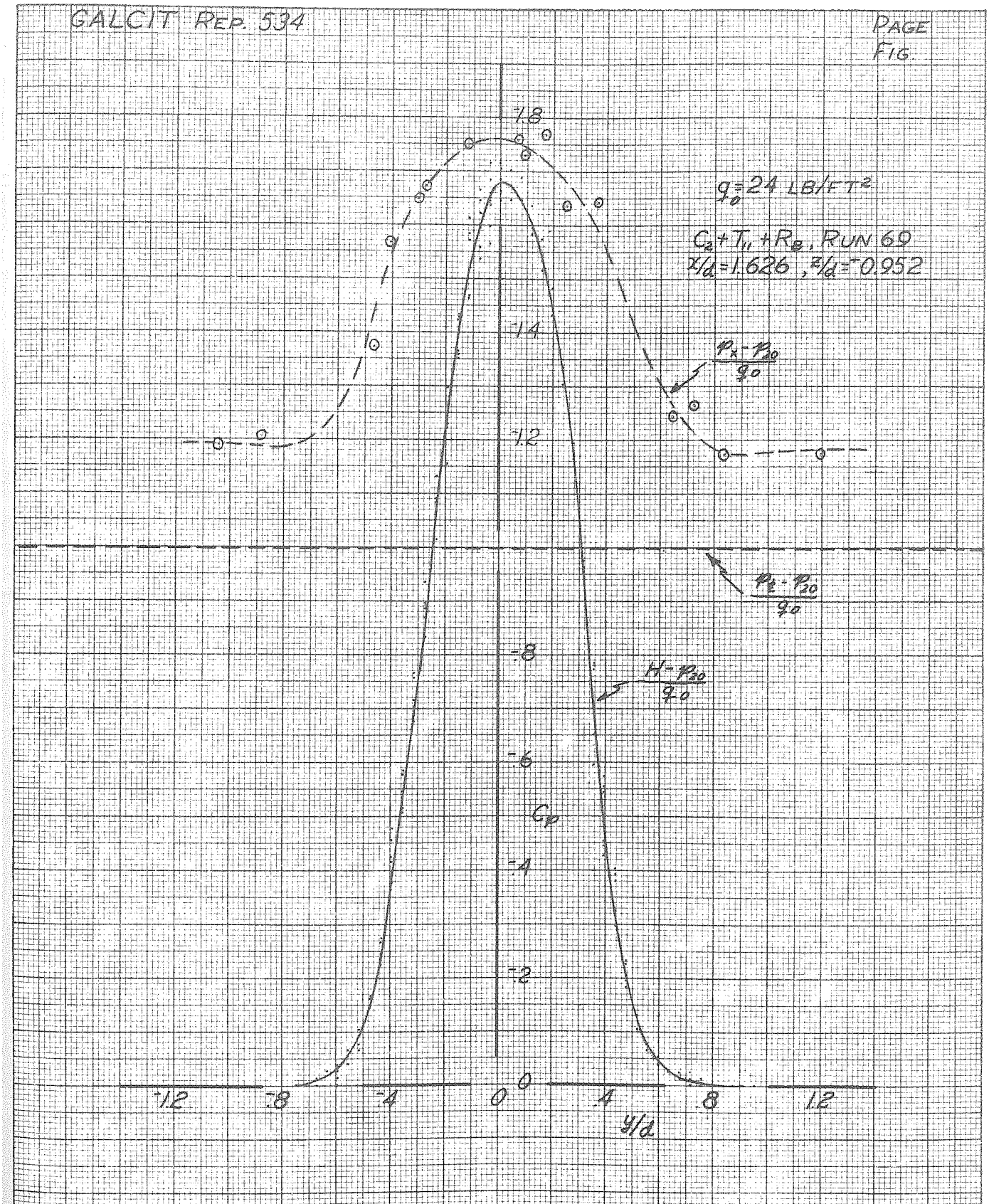

FIGURE 24a
WAKE PATTERN AFT OF CYLINDER ($C_2 + T_{11}$)
$x/d = 1.626$, $z/d = -0.952$

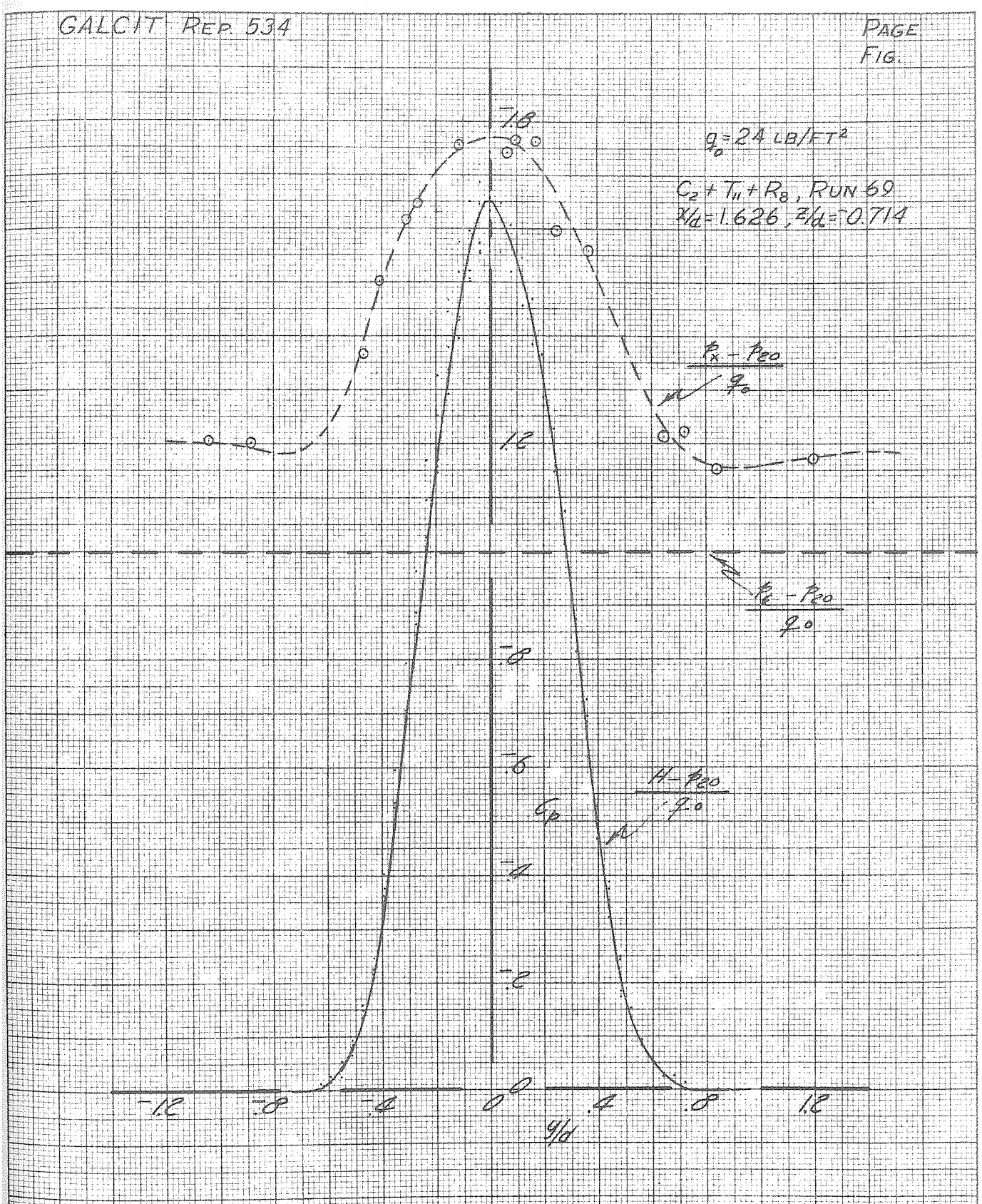

FIGURE 24b
WAKE PATTERN AFT OF CYLINDER (C_2+T_{11})
$x/d = 1.626$, $z/d = -0.714$

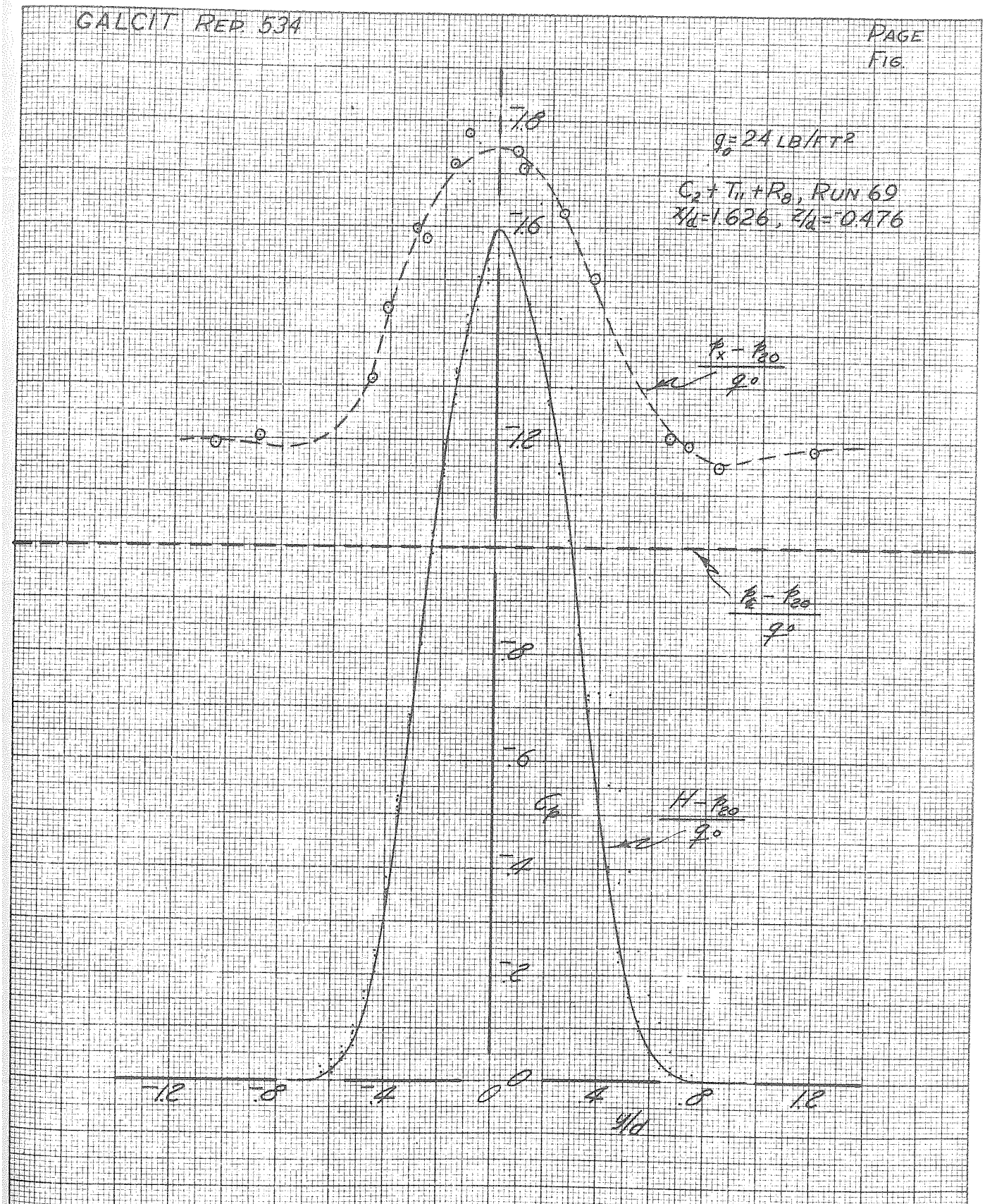

FIGURE 24c
WAKE PATTERN AFT OF CYLINDER ($C_2 + T_{11}$)
$x/d = 1.626$, $z/d = -0.476$

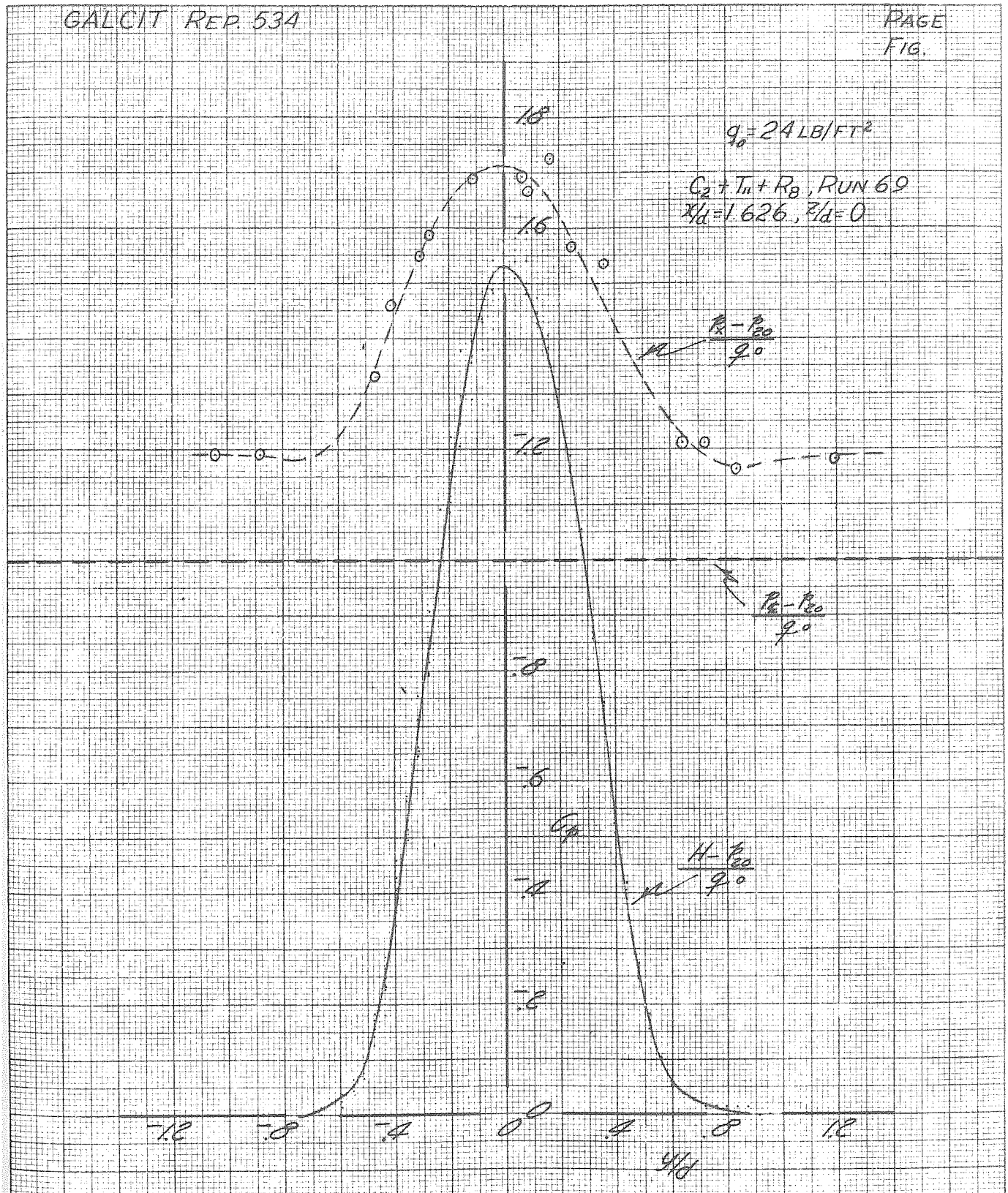

FIGURE 24d
WAKE PATTERN AFT OF CYLINDER ($C_2 + T_{11}$)
$x/d = 1.626$, $z/d = 0$

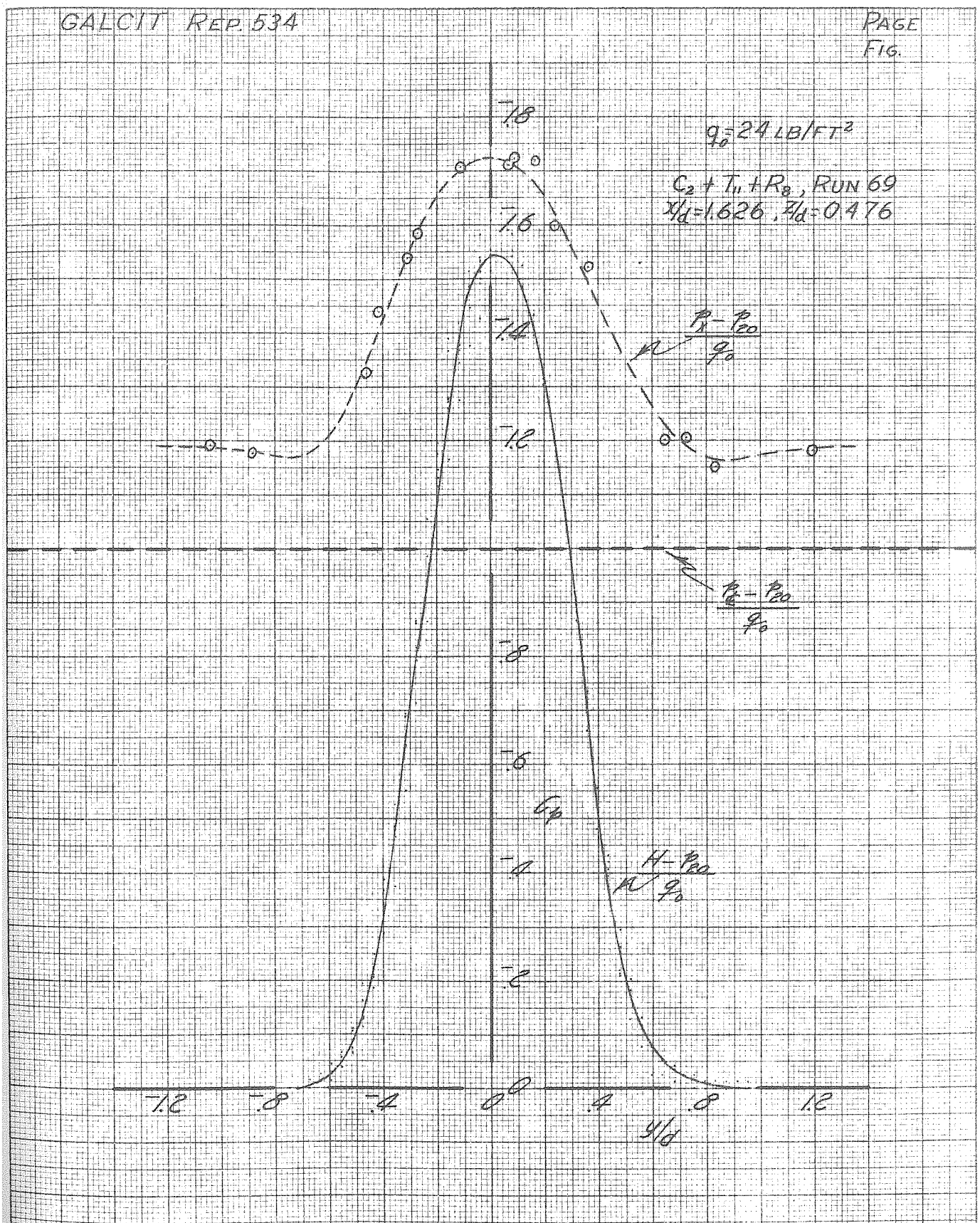

FIGURE 24c
WAKE PATTERN AFT OF CYLINDER ($C_2 + T_{11}$)
$x/d = 1.626$, $z/d = 0.476$

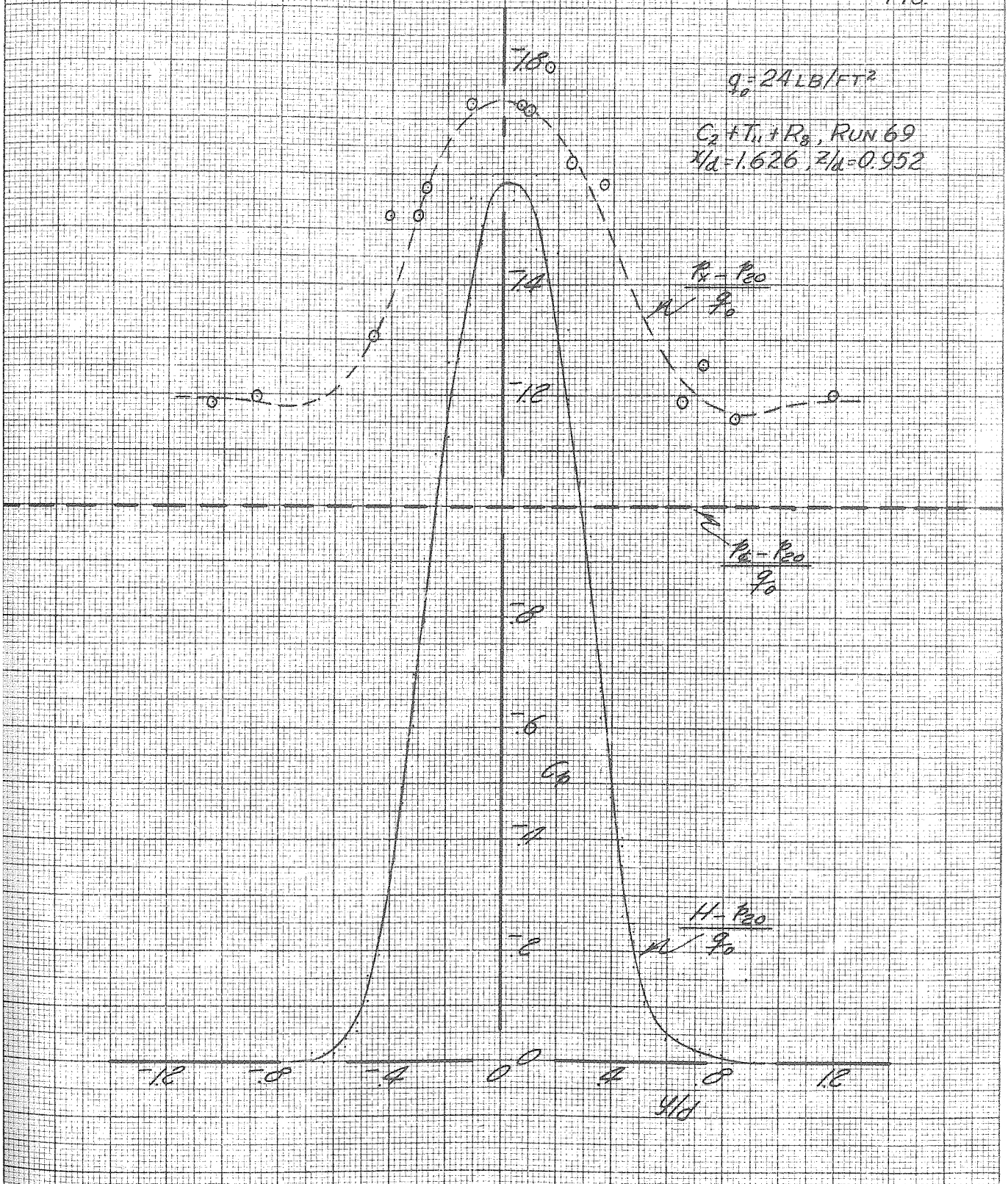

FIGURE 24 f
WAKE PATTERN AFT OF CYLINDER ($C_2 + T_{11}$)
$x/d = 1.626$, $z/d = 0.952$

GALCIT REP 534

PAGE
FIG.

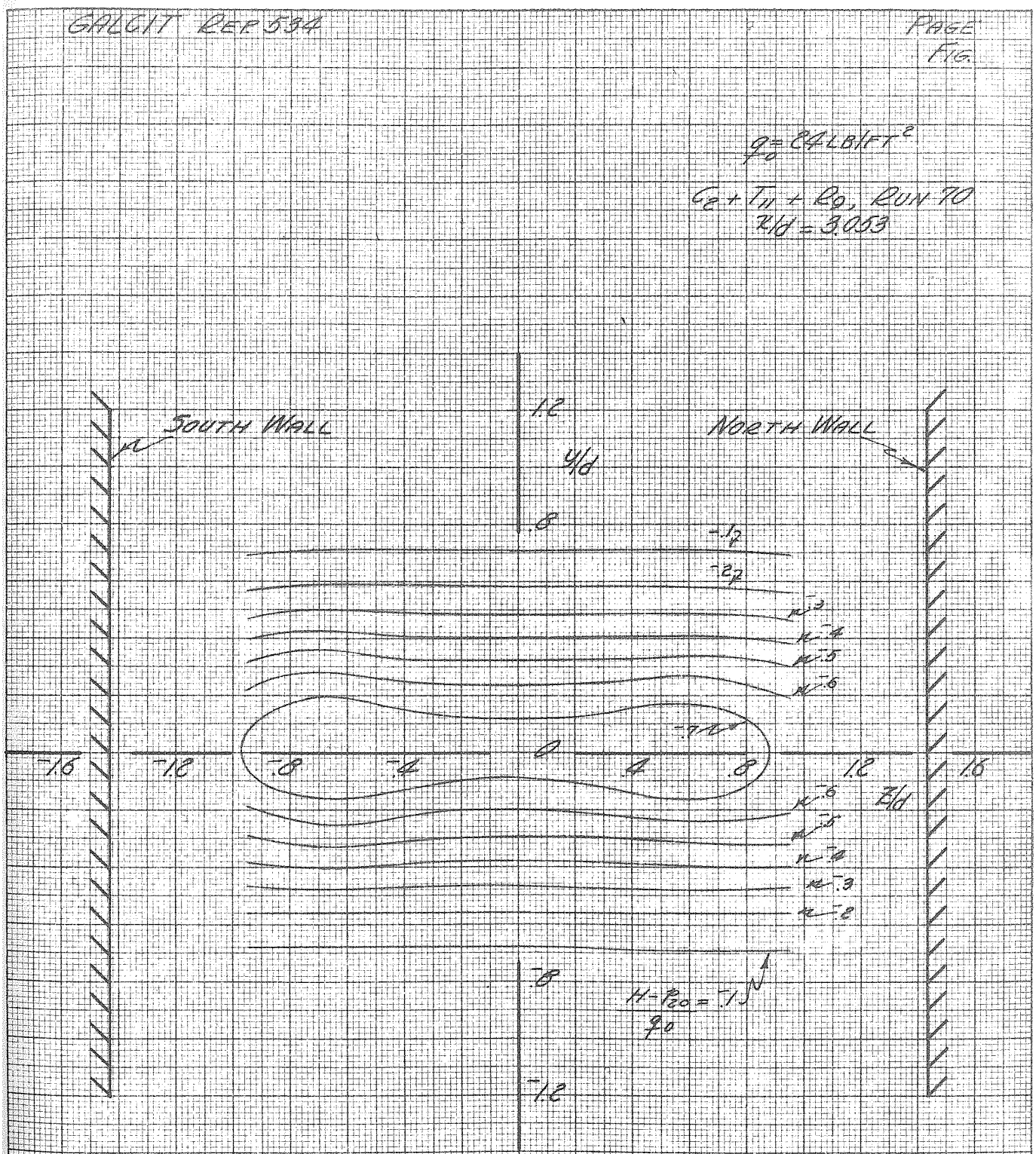

FIGURE 25
CONTOURS OF CONSTANT TOTAL HEAD DECREMENTS AFT OF CYLINDER ($G_2 + T_{11}$)
$Y/d = 3.053$

GALCIT REP. 534 PAGE FIG.

$q_{\infty} = 24 \text{ LB/FT}^2$

$C_2 + T_{III} + R_9$, RUN 70

$x/d = 3.053$

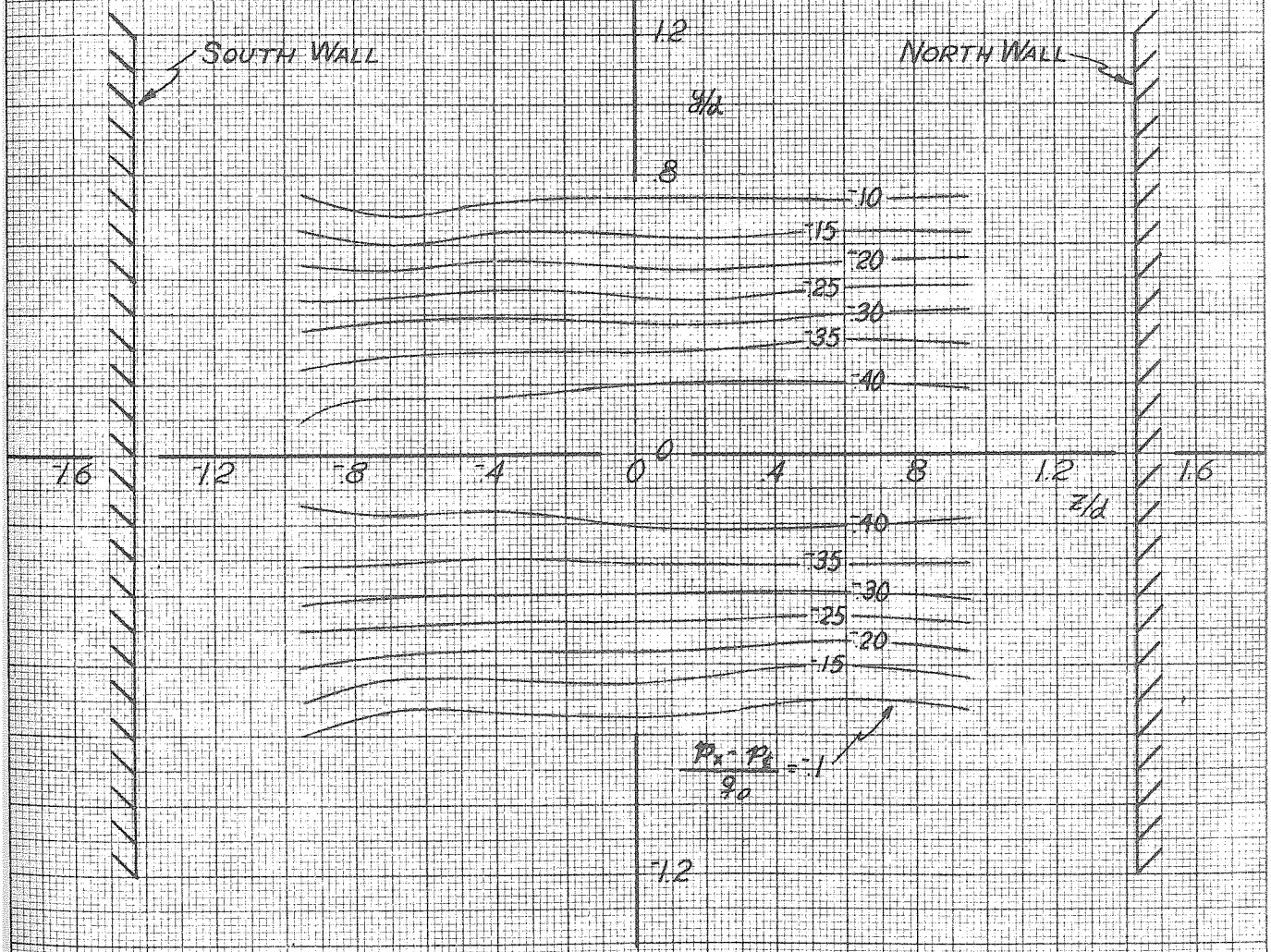

FIGURE 25-1

CONTOURS OF CONSTANT STATIC PRESSURE DECREMENTS AFT OF CYLINDER

$(C_2 + T_{III})$

$x/d = 3.053$

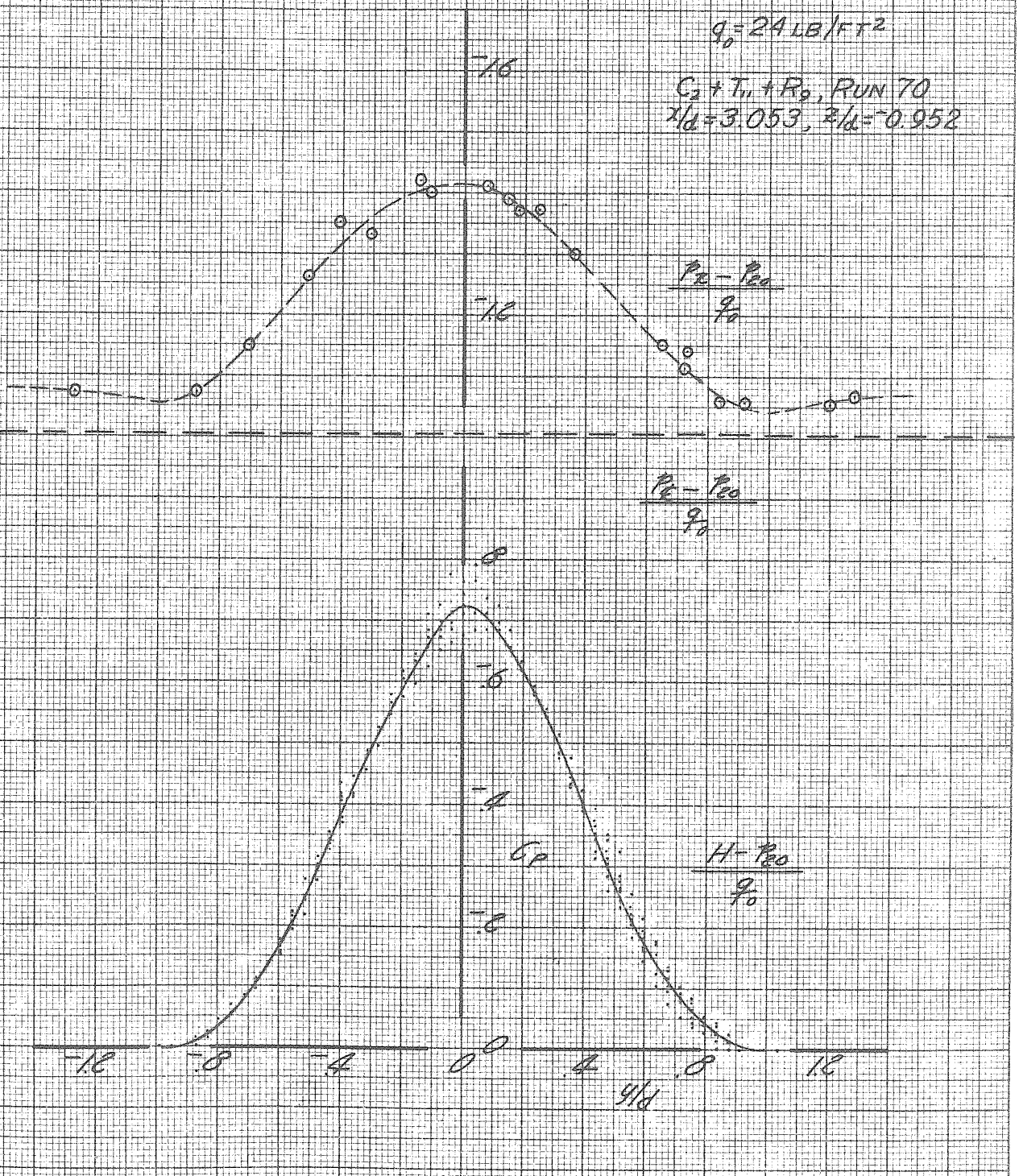

FIGURE 25a
WAKE PATTERN AFT OF CYLINDER ($C_2 + T_{11}$)
$x/d = 3.053$, $z/d = 0.952$

GALCIT REP. 584

PAGE
FIG.

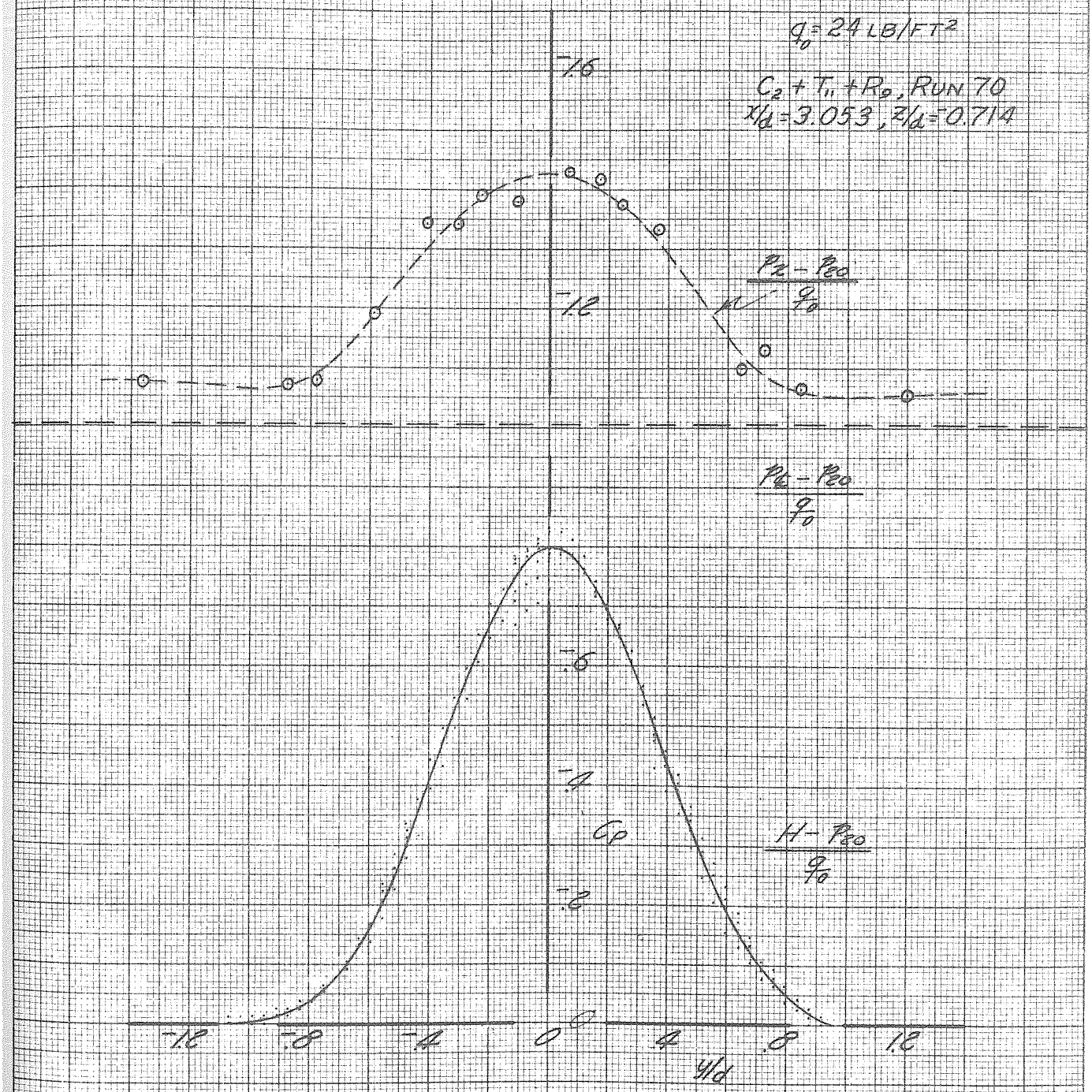

FIGURE 25b
WAKE PATTERN AFT OF CYLINDER ($C_2 + T_{11}$)
$x/d = 3.053$, $z/d = 0.714$

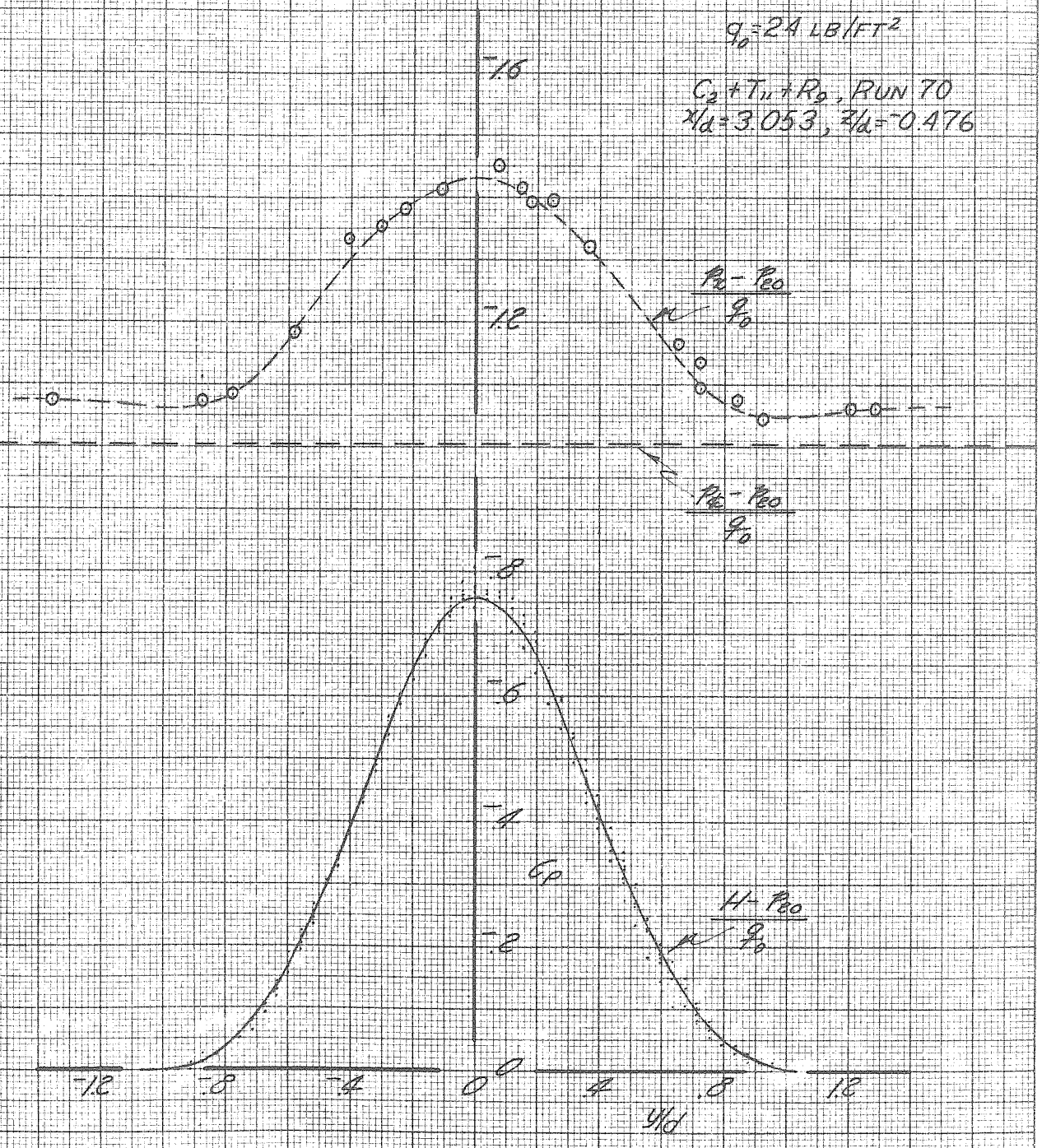

FIGURE 25c
WAKE PATTERN AFT OF CYLINDER ($C_2 + T_{11}$)
$x/d = 3.053$, $z/d = -0.476$

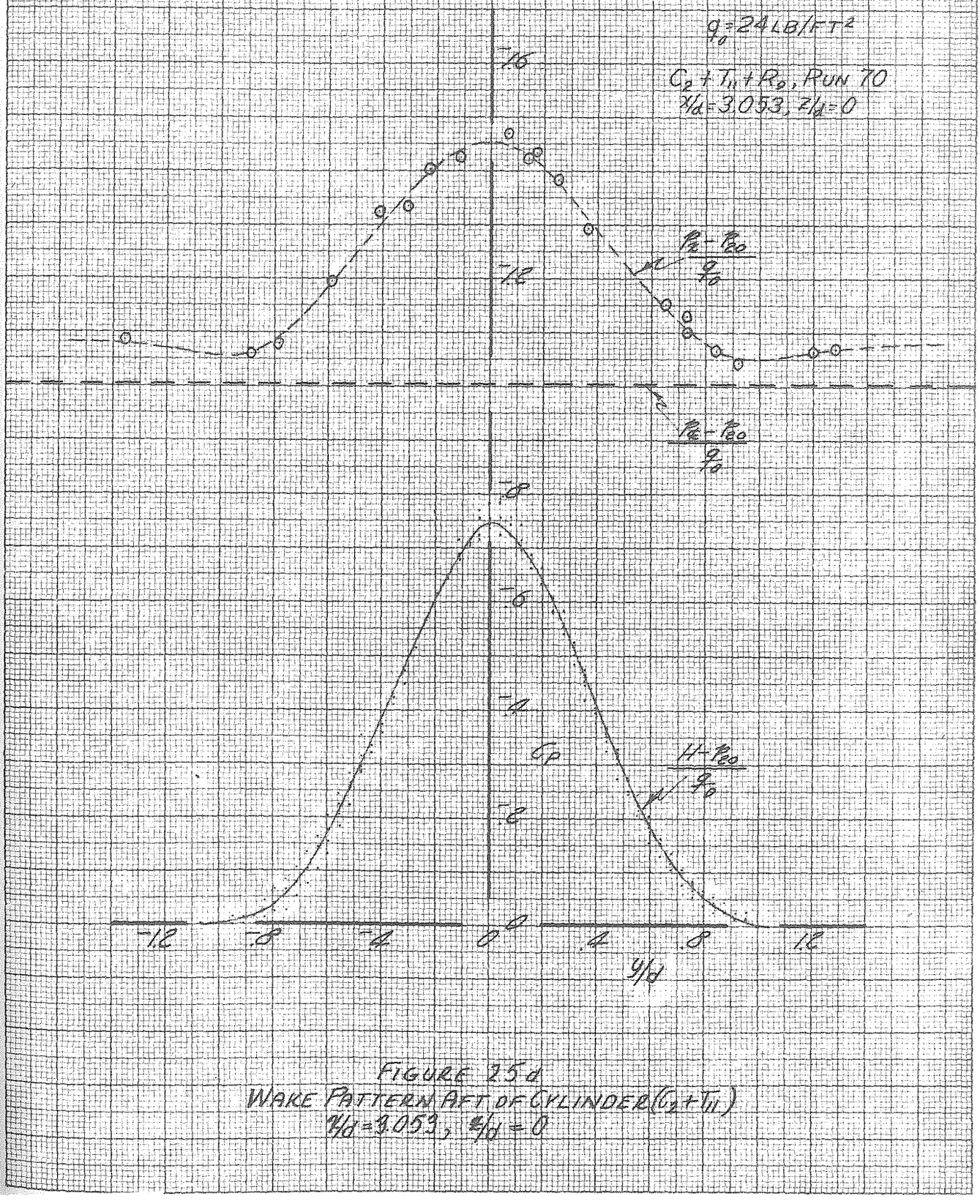

FIGURE 25 d
WAKE PATTERN AFT OF CYLINDER ($C_2 + T_{11}$)
$x/d = 3.053$, $z/d = 0$

GALCIT REA 534

PAGE
FIG.

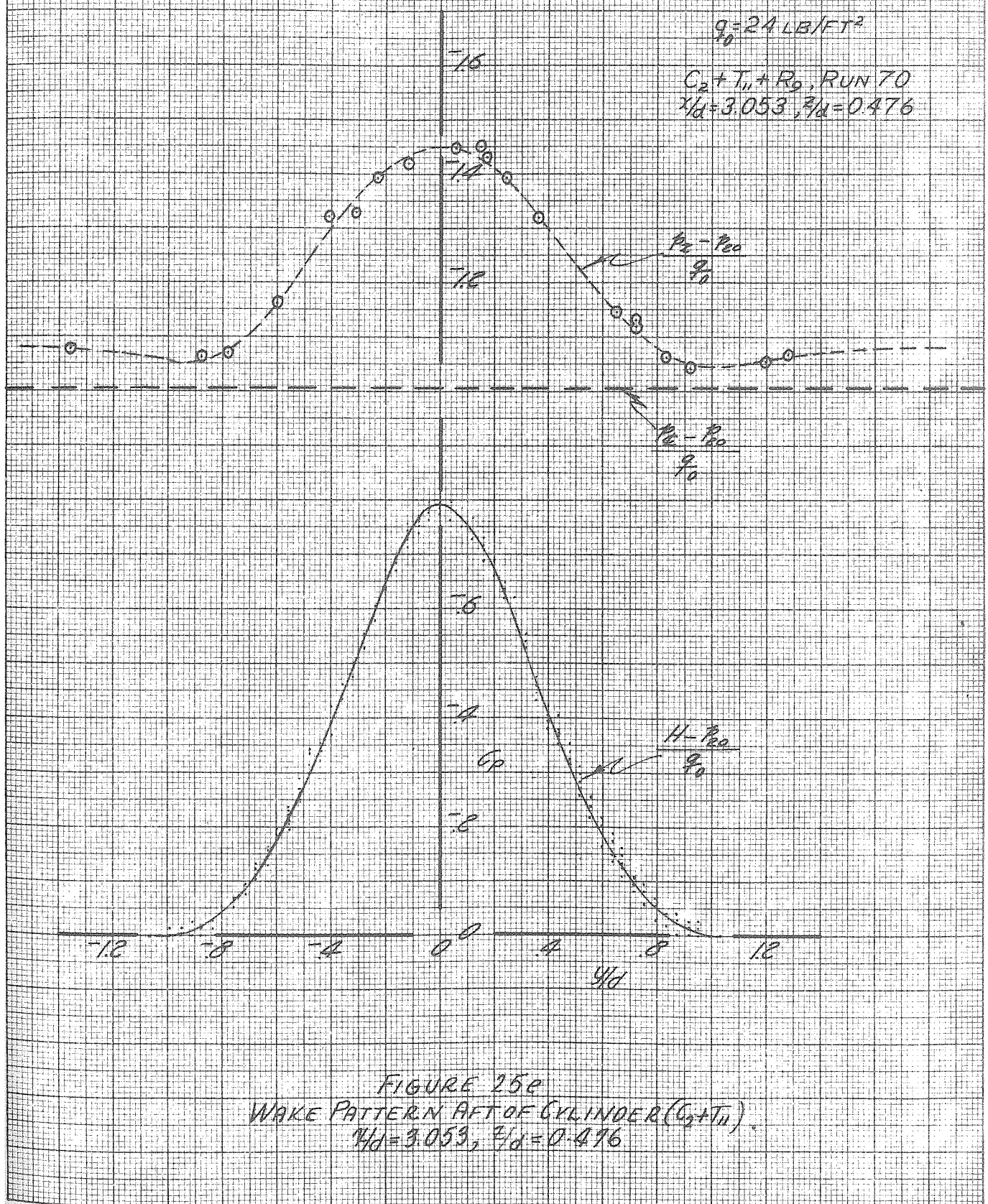

FIGURE 25e
WAKE PATTERN AFT OF CYLINDER ($C_2 + T_{11}$).
$x/d = 3.053$, $z/d = 0.476$

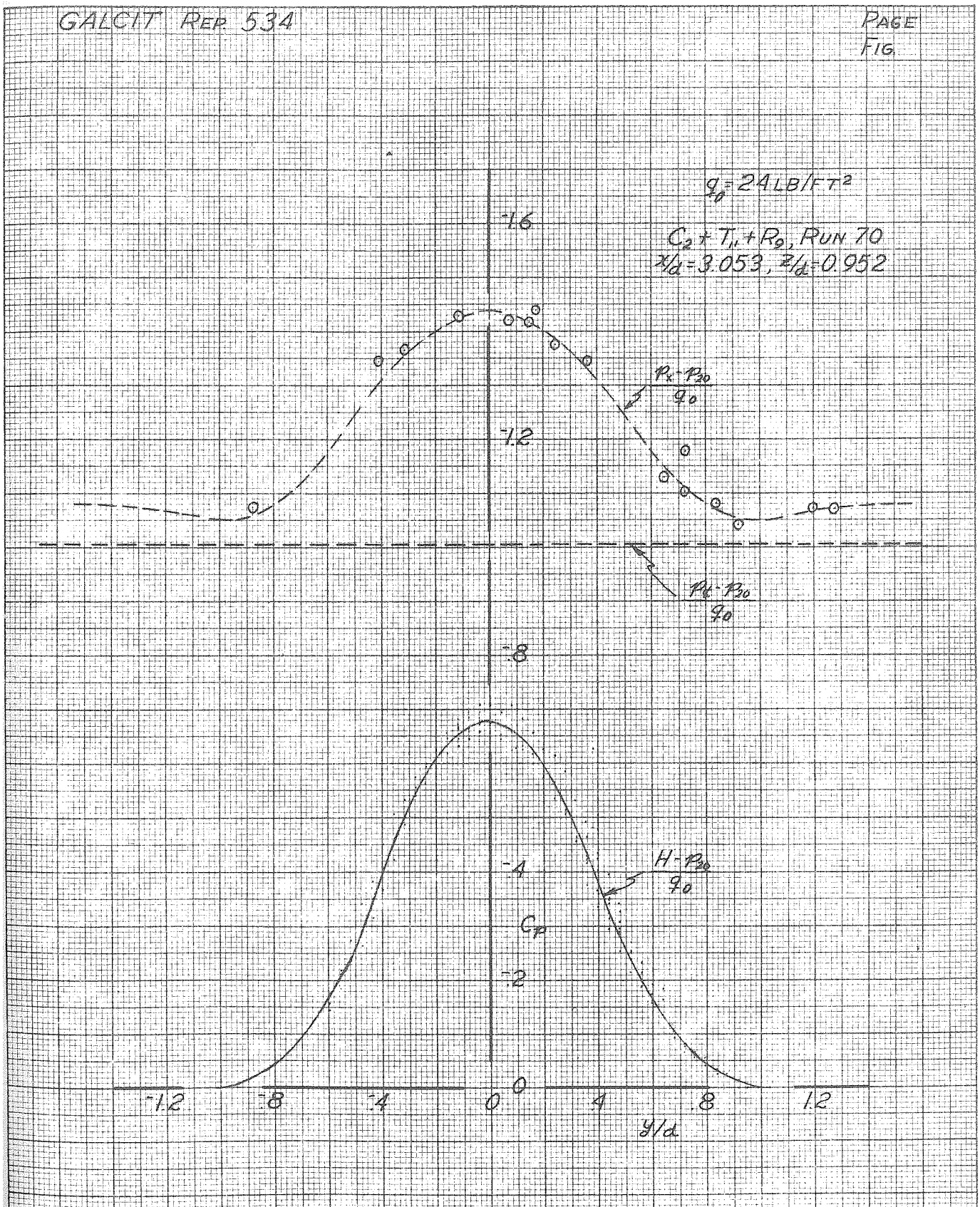

FIGURE 25f
WAKE PATTERN AFT OF CYLINDER (C_2+T_1)
$x/d = 3.053$, $z/d = 0.952$

GALCIT REP. 534

PAGE
FIG.

$q_0 = 24$ LB/FT^2

$C_2 + T_{12} + R_8$, RUN 72
$x/d = 1.626$

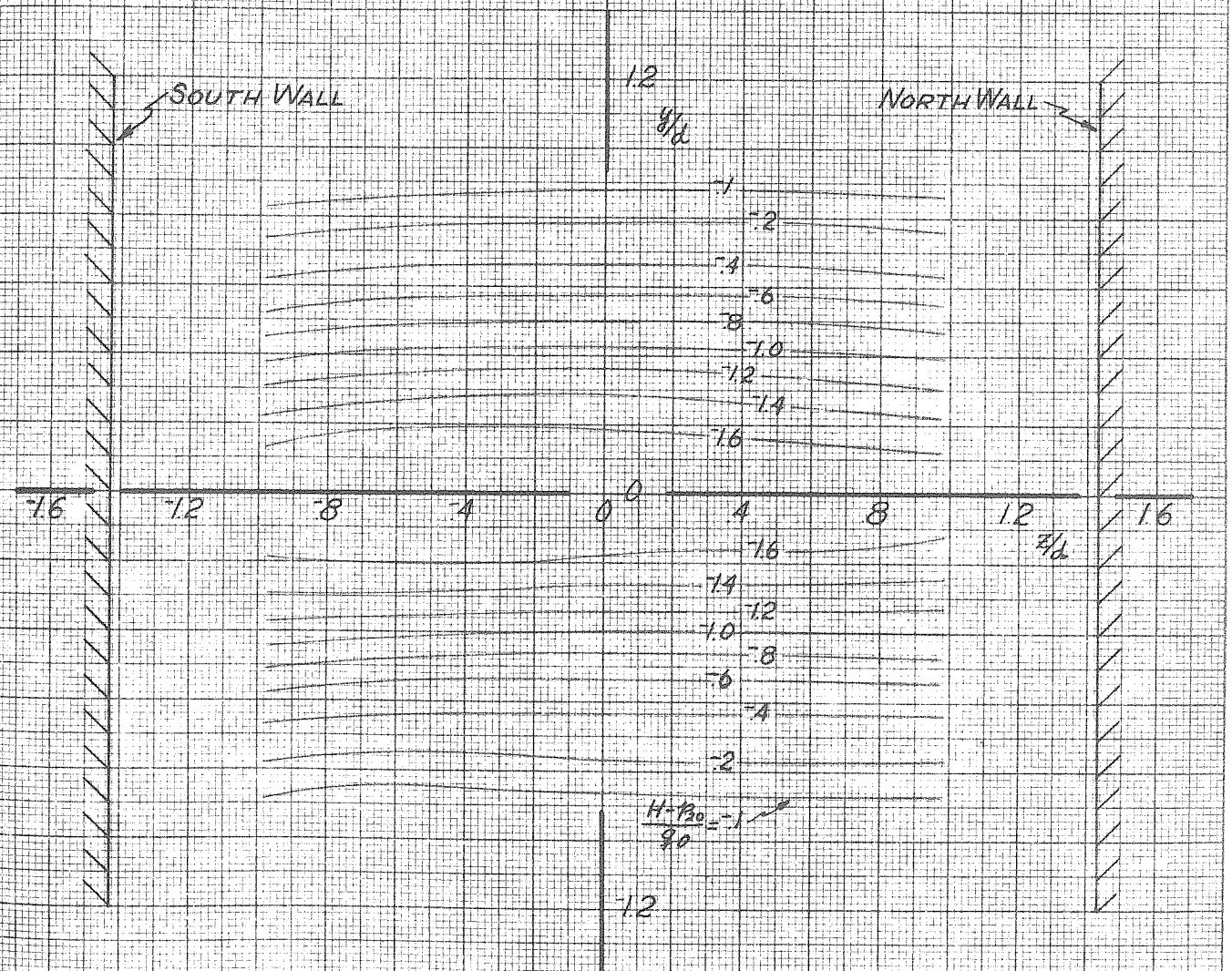

FIGURE 26
CONTOURS OF CONSTANT TOTAL HEAD DECREMENTS AFT OF CYLINDER ($C_2 + T_{12}$)
$x/d = 1.626$

GALCIT REP 534

PAGE
FIG

$q_0 = 24 \text{ LB/FT}^2$

$C_2 + T_{12} + R_B$, RUN 72

$x/d = 1.626$

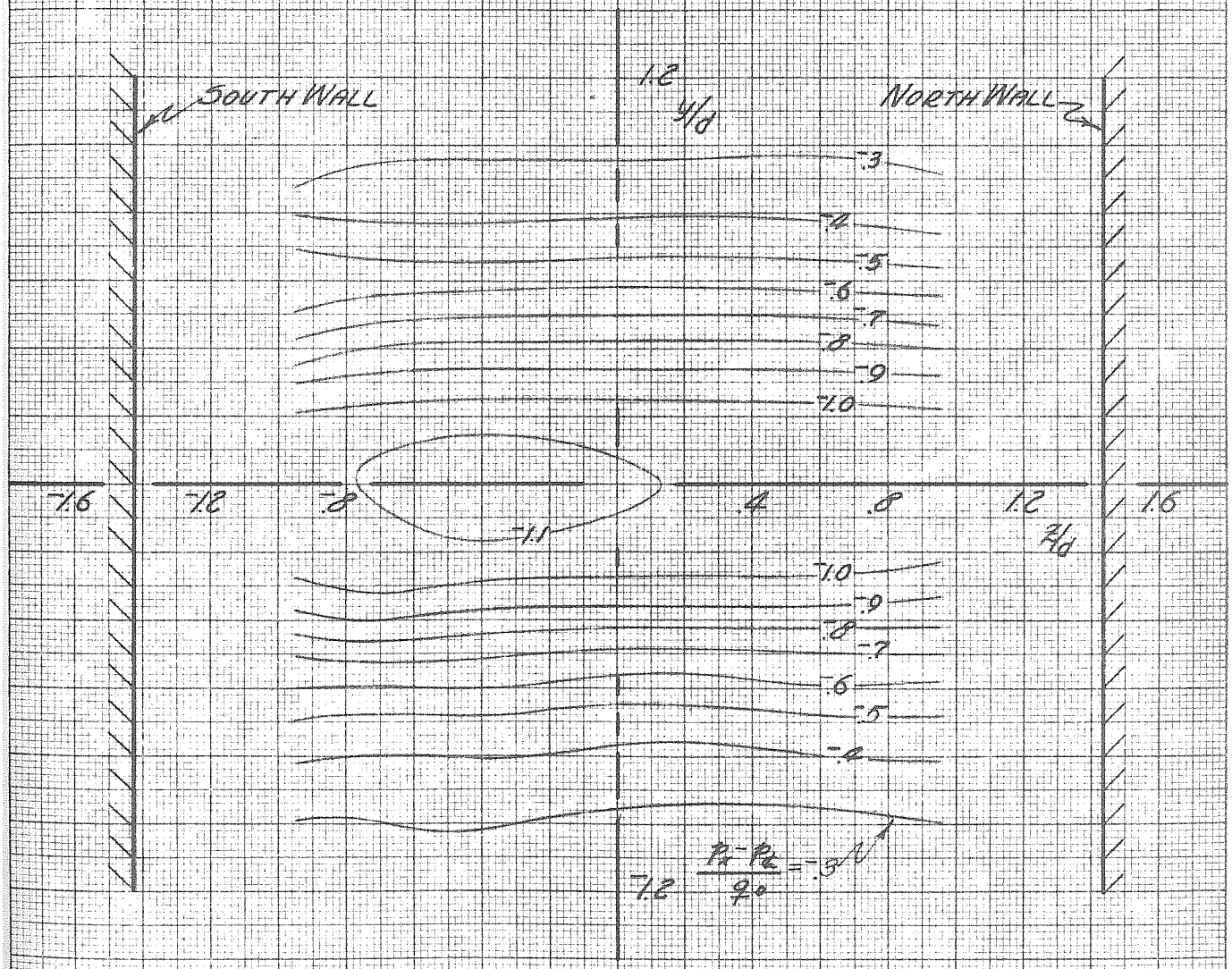

FIGURE 26-1

CONTOURS OF CONSTANT STATIC PRESSURE DECREMENTS AFT OF CYLINDER $(C_2 + T_{12})$

$x/d = 1.626$

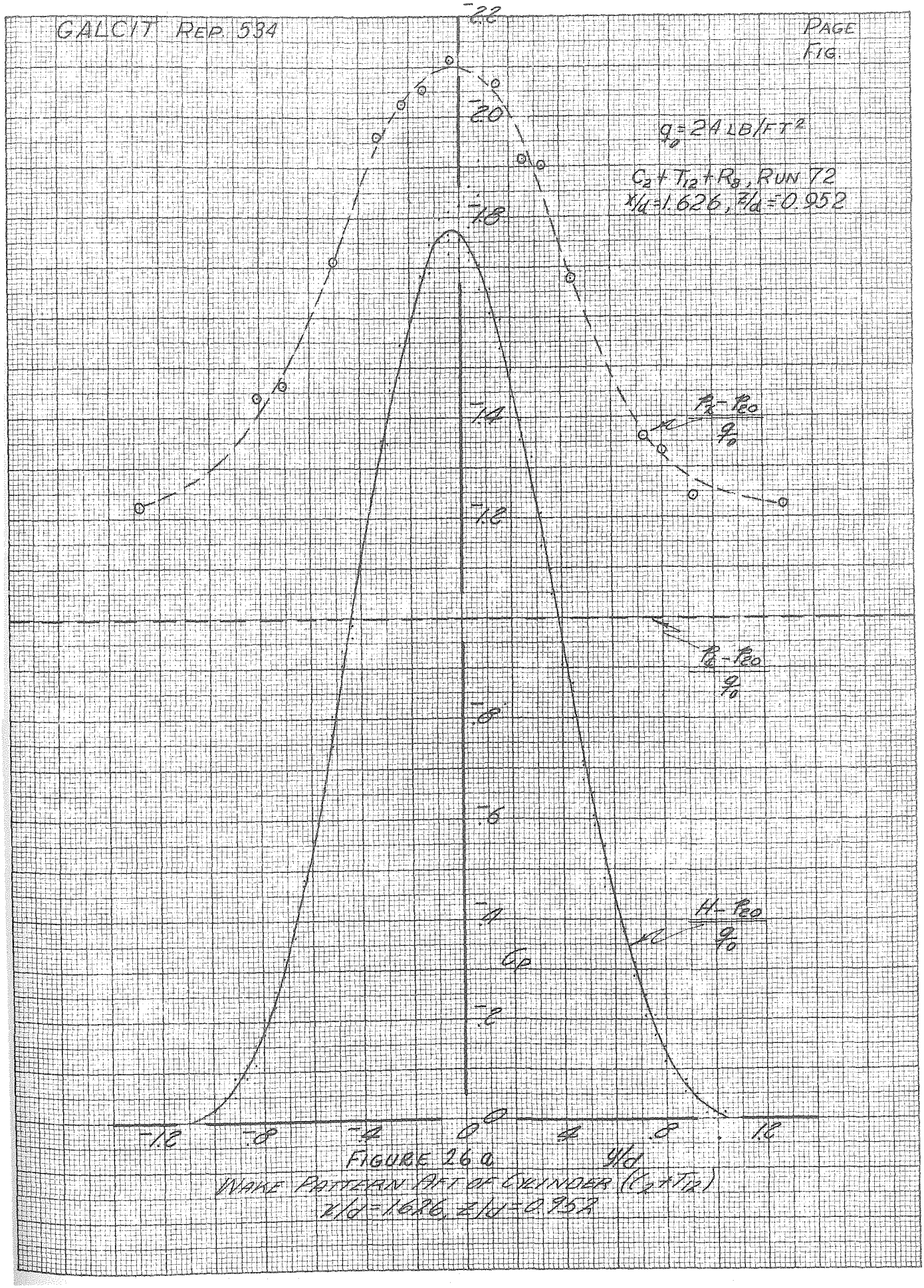

FIGURE 26a

WAKE PATTERN AFT OF CYLINDER ($C_2 + T_{12}$)
$x/d = 1.626$, $z/d = 0.952$

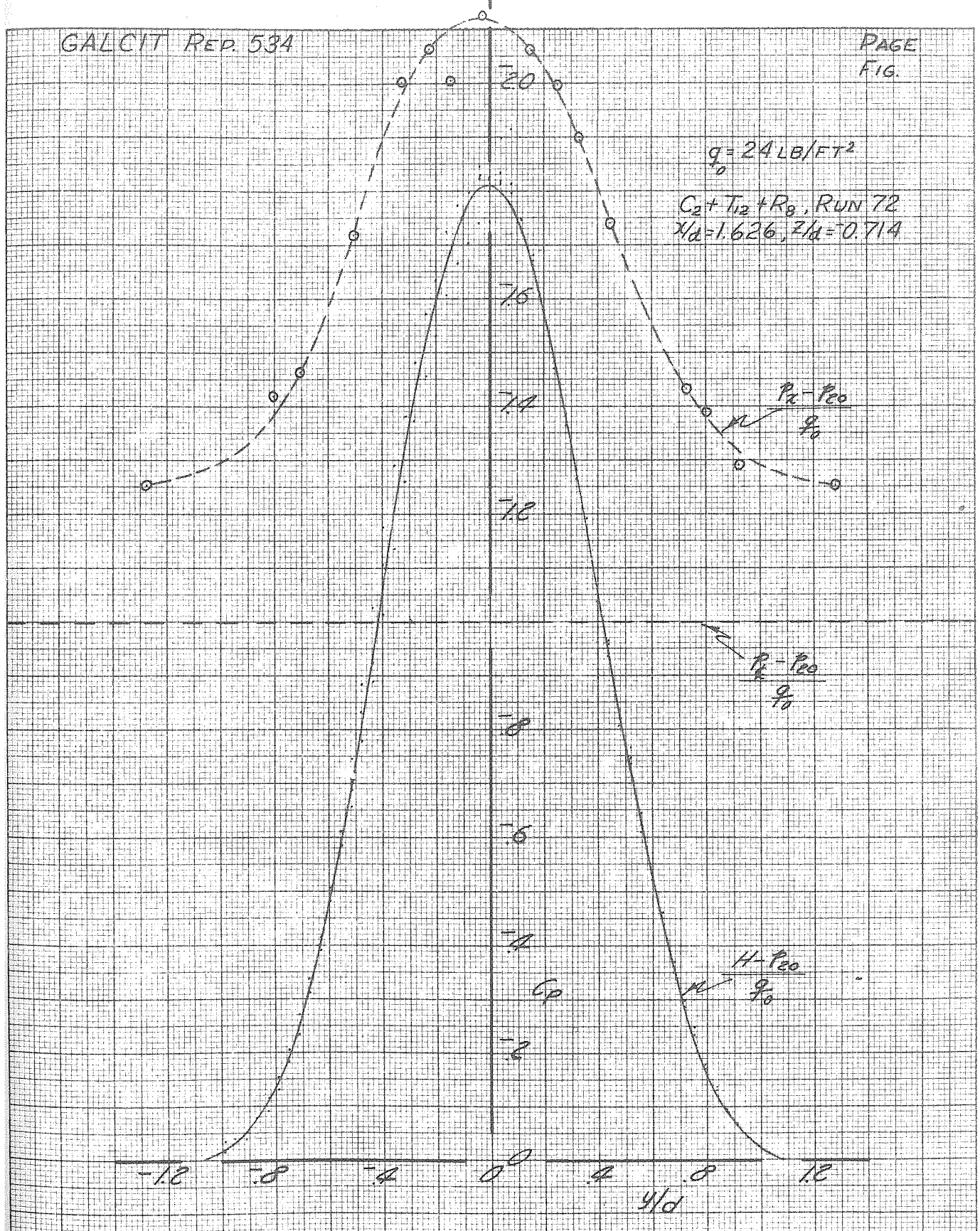

FIGURE 26b
WAKE PATTERN AHEAD OF CYLINDER ($C_2 + T_{12}$)
$x/d = 1.626$, $z/d = 0.714$

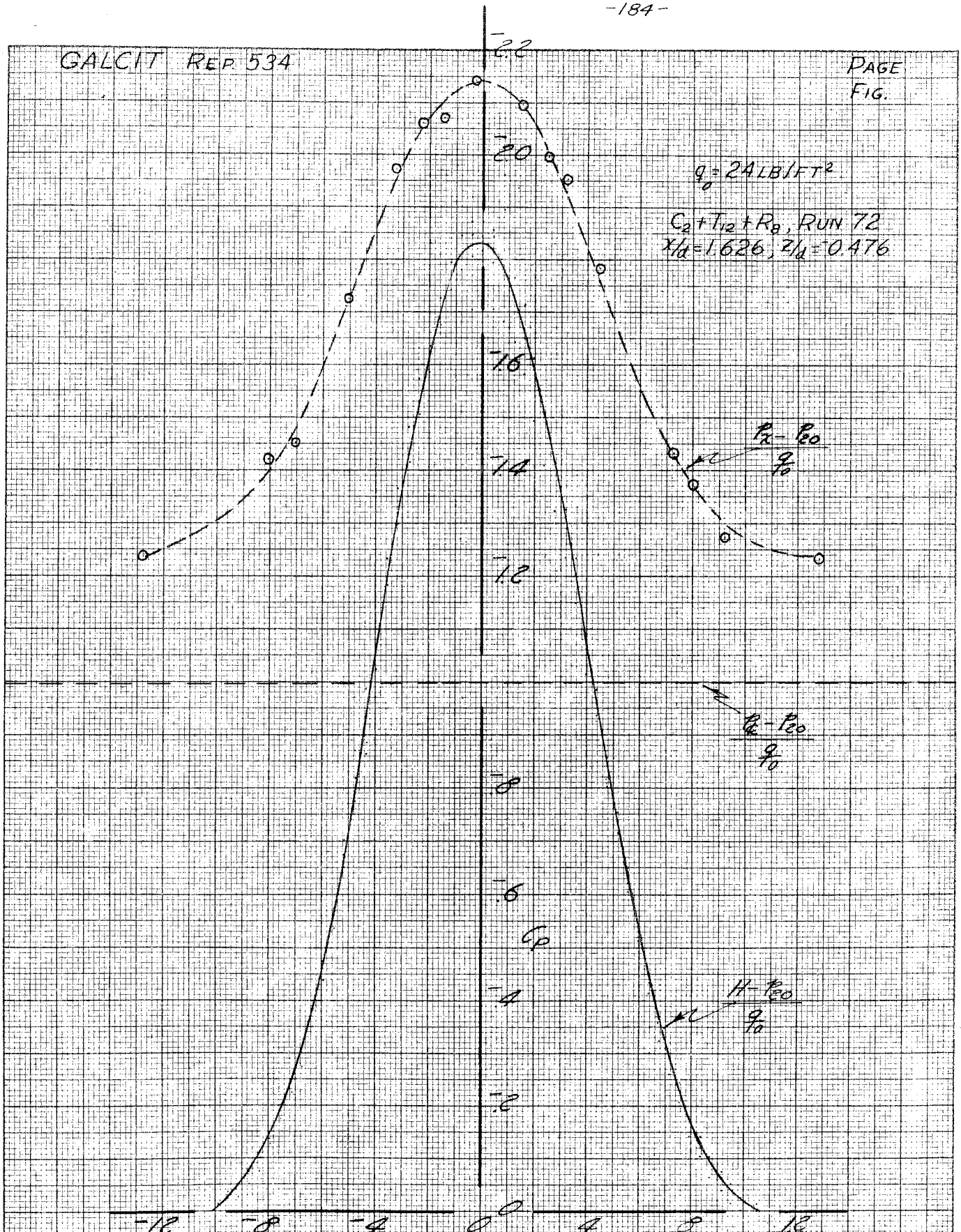

FIGURE 26c

WAKE PATTERN AFT OF CYLINDER ($C_2 + T_{12}$)
$x/d = 1.626$, $z/d = 0.476$

GALCIT REP 534

PAGE
FIG.

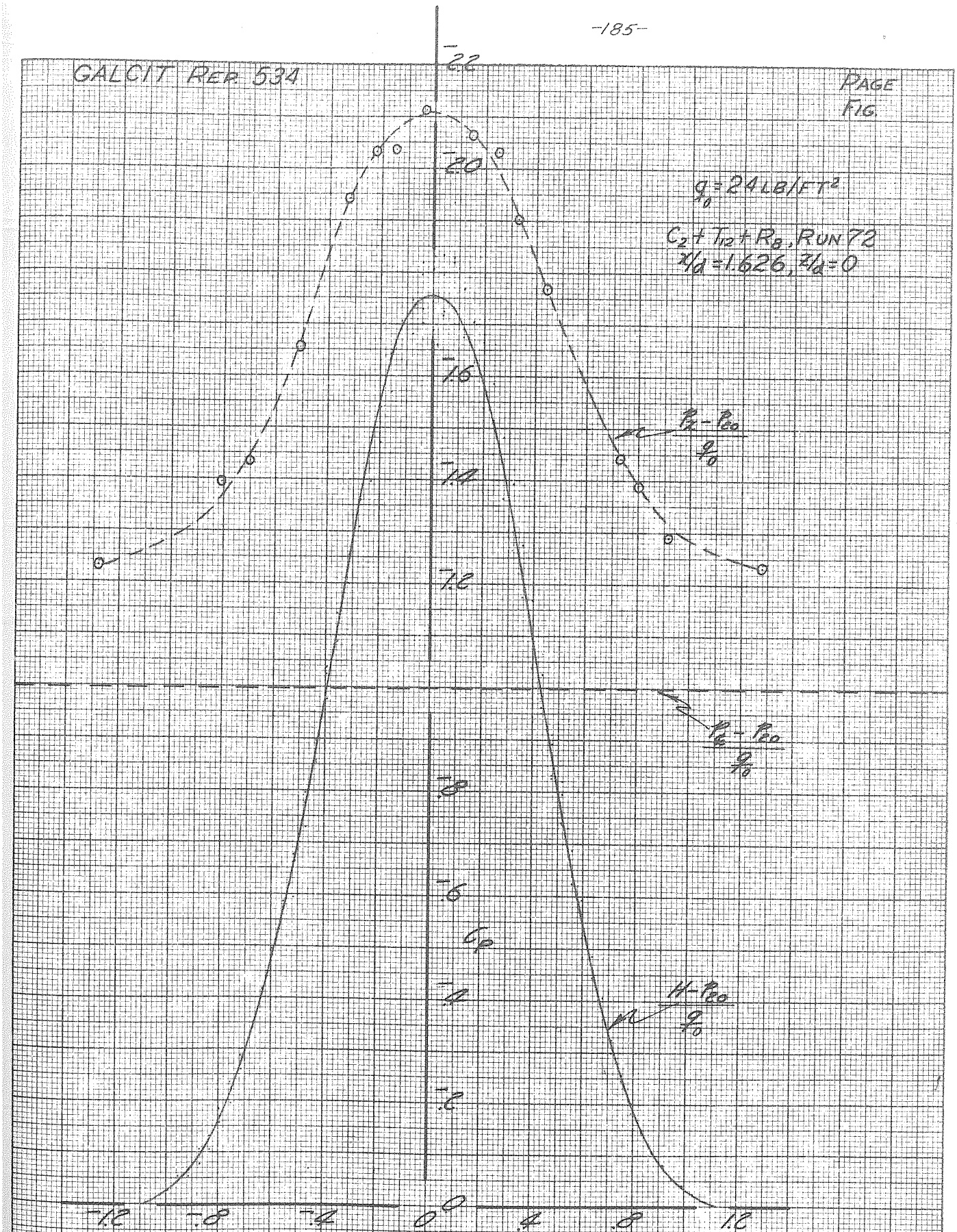

FIGURE 26d

WAKE PATTERN AHT OF CYLINDER ($C_2 + T_{12}$)
$x/d = 1.626$, $z/d = 0$

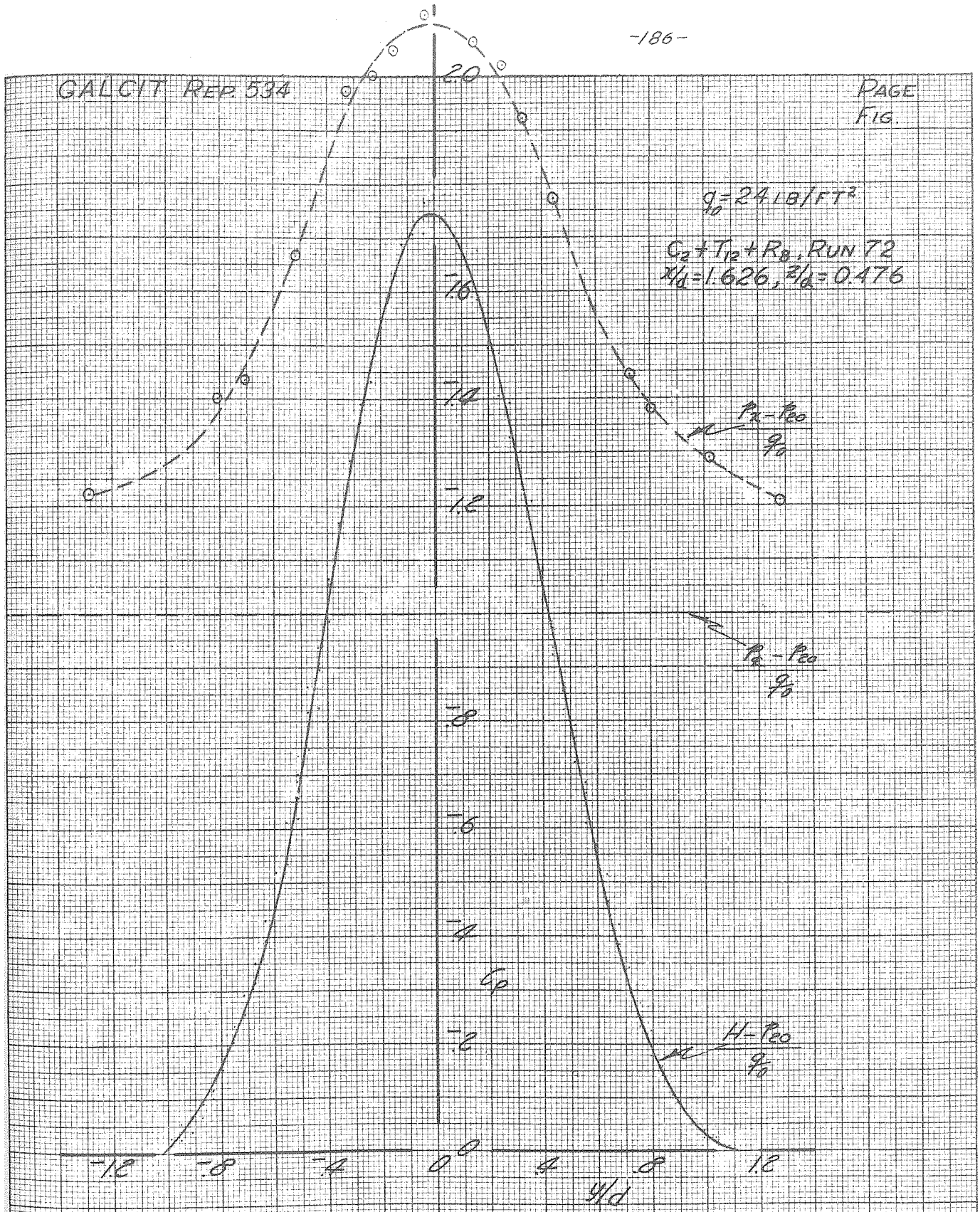

FIGURE 26 e
WAKE PATTERN AFT OF CYLINDER (C_2+T_{12})
$z/d = 1.626$, $z/d = 0.476$

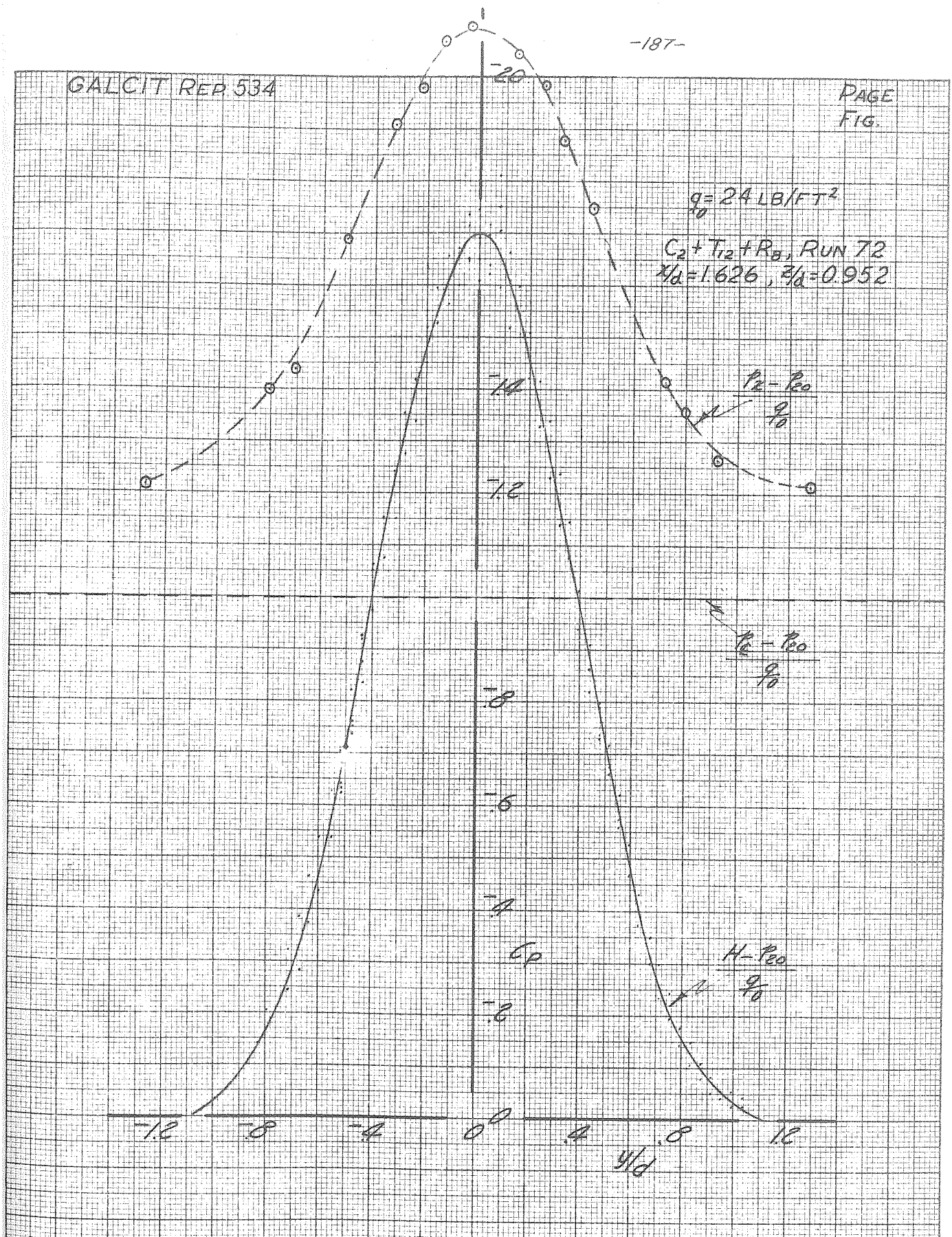

FIGURE 26 A
WAKE PATTERN AFT OF CYLINDER ($C_2 + T_{12}$)
$x/d = 1.626$, $z/d = 0.952$

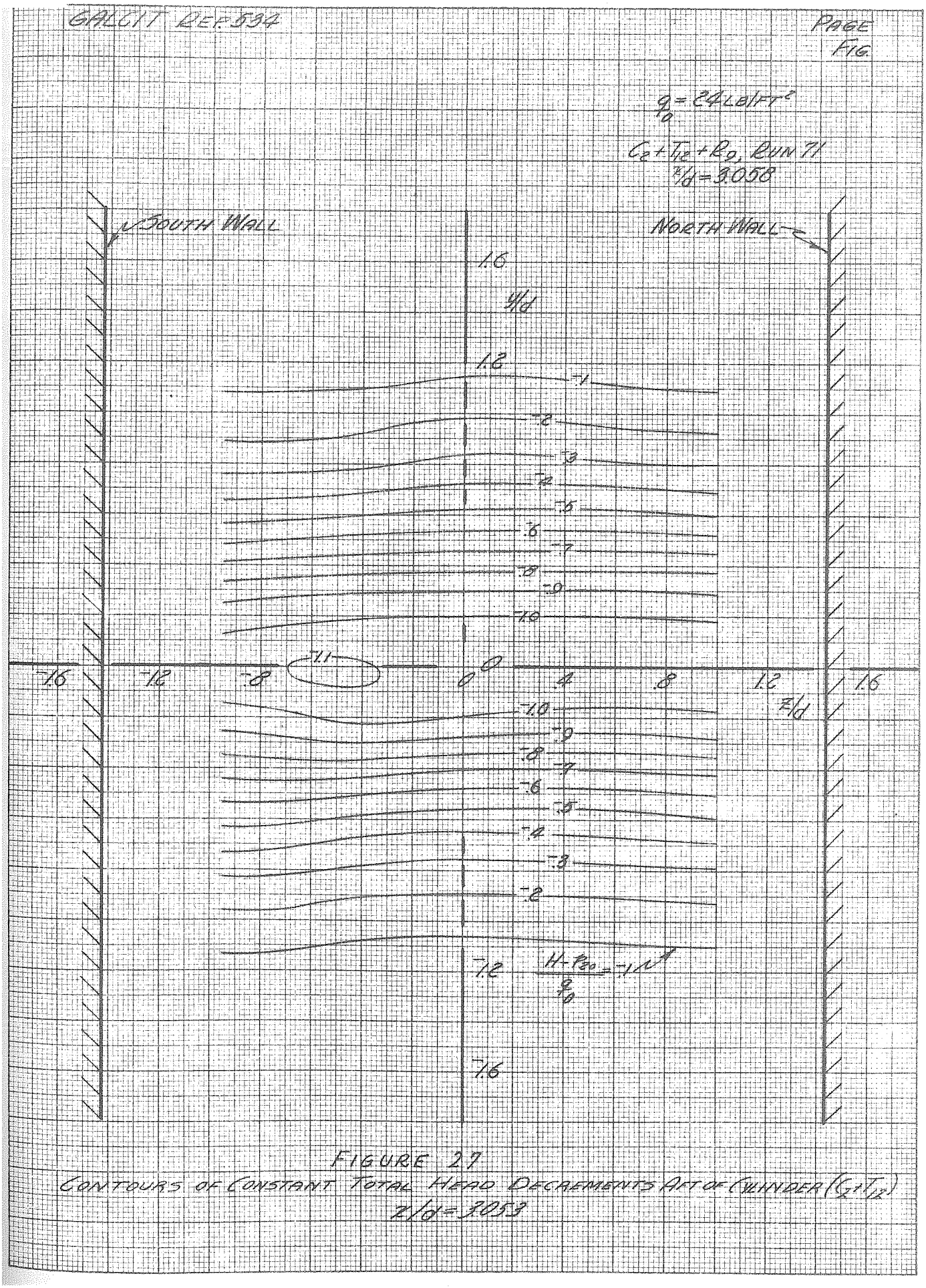

FIGURE 27
CONTOURS OF CONSTANT TOTAL HEAD DECREMENTS AFT OF CYLINDER ($C_2 + T_{12}$)
$z/b = 3.053$

GALCIT REF. 534

PAGE
FIG.

$q_0 = 24$ LB/FT^2

$C_2 + T_{12} + R_9$, RUN 71

$Z/d = 3.053$

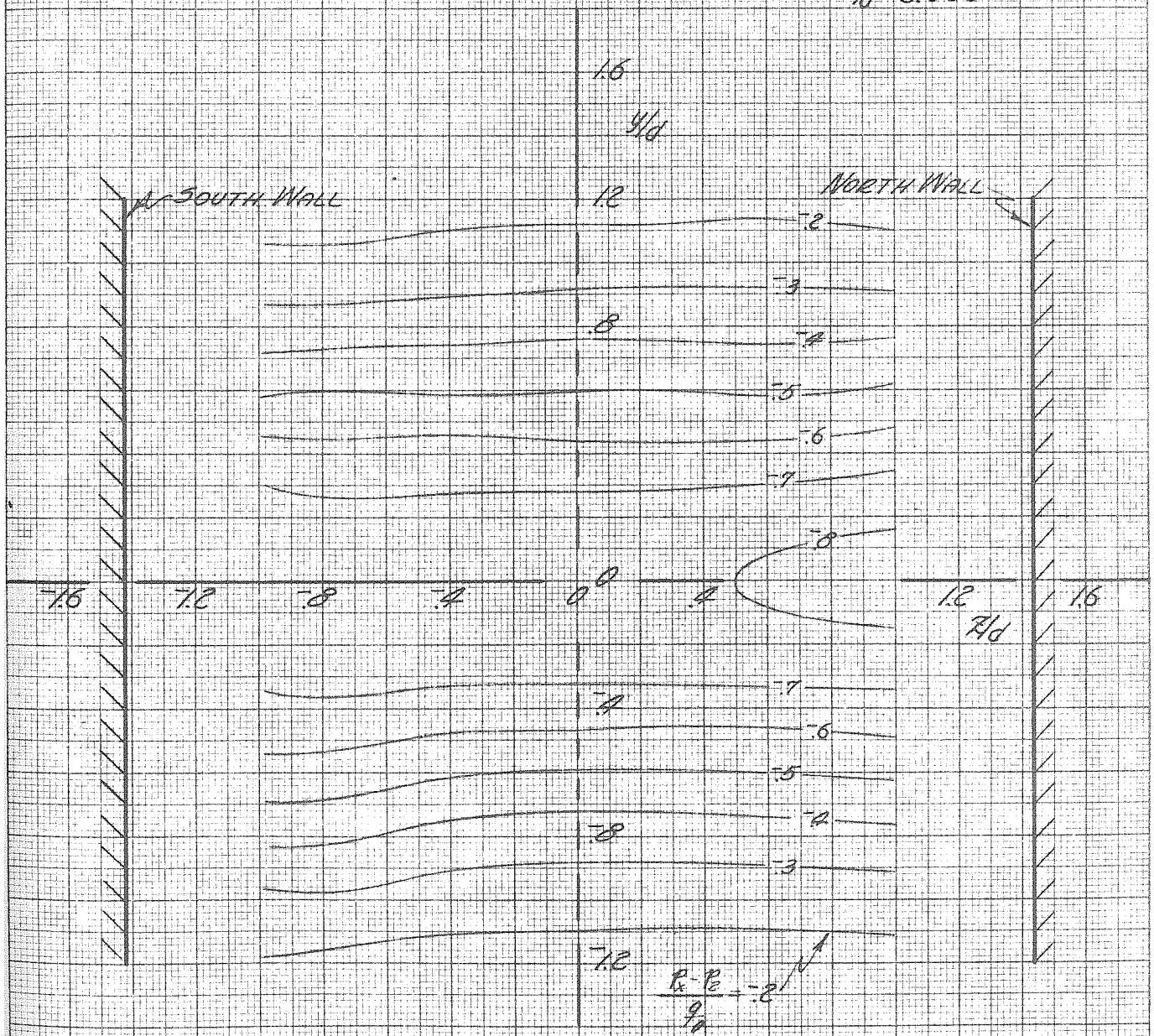

FIGURE 27-1

CONTOURS OF CONSTANT STATIC PRESSURE DECREMENTS AFT OF CYLINDER ($C_2 + T_{12}$)

$Z/d = 3.053$

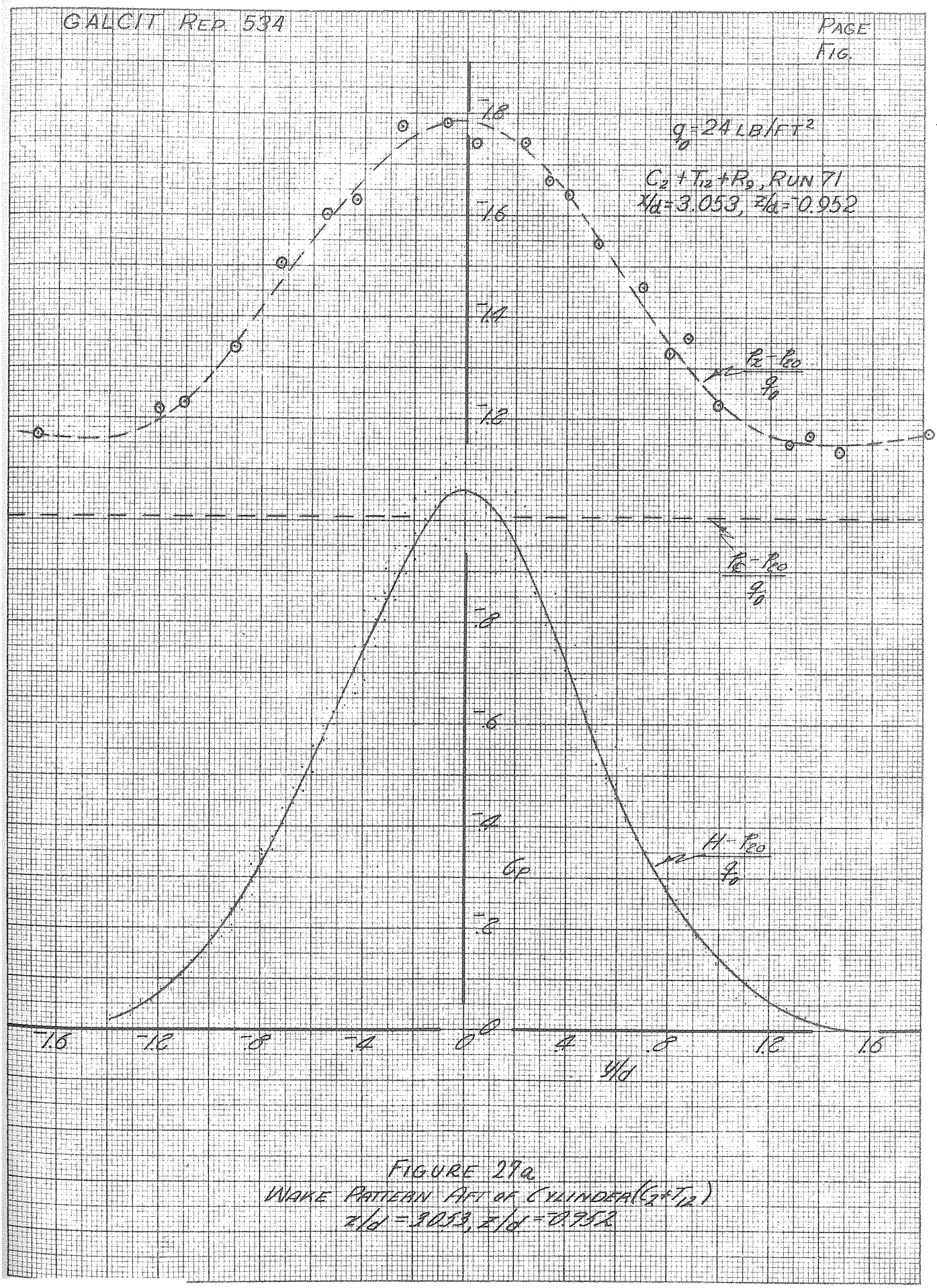

FIGURE 29a
WAKE PATTERN AFT OF CYLINDERS (C_2+T_{12})
$x/d = 3.053$, $z/d = 0.952$

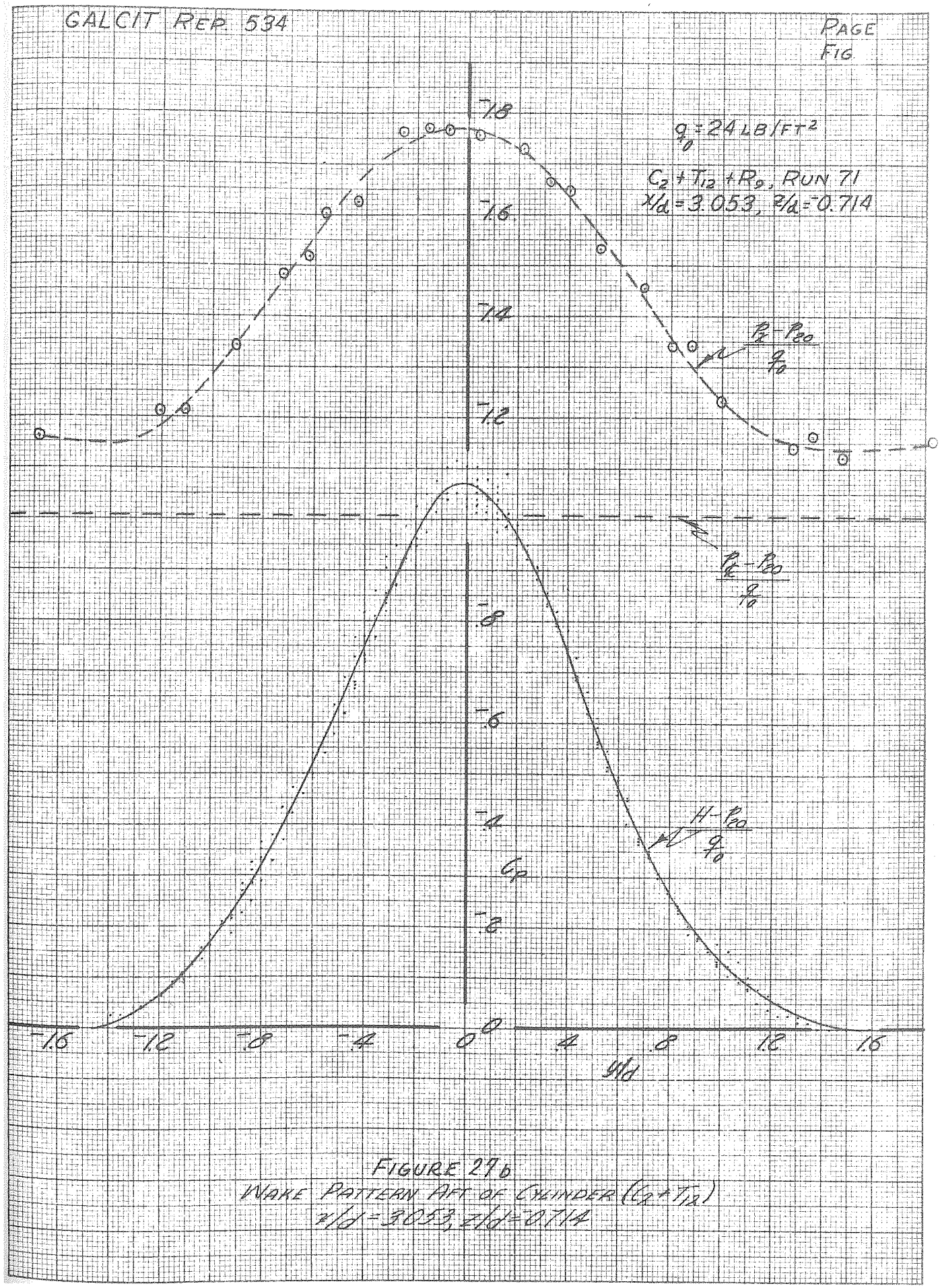

FIGURE 29b
WAKE PATTERN AFT OF CYLINDER ($C_2 + T_{12}$)
$x/d = 3.053$, $z/d = -0.714$

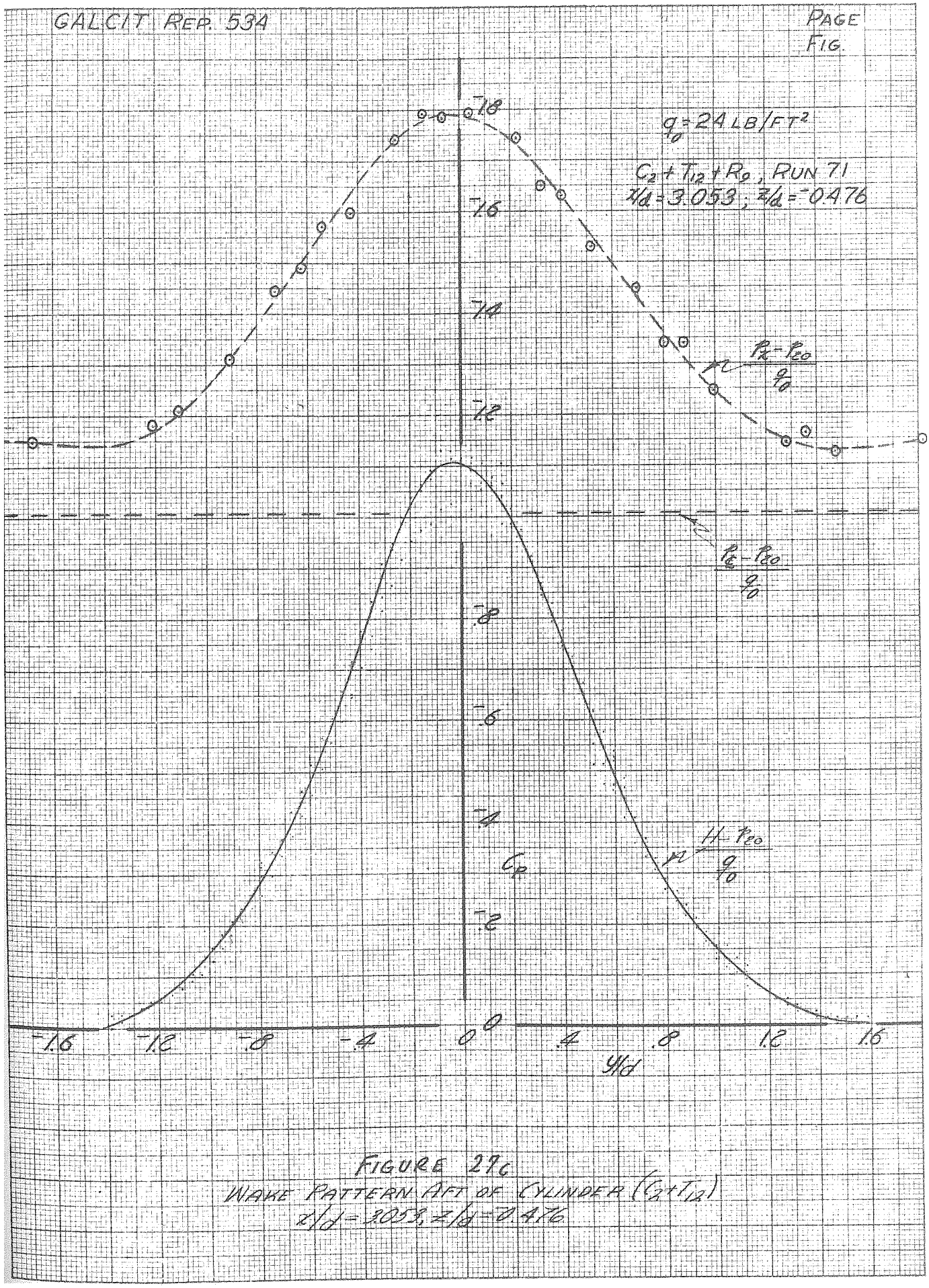

FIGURE 27c
WAKE PATTERN AFT OF CYLINDER (C_2+T_{12})
$z/d = 3.053$, $z/d = -0.476$

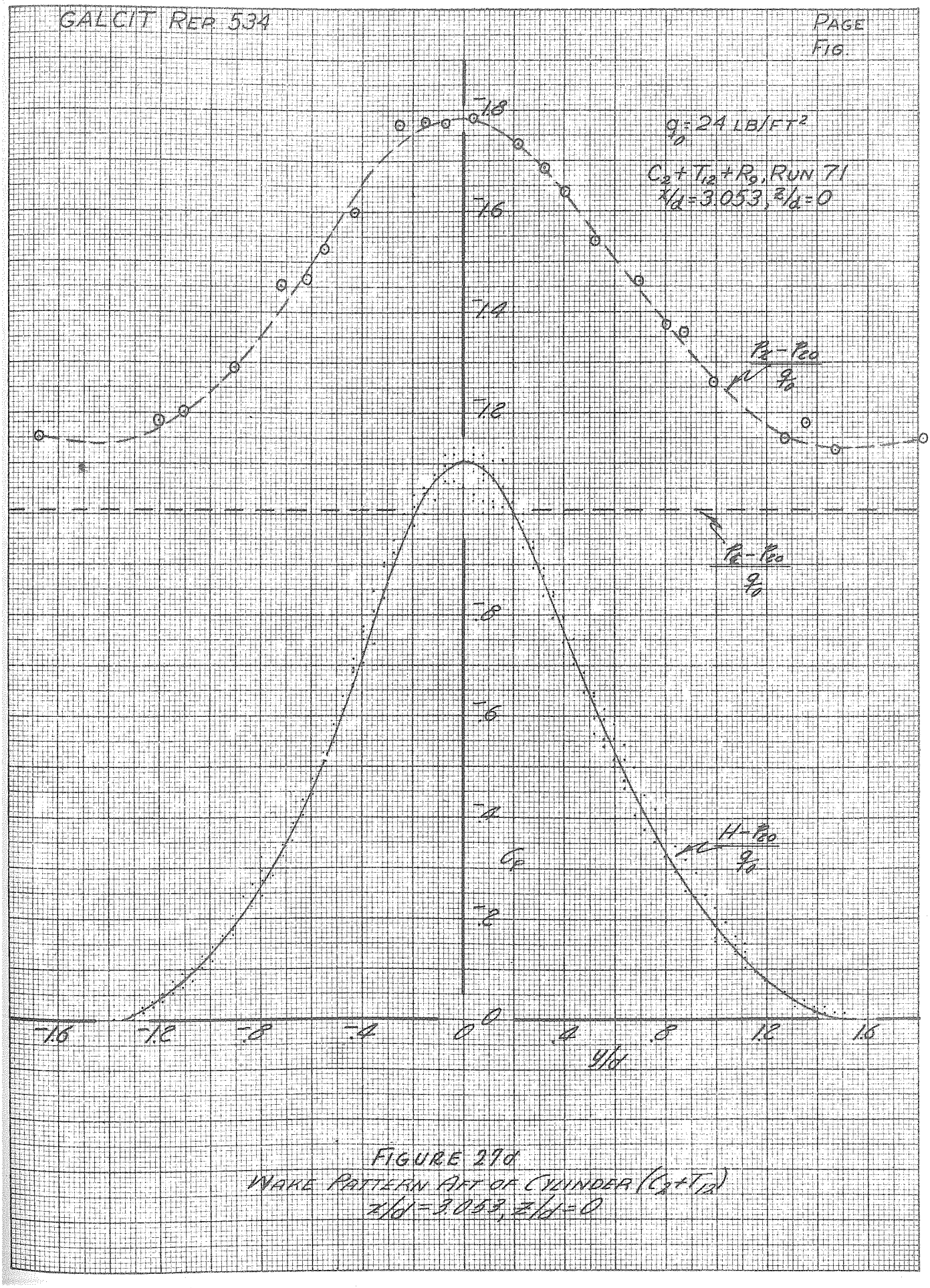

FIGURE 27d
WAKE PATTERN AFT OF CYLINDER (C_2+T_{12})
$x/d = 3.053$, $z/d = 0$

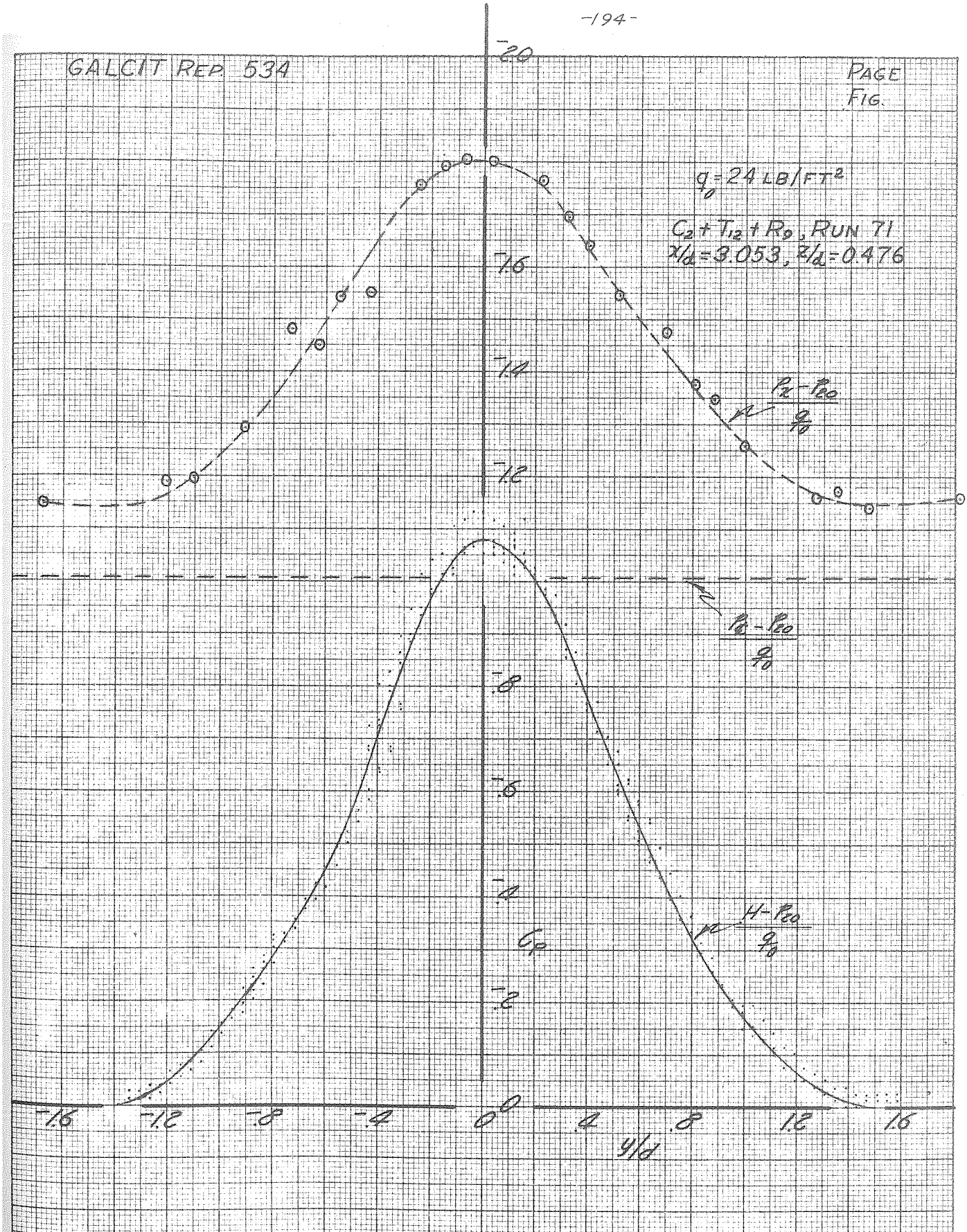

FIGURE 27e
WAKE PATTERN AFT OF CYLINDER (C_2+T_{12})
$x/d = 3.053$, $z/d = 0.476$

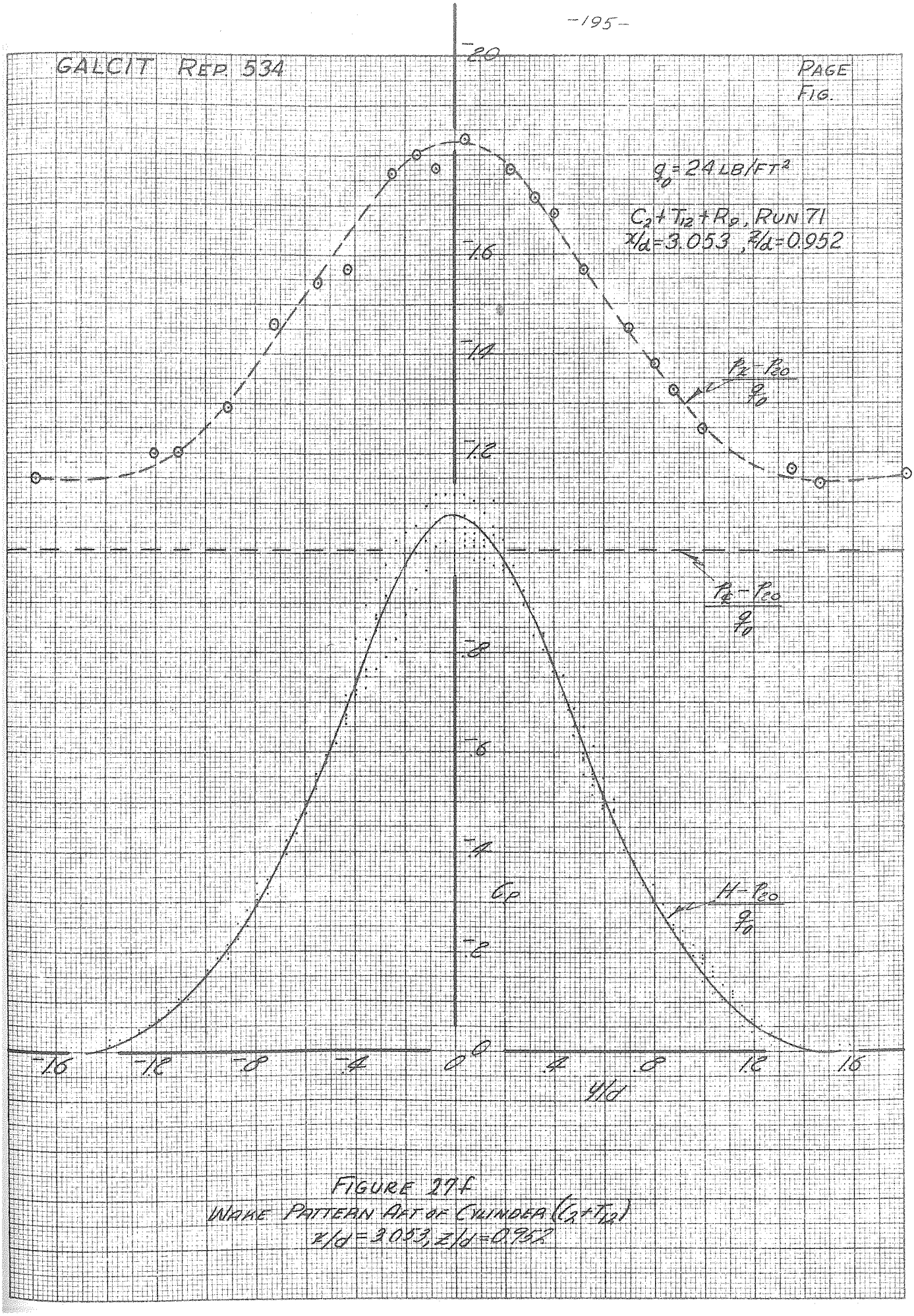

FIGURE 29f
WAKE PATTERN AFT OF CYLINDER ($C_2 + T_{12}$)
$x/d = 3.053$, $z/d = 0.952$

$q_0 = 10 \text{ LB/FT}^2$

$C_3 + R_8$, RUN 73

$z/d = 1.150$

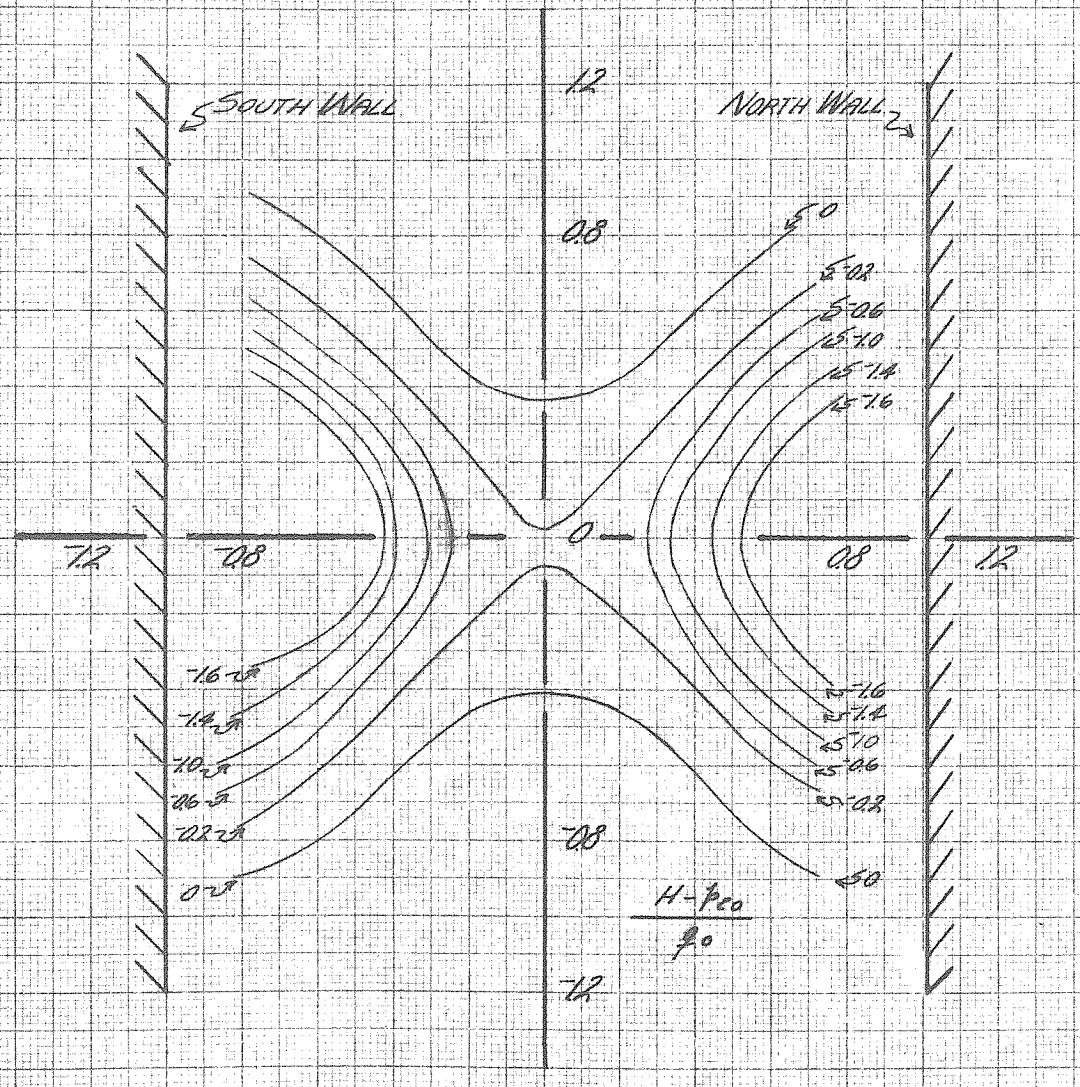

FIGURE 28
CONTOURS OF CONSTANT TOTAL HEAD DEGREMENTS
AFT OF CYLINDER C_3 WITHOUT SEPARATION STRIPS
$z/d = 1.150$

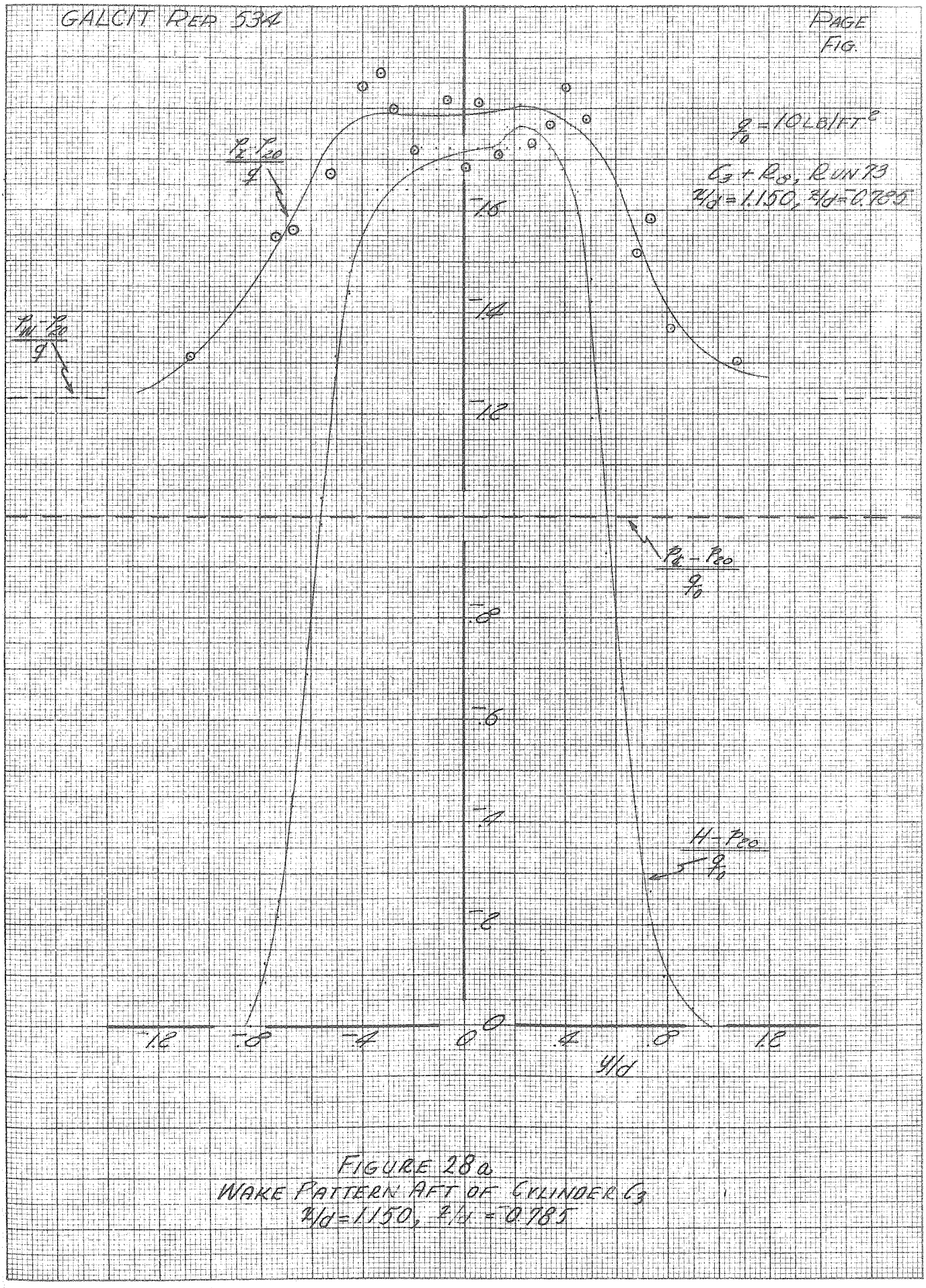

FIGURE 28a
WAKE PATTERN AFT OF CYLINDER G_3
$y/d = 1.150$, $z/d = 0.785$

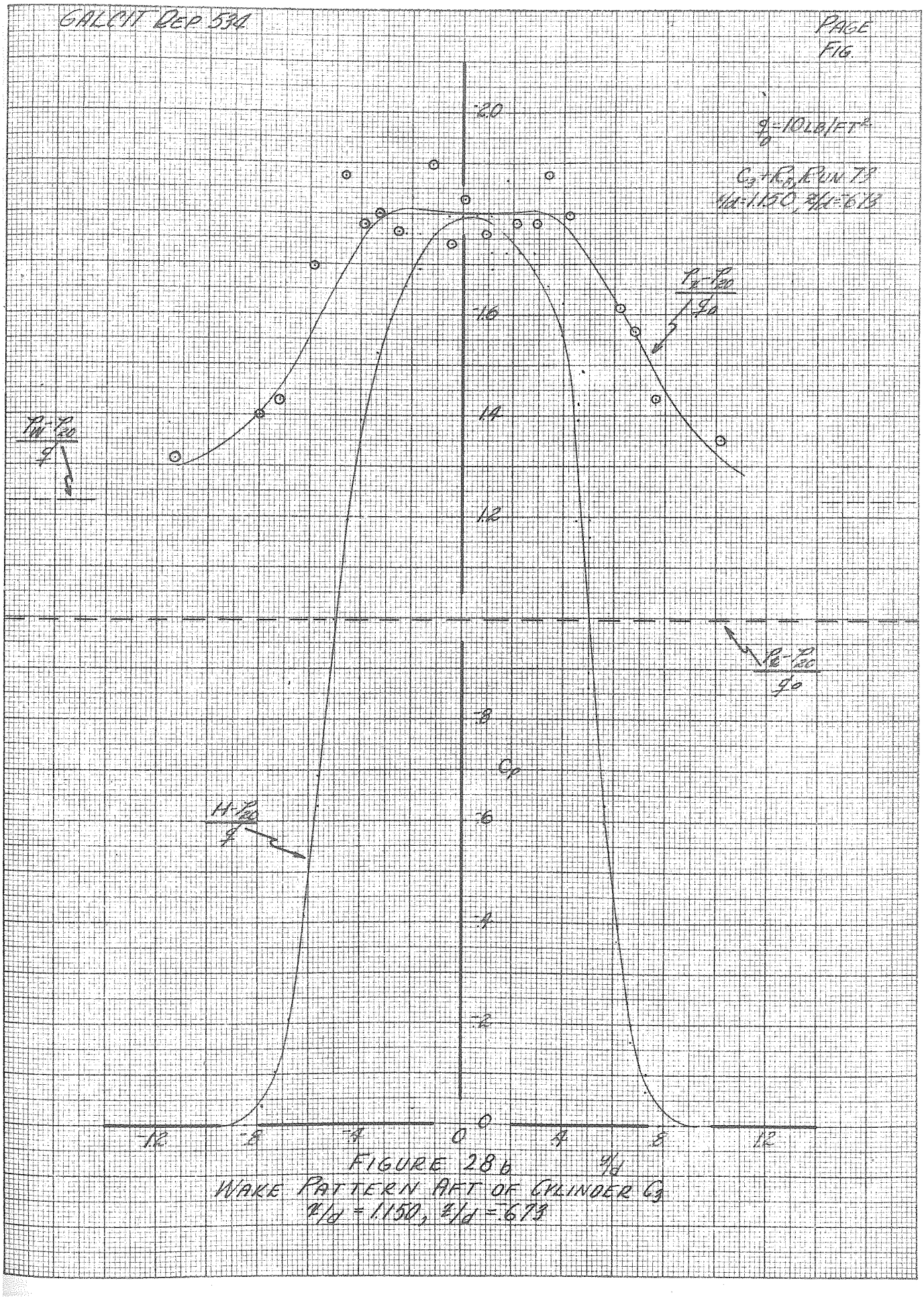

FIGURE 28b

WAKE PATTERN AFT OF CYLINDER C_3

$\frac{x}{d}$ = 1.150, $\frac{z}{d}$ = .673

GALCIT REP 53A

PAGE
FIG

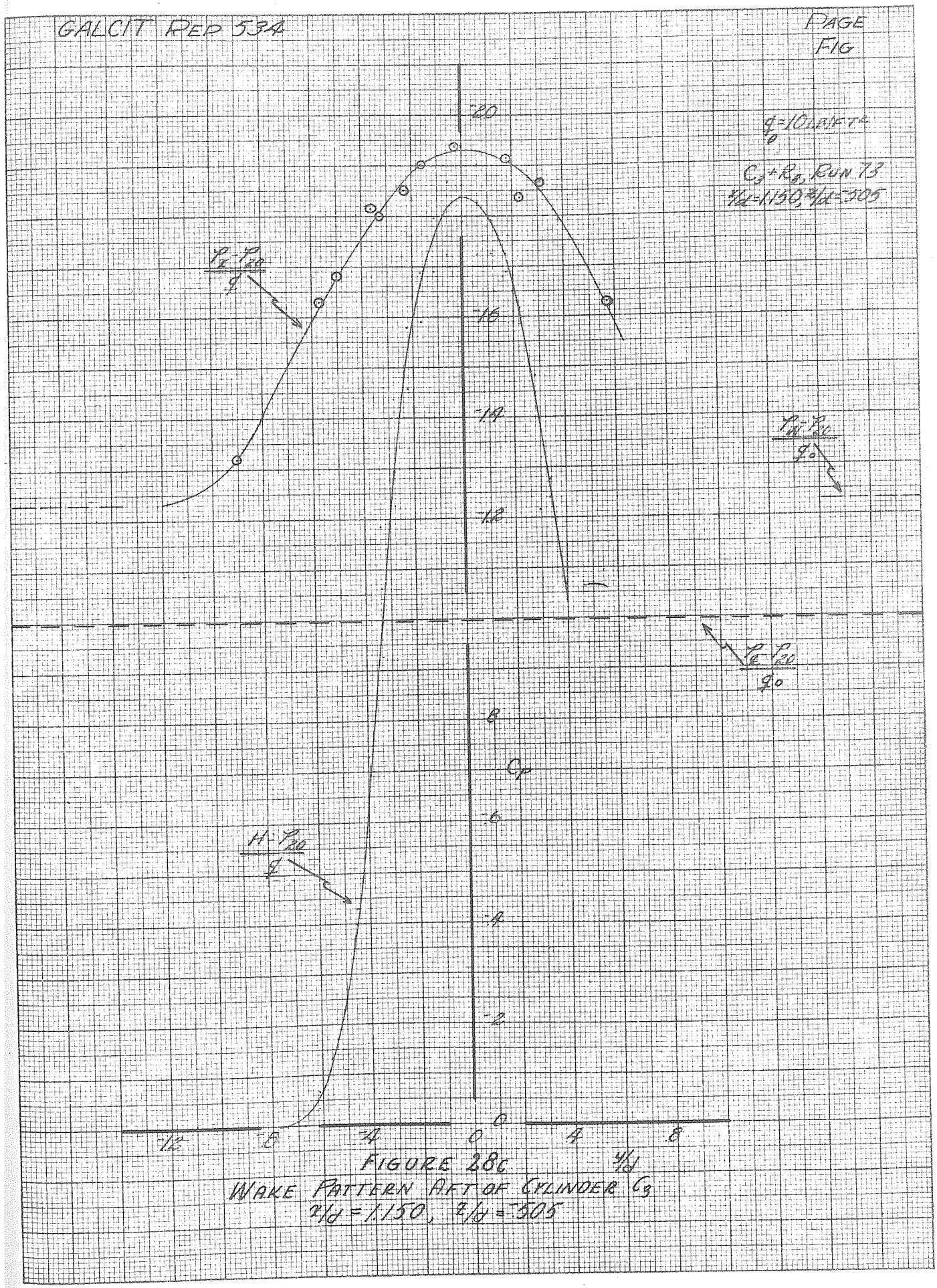

FIGURE 28c
WAKE PATTERN AFT OF CYLINDER C_3
x/d = 1.150, z/d = .505

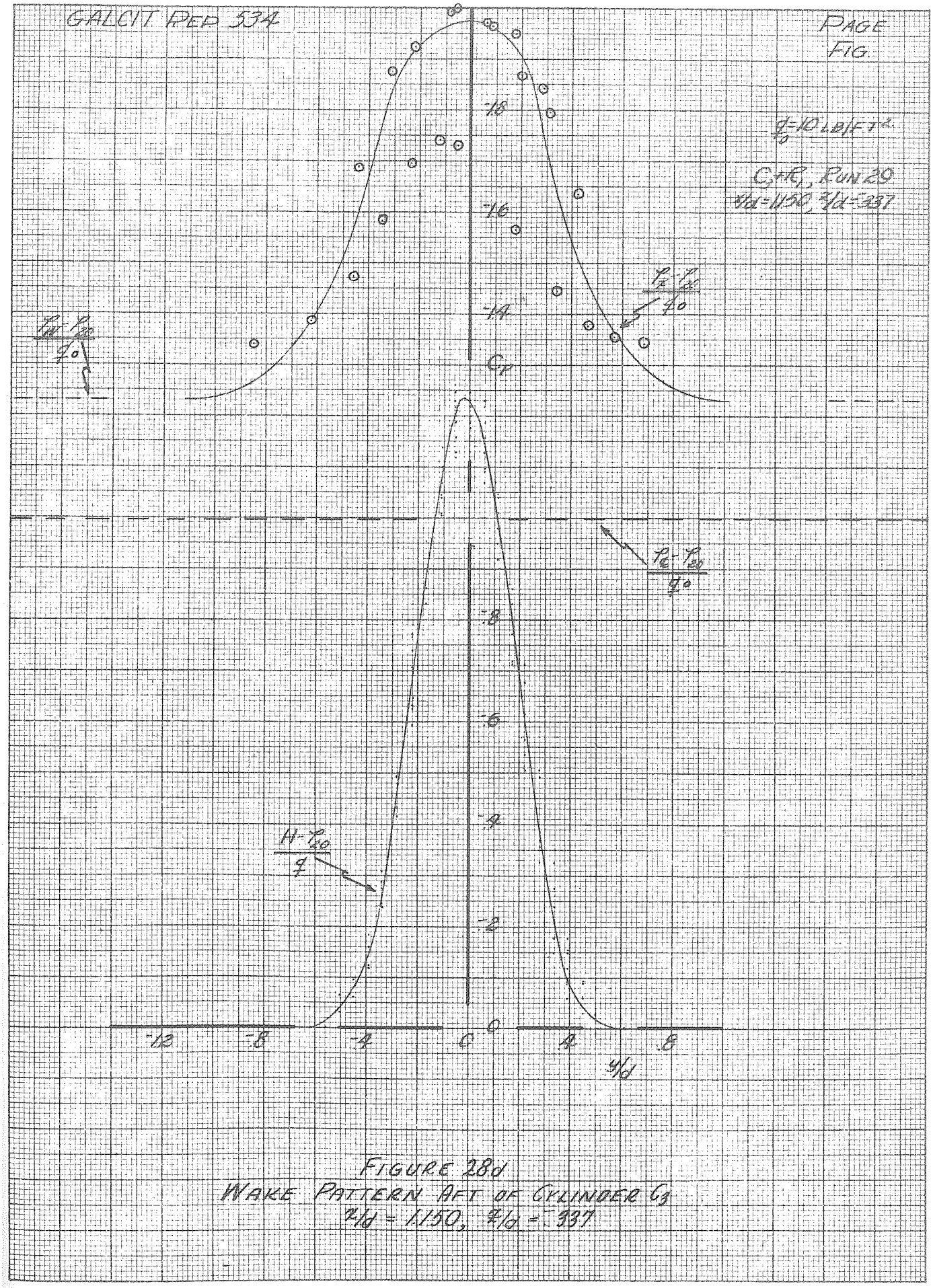

FIGURE 28d
WAKE PATTERN AFT OF CYLINDER C_3
$x/d = 1.150$, $y/d = .337$

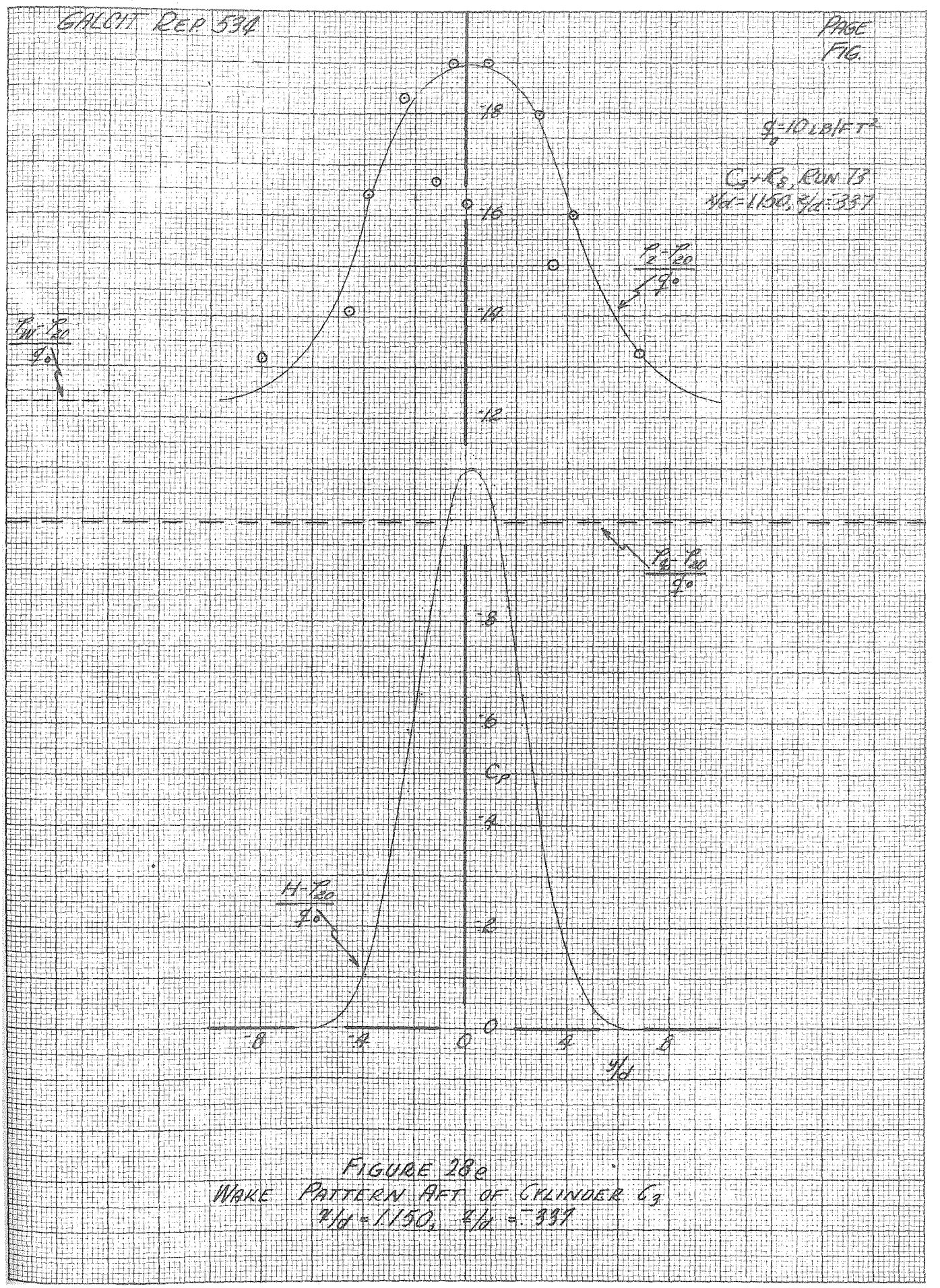

FIGURE 28e
WAKE PATTERN AFT OF CYLINDER C_3
x/d = 1.150, z/d = .337

GALCIT DEP 534.

PAGE
FIG.

q_0 = 12.4 LB/FT²

C_3 + R_6, RUN 73
Y/d = 1.150, Z/d = 0

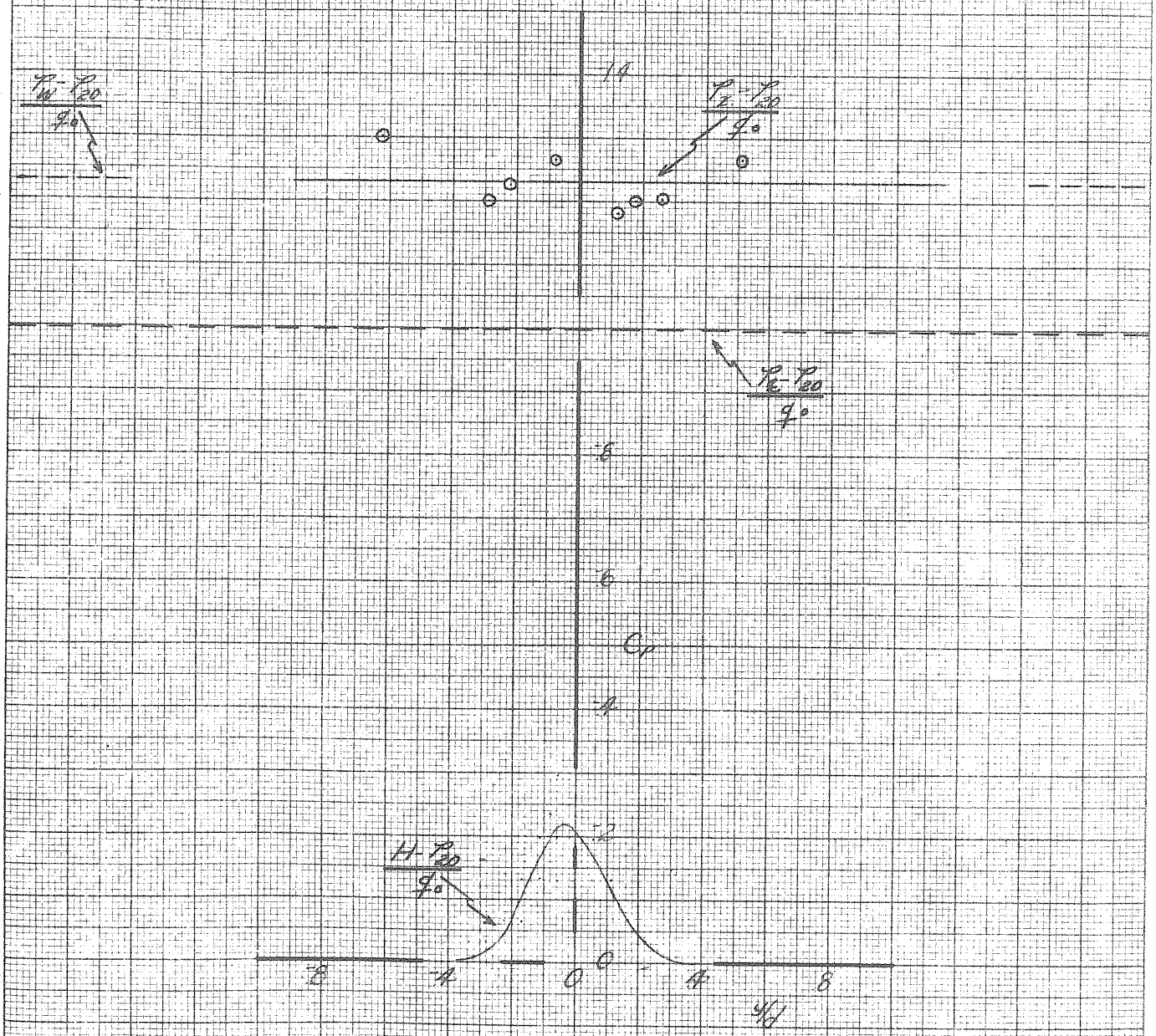

FIGURE 28f
WAKE PATTERN AFT OF CYLINDER C_3
Y/d = 1.150, Z/d = 0

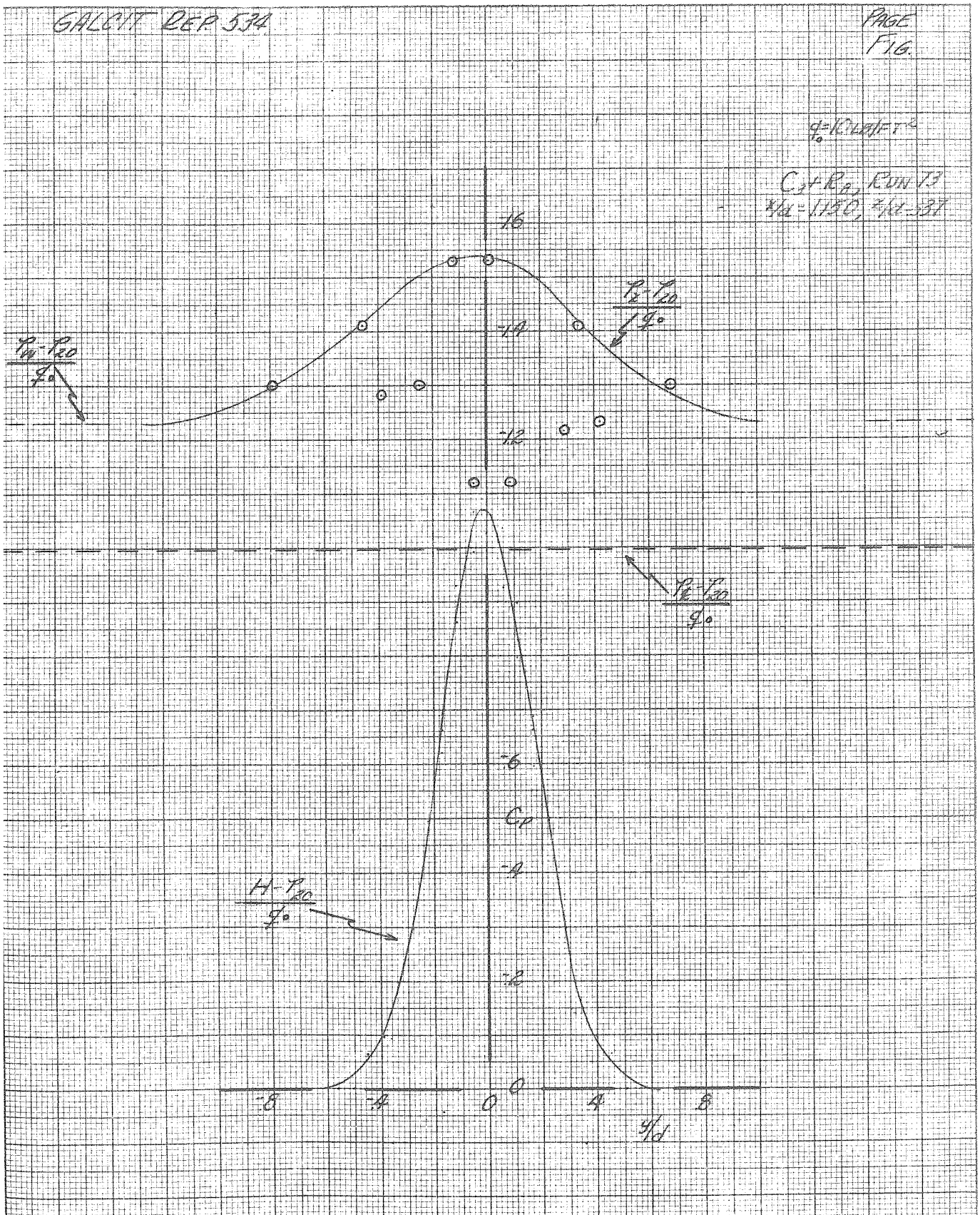

FIGURE 28g
WAKE PATTERN AFT OF CYLINDER C_3
x/d = 1.150, z/d = .937

GALCIT REP 534

PAGE
FIG.

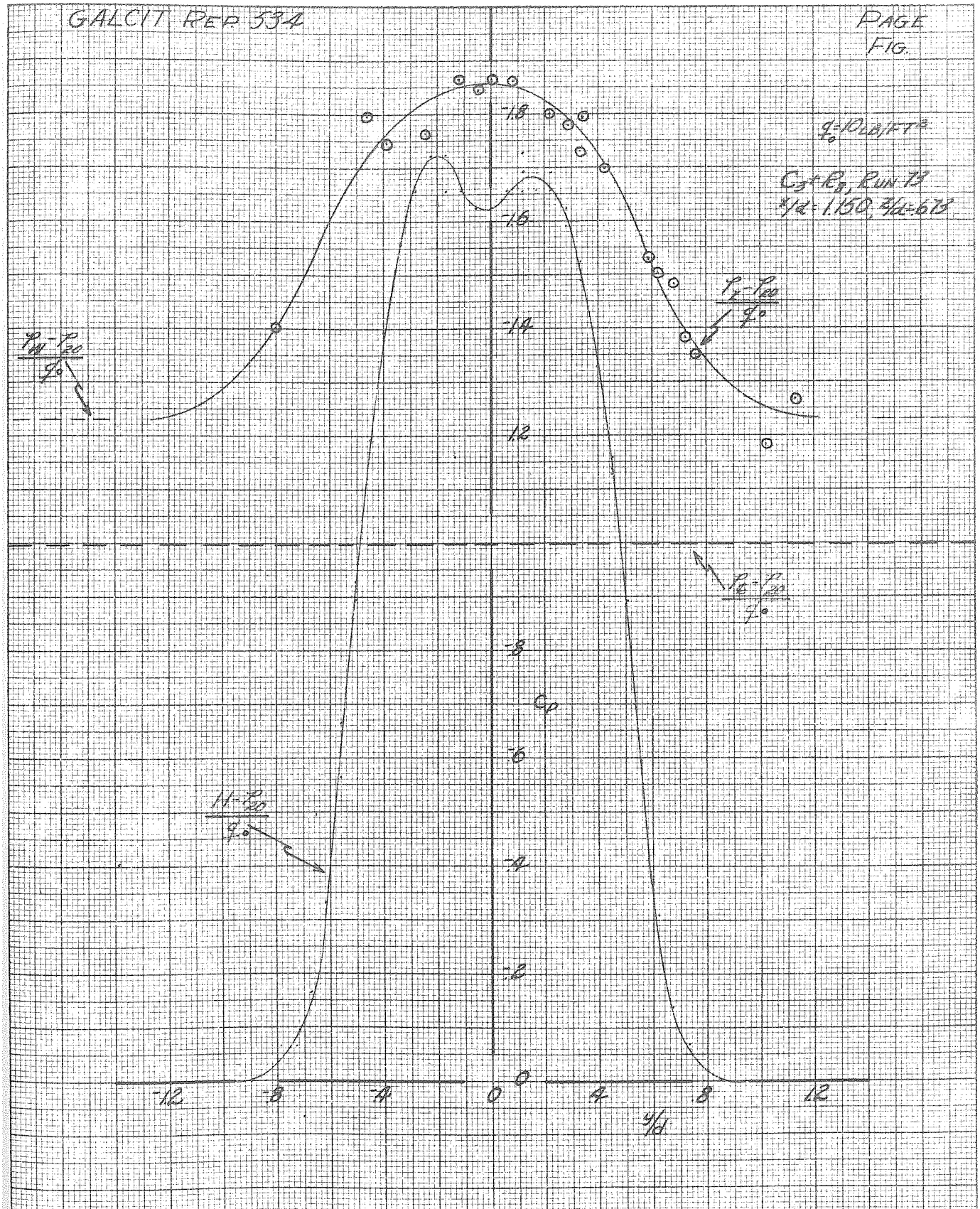

FIGURE 28R
WAKE PATTERN AFT OF CYLINDER C_3
$x/d = 1.150$, $z/d = .673$

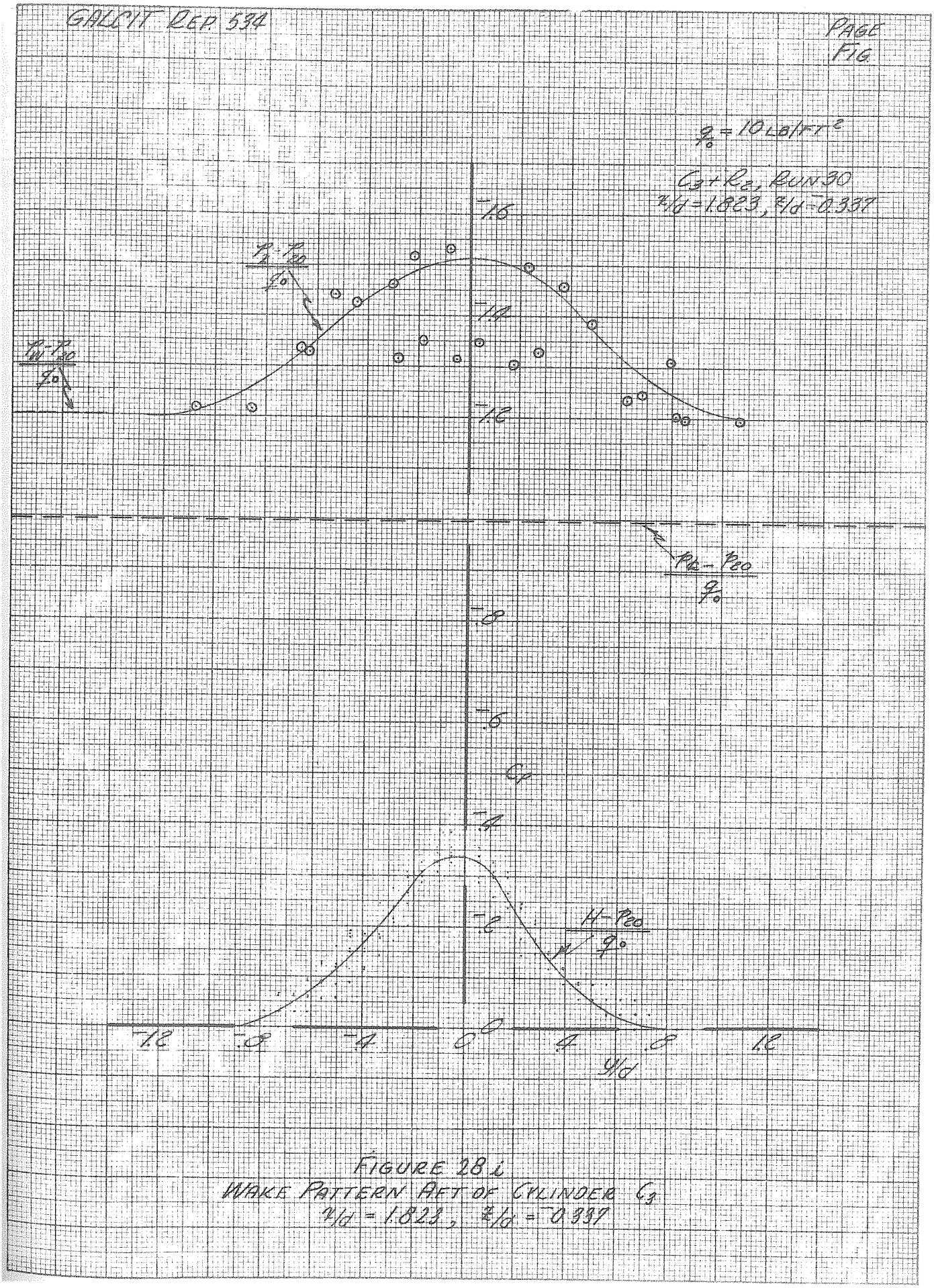

FIGURE 28.2
WAKE PATTERN AFT OF CYLINDER C_3
$x/d = 1.823$, $z/d = 0.337$

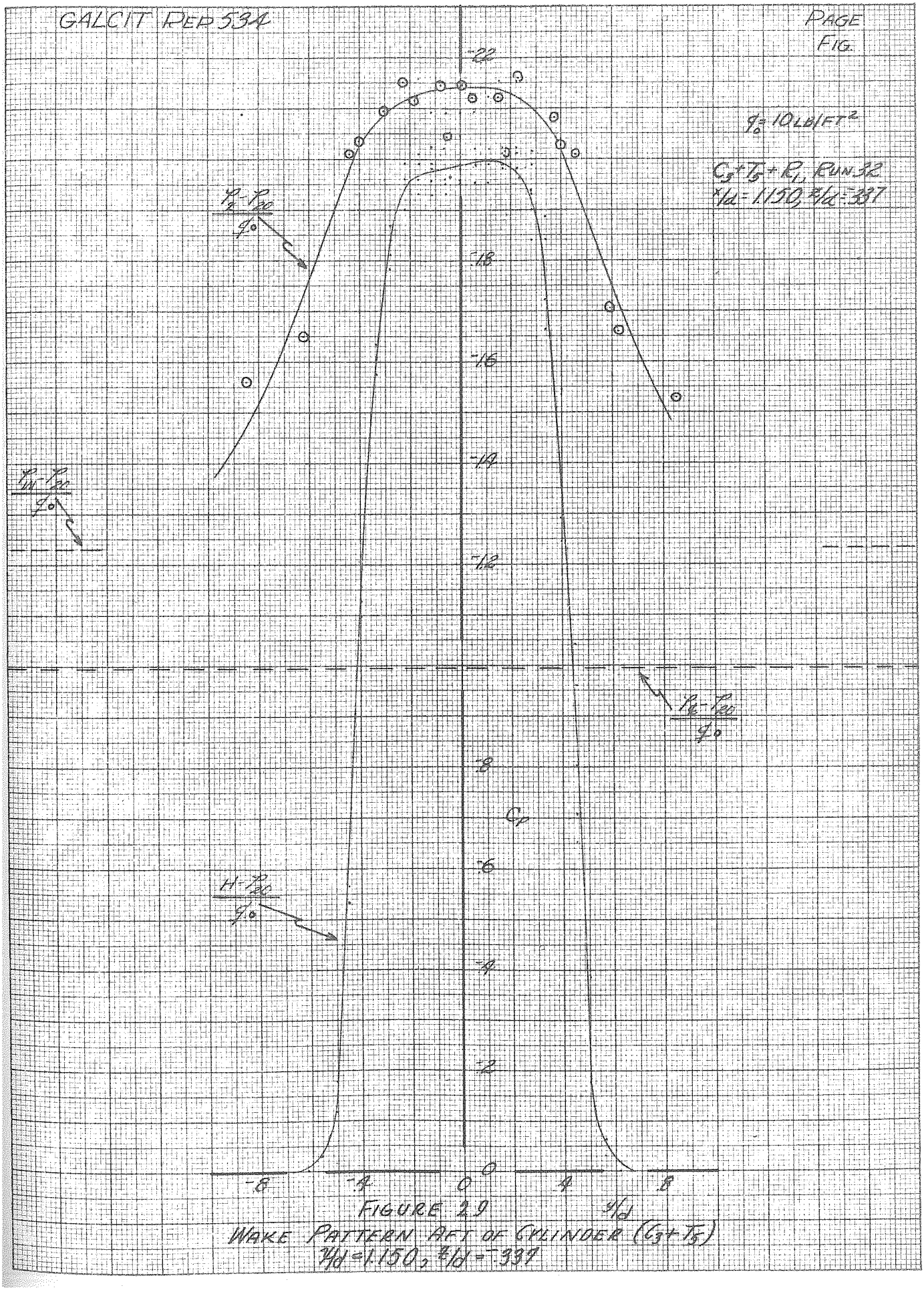

FIGURE 29
WAKE PATTERN AFT OF CYLINDER ($C_3 + T_5$)
$Y/d = 1.150$, $X/d = -.337$

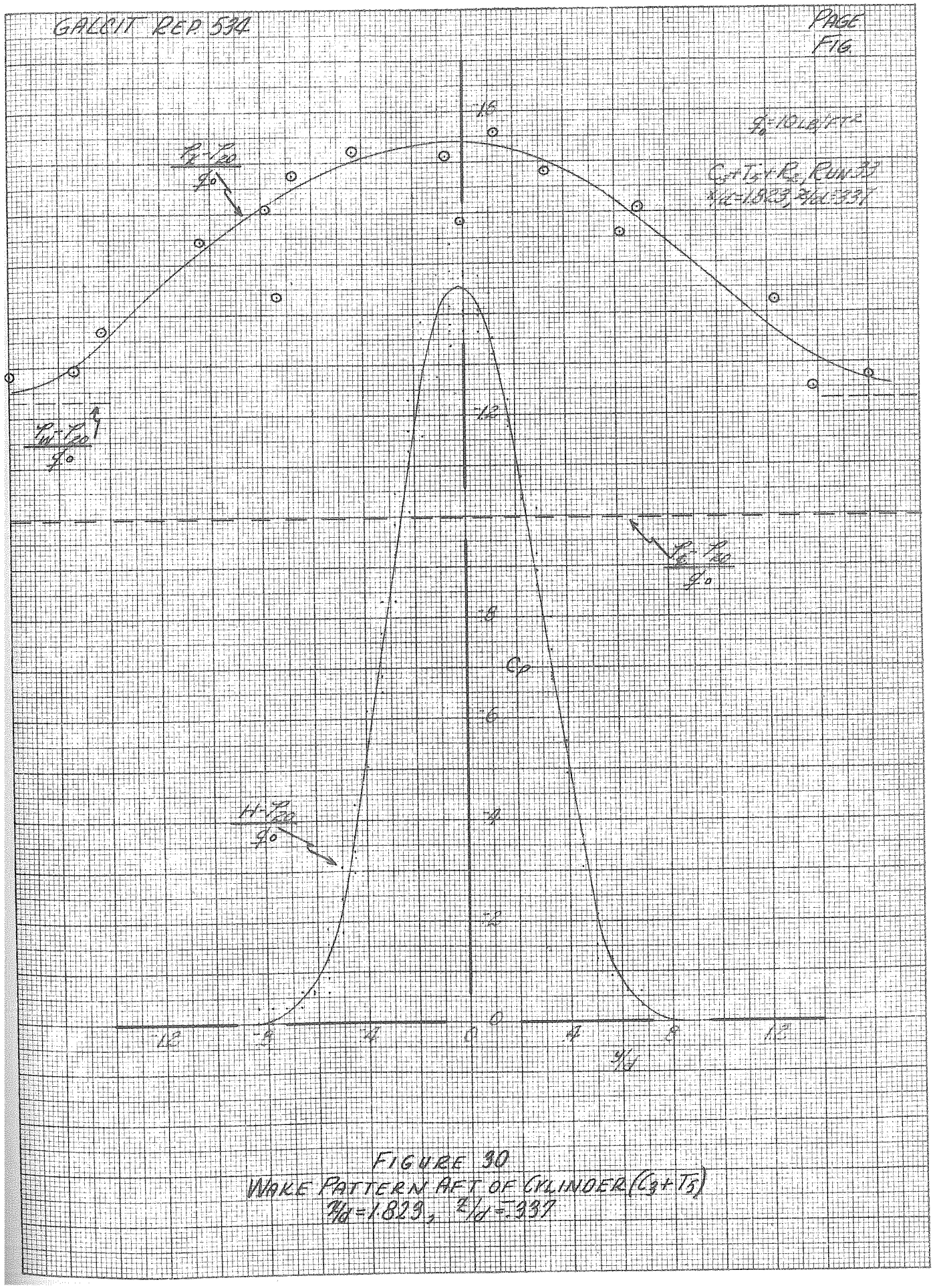

FIGURE 30
WAKE PATTERN AFT OF CYLINDER (C_3+T_5)
x/d=1.829, z/d=.337

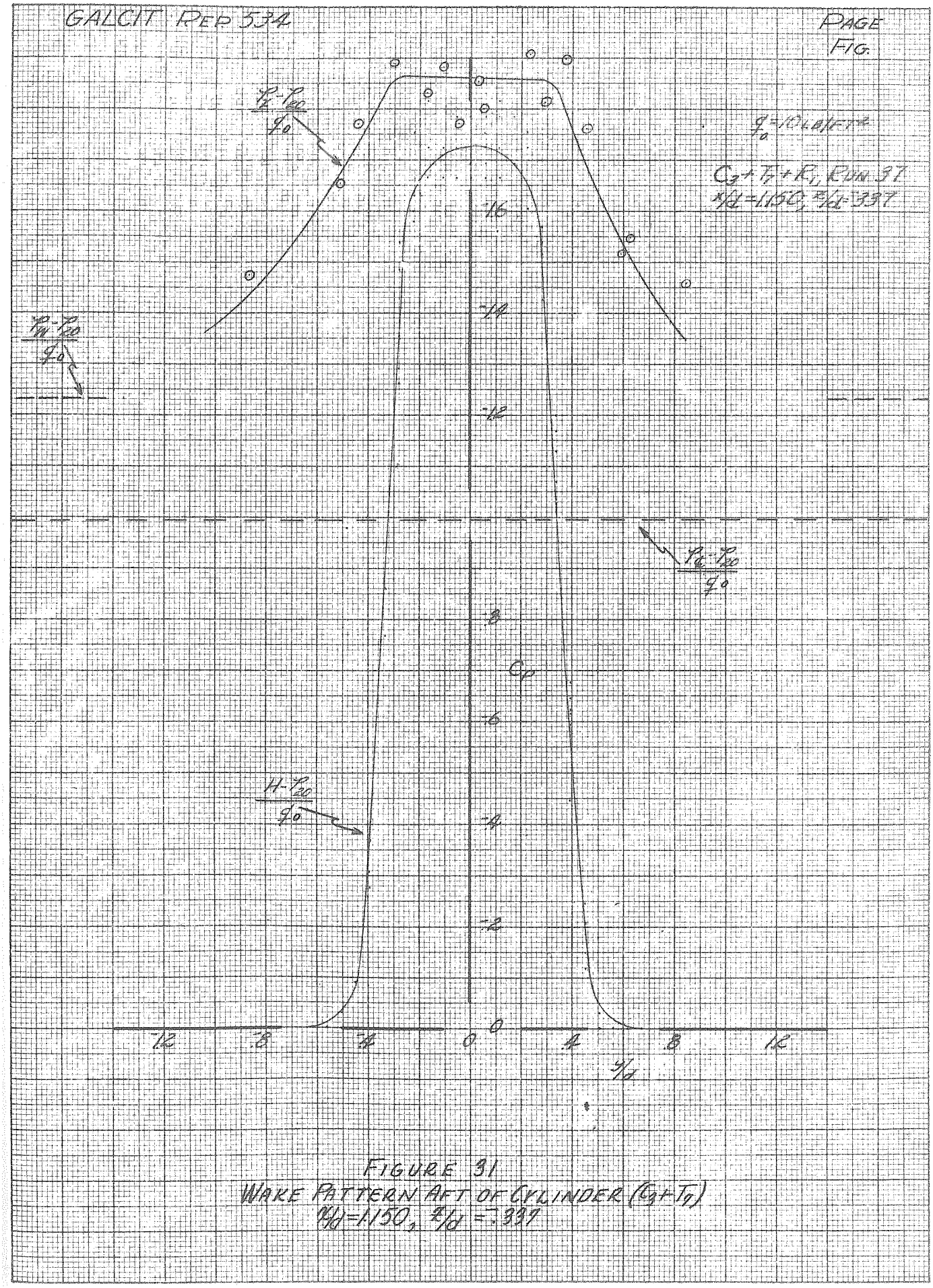

FIGURE 31
WAKE PATTERN AFT OF CYLINDER (C_3+T_7)
x/d=1.150, z/d=.337

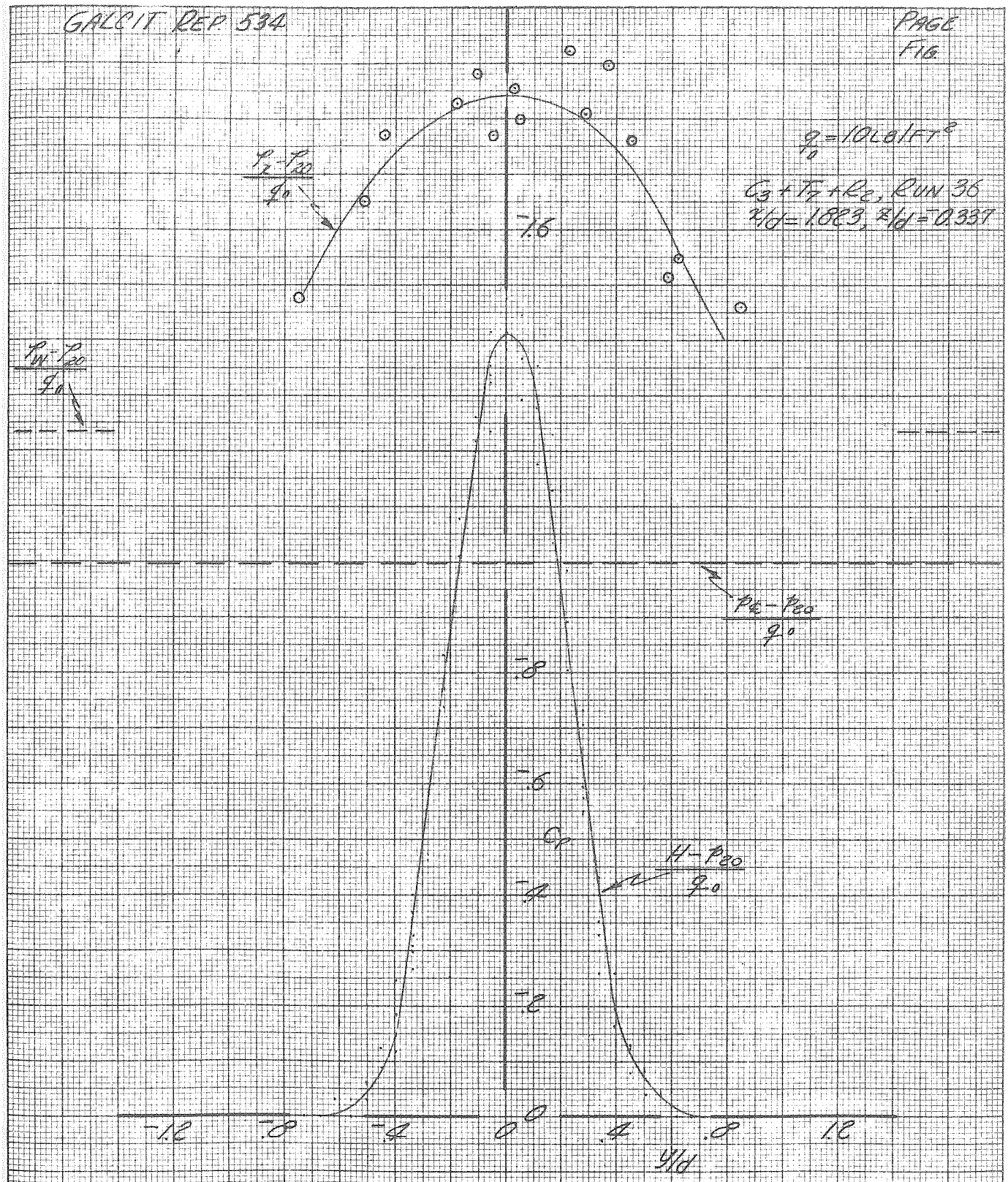

FIGURE 32
WAKE PATTERN AFT OF CYLINDER (C_3+T_7)
$x/d = 1.823$, $z/d = 0.337$

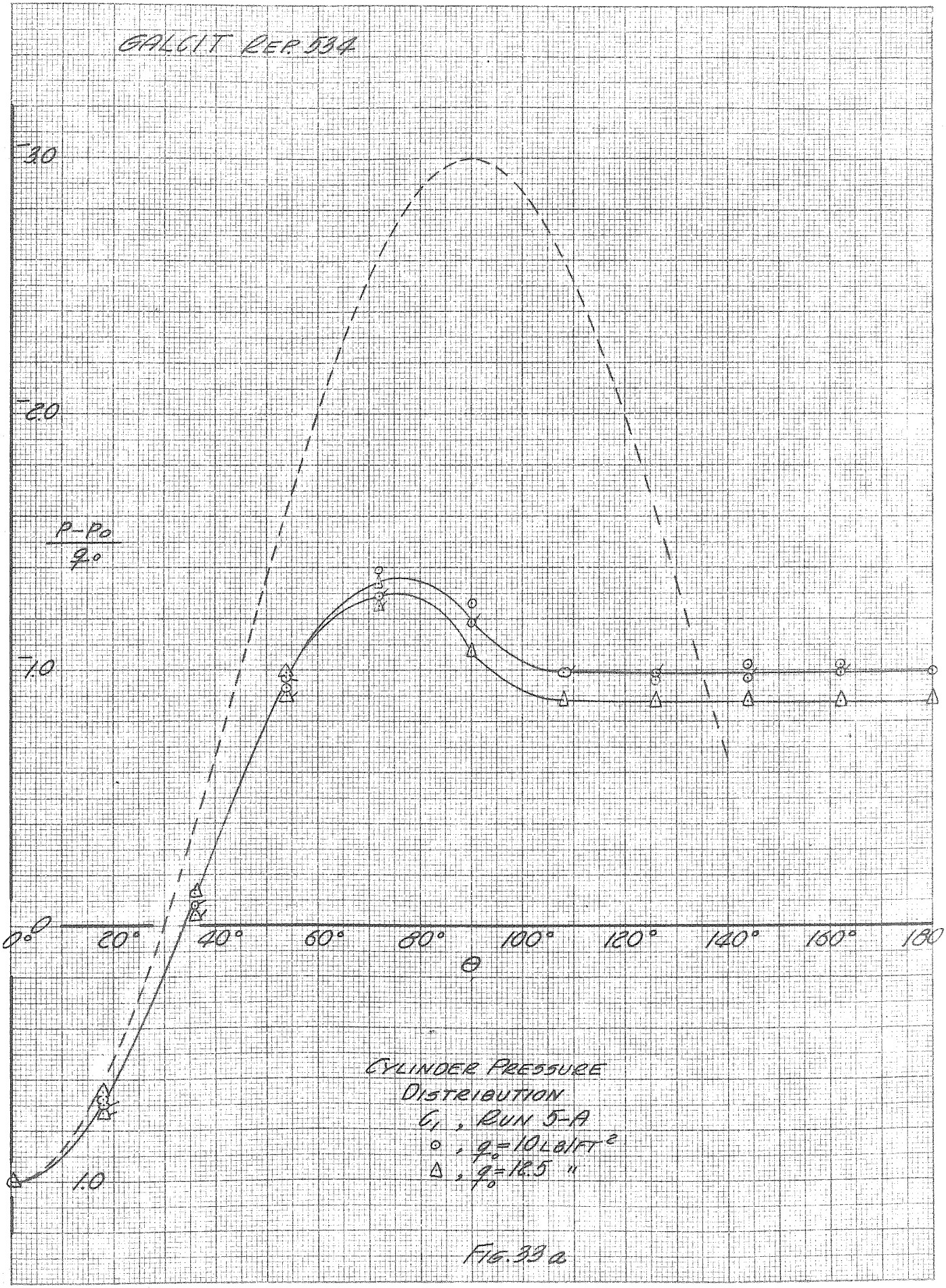

CYLINDER PRESSURE DISTRIBUTION
C_1, RUN 5-A
○, $q_0 = 10$ LB/FT^2
△, $q_0 = 12.5$ "

FIG. 39a

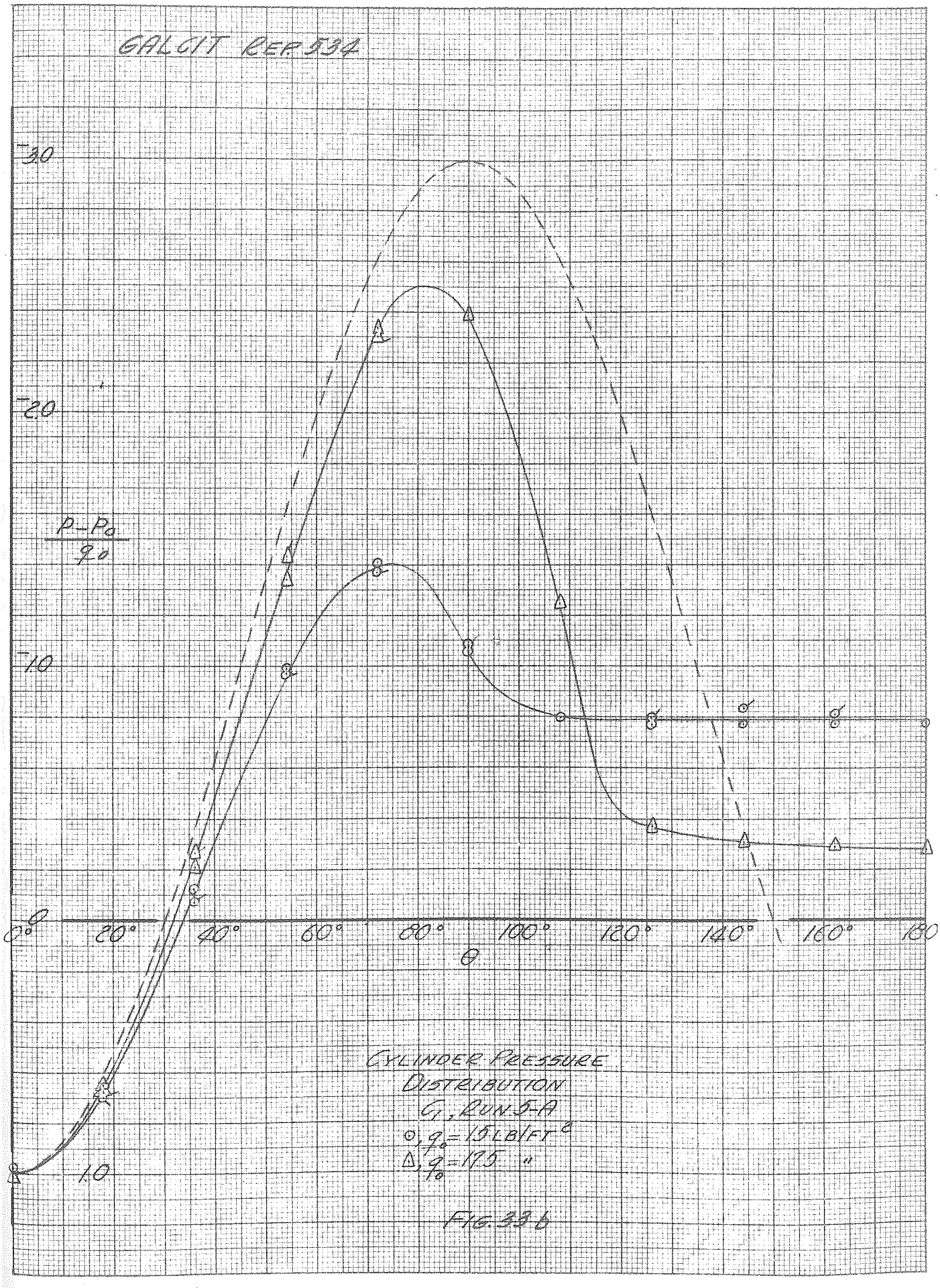

CYLINDER PRESSURE DISTRIBUTION
G, RUN 5-A
⊙, q_0 = 15 LB/FT²
△, q_0 = 17.5 "

FIG. 39 b

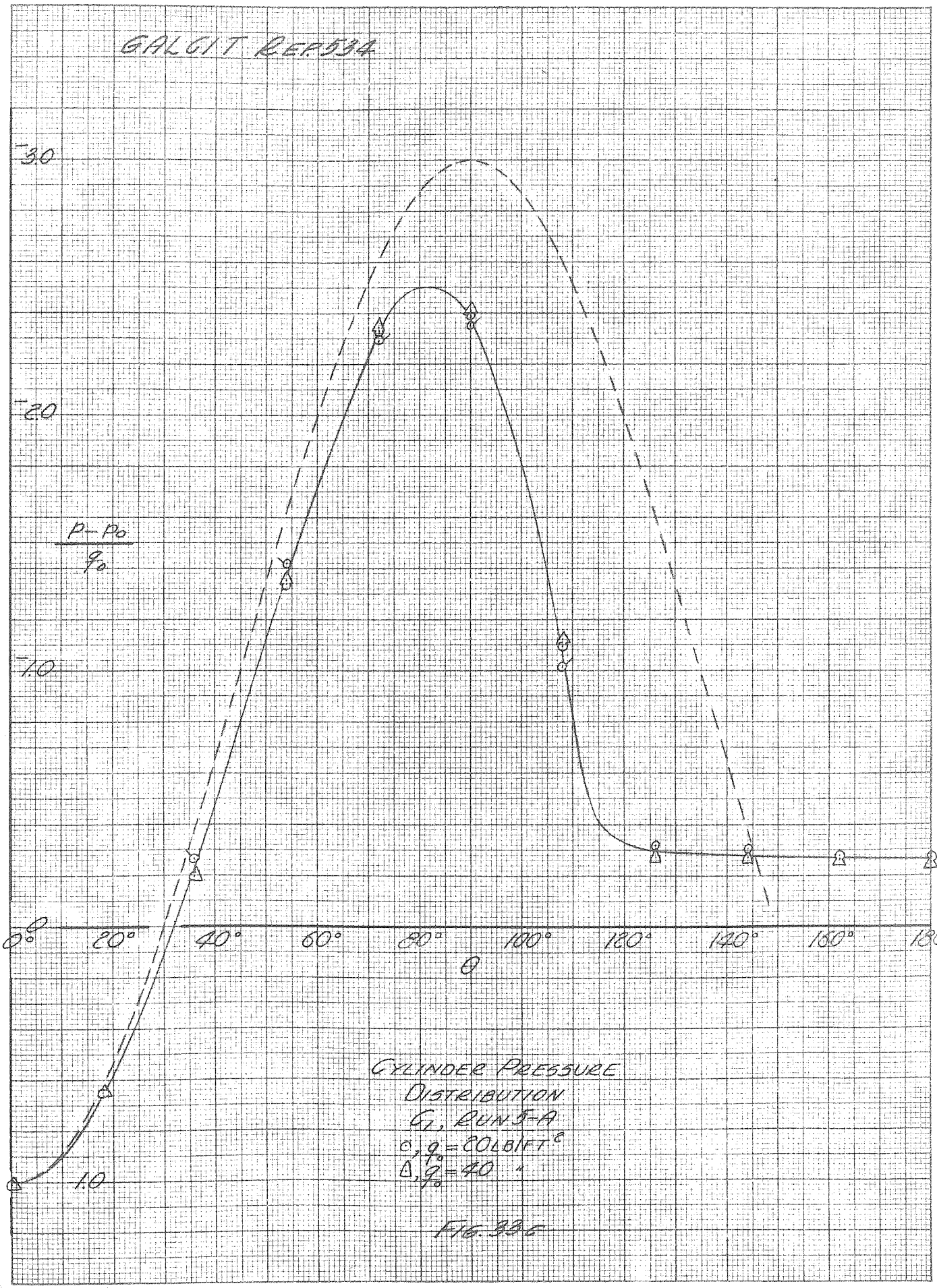

CYLINDER PRESSURE DISTRIBUTION
C_1, RUN 5-A
○, q_0 = 20 LB/FT.^{c}
△, q_0 = 40 "

FIG. 33 c

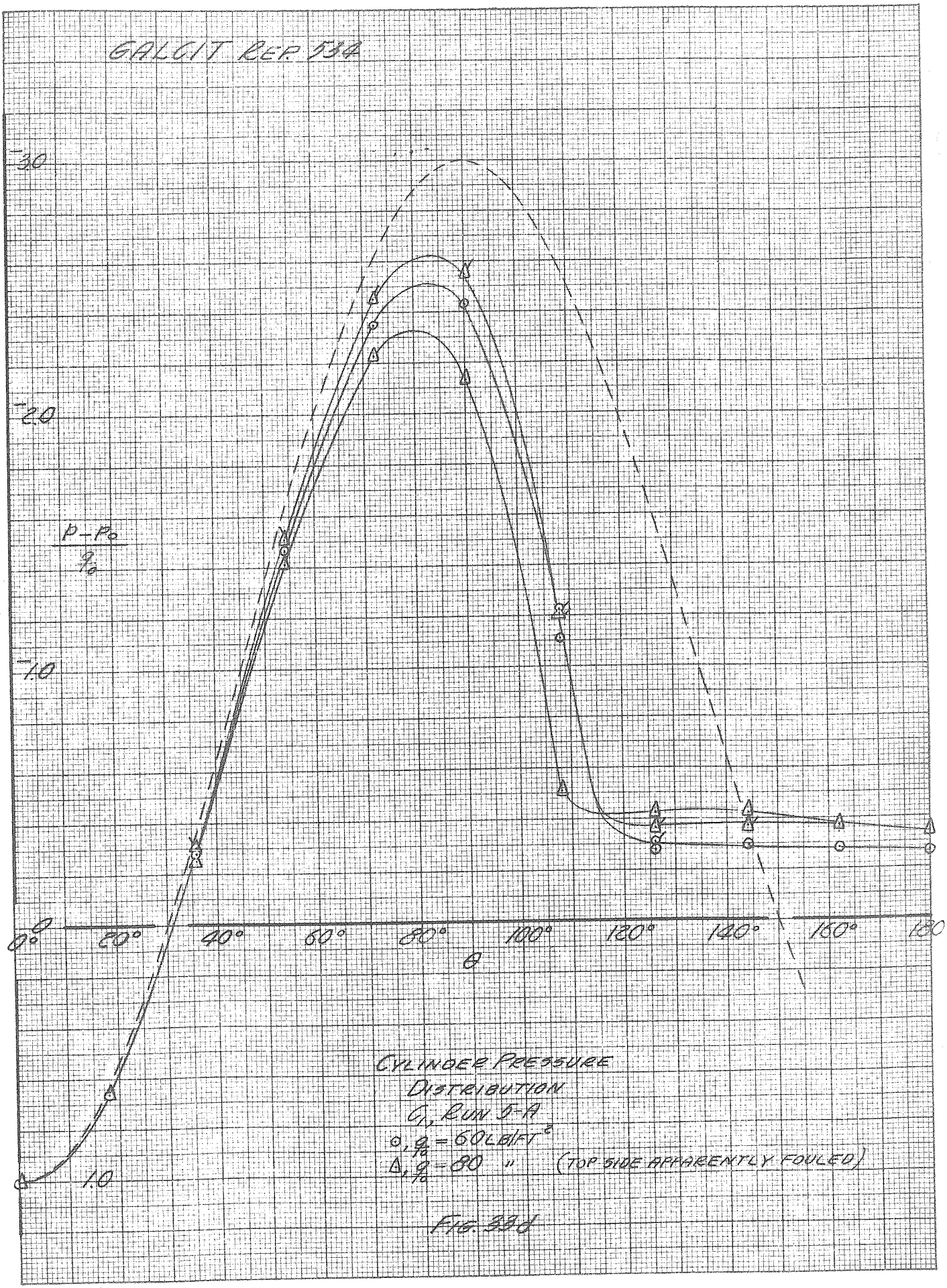

CYLINDER PRESSURE DISTRIBUTION
C_L, RUN 5-A
○, $\frac{q}{p_0}$ = 60 LB/FT²
△, $\frac{q}{p_0}$ = 80 " (TOP SIDE APPARENTLY FOULED)

FIG. 33d

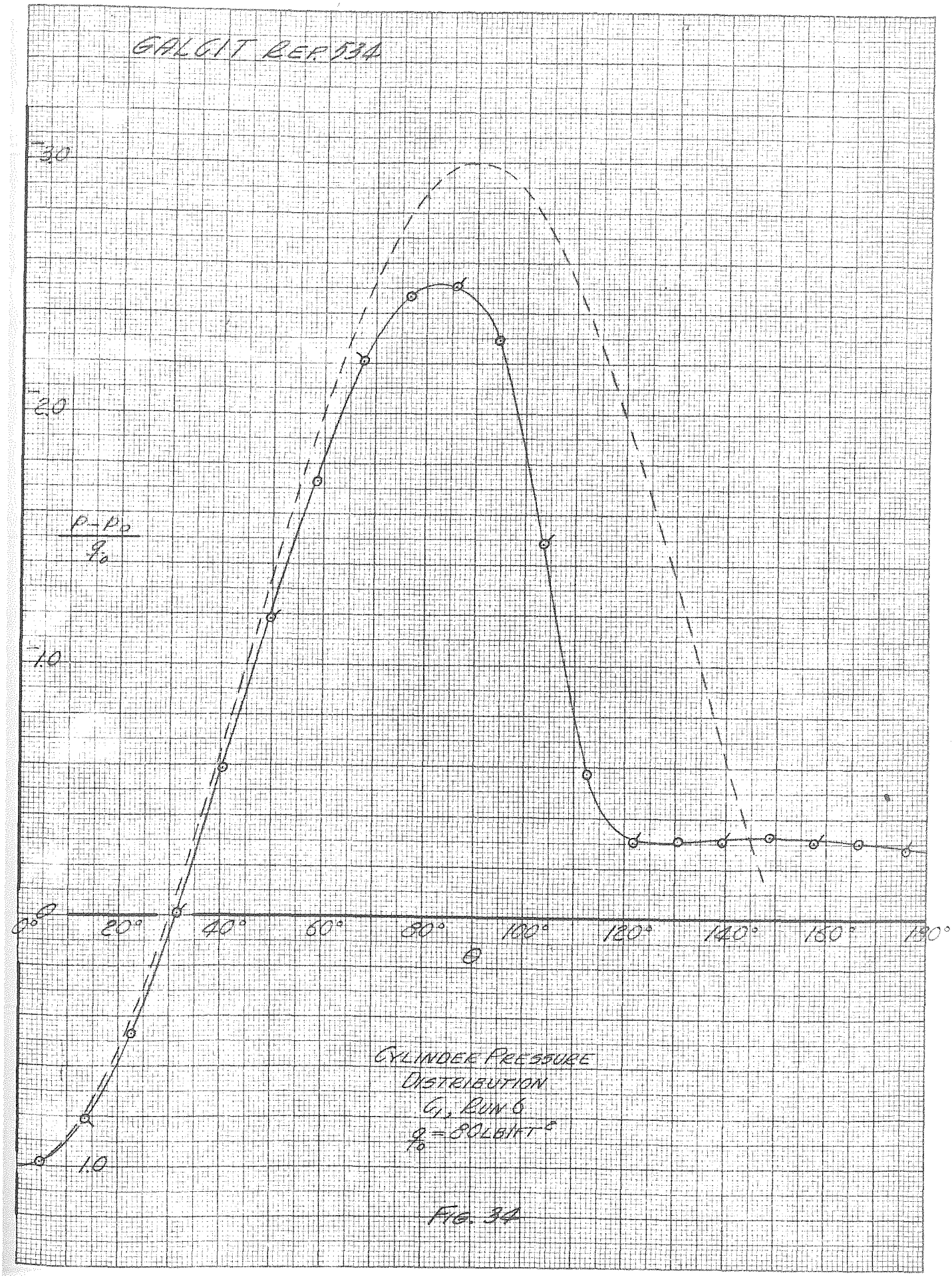

CYLINDER PRESSURE DISTRIBUTION
G_1, RUN 6
$q_0 = 80 \text{ LB/FT}^2$

FIG. 34

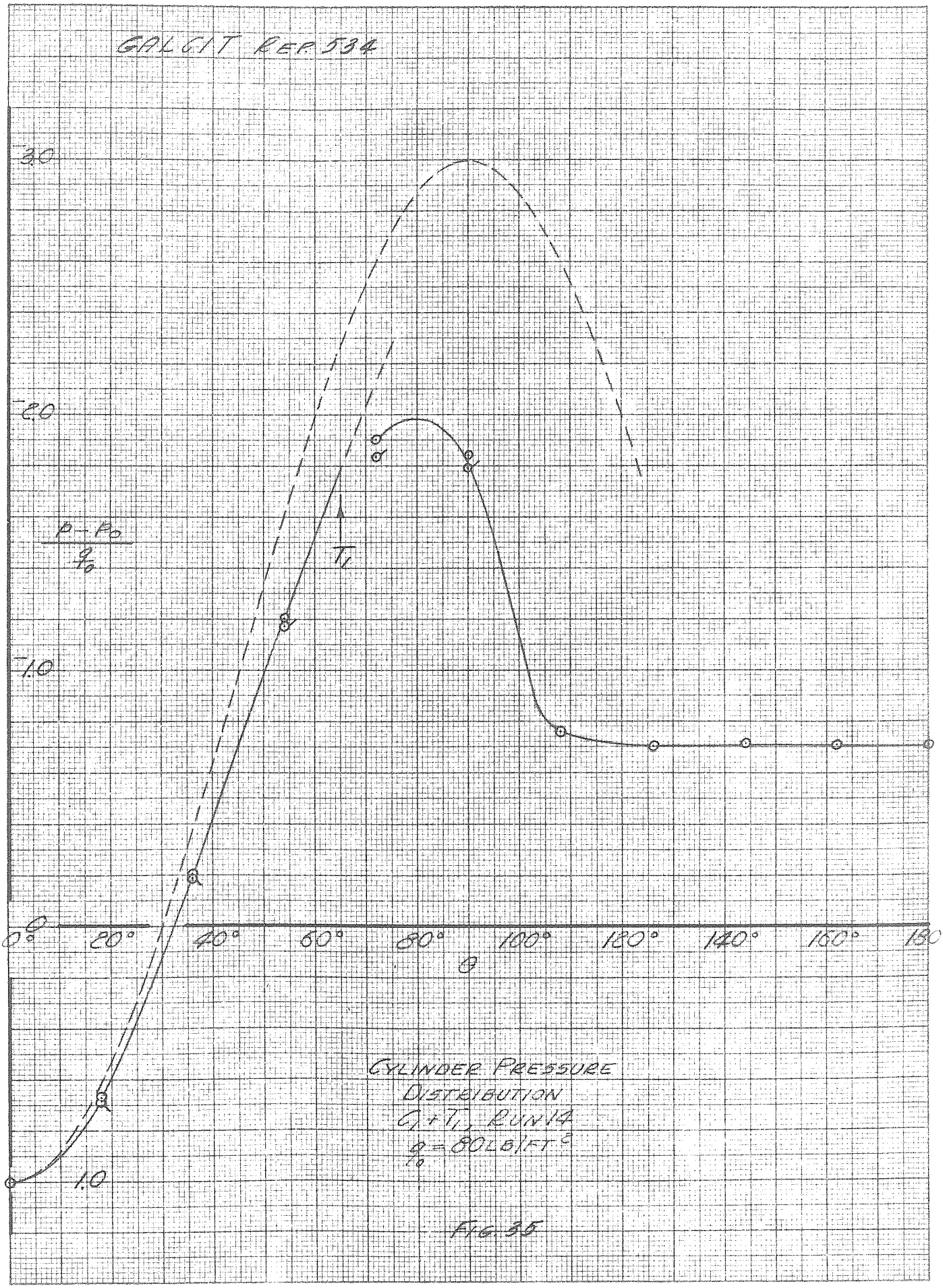

CYLINDER PRESSURE DISTRIBUTION
$C_1 + T_1$, RUN 14
$q_0 = 80$ LB/FT^2

FIG. 35

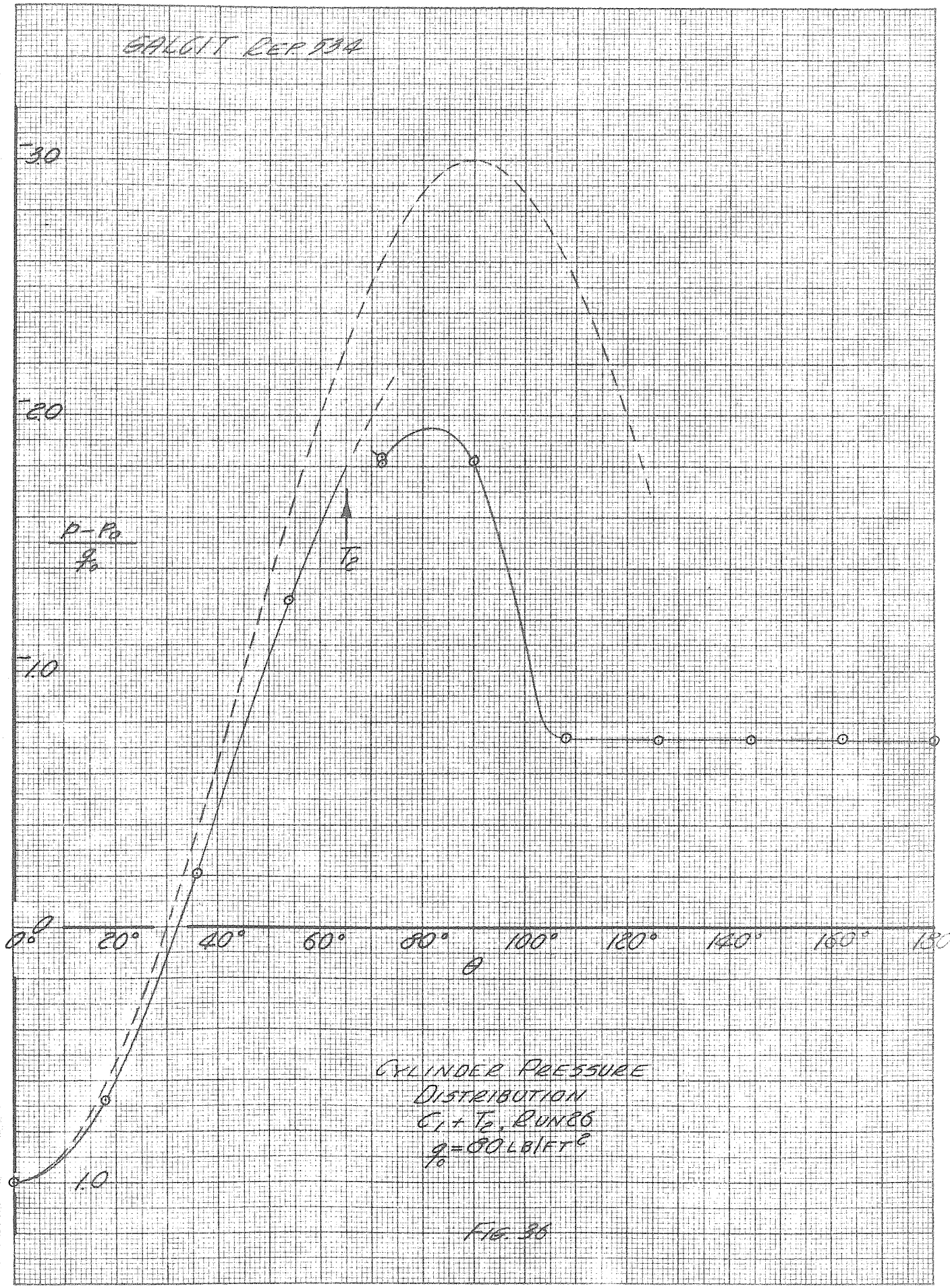

CYLINDER PRESSURE DISTRIBUTION
$C_1 + T_2$, RUN 26
$q_0 = 80$ LB/FT^2

FIG. 38

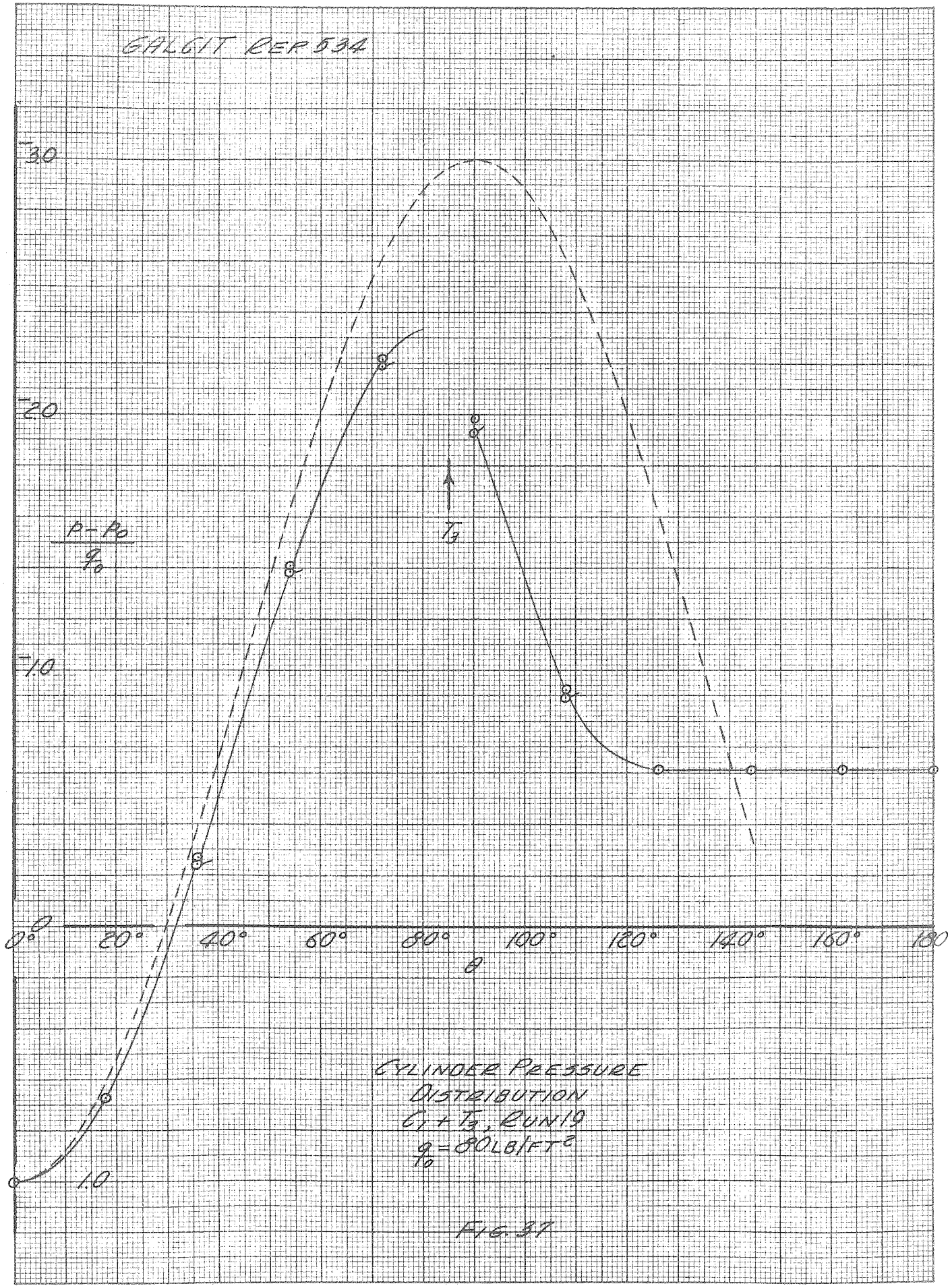

CYLINDER PRESSURE DISTRIBUTION
$C_1 + T_3$, RUN 19
$q_0 = 80$ LB/FT^2

FIG. 31

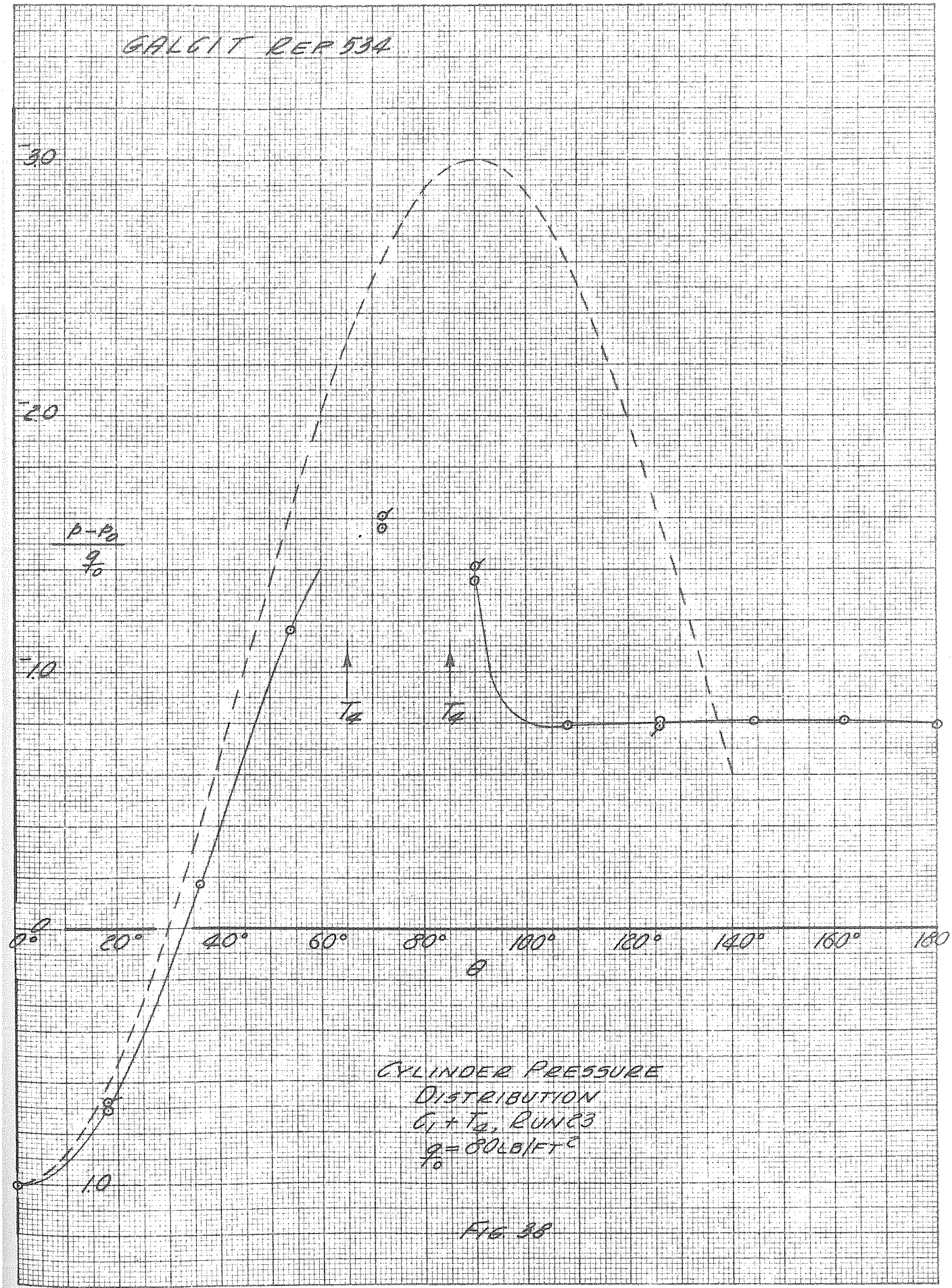

CYLINDER PRESSURE DISTRIBUTION
$C_1 + T_2$, RUN 23
$q_0 = 80$ LB/FT^2

FIG. 38

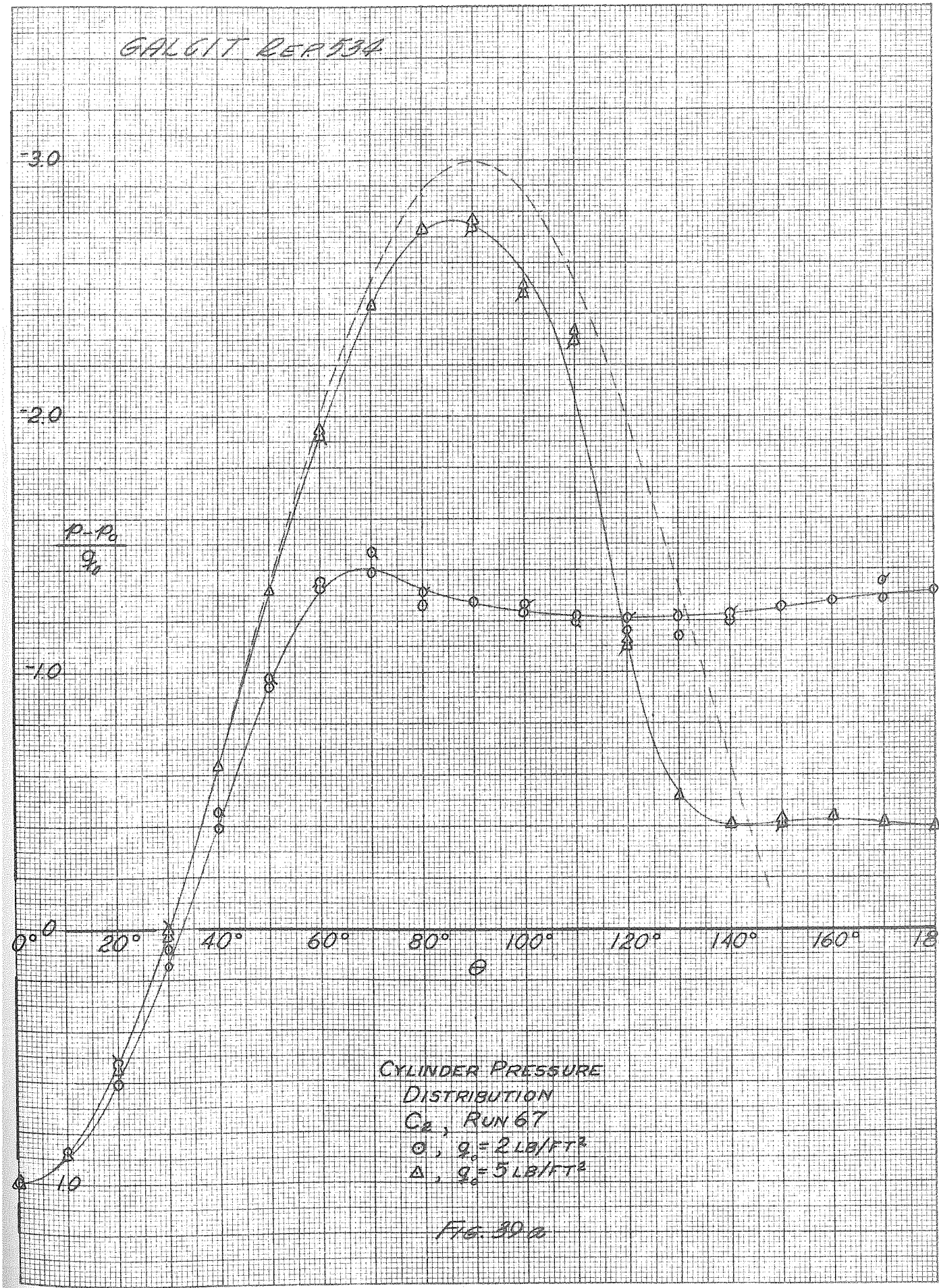

CYLINDER PRESSURE DISTRIBUTION
C_2, RUN 67
⊙, $q_0 = 2$ LB/FT^2
△, $q_0 = 5$ LB/FT^2

FIG. 39a

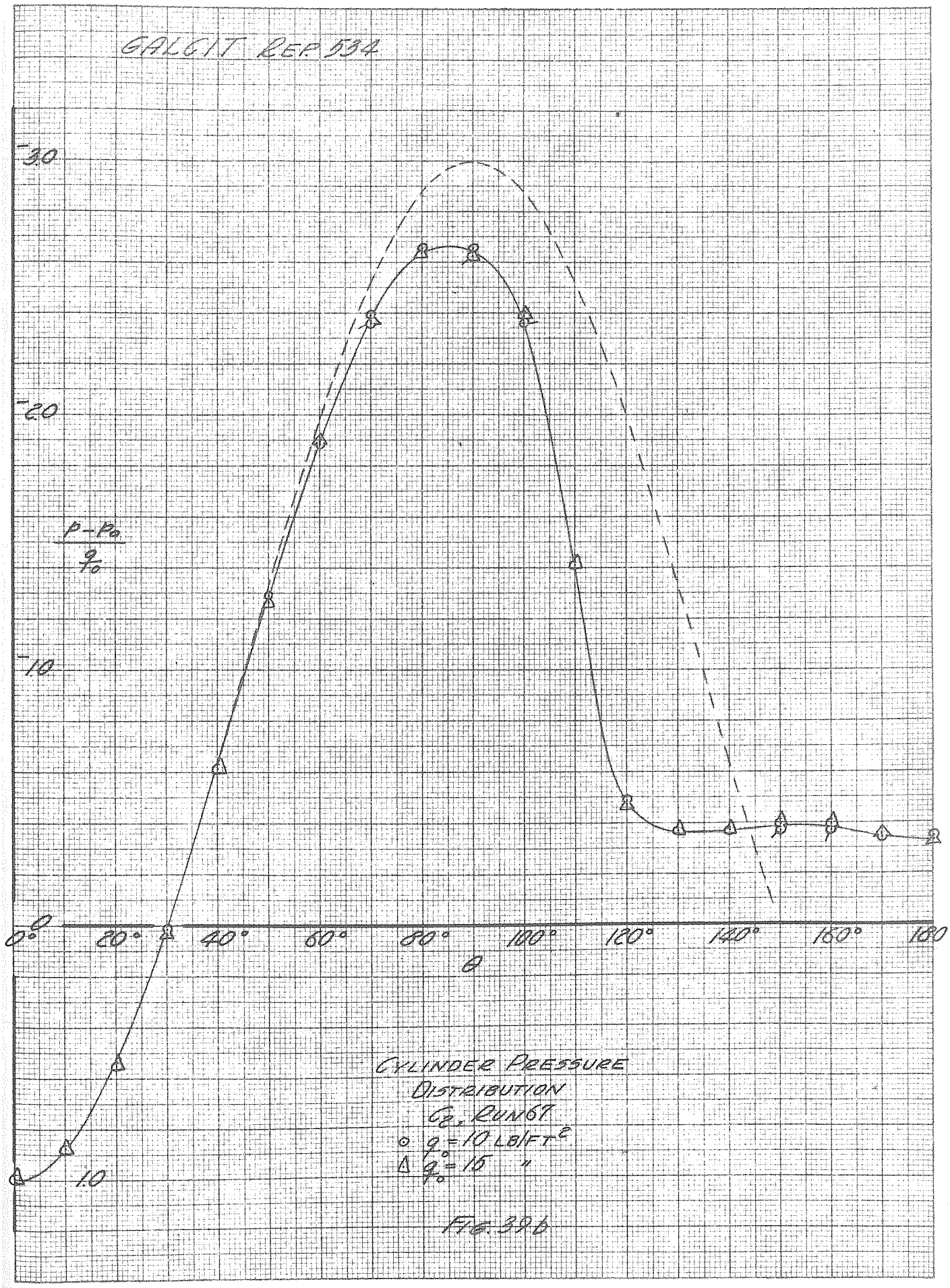
GALCIT REF 534
-30
-20
-10
1.0
$\frac{p-p_0}{q_0}$
0°
20°
40°
60°
80°
100°
120°
140°
160°
180°
θ
CYLINDER PRESSURE DISTRIBUTION
C_L, RUN 69
⊙ q_0 = 10 LB/FT²
△ q_0 = 15 "

FIG. 39b

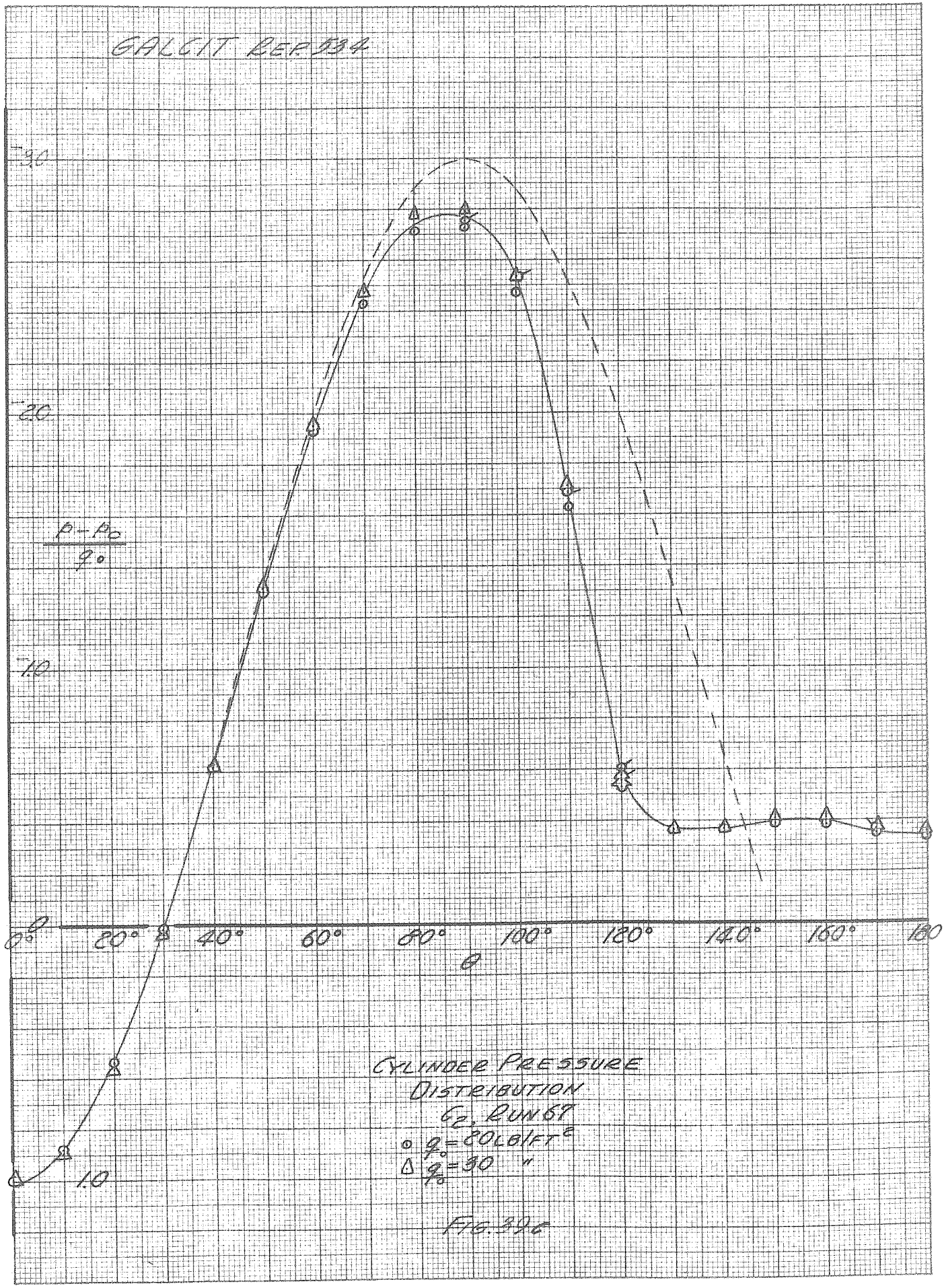

CYLINDER PRESSURE DISTRIBUTION
62, RUN 67
○ q_0 = 20 LB/FT²
△ q_0 = 30 "

FIG. 32c

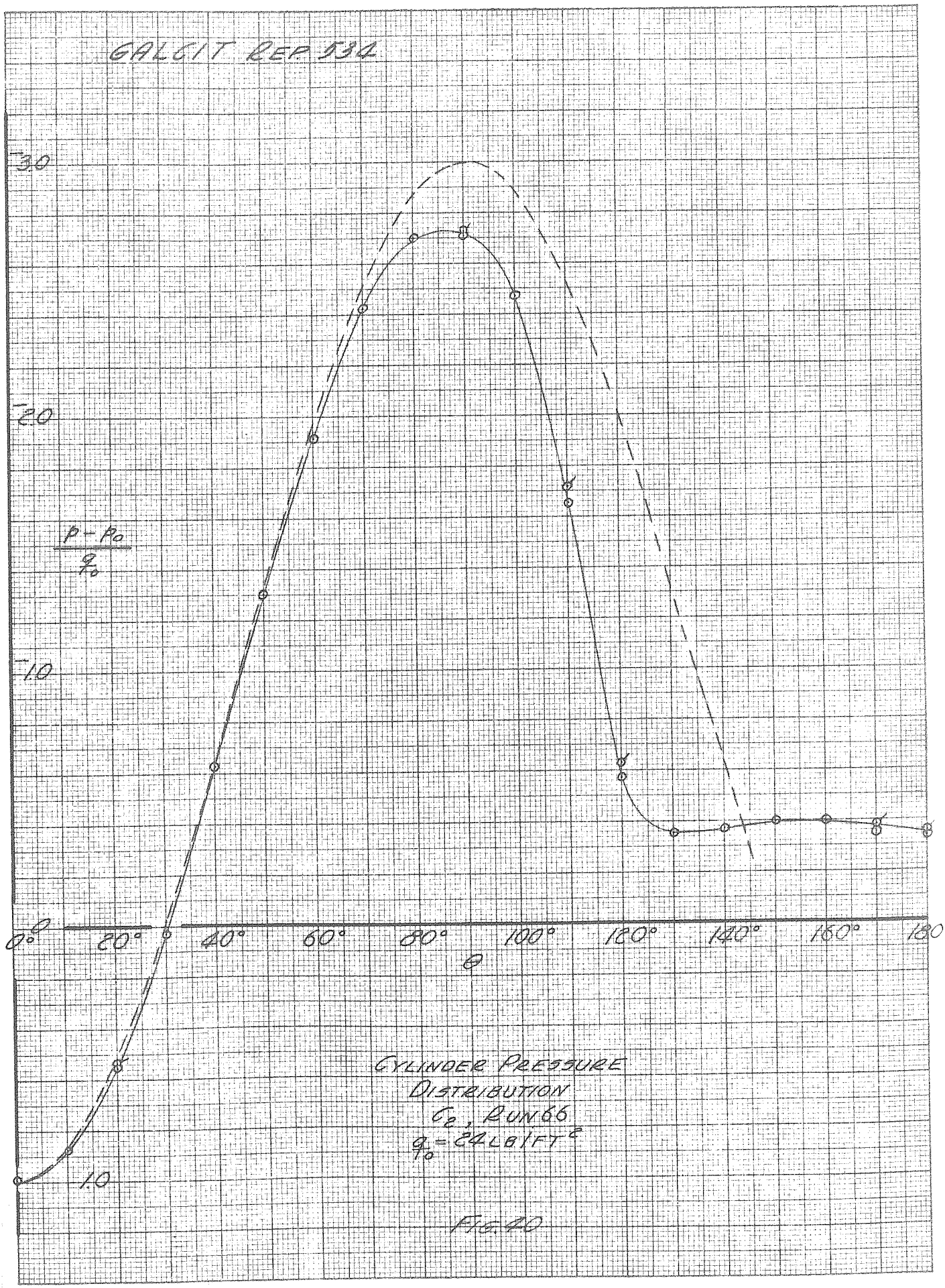

CYLINDER PRESSURE DISTRIBUTION
C_D, RUN 66
$q_0 = 24$ LB/FT^2

FIG. 40

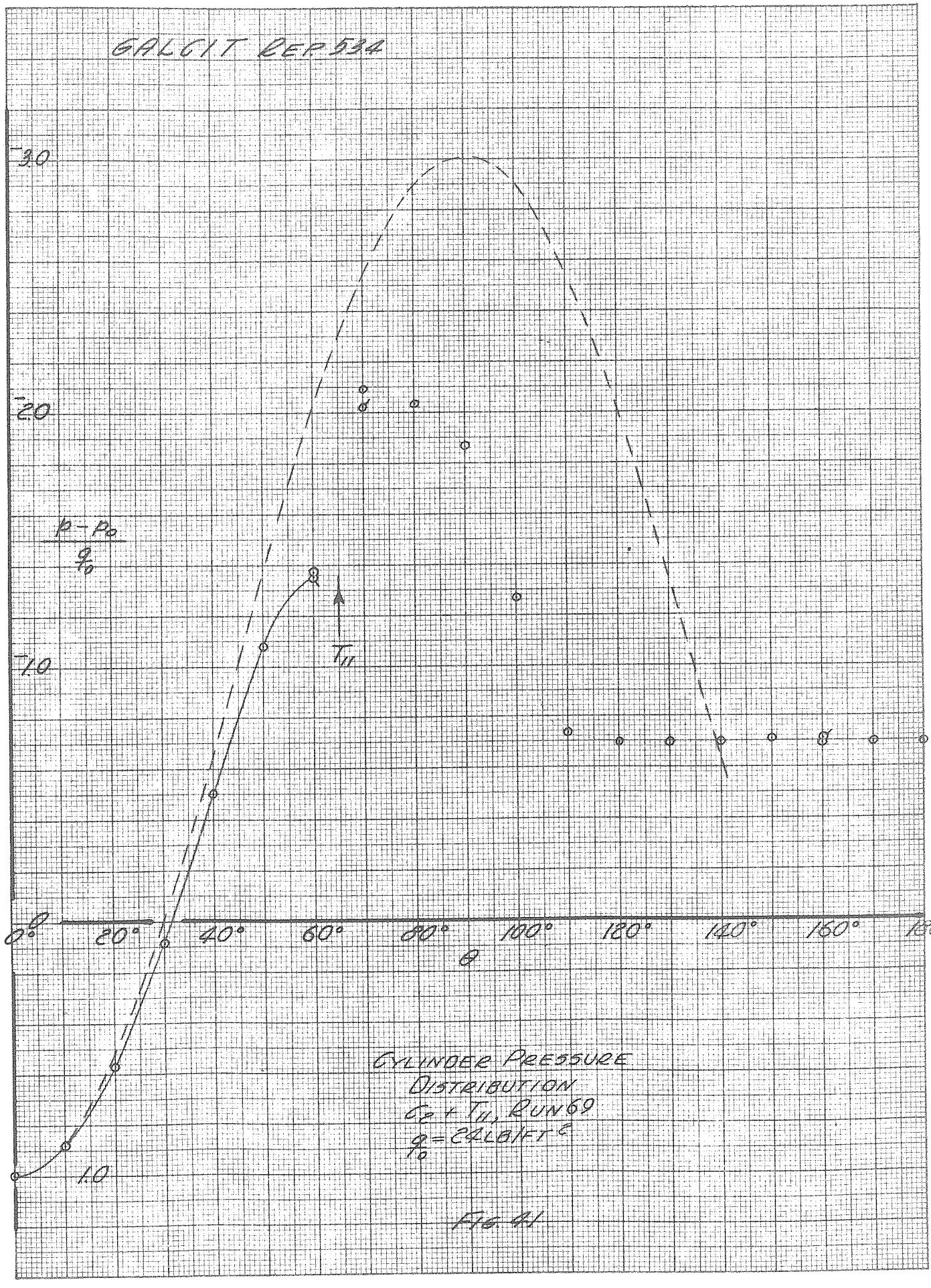

CYLINDER PRESSURE DISTRIBUTION
C_p + T_{tr}, RUN 69
$\frac{q}{q_0}$ = CALCULATED

FIG. 41

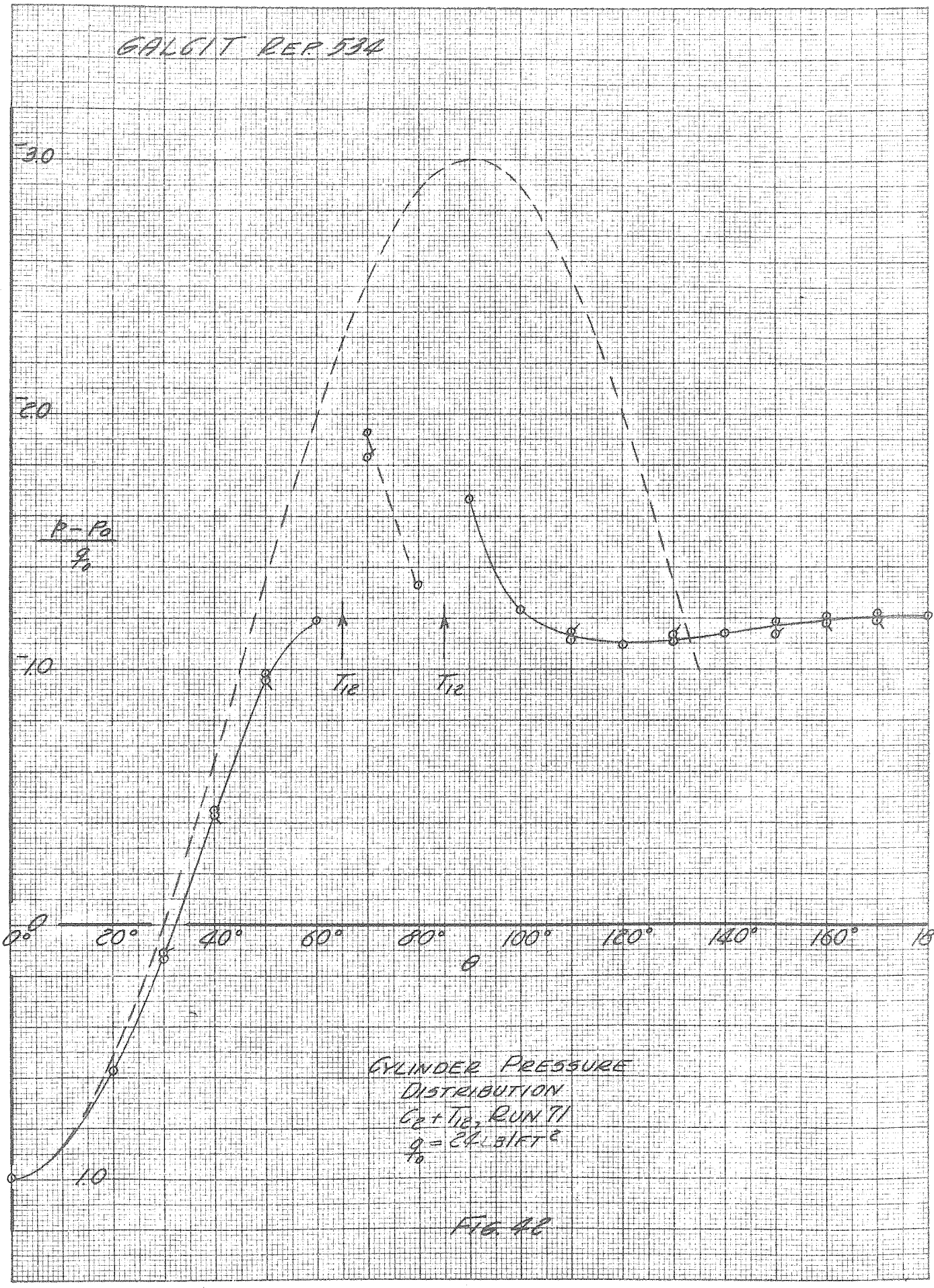

CYLINDER PRESSURE DISTRIBUTION
$C_2 + T_{12}$, RUN 71
$\frac{q}{q_0} = 24.31 ft^2$

FIG. 42

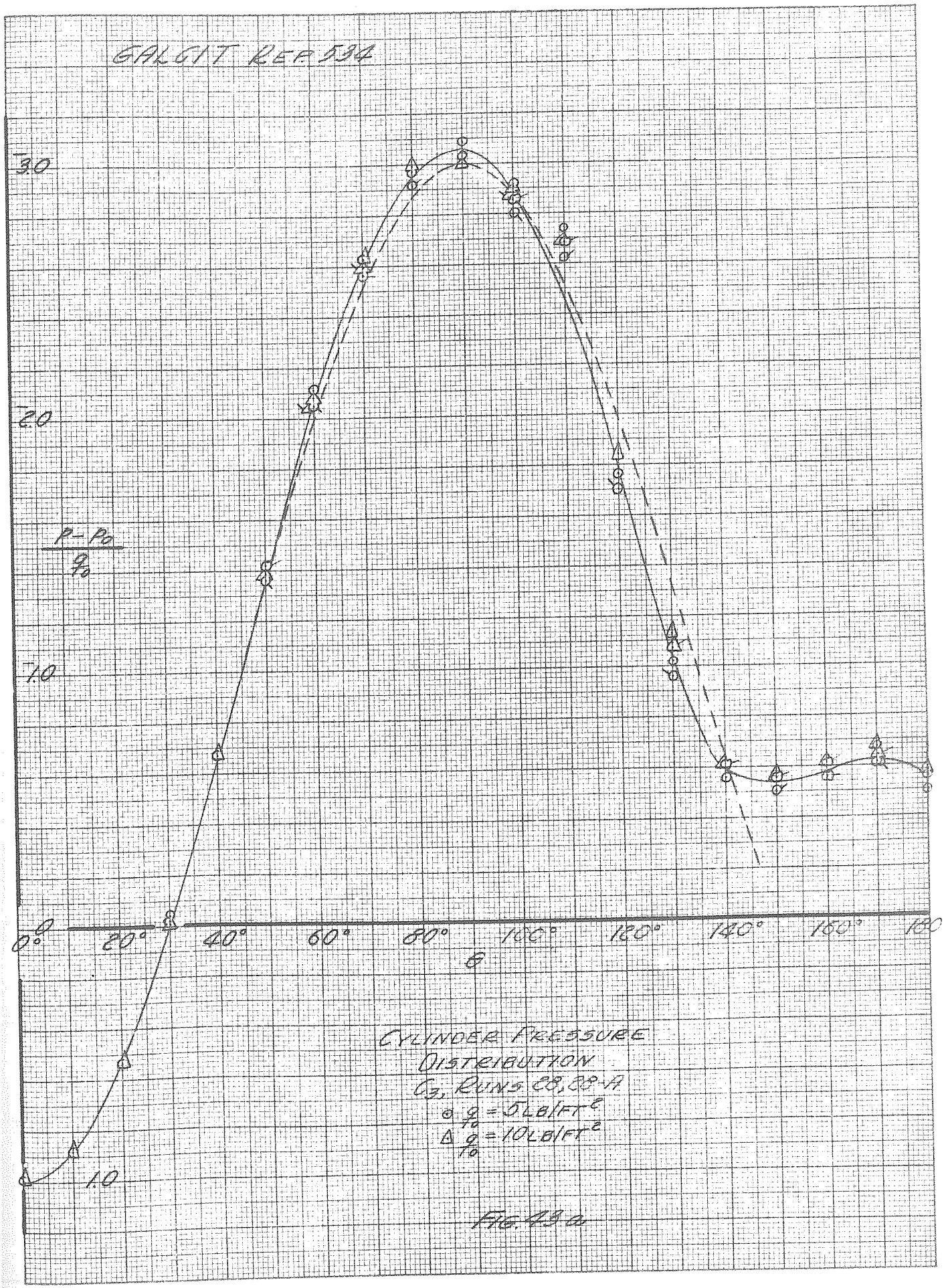

CYLINDER PRESSURE DISTRIBUTION
C_2, RUNS 88, 88-A
○ $\frac{q}{q_0}$ = .5 LB/FT²
Δ $\frac{q}{q_0}$ = 1.0 LB/FT²

FIG. 43a

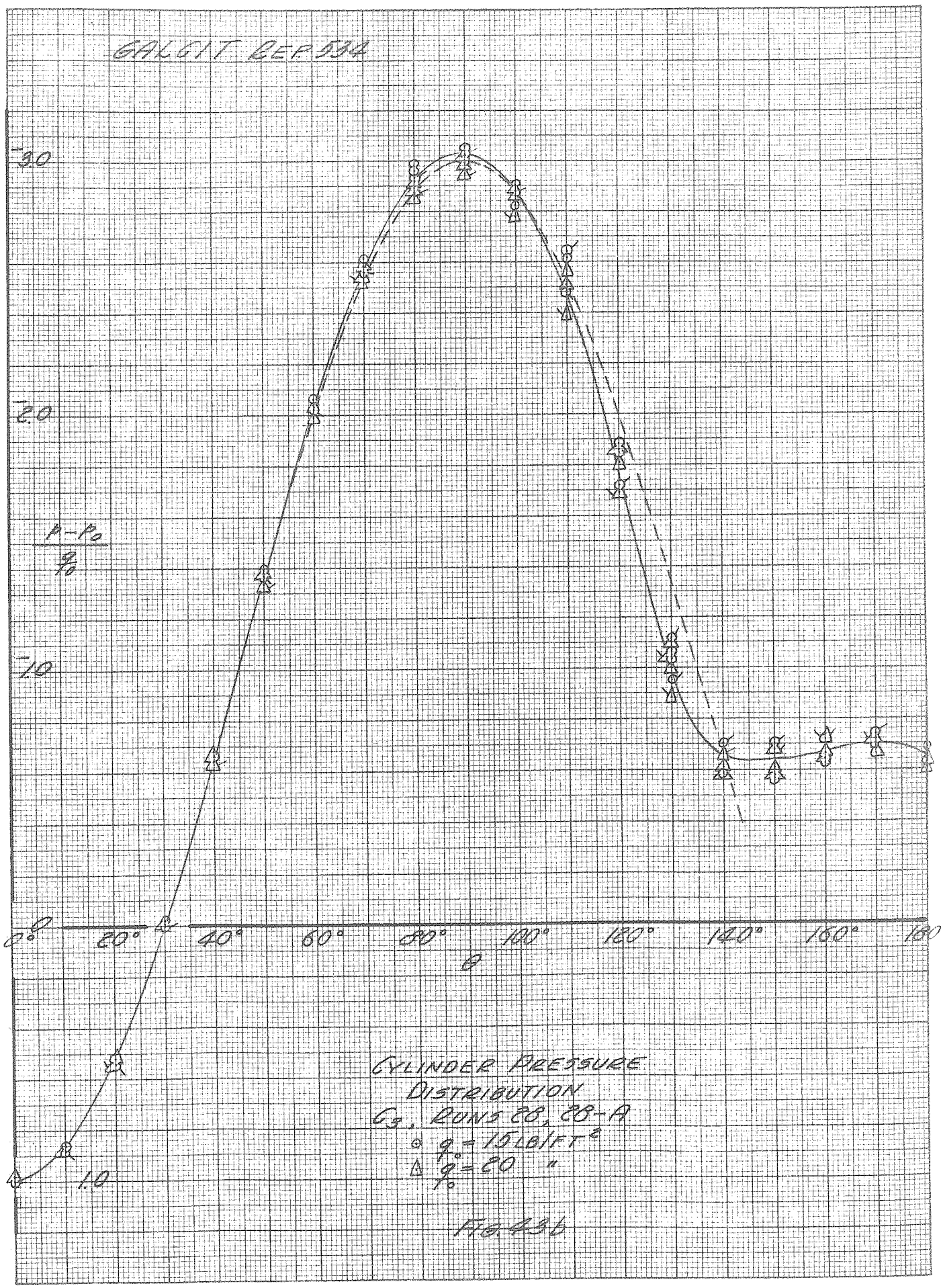

CYLINDER PRESSURE DISTRIBUTION
G3, RUNS 28, 28-A
⊙ q_0 = 15 LB/FT²
△ q_0 = 20 "

FIG. 43b

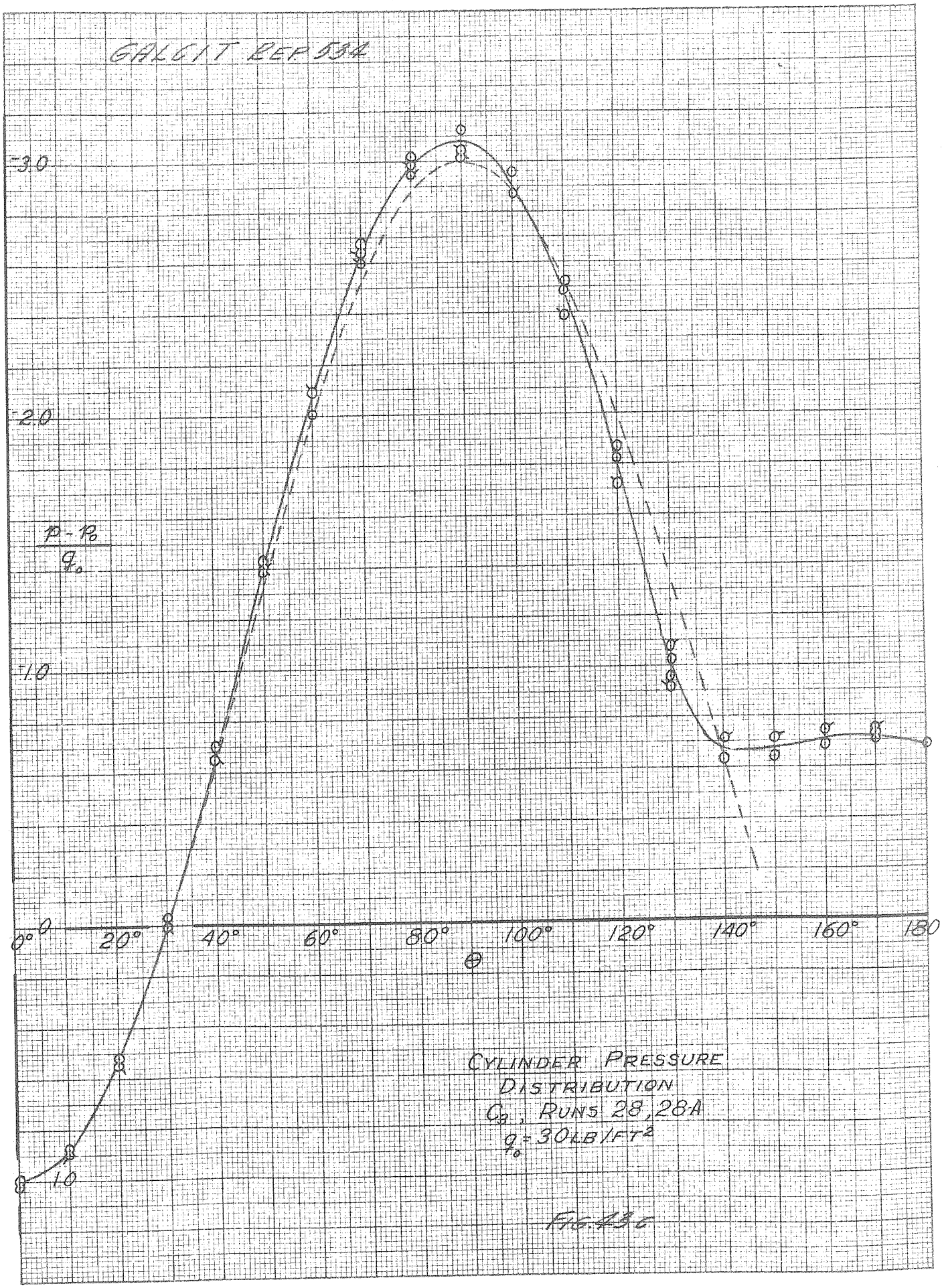

CYLINDER PRESSURE DISTRIBUTION
C_D, RUNS 28, 28A
$q_0 = 30 \text{ LB/FT}^2$

FIG. 43c

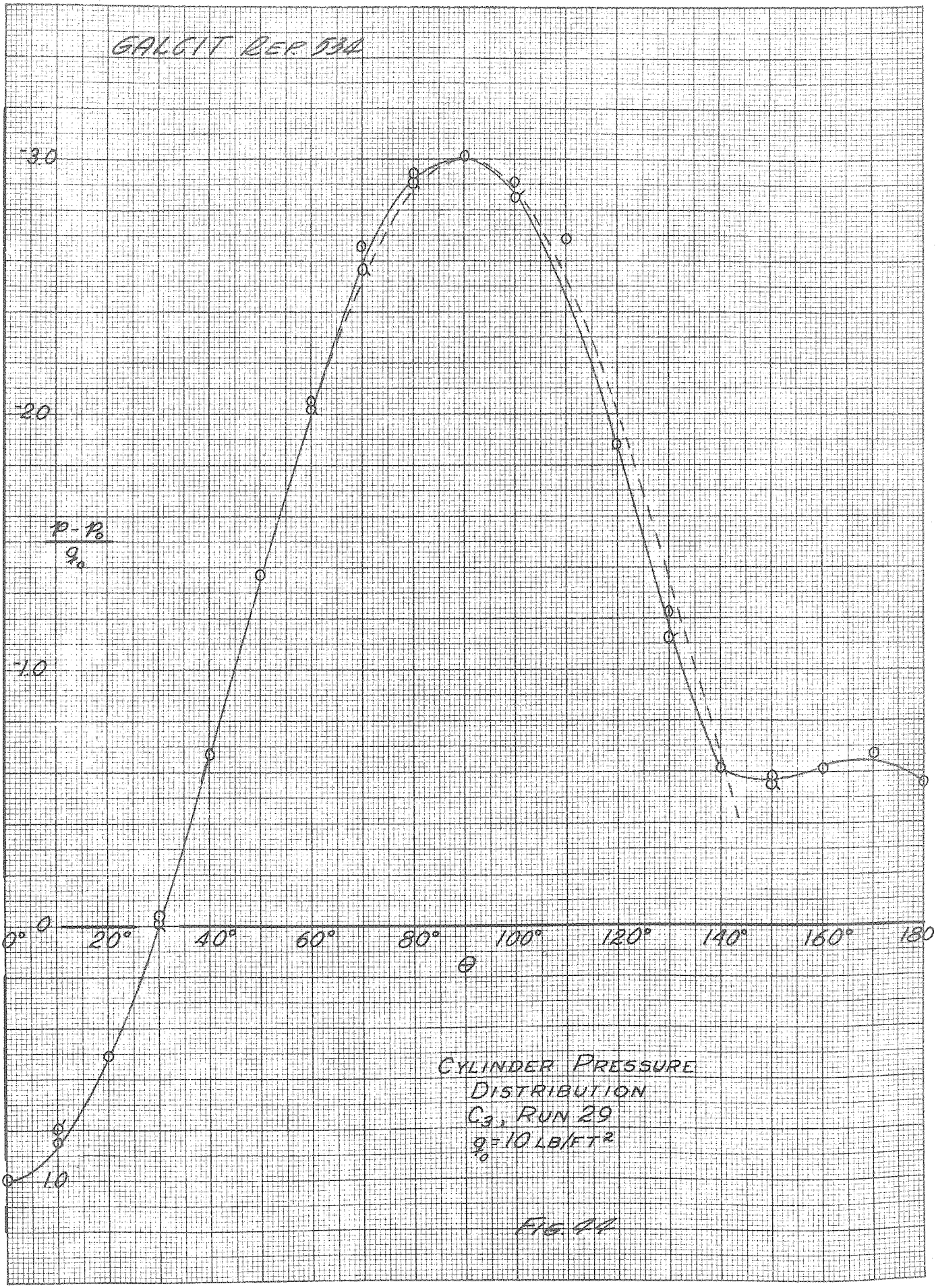

CYLINDER PRESSURE DISTRIBUTION
C_3, RUN 29
$q_0 = 10$ LB/FT^2

FIG. 44

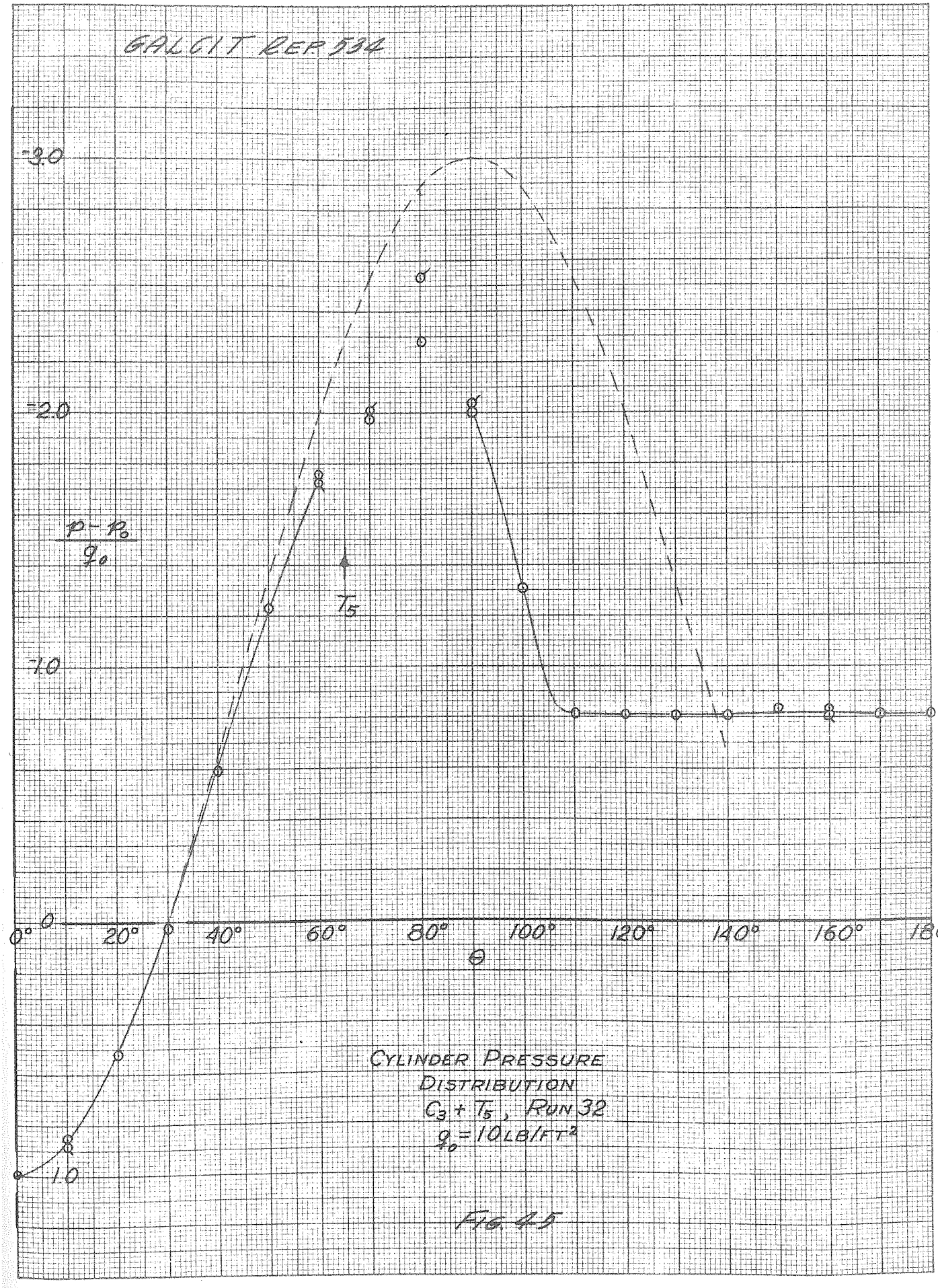

CYLINDER PRESSURE DISTRIBUTION
$C_3 + T_5$, RUN 32
$q_0 = 10$ LB/FT^2

FIG. 45

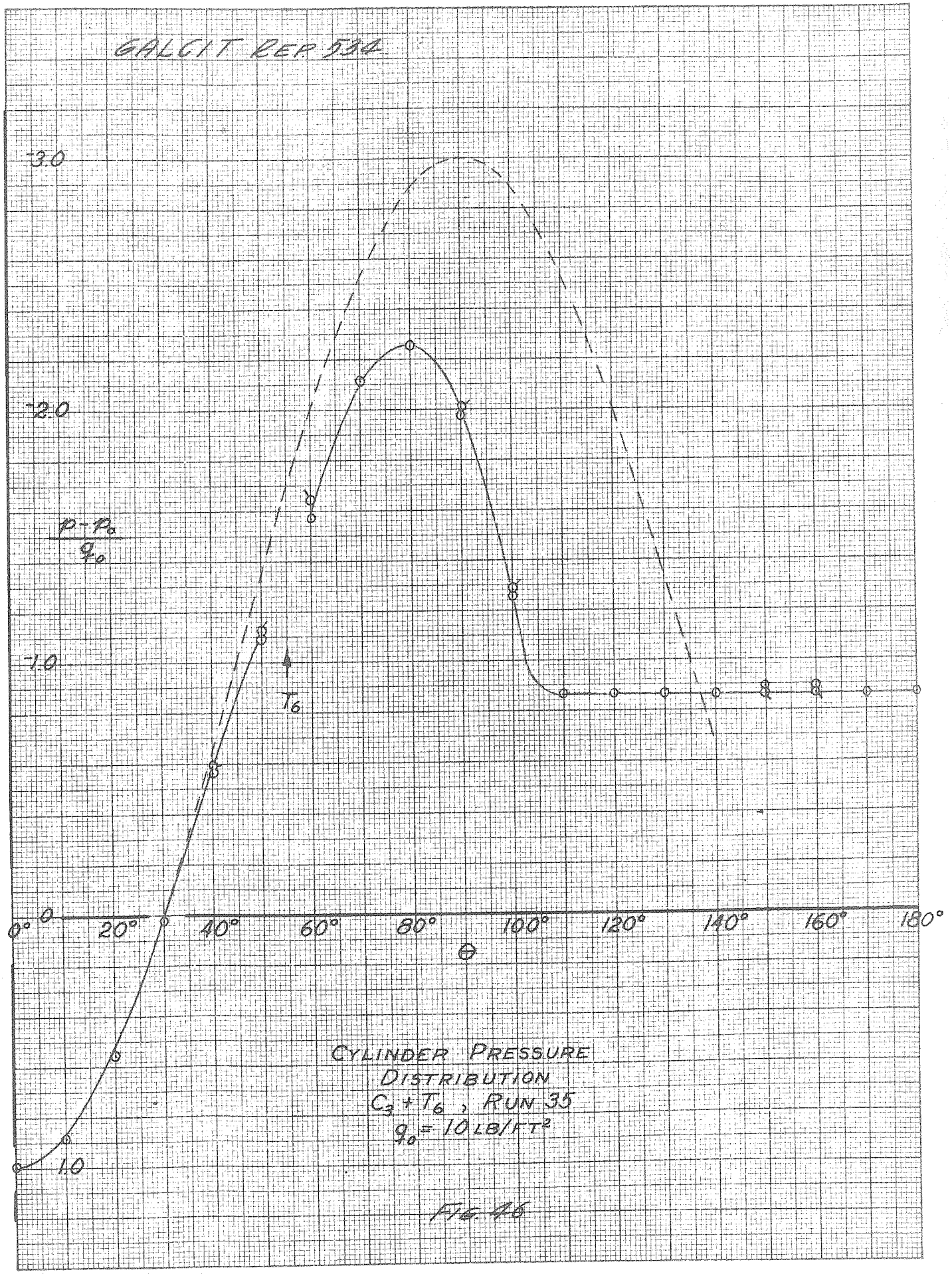

CYLINDER PRESSURE DISTRIBUTION
$C_3 + T_6$, RUN 35
$q_0 = 10$ LB/FT^2

FIG. 26

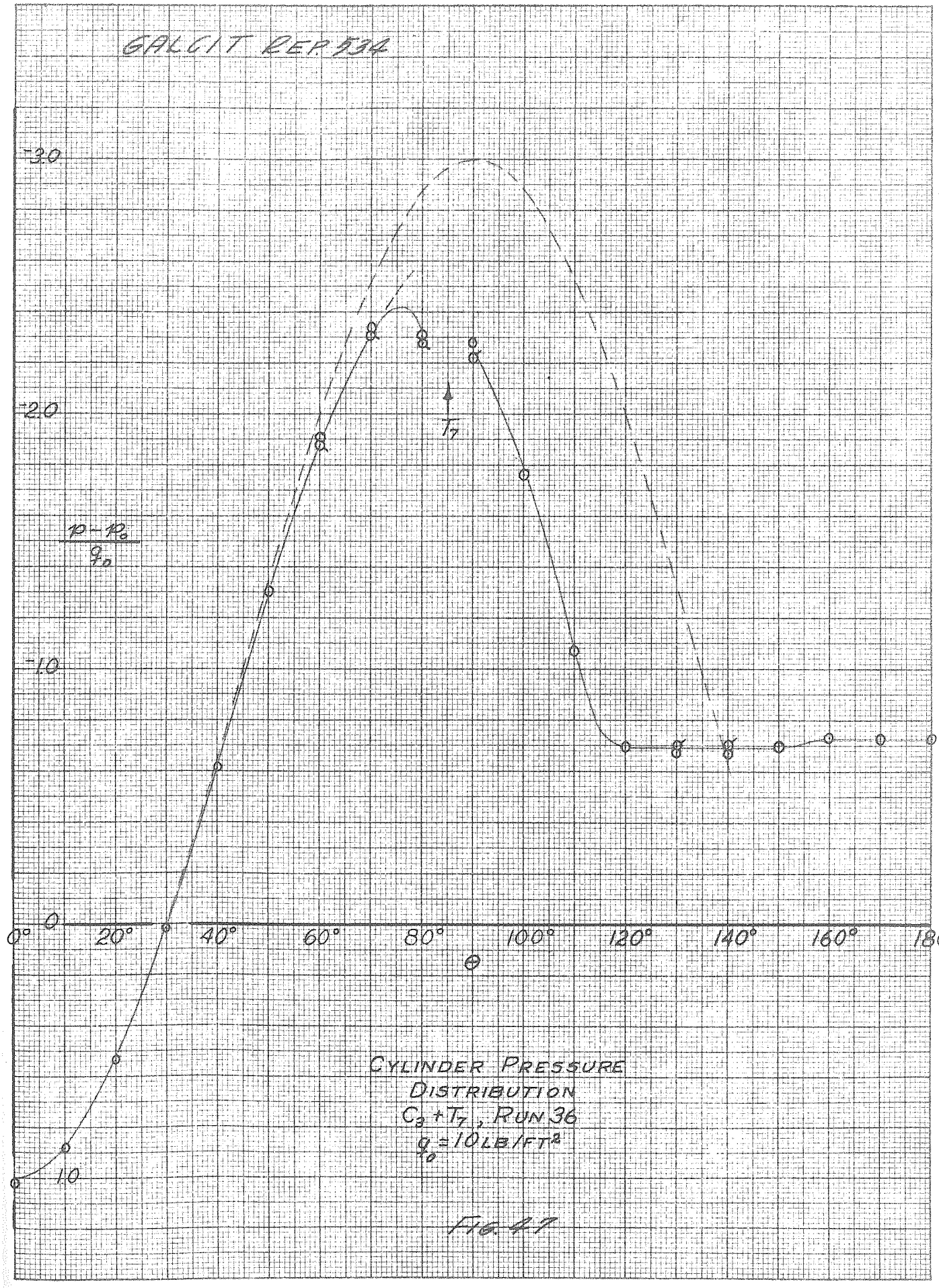

CYLINDER PRESSURE DISTRIBUTION
$C_3 + T_7$, RUN 36
$q_0 = 10$ LB/FT^2

FIG. 47

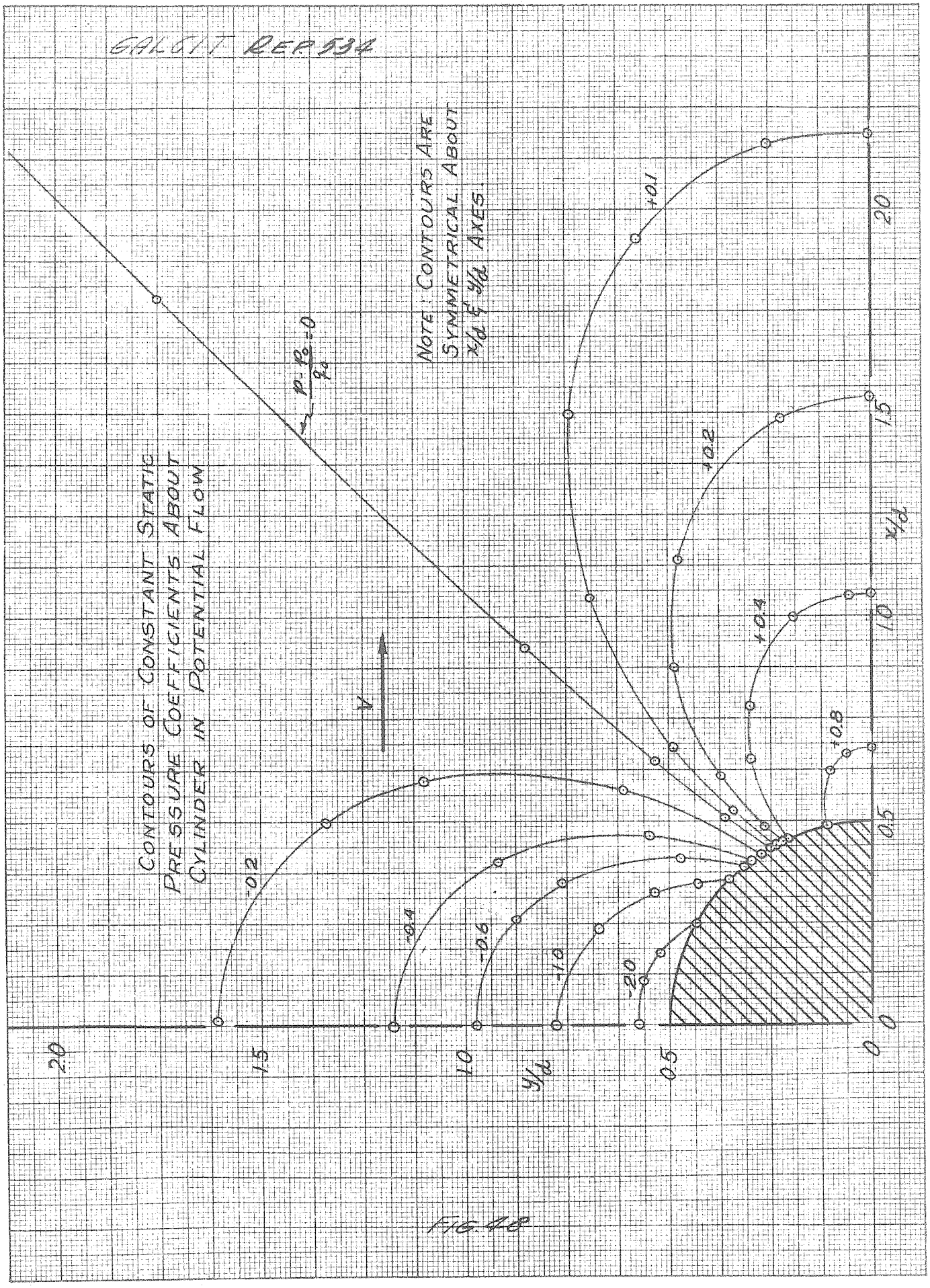
GALCIT REP 534
CONTOURS OF CONSTANT STATIC PRESSURE COEFFICIENTS ABOUT CYLINDER IN POTENTIAL FLOW
NOTE: CONTOURS ARE SYMMETRICAL ABOUT x/d & y/d AXES
p - p∞ / q
V
+.01
+.02
+.04
+.08
-.02
-.04
-.06
-.10
-.20
y/d
x/d
0
0.5
1.0
1.5
2.0

FIG. 48

GALCIT RE A 54

CONTOURS OF CONSTANT STATIC PRESSURE
COEFFICIENTS ABOUT CYLINDER AT NORTH END PLATE

○ { C_1, RUNS 49A,B } $q_o = 80 LB/FT^2$
{ $C_1 + X_1$, RUN 53 }

□ C_2, $q_o = 24 LB/FT^2$, RUN 65

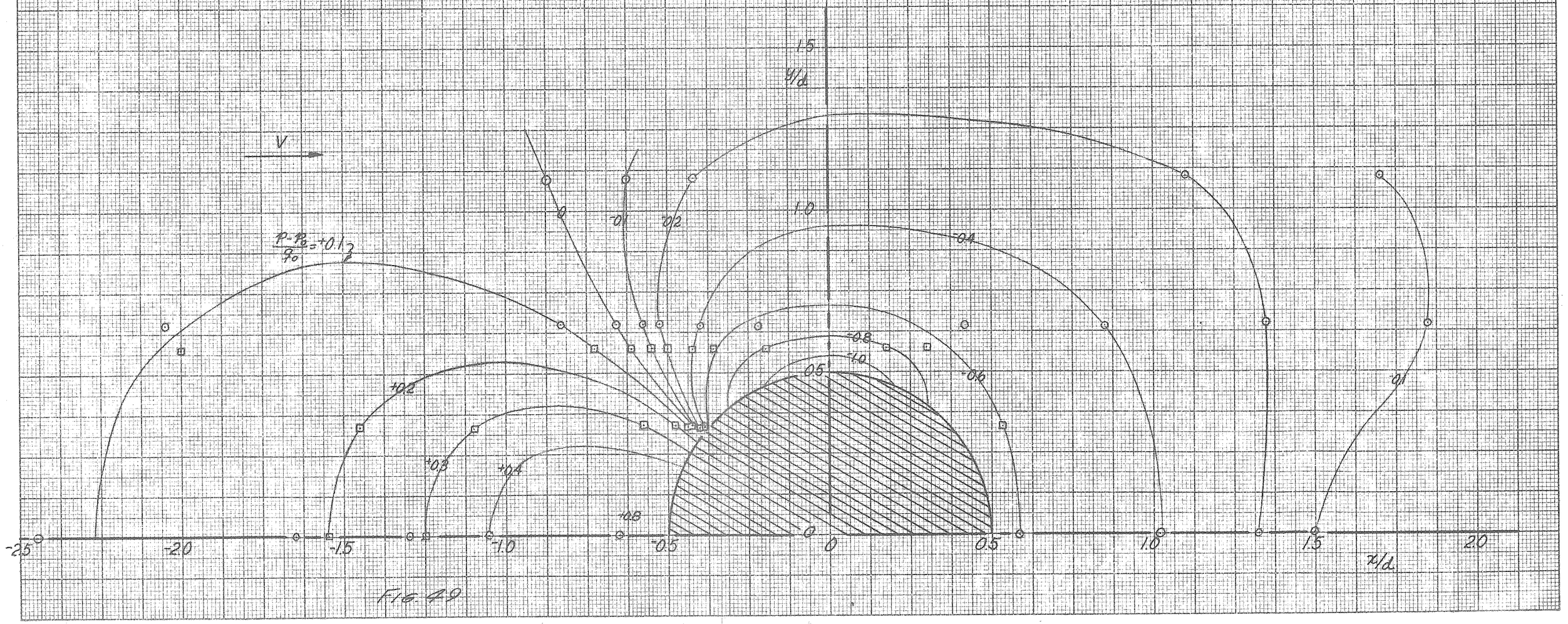

FIG 29

GALCIT REP 934

CONTOURS OF CONSTANT STATIC PRESSURE COEFFICIENTS ABOUT CYLINDER AT NORTH ENDPLATE
$C_1 + T_{10}$, RUN 52
$q_0 = 80 LB/FT^2$

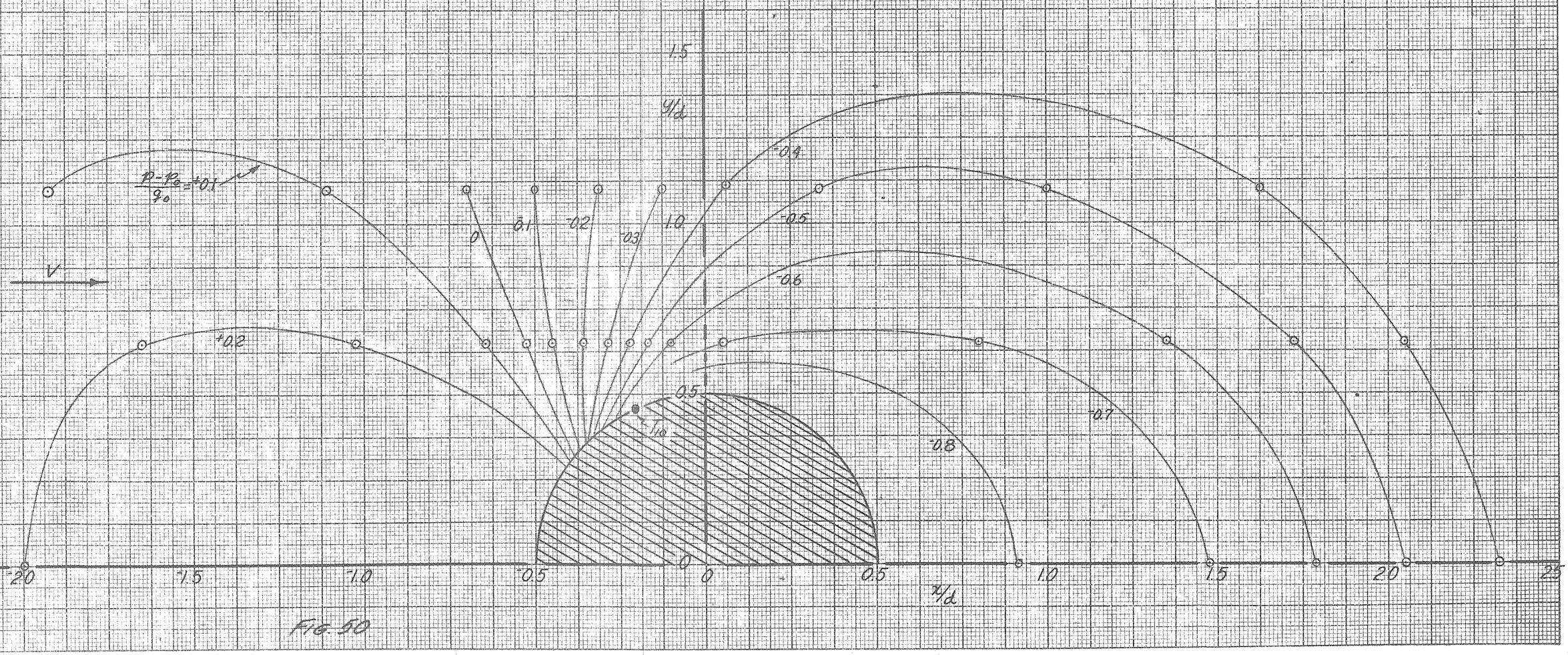

FIG 50

GALCIT REP 534

FIG.

$\frac{q}{P_0} = 80 \text{ LB/FT}^2$

- ○ C_1', RUN 74
- △ C_1, RUNS 6, 13, 56, 57
- □ $C_1 + T_3$, " 18, 19, 63
- ◇ $C_1 + T_4$, " 24, 61

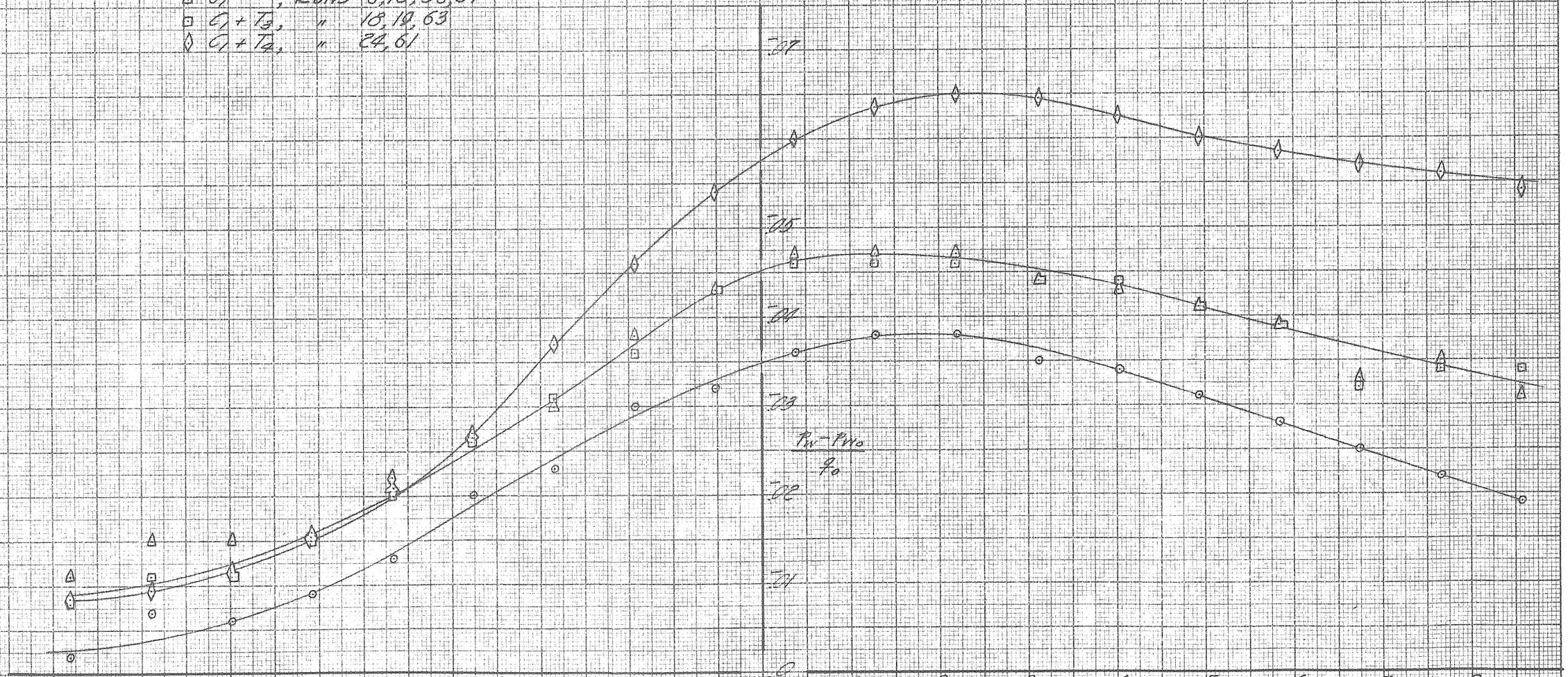

STATIC PRESSURE DISTRIBUTION ON TUNNEL FLOOR AND CEILING, CYLINDER C, WITH AND WITHOUT SEPARATION STRIPS

FIG. 51

GALCIT REP 534

PAGE
FIG

$q_o = 24$ LB/FT^2

○ C_2 , RUNS 66, 68
△ $C_2 + T_H$, RUN 69
□ $C_2 + T_E$, RUNS 71, 72

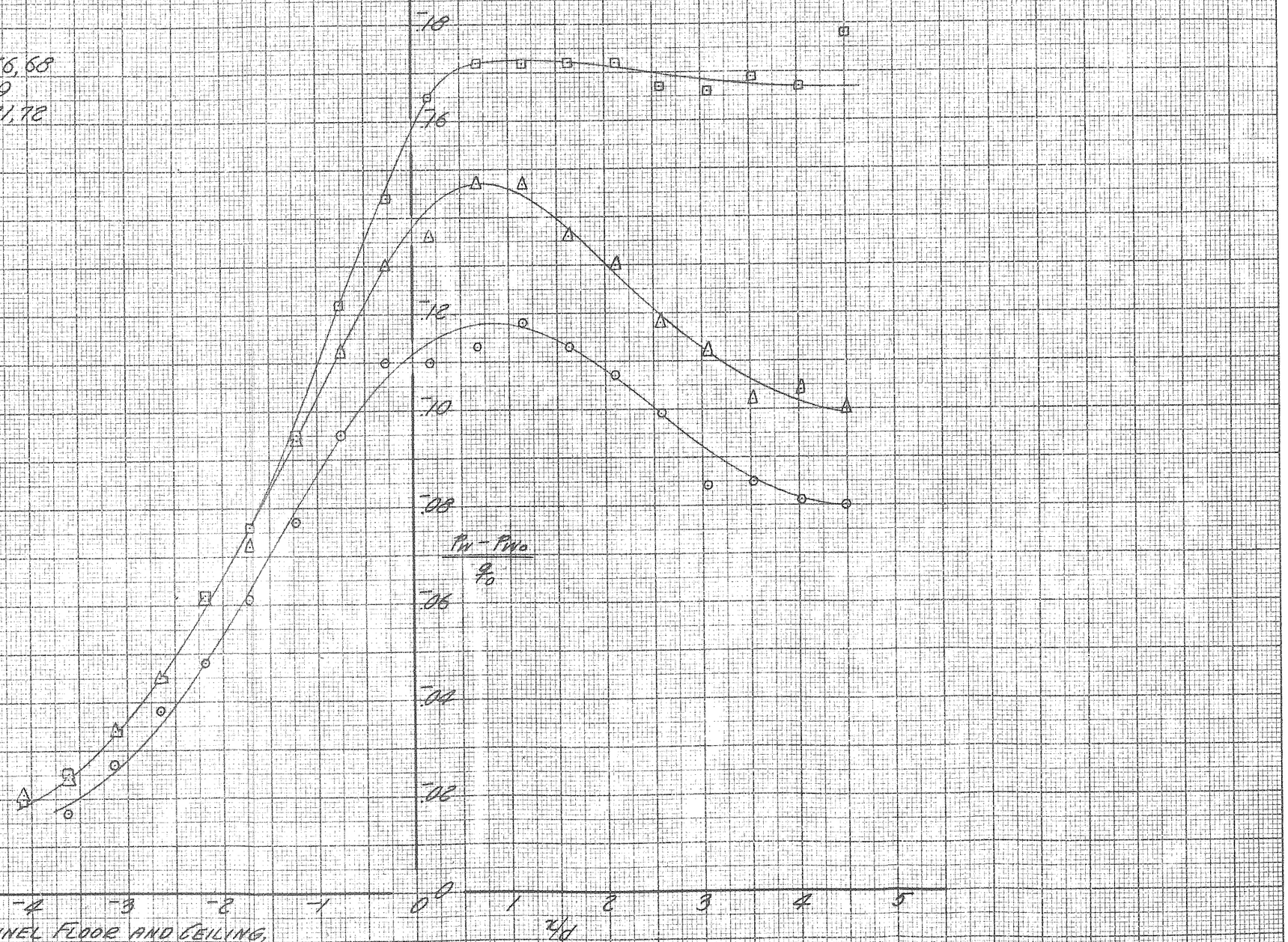

STATIC PRESSURE DISTRIBUTION ON TUNNEL FLOOR AND CEILING, CYLINDER C_2 WITH AND WITHOUT SEPARATION STRIPS
FIG. 52

GALCIT REF 534

PAGE
FIG

$q_0 = 10 LB/FT^2$

○ C_3 , RUNS 29, 31, 73

△ $C_3 + T_6$, " 32, 34

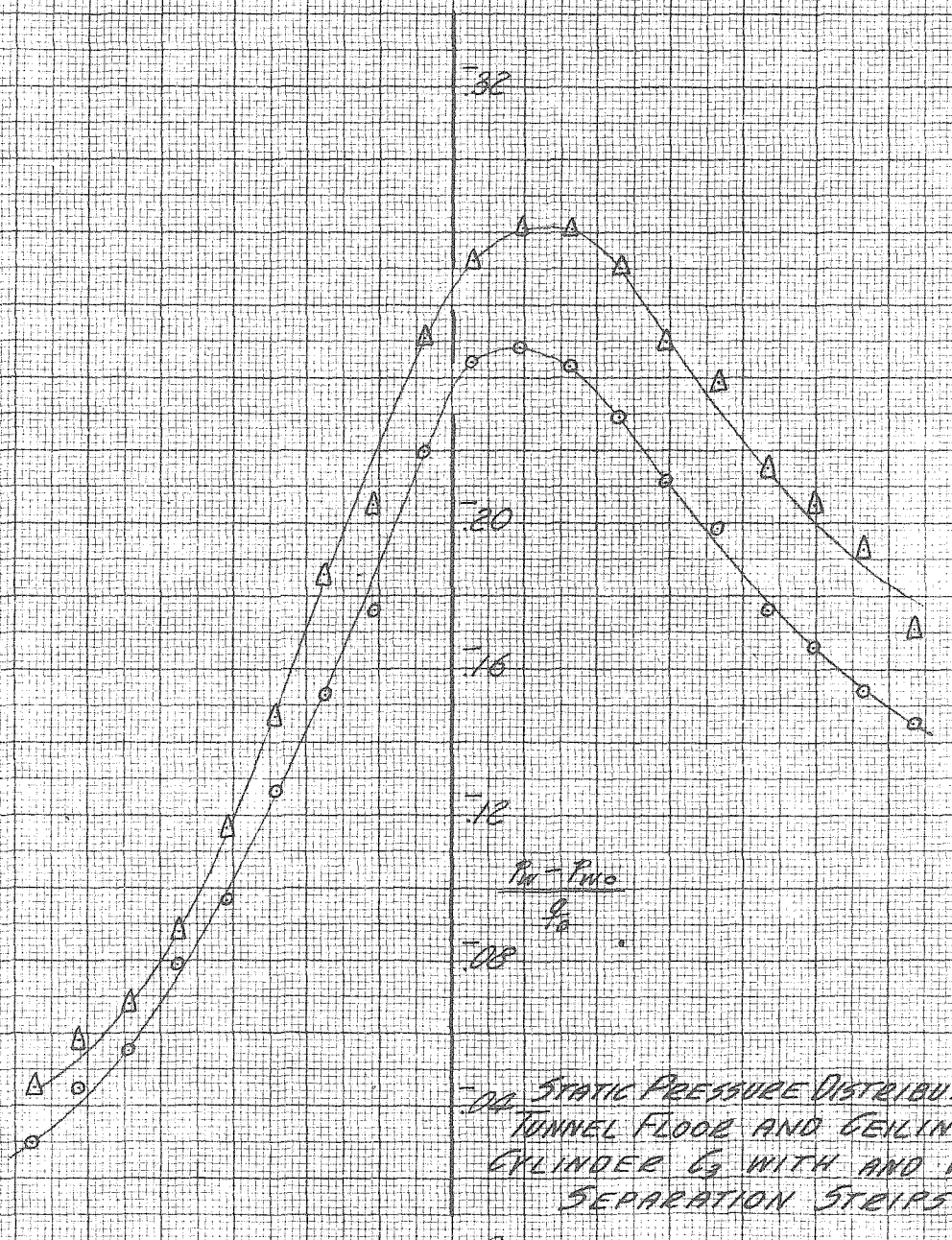

STATIC PRESSURE DISTRIBUTION ON TUNNEL FLOOR AND CEILING, CYLINDER C_3 WITH AND WITHOUT SEPARATION STRIPS

FIG 33

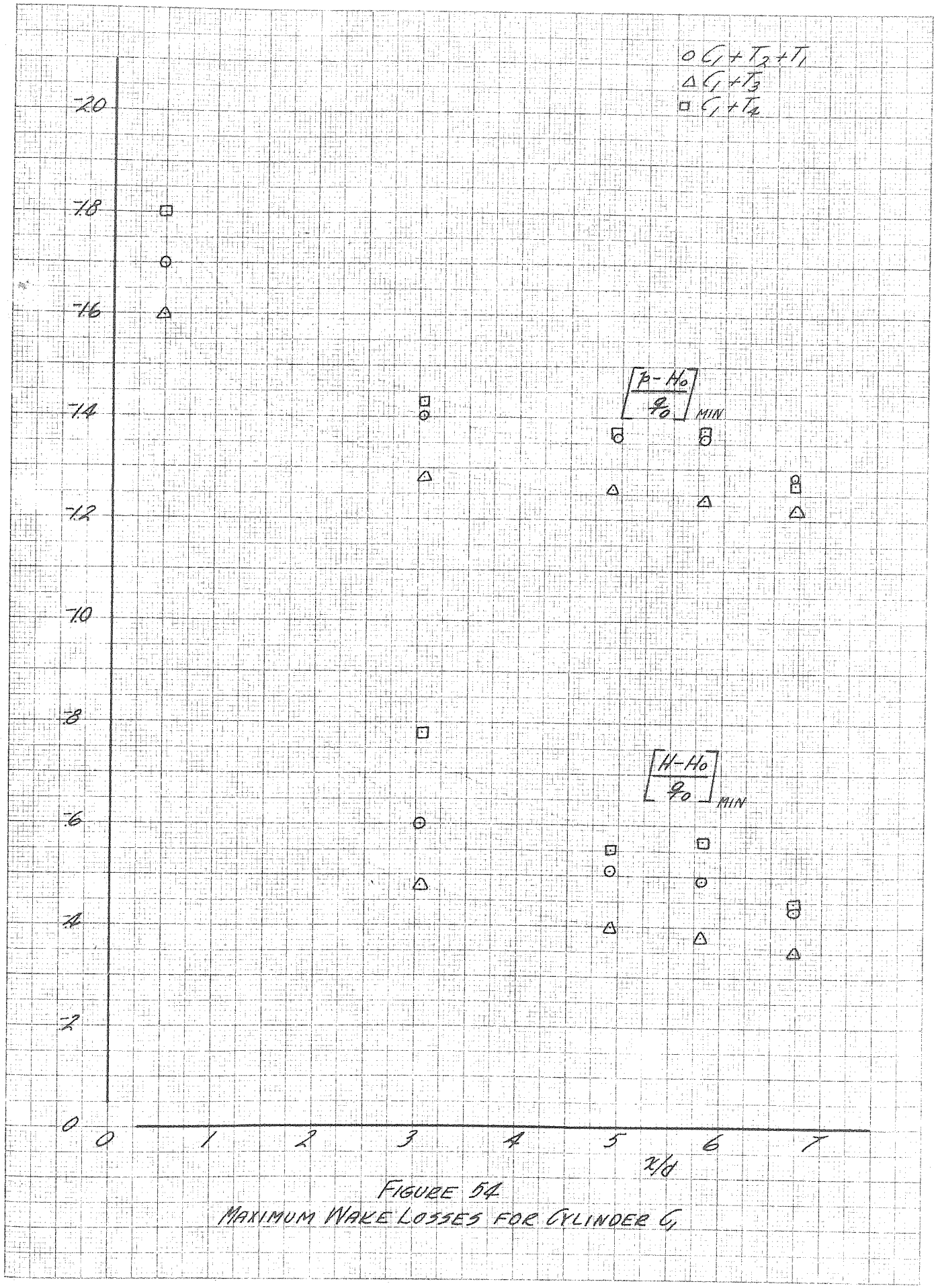

FIGURE 54
MAXIMUM WAKE LOSSES FOR CYLINDER G

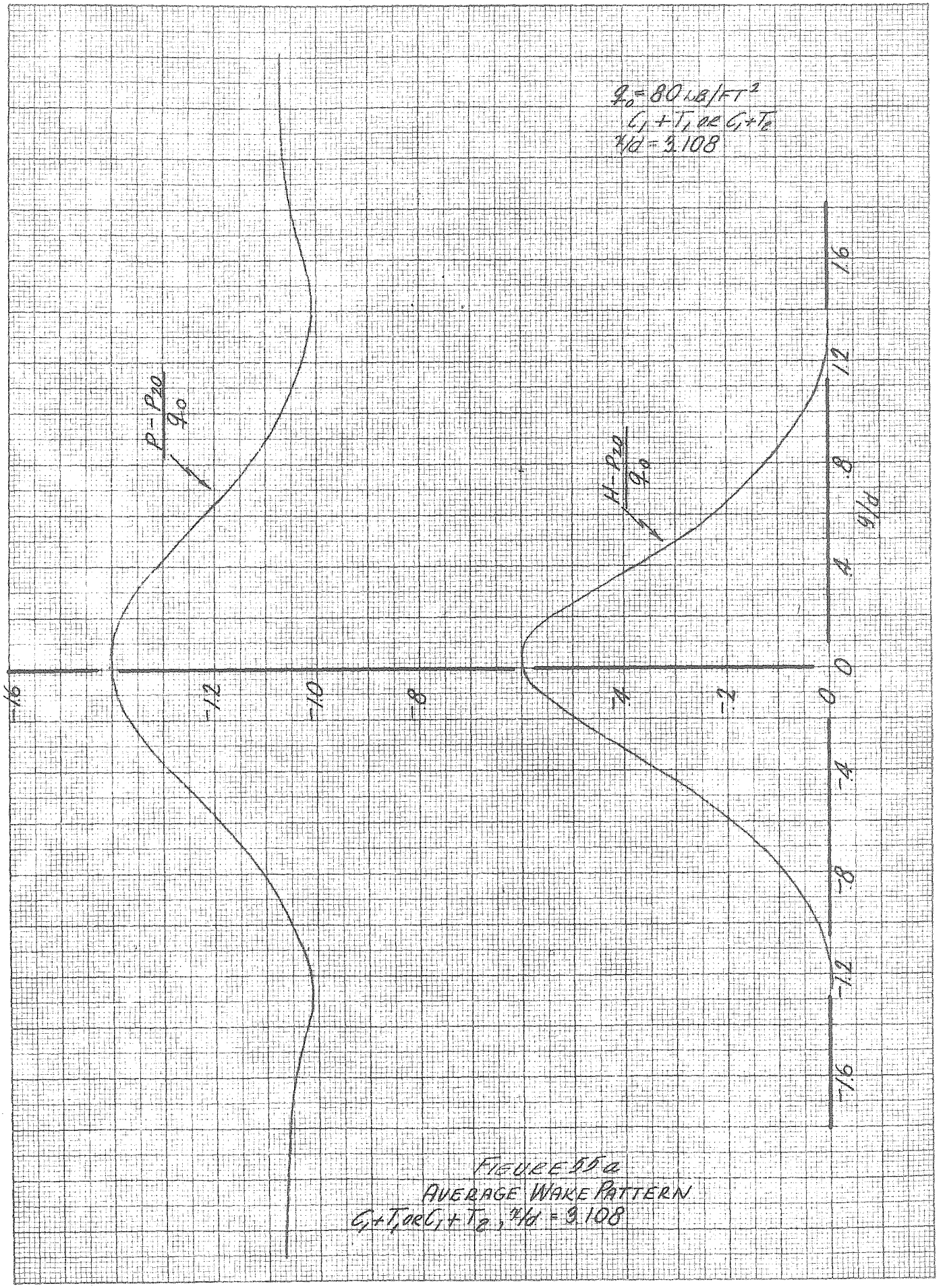

FIGURE 55a
AVERAGE WAKE PATTERN
$C_1 + T_1$ OR $C_1 + T_2$, $Y/d = 3.108$

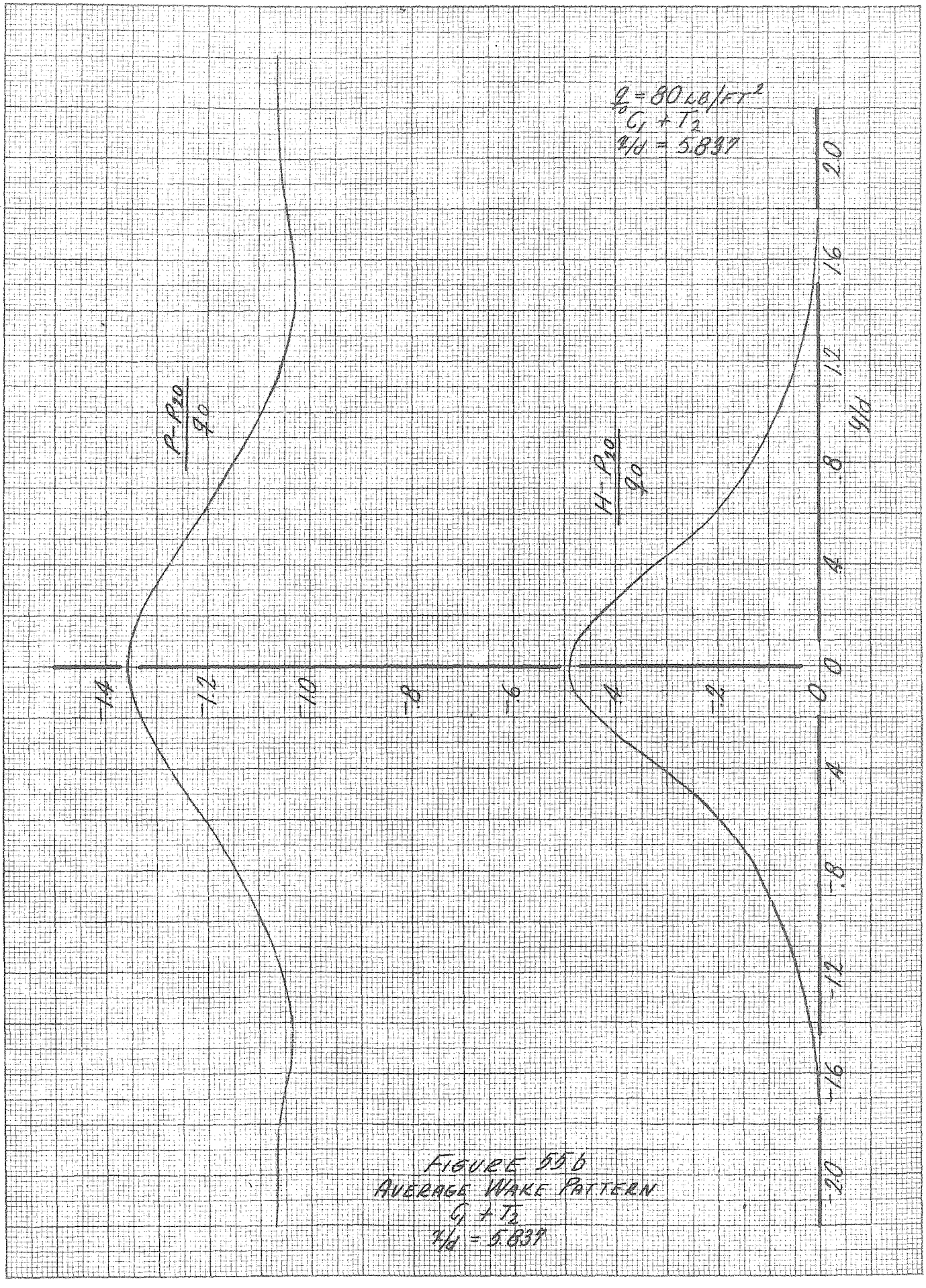

FIGURE 55b
AVERAGE WAKE PATTERN
$C_1 + T_2$
$x/d = 5.833$

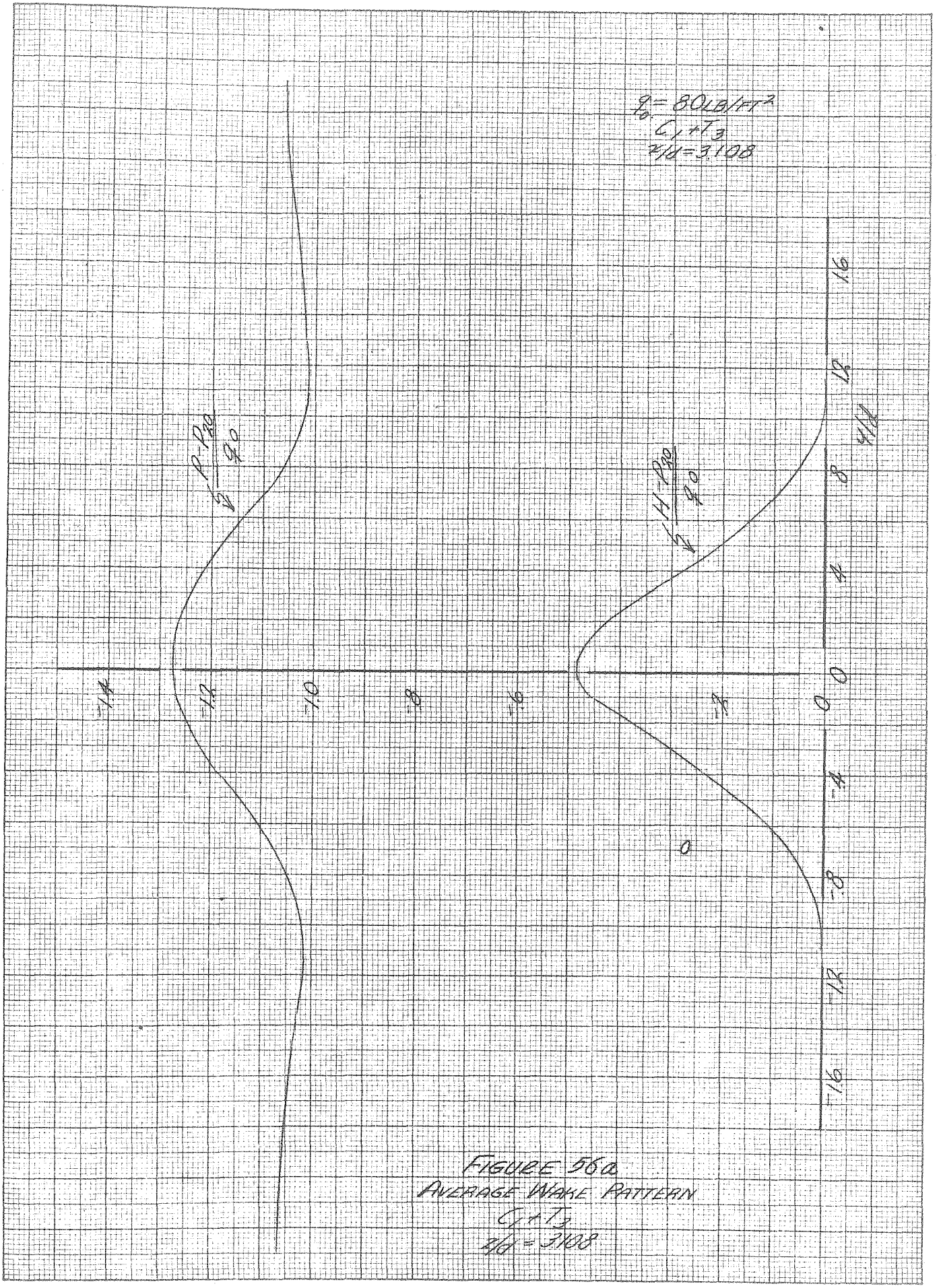

FIGURE 56a
AVERAGE WAKE PATTERN
$C_L + T_3$
$z/d = 3.108$

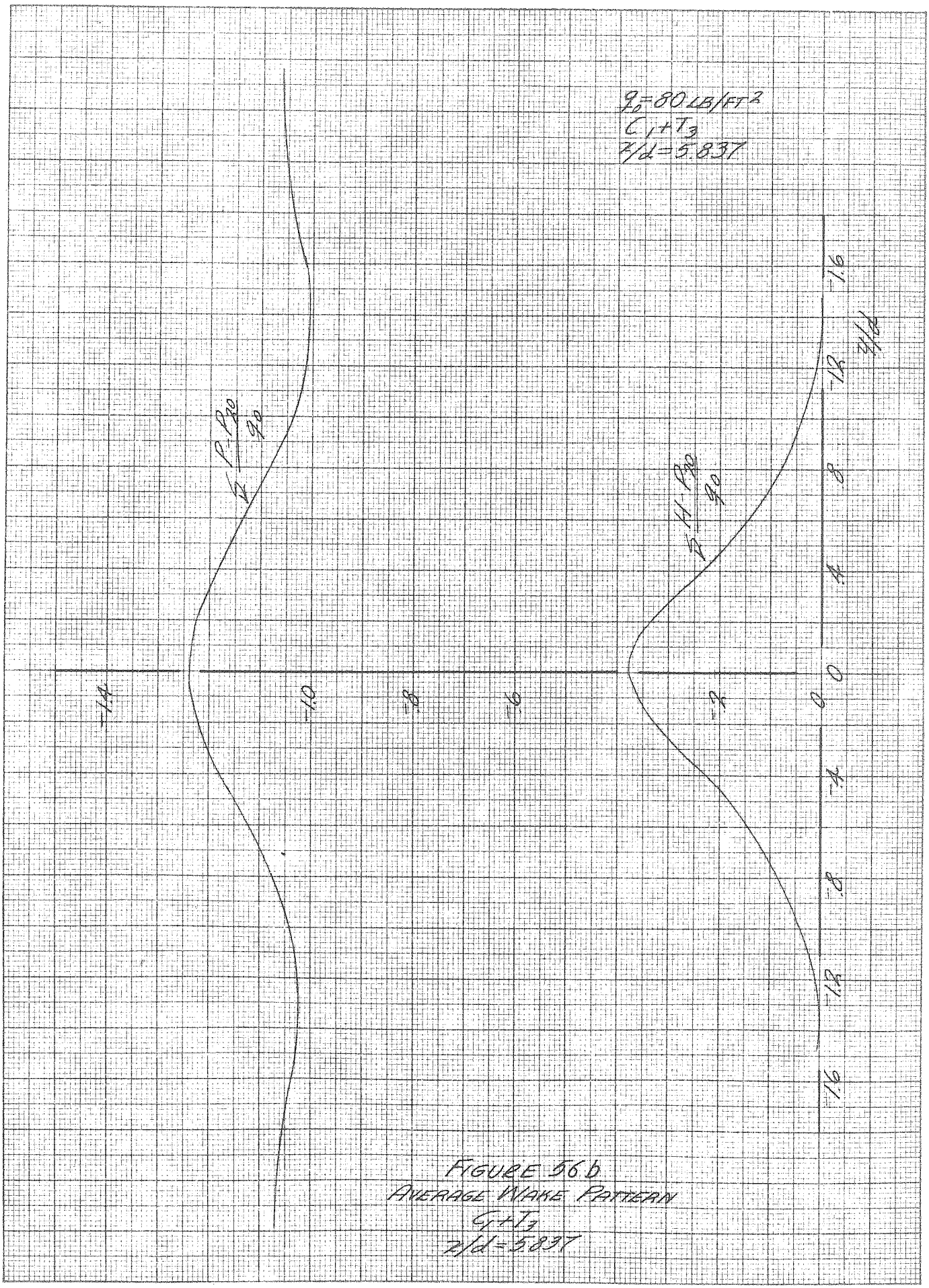

FIGURE 56 b
AVERAGE WAKE PATTERN
C_1+T_3
z/d=5.837

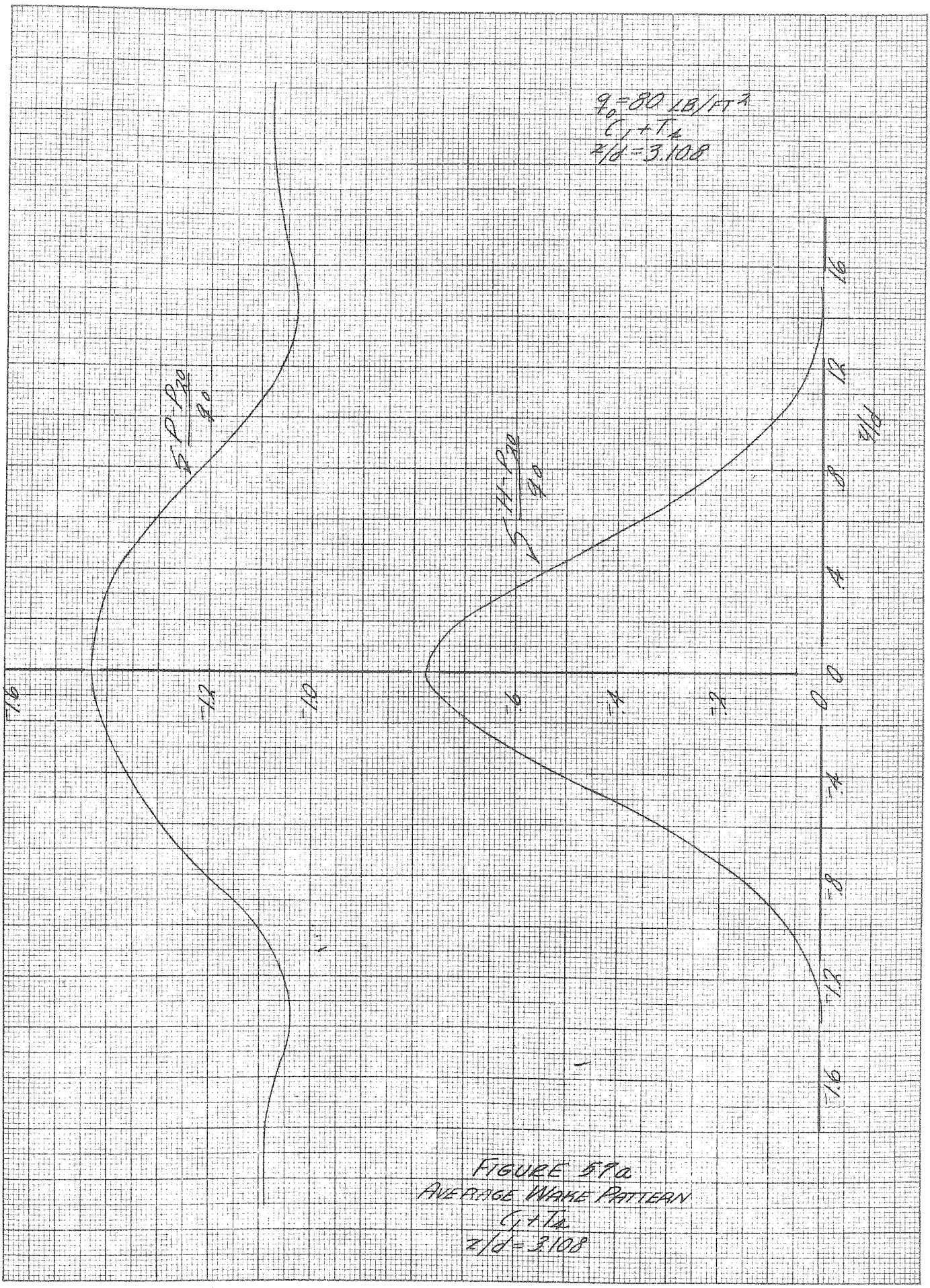

FIGURE 57a
AVERAGE WAKE PATTERN
$C_f + T_R$
$z/d = 3.108$

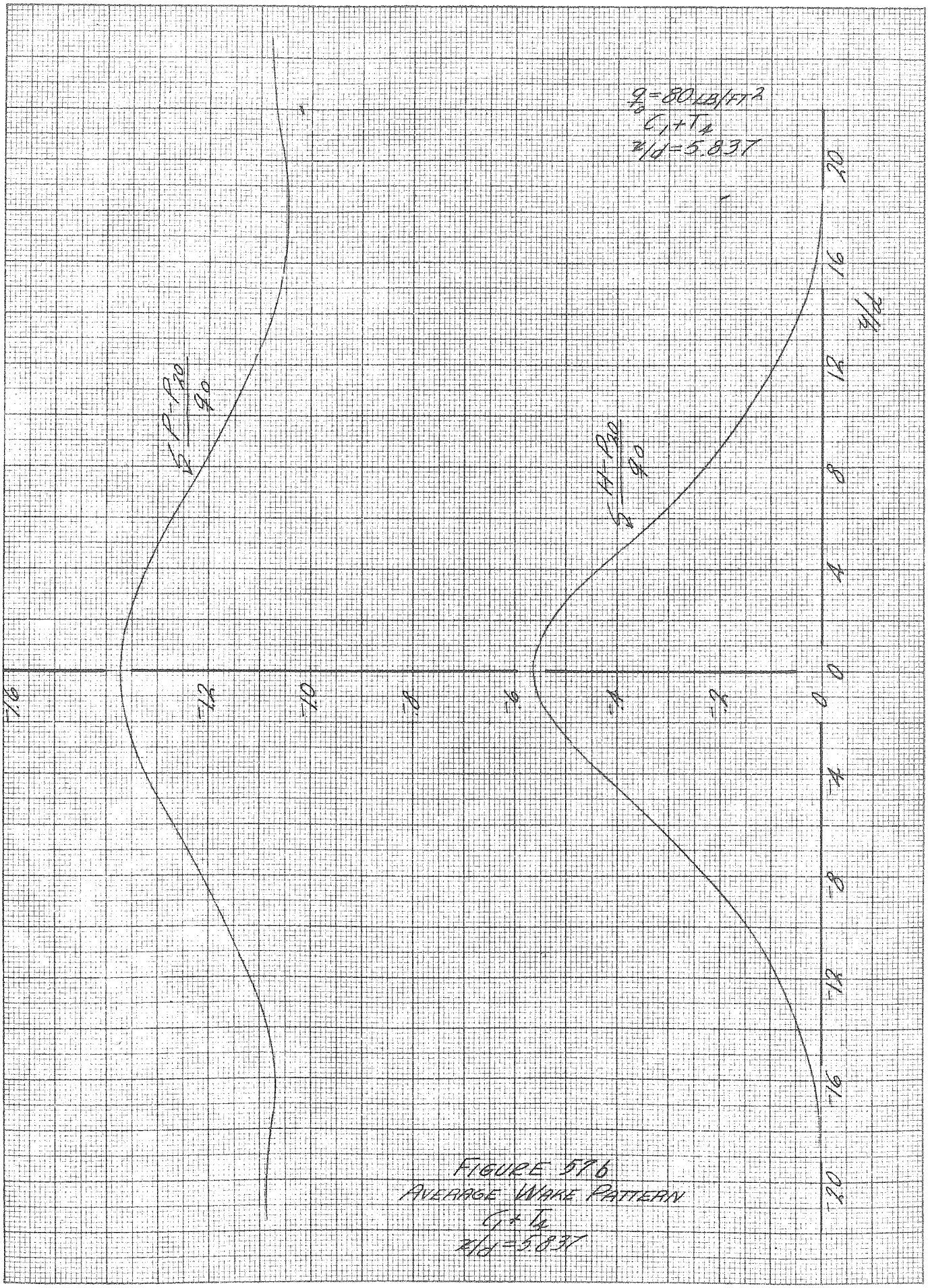

FIGURE 57b
AVERAGE WAKE PATTERN
$C + T_4$
$z/d = 5.83T$

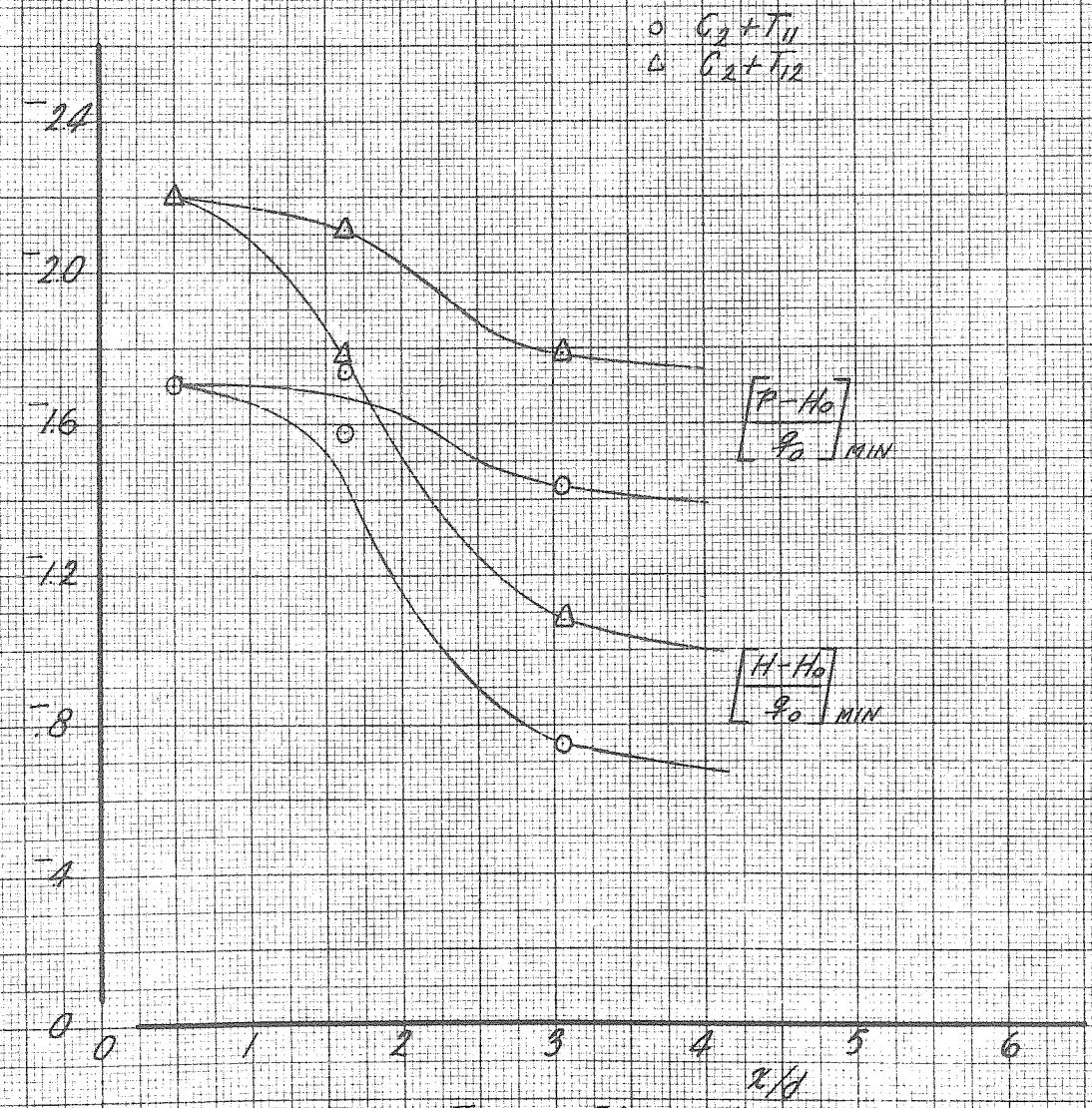

FIGURE 58
MAXIMUM WAKE LOSSES FOR CYLINDER C_2

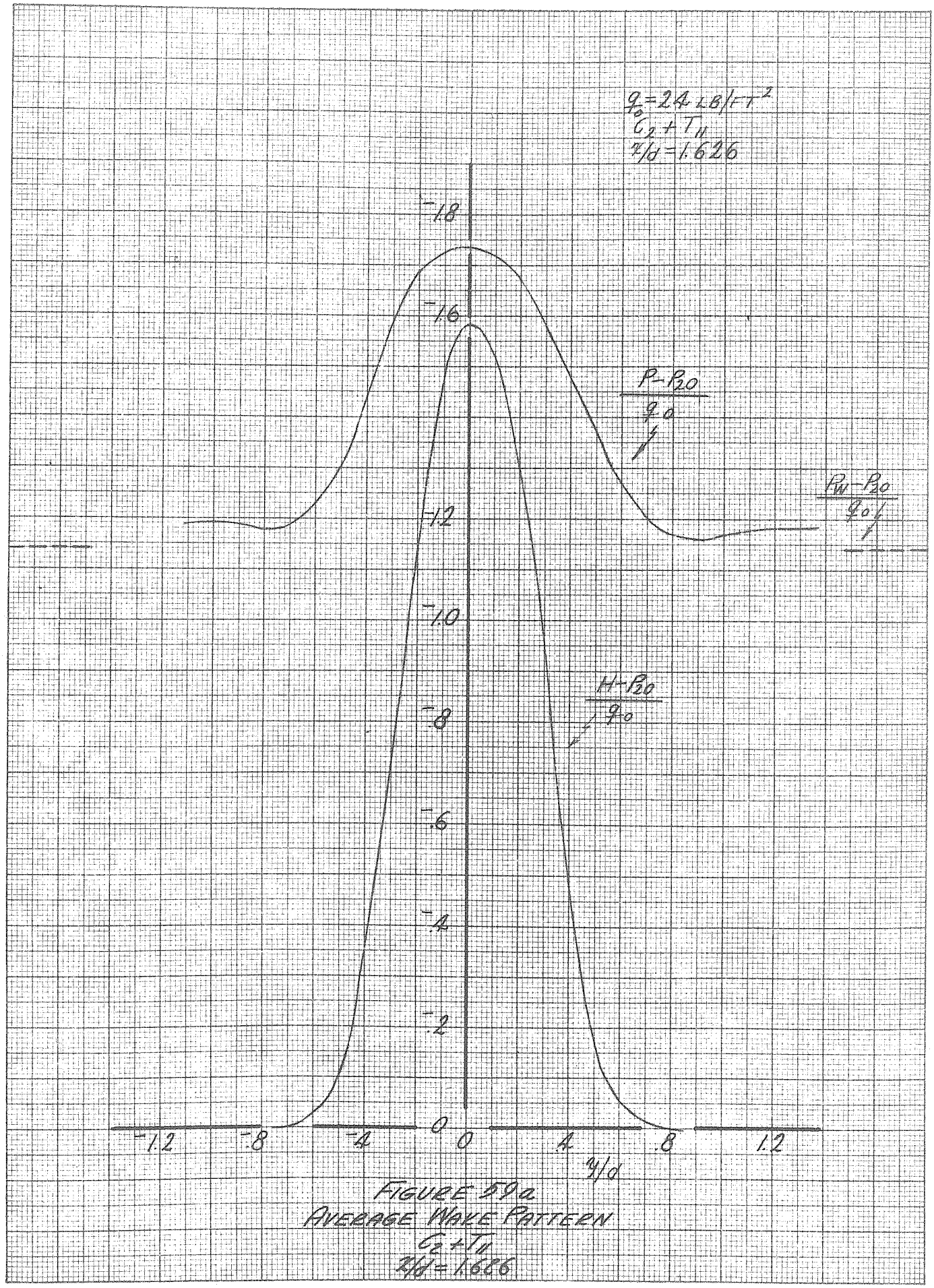

FIGURE 59a
AVERAGE WAKE PATTERN
$\frac{C_2+T_{11}}{y/D = 1.626}$

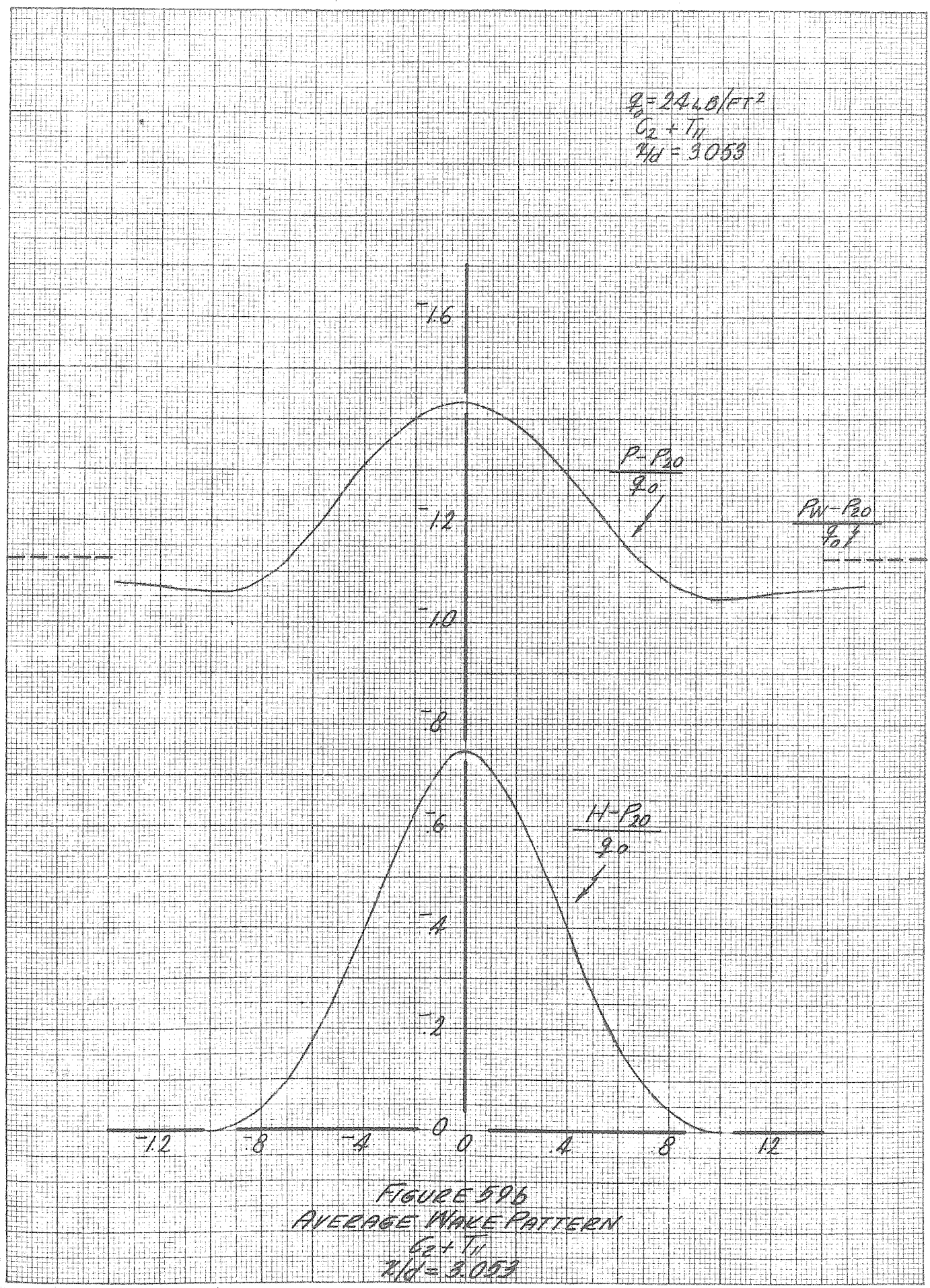

FIGURE 59b
AVERAGE WAKE PATTERN
$C_2 + T_{11}$
$x/d = 3.053$

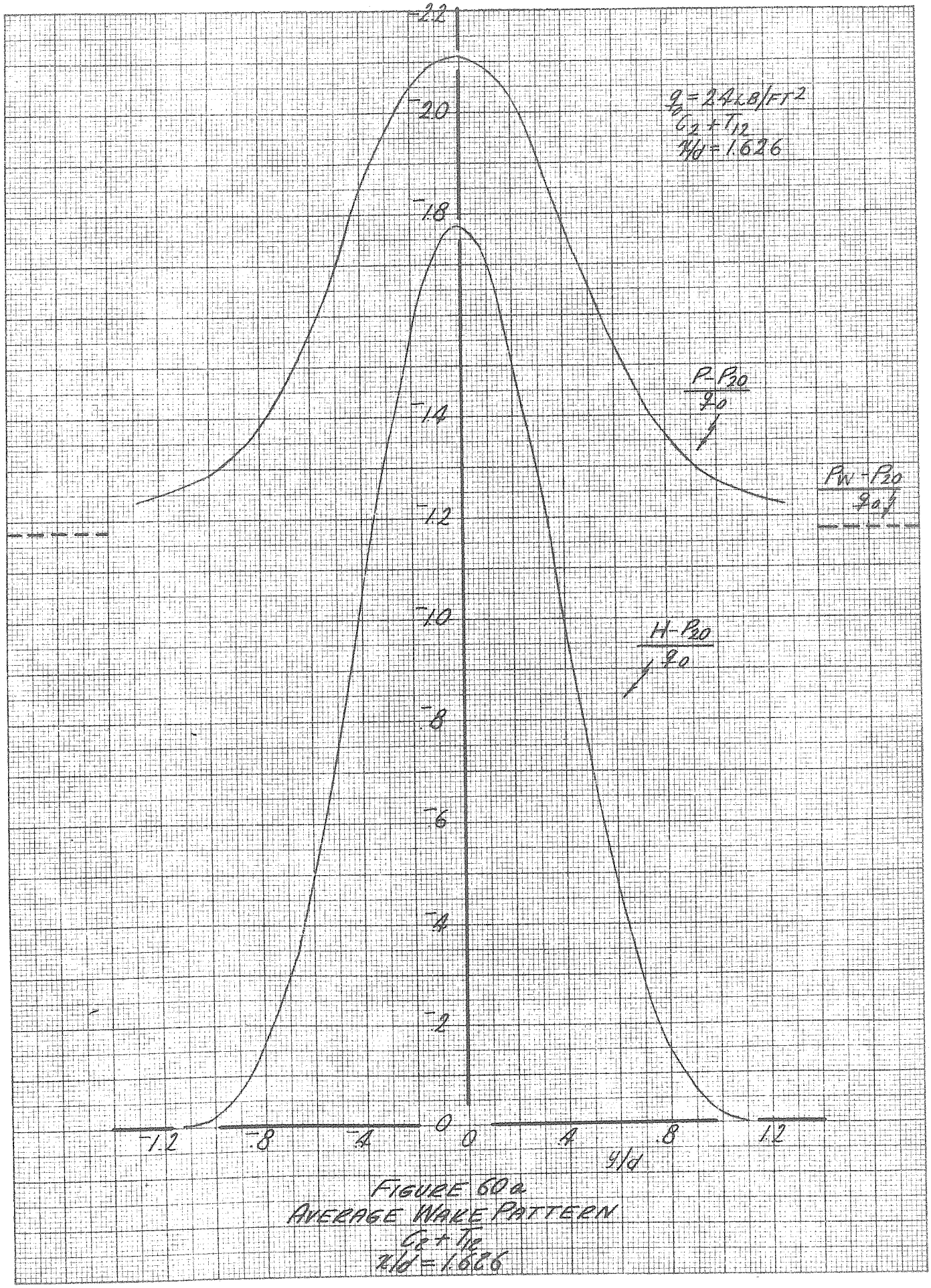

FIGURE 60a
AVERAGE WAKE PATTERN
$C_L + T_E$
π/d = 1.626

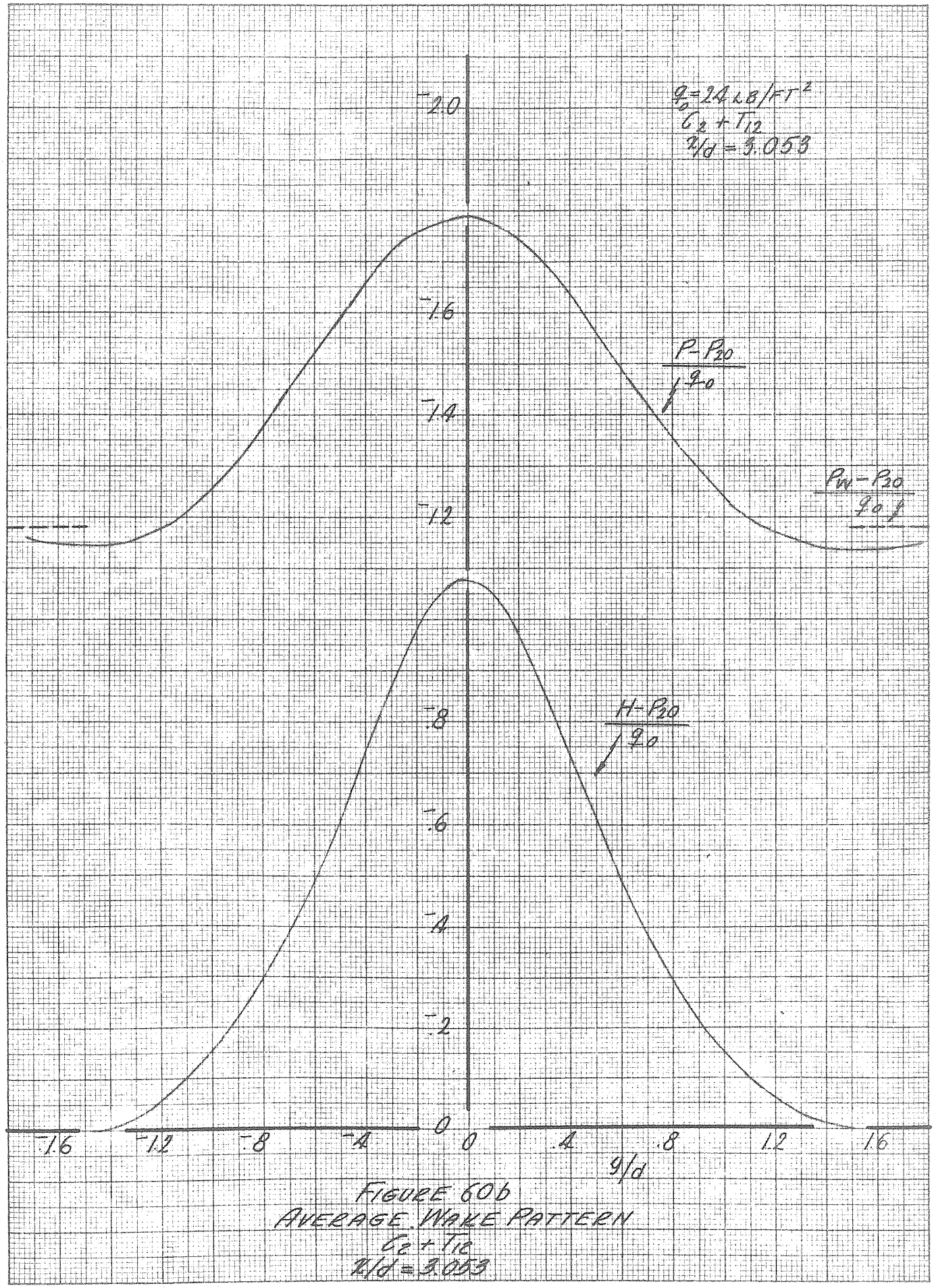

FIGURE 60b
AVERAGE WAKE PATTERN
$C_2 + T_{12}$
$x/d = 3.053$

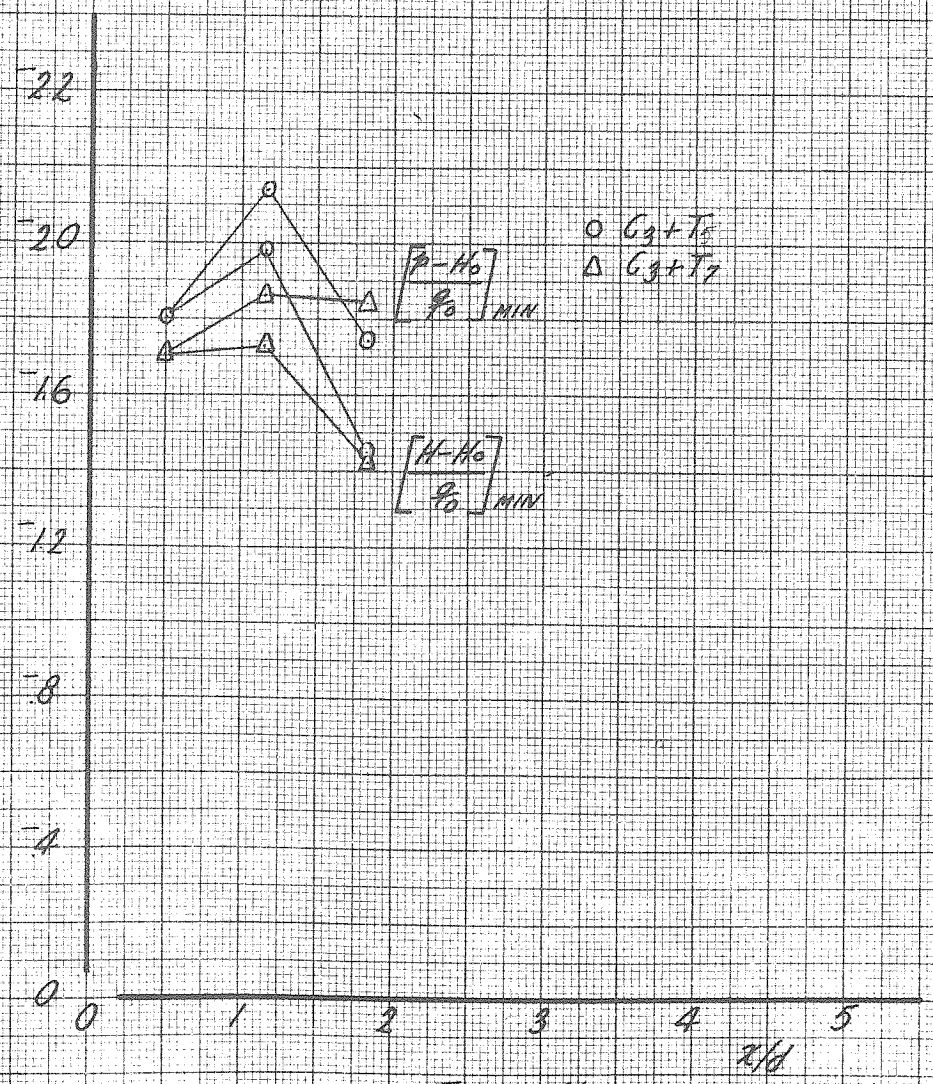

FIGURE 61
MAXIMUM WAKE LOSSES FOR CYLINDER G_3

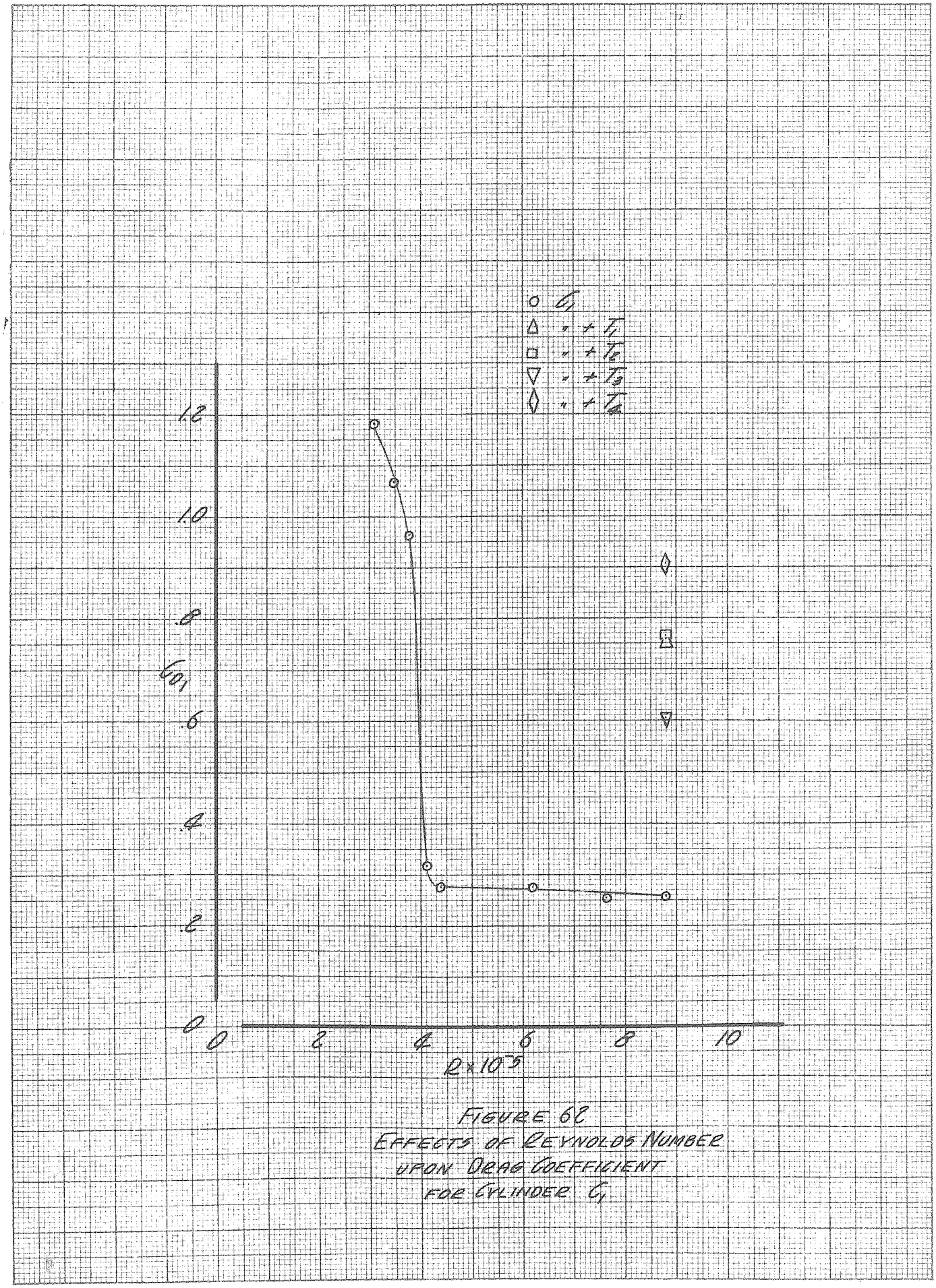

FIGURE 62
EFFECTS OF REYNOLDS NUMBER
UPON DRAG COEFFICIENT
FOR CYLINDER C_1

Cylinder	θ^{o} Separation Wire	C_{D_1}	C_{D_w}	at x/d
$C_1 + T_1$	65	.759		
$C_1 + T_2$	65	.764	.635 .607	3.108 5.837
$C_1 + T_3$	85	.603	.433 .419	3.108 5.837
$C_1 + T_4$	65 and 85	.907	.904 .848	3.108 5.837
$C_2 + T_{21}$	65	.714	.911 .642	1.626 3.053
$C_2 + T_{22}$	65 and 85	1.243	1.690 1.377	1.626 3.053
$C_3 + T_5$	65	.747		
$C_3 + T_6$	55	.805		
$C_3 + T_7$	85	.632		

C_{D_1} = pressure drag coefficient (equation (1))

C_{D_w} = wake drag coefficient (equation (1a))

Figure 63

TABLE OF PRESSURE AND WAKE DRAG COEFFICIENTS FOR TWO-DIMENSIONAL WAKE CONFIGURATIONS

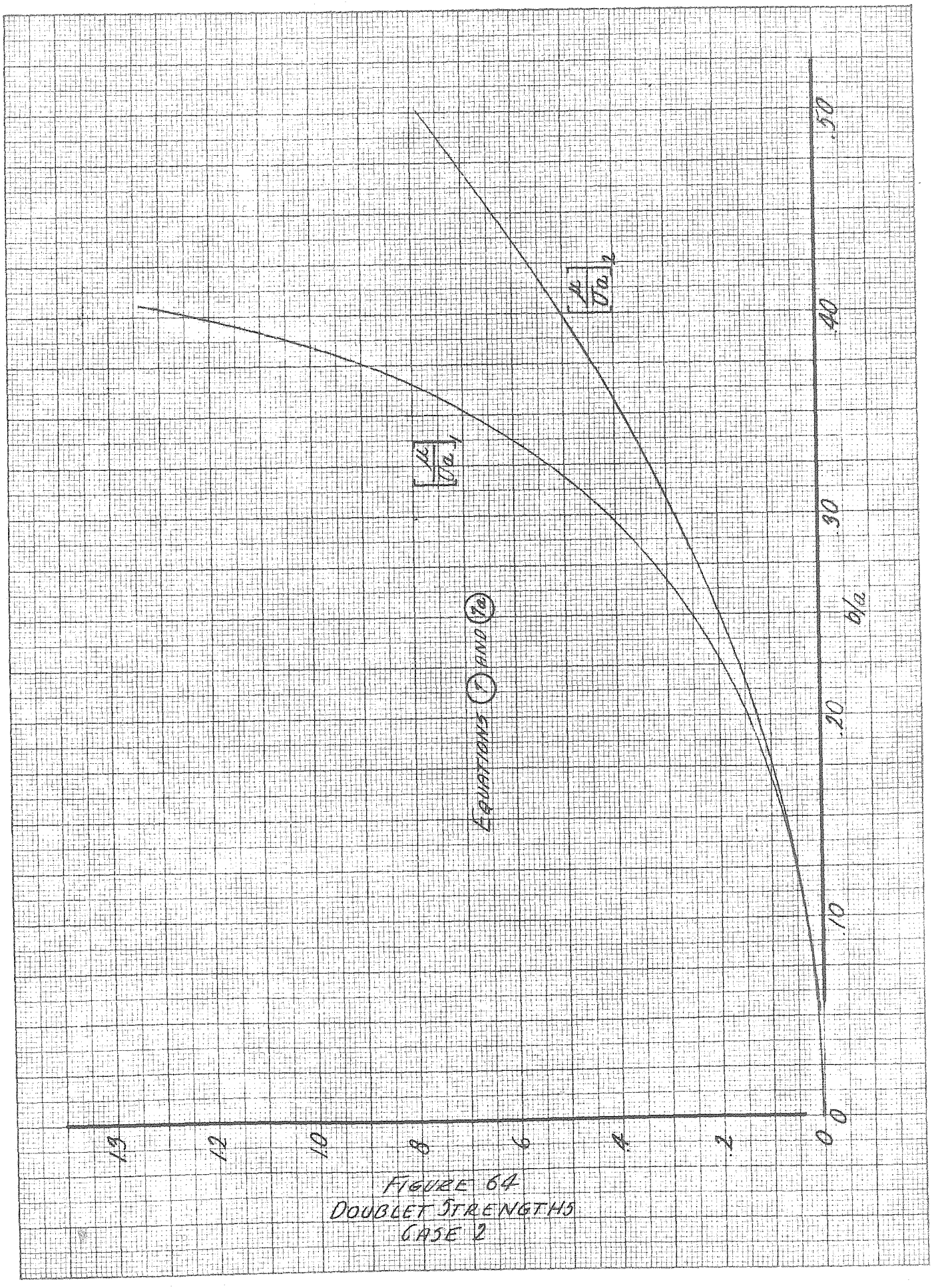

FIGURE 64
DOUBLET STRENGTHS
CASE 2

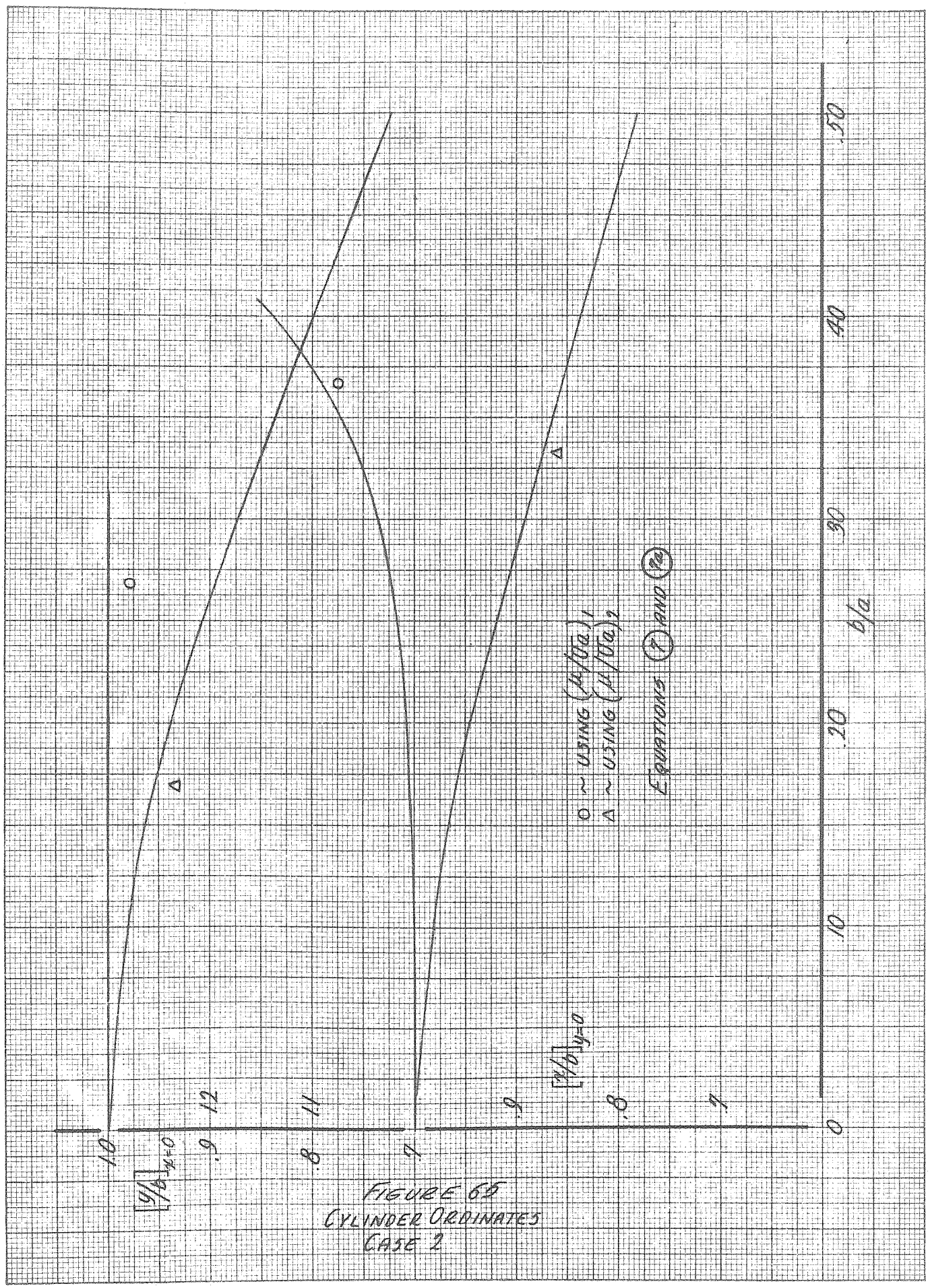

FIGURE 65
CYLINDER ORDINATES
CASE 2

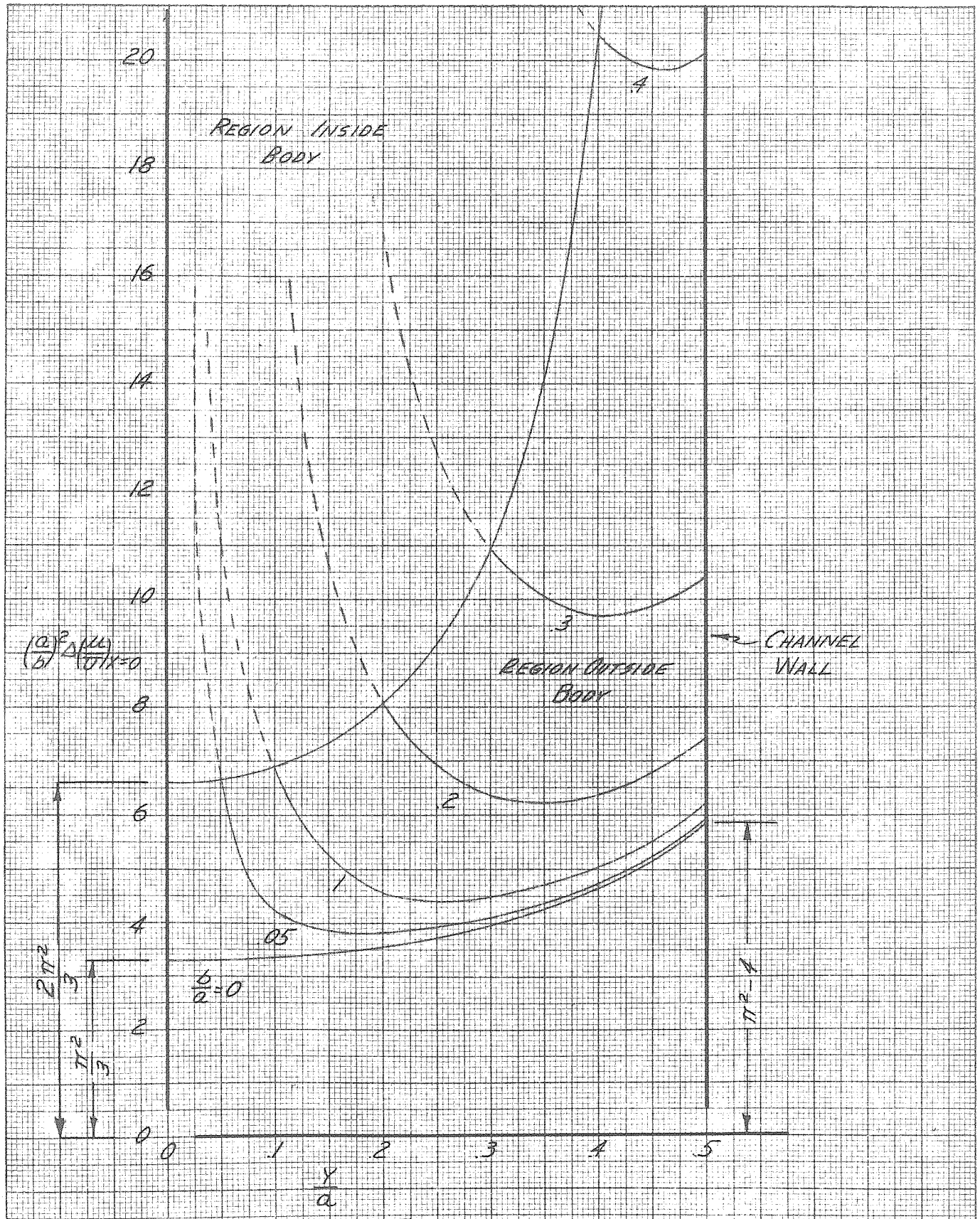

FIGURE 66
BLOCKAGE FACTOR AT X=0 WITHOUT WAKE
EQUATION (9)

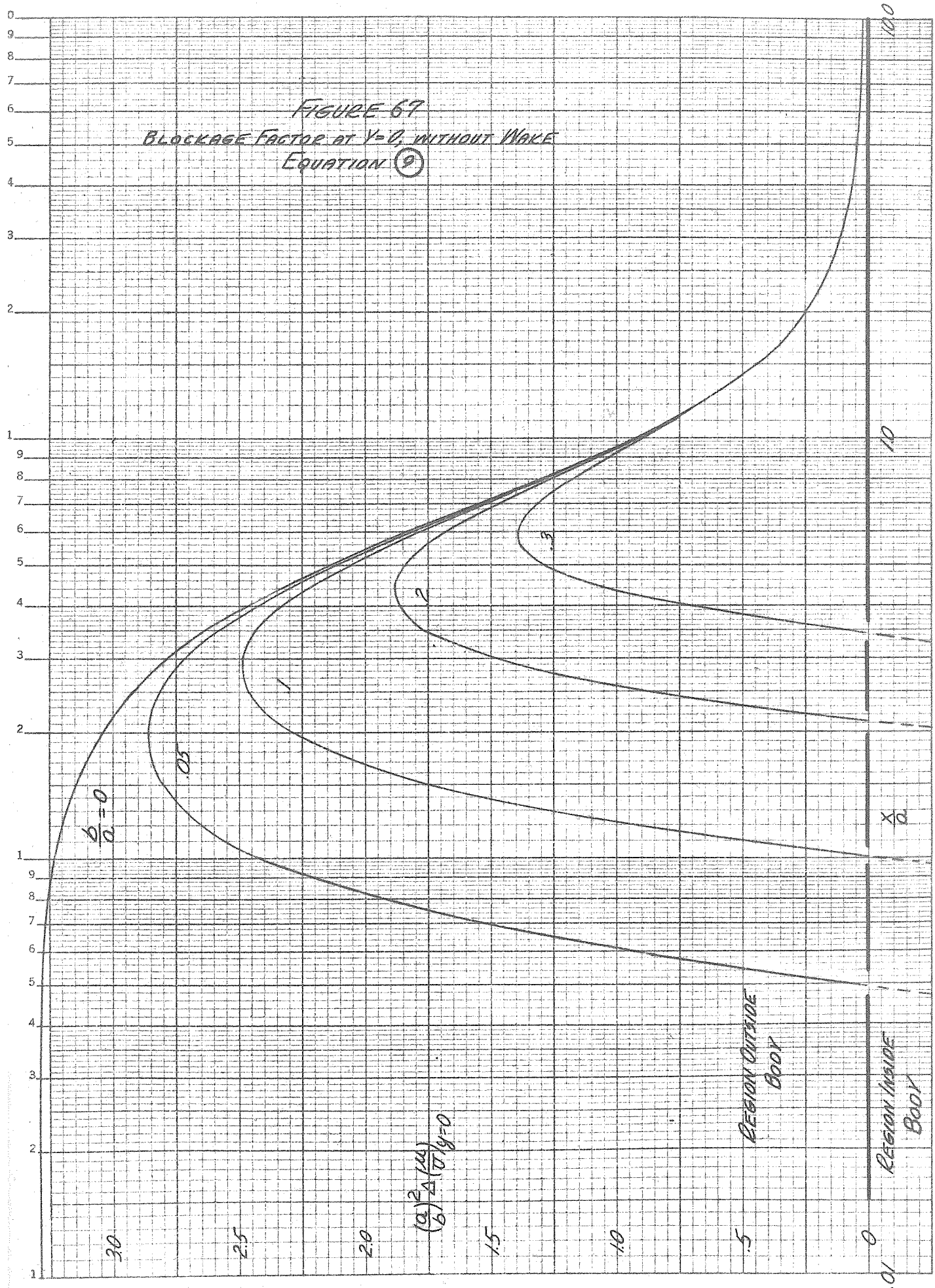
FIGURE 67
BLOCKAGE FACTOR AT Y=0, WITHOUT WAKE
EQUATION (9)
b/a = 0
.5
1
2
5
∞
x/a
REGION OUTSIDE BODY
REGION INSIDE BODY
(a/b)² Δ(u/U)y=0
3.0
2.5
2.0
1.5
1.0
.5
0
.01
.10
1.0
10.0

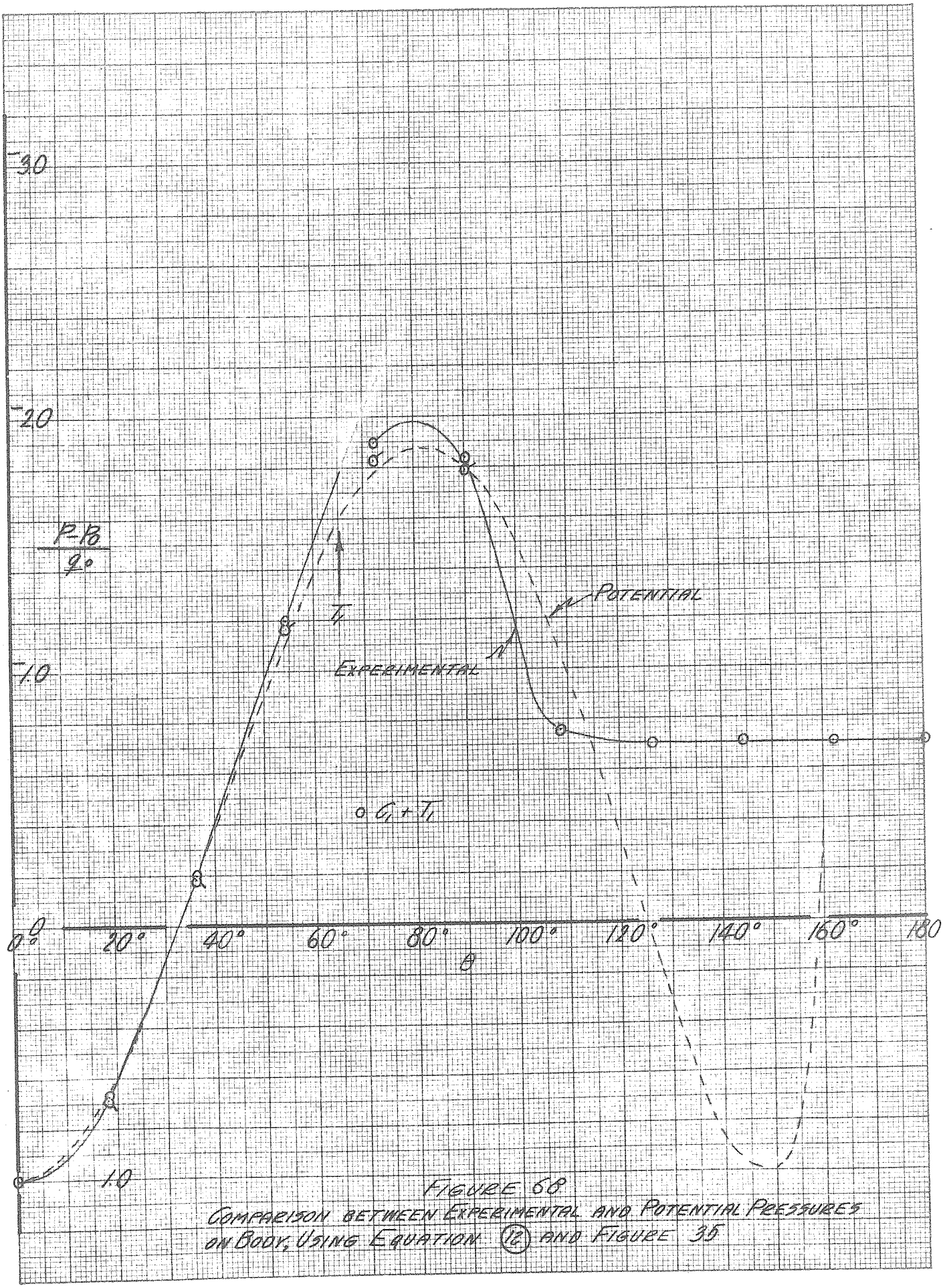

FIGURE 68
COMPARISON BETWEEN EXPERIMENTAL AND POTENTIAL PRESSURES ON BODY, USING EQUATION (12) AND FIGURE 35

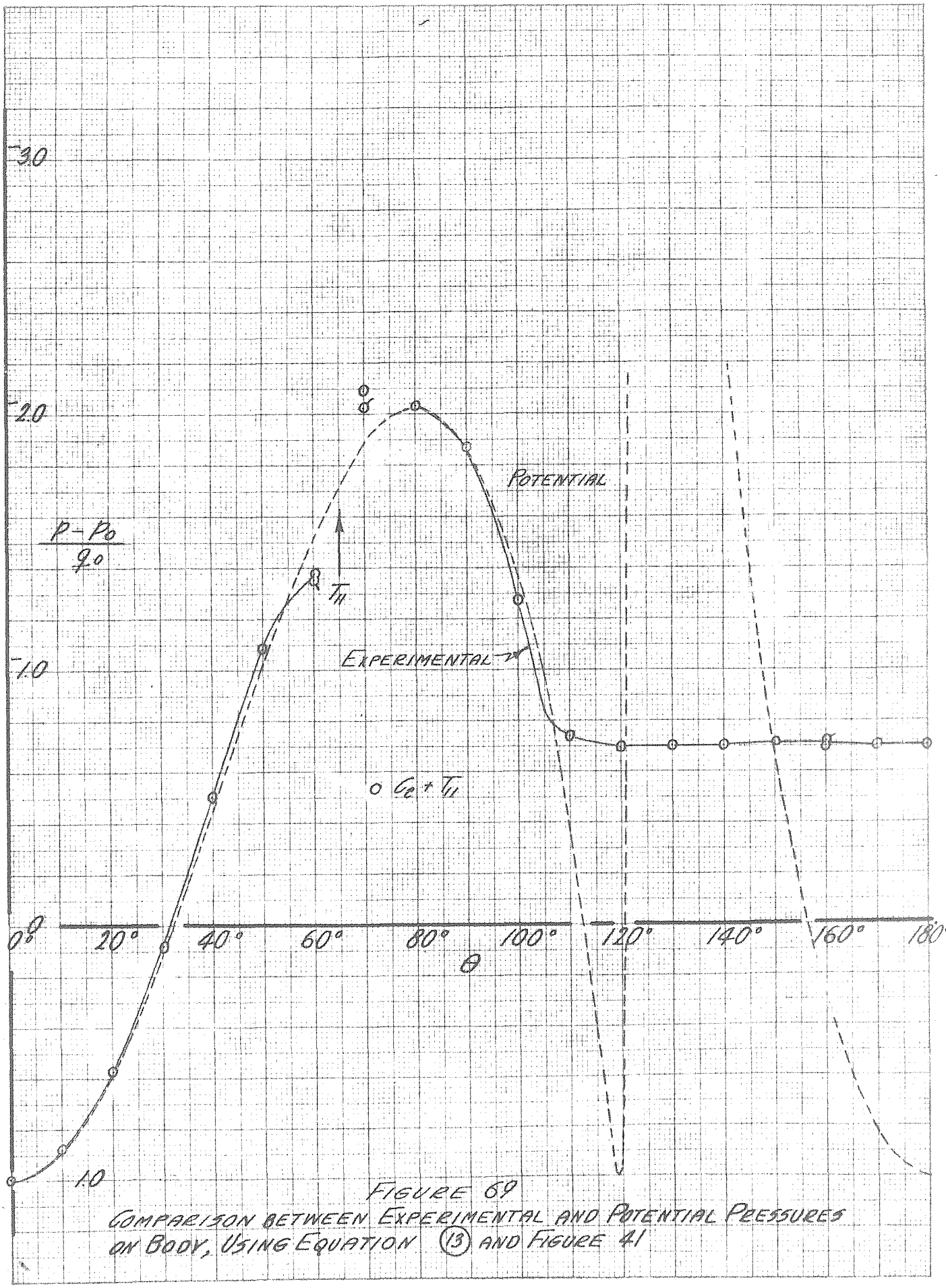

FIGURE 69
COMPARISON BETWEEN EXPERIMENTAL AND POTENTIAL PRESSURES ON BODY, USING EQUATION (13) AND FIGURE 41

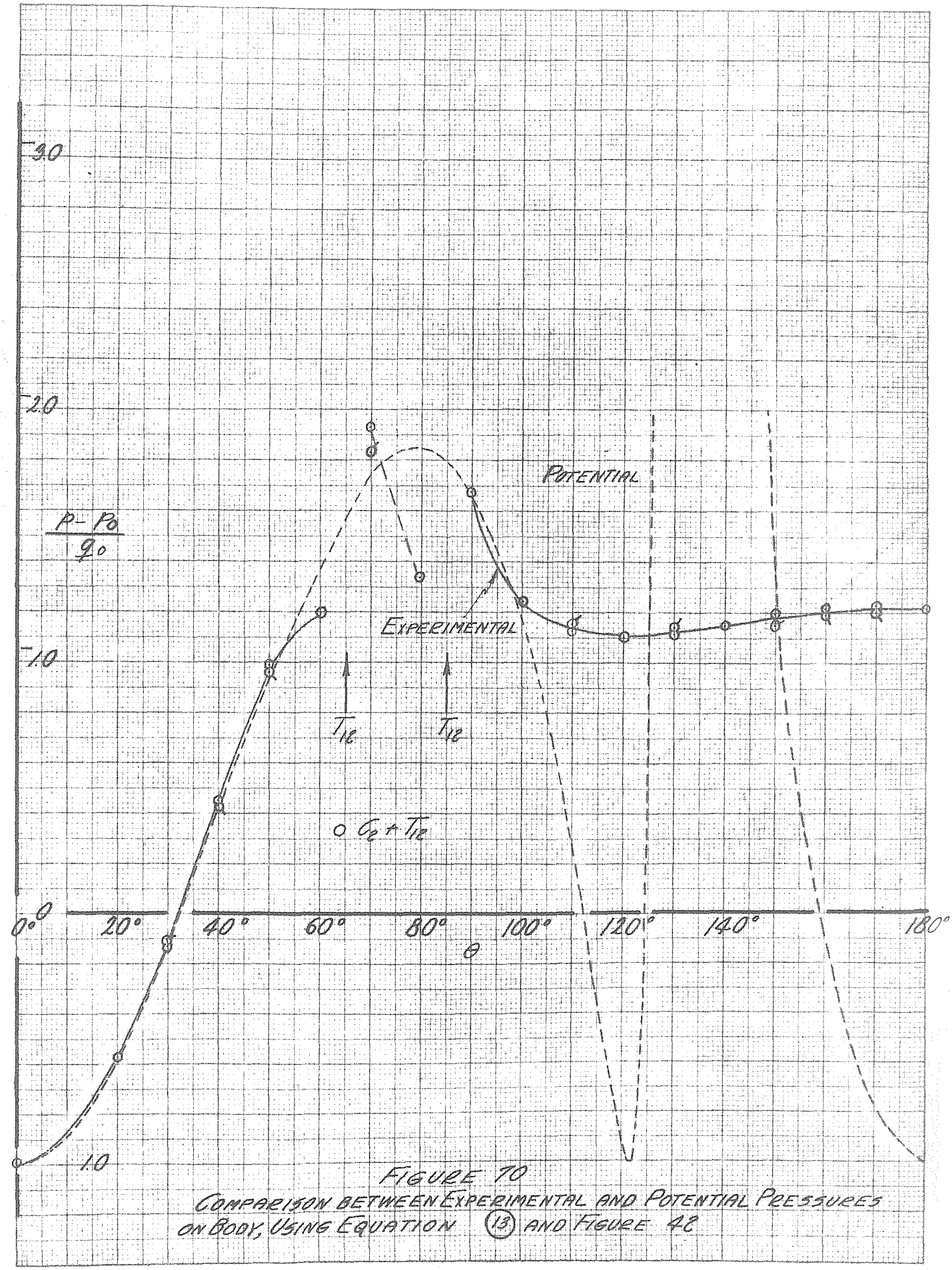

FIGURE 70
COMPARISON BETWEEN EXPERIMENTAL AND POTENTIAL PRESSURES ON BODY, USING EQUATION (13) AND FIGURE 42

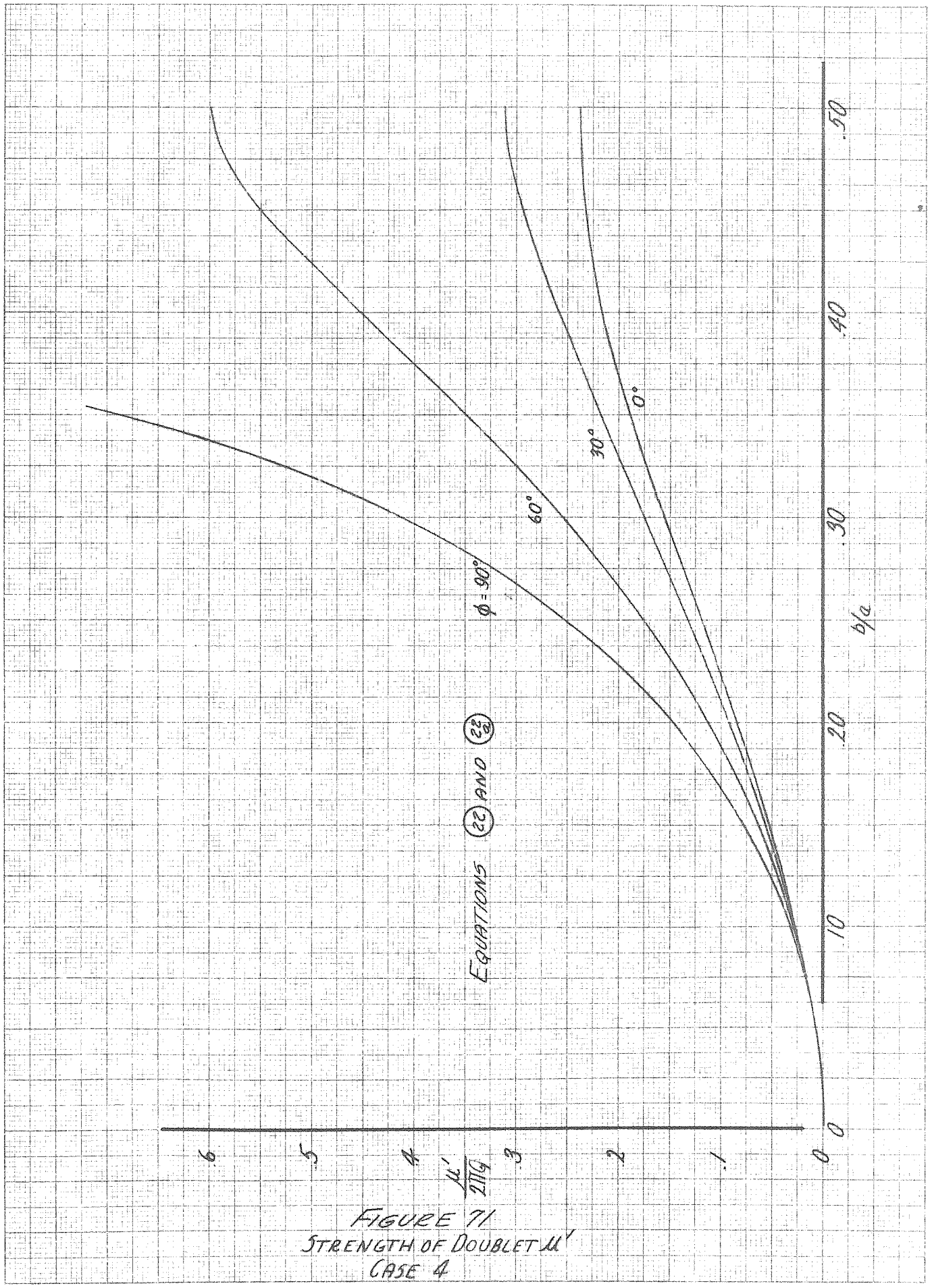

FIGURE 71
STRENGTH OF DOUBLET μ'
CASE 4

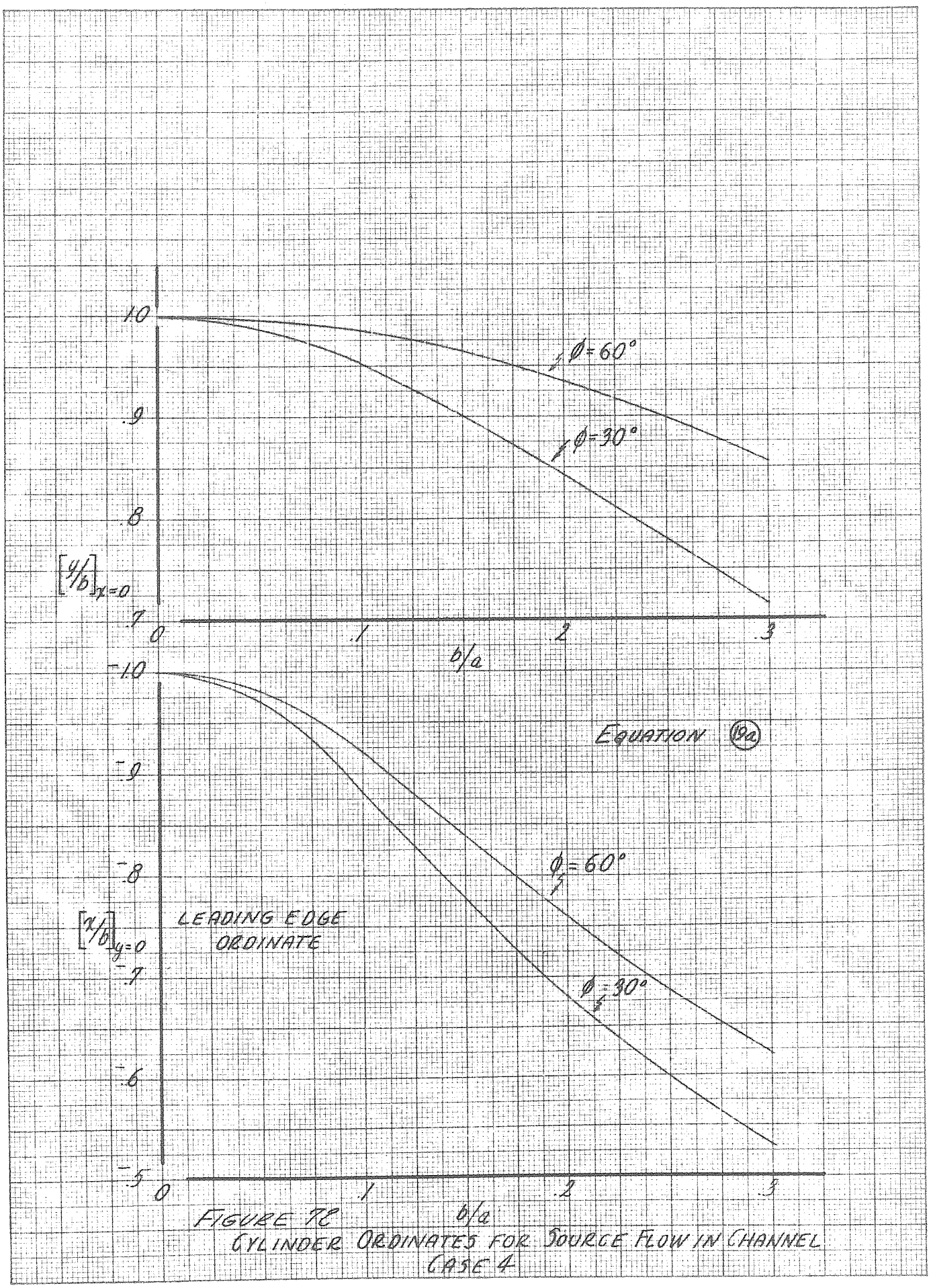

FIGURE 7C
CYLINDER ORDINATES FOR SOURCE FLOW IN CHANNEL
CASE 4

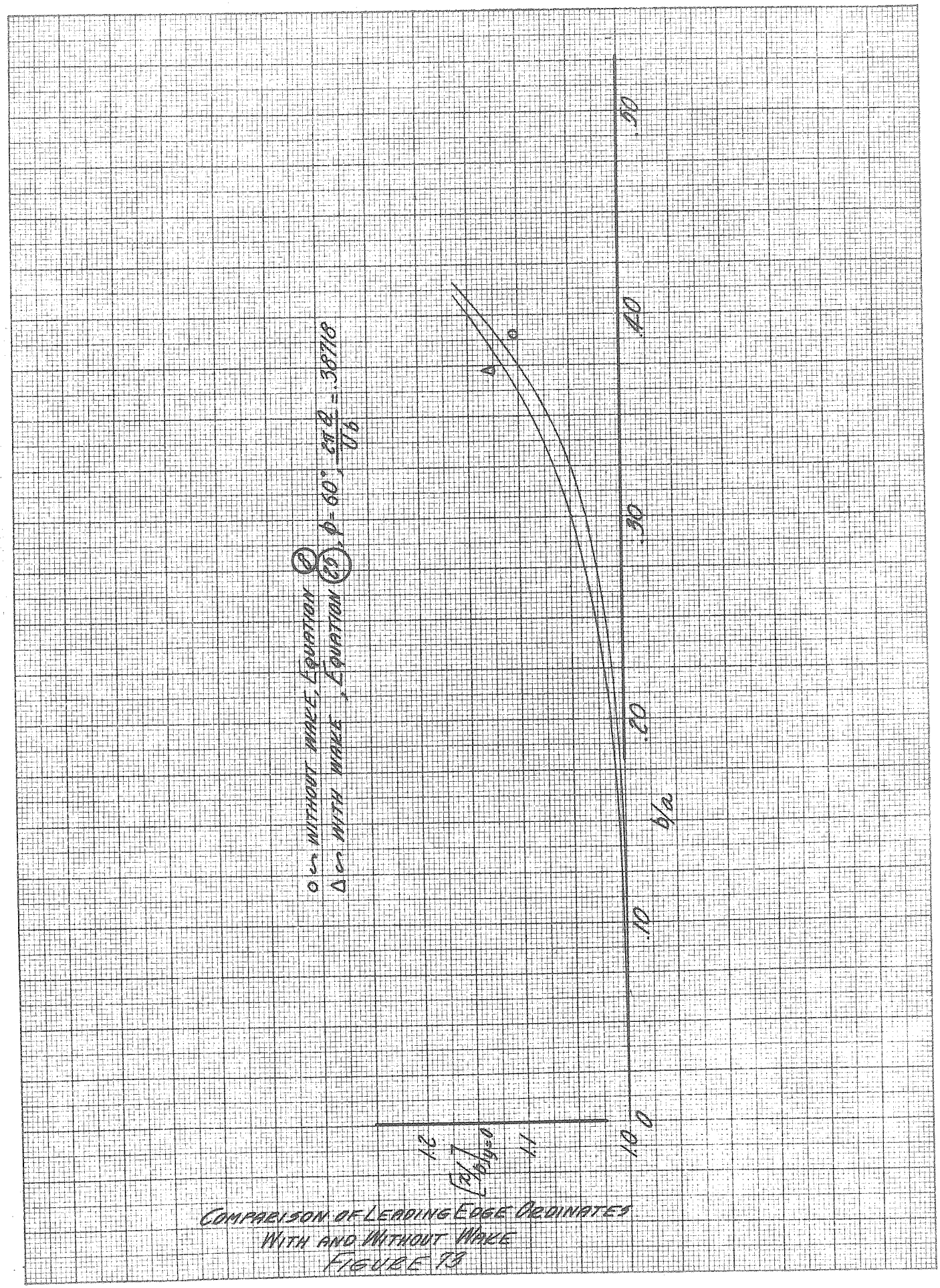

COMPARISON OF LEADING EDGE ORDINATES
WITH AND WITHOUT WAKE
FIGURE 13

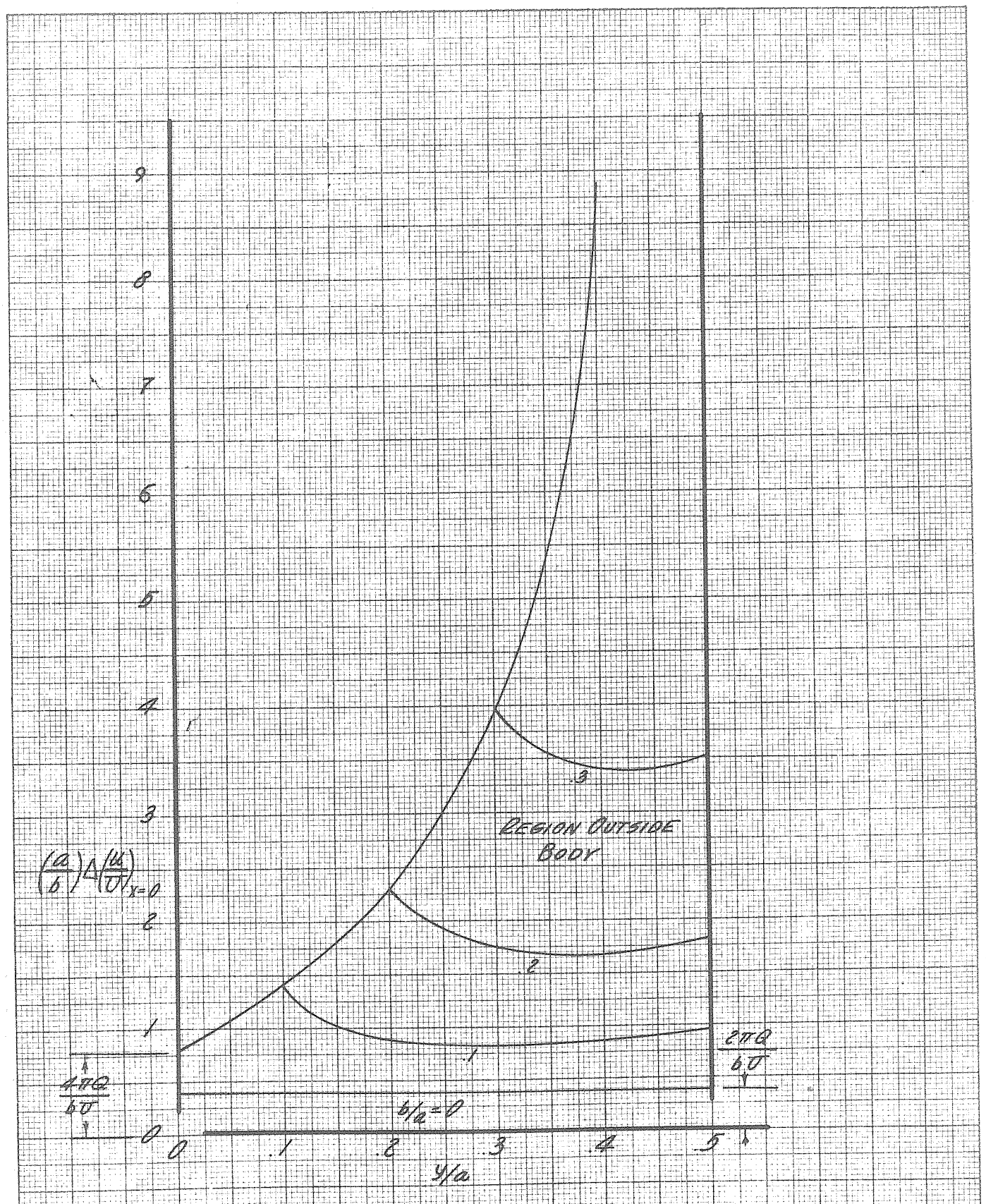

FIGURE 14
BLOCKAGE FACTOR AT x=0 WITH WAKE
EQUATIONS (16) AND (26)
$\phi = 60°$, $\frac{4\pi Q}{Ub} = 0.387$

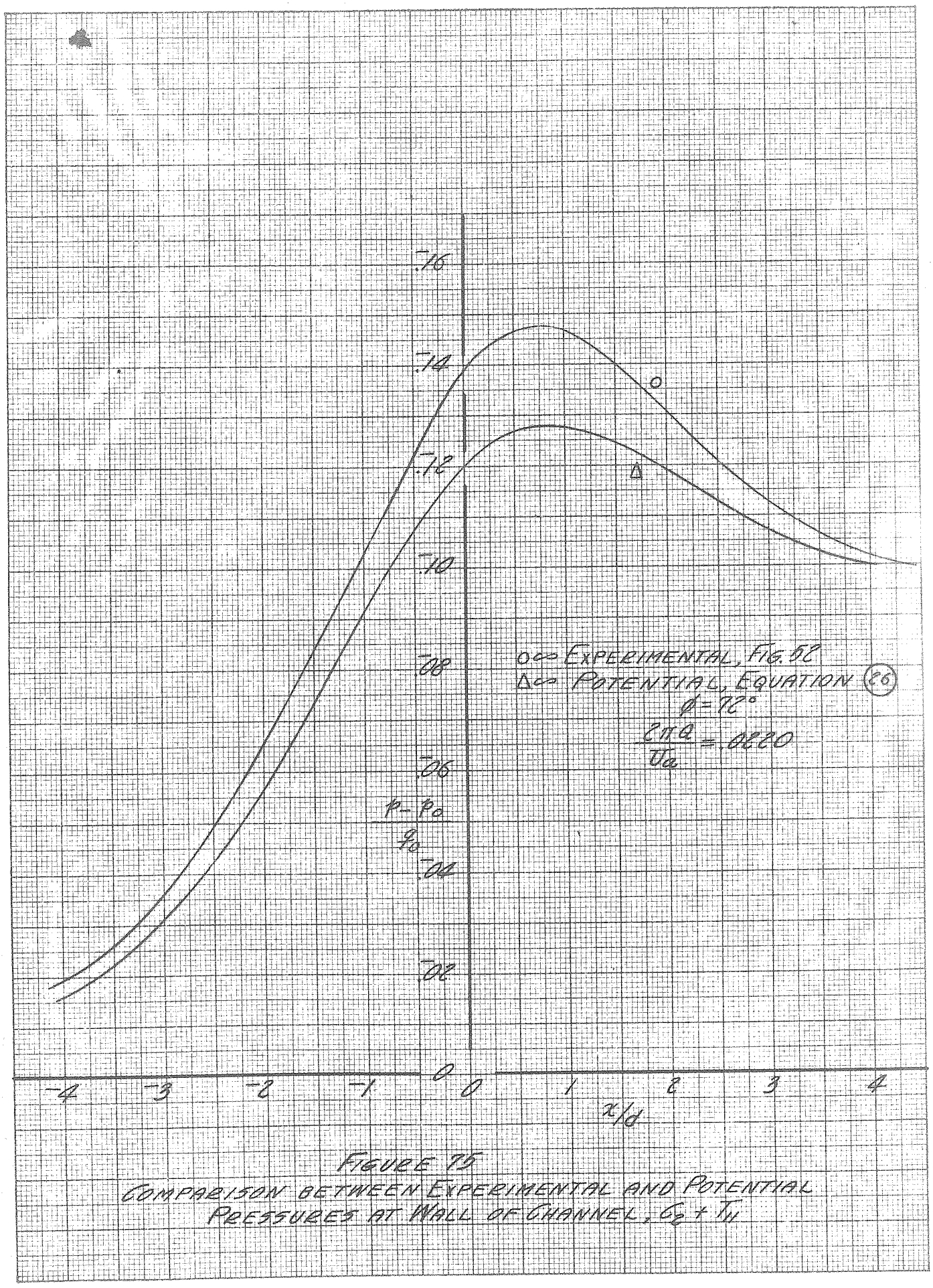

FIGURE 75
COMPARISON BETWEEN EXPERIMENTAL AND POTENTIAL PRESSURES AT WALL OF CHANNEL, $G_2 + T_4$

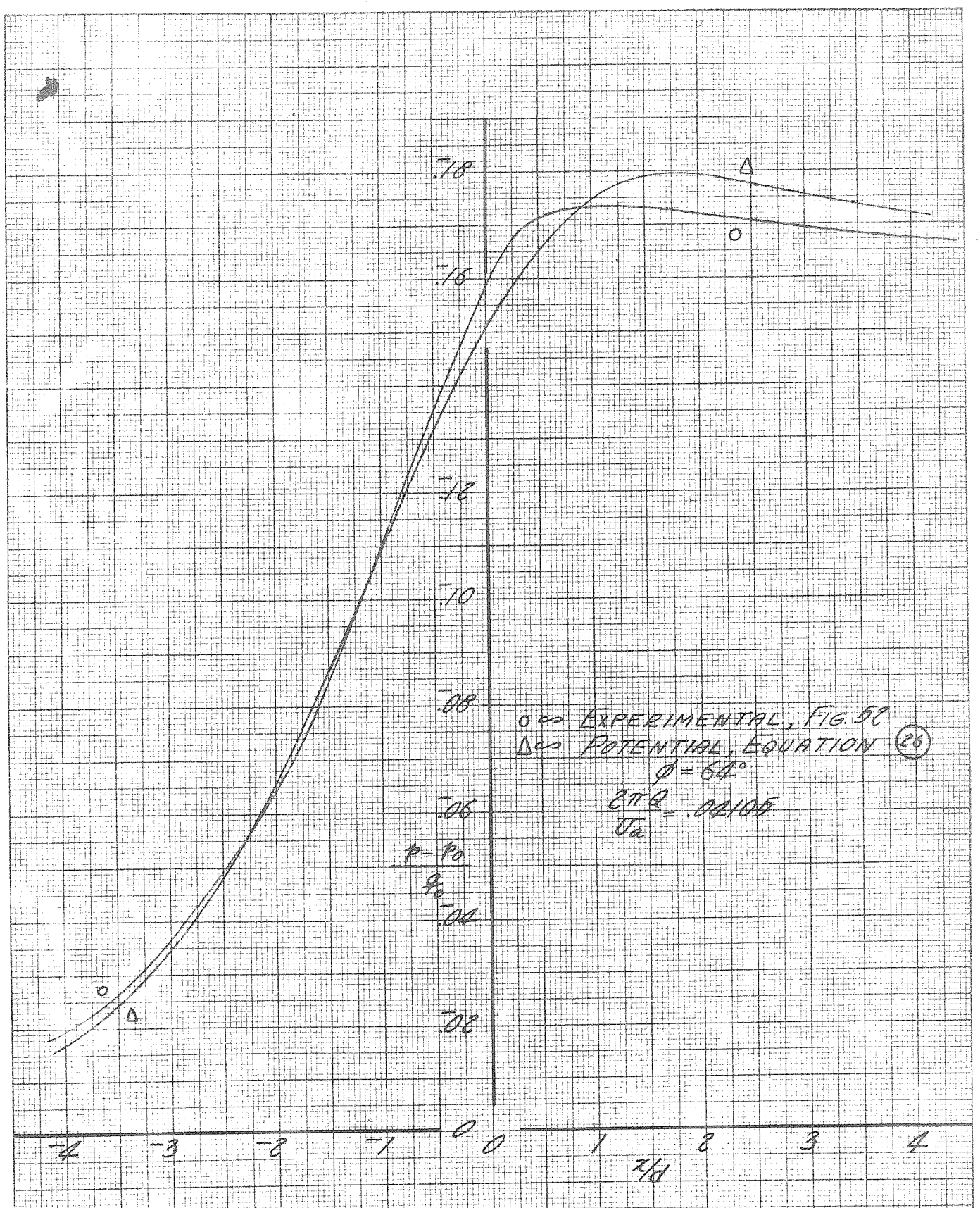

FIGURE 76
COMPARISON BETWEEN EXPERIMENTAL AND POTENTIAL PRESSURES AT WALL OF CHANNEL, $C_2 + T_{12}$